

Cell Individuality in Adhesin Expression of *Candida glabrata*

Samantha Clare Halliwell, MBIolSci.

Thesis submitted to the University of Nottingham for
the degree of Doctor of Philosophy

July 2012

Abstract

Clonal cell populations are known to exhibit marked phenotypic heterogeneity at the single cell level, a phenomenon usually masked by conventional population-wide analyses. Two models of yeast cell heterogeneity were investigated during this study. First, expression of the *Saccharomyces cerevisiae* Rad6 protein, known to facilitate DNA damage tolerance, was investigated. However, apparent bimodal Rad6 expression proved to be an artefact of a mixed-genotype culture source. The other model was adhesin expression heterogeneity in the opportunistic yeast pathogen *Candida glabrata*. Adherence to the host cell is an important step in the establishment of *C. glabrata* infection, mediated by adhesin proteins. The subtelomeric *EPA* family of adhesin genes encodes a large class of GPI-anchored cell wall proteins in *C. glabrata*, among which Epa1 is the best studied. Epa1 expression is highly heterogeneous between individual *C. glabrata* cells, a factor that can dictate adherence capacity and may have important implications for infection. Such cell-to-cell variability was dependent upon strain background. Variation in cell surface Epa1 level was correlated with variation in *EPA1* mRNA, consistent with transcriptional regulation of heterogeneity. Indeed Sir-dependent silencing was found to be a major driver of heterogeneous Epa1 expression in a strain demonstrating high cell-to-cell variability but not in an alternative genetic background demonstrating lower heterogeneity. Inefficient silencing in the latter strain was overcome by ectopic *SIR3* expression, and was not due to differences in *EPA1* sequence or distance from the chromosome end compared with the heterogeneous strain. Moreover, strain-to-strain variation in the silencing-dependence of *EPA1* expression was observed across a range of clinical isolates and was found to correlate with the extent of Epa1 heterogeneity. Thus, marked variation in adhesin expression exists between cells and between strains of *C. glabrata*. In addition, the data presented shed light on the regulation of such heterogeneity in particular the role of Sir-dependent transcriptional silencing.

Published Papers

Halliwell, S. C., Smith, M. C. A., Muston, P., Holland, S. L. & Avery, S. V. 2012. Heterogeneous expression of the virulence-related adhesin Epa1 between individual cells and strains of the pathogen *Candida glabrata*. *Eukaryot. Cell*, 11,141-150.

Acknowledgements

Firstly I would like to thank Dr Simon Avery for supervising the work performed during this study. I would also like to thank Dr Alistair Chambers for useful discussions and all other members of my lab, in particular, Dr Sara Holland and Lee Shunburne. Thanks must be given to Prof Neil Gow for initially suggesting Epa1 as a model for heterogeneity study along with Dr Michael Petrou for providing clinical *C. glabrata* isolates, and Prof Ken Haynes and Prof Brendan Cormack for donating additional strains and plasmids. For initial suggestions involving lipid rafts my thanks also go to Dr Carol Munro. I would also like to thank Prof Ed Louis and Philippa Muston in addition to Kelly Vere and Prof Paul O'Shea for useful discussion and technical assistance.

Table of Contents

Chapter 1 - Introduction	6
1.1 Introduction.....	7
1.2 Classification of Fungi and the Yeasts.....	7
1.3 <i>Candida glabrata</i>	9
1.3.1 <i>The Genomics of C. glabrata</i>	12
1.3.2 <i>Clinical Relevance and Incidence of C. glabrata Infections</i>	14
1.3.3 <i>Treatment and Azole Resistance of Candida glabrata Infections</i>	16
1.4 The Fungal Cell Wall	18
1.4.1 <i>Cell Wall Structure</i>	19
1.4.2 <i>GPI-Anchored Cell Wall Proteins</i>	22
1.4.2.1 <i>GPI-Anchored Adhesins</i>	25
1.5 Sir-Dependent Transcriptional Silencing in Yeasts.....	28
1.5.1 <i>Telomeric Silencing</i>	31
1.5.1.1 <i>Assembly and Propagation of the Telomeric Sir Complex</i> ...	32
1.6 DNA Damage Tolerance in Yeast	37
1.6.1 <i>Translesion Synthesis</i>	38
1.6.2 <i>Error Free Damage Tolerance</i>	43
1.6.3 <i>Conservation of DNA Damage Tolerance from Yeast to Humans</i>	44
1.7 Microbial Cell Individuality	45
1.7.1 <i>Cell Surface Variation</i>	47
1.7.1.1 <i>Protozoan Cell Surface Variation</i>	47
1.7.1.2 <i>Yeast Cell Surface Variation</i>	54
1.8 Aims of the Current Work.....	57
Chapter 2 - Materials and Methods	59
2.1 Strains and Plasmids.....	60
2.1.1 <i>Construction of CG2001-Epa1-HA</i>	60
2.1.2 <i>Construction of sir3Δ Strains</i>	62
2.1.3 <i>Construction of pCgACT-14-SIR3 Single Copy Plasmid</i>	63
2.1.4 <i>Construction of yps7Δ and yps1yps7Δ Mutant Strains</i>	63
2.1.5 <i>S. cerevisiae Strains and Plasmids</i>	64
2.2 Growth Conditions for Experiments and Storage.....	65
2.3 Isolation of DNA.....	67
2.3.1 <i>Genomic DNA Isolation from Yeast</i>	67
2.3.2 <i>Plasmid Isolation from E. coli</i>	68
2.3.3 <i>Plasmid Isolation from C. glabrata and S. cerevisiae</i>	68
2.4 Polymerase Chain Reaction (PCR).....	69
2.4.1 <i>Phusion® High-Fidelity Polymerase PCR Reaction</i>	69

2.4.2 <i>Taq</i> DNA Polymerase PCR Reaction.....	70
2.4.3 Yeast Colony PCR.....	71
2.4.4 Bacterial Colony PCR.....	71
2.5 DNA Sequencing	73
2.6 Digestion of DNA with Restriction Enzymes.....	73
2.7 Agarose Gel Electrophoresis.....	73
2.8 Purification of DNA from Agarose Gels.....	74
2.9 DNA Ligations	74
2.9.1 Ethanol Precipitation.....	76
2.10 Transformations	76
2.10.1 Yeast Transformation.....	76
2.10.2 Bacterial Transformation	77
2.10.2.1 Preparation of Electro-competent <i>E. coli</i> XLI Blue Cells	77
2.11 Cell Staining/Probing.....	78
2.11.1 Probing for <i>Epa1</i>	78
2.11.2 Probing for Mannoprotein	78
2.11.3 Filipin Staining	79
2.11.4 Dual Staining.....	79
2.11.5 Actin Staining	79
2.12 Flow Cytometry and Fluorescence Activated Cell Sorting (FACS)	79
2.13 Fluorescence Microscopy.....	80
2.13.1 Time Lapse Microscopy	80
2.14 Adherence Assay	81
2.15 RNA Extraction	81
2.16 Reverse Transcription.....	82
2.17 Quantitative RT-PCR (qRT-PCR).....	82
2.17.1 Calculation of DNA Copy Number for qRT-PCR Standard Curves	83
2.18 Digestion, Separation and Probing of <i>EPA1</i> -containing High Molecular Weight DNA	84
2.18.1 Isolation of High Molecular Weight DNA in Agarose Plugs	84
2.18.2 Digestion of DNA Isolated in Agarose Plugs.....	85
2.18.3 Field Inversion Gel Electrophoresis (FIGE)	85
2.18.4 Southern Transfer and Probing for <i>EPA1</i>	87
2.19 Statistical Analysis	88
Chapter 3 - Heterogeneity in Rad6 Expression	89
3.1 Introduction.....	90
3.2 Complementation of the <i>sir2Δ</i> and <i>swi6Δ</i> Deletions in Rad6- GFP Expressing Cells	94

3.2.1 Construction of SIR2 and SWI6 Single Copy Plasmids	94
3.2.2 Complementation of Rad6-GFP sir2 Δ and Rad6-GFP swi6 Δ Strains does not restore Bimodal Rad6-GFP Expression	94
3.3 Rad6 Expression Levels are Maintained for Many Generations	97
3.4 Rad6 Does Not Exhibit Bi-stable Gene or Protein Expression	99
3.4.1 Analysis of a RAD6-GFP Transcriptional Fusion	99
3.4.2 Analysis of a Newly Constructed Rad6-GFP Translational Fusion	101
3.5 Discussion	103
Chapter 4 - <i>Candida glabrata</i> exhibits Strain Background-Dependent Heterogeneous Epa1 Expression	105
4.1 Introduction	106
4.2 Cell-to-Cell Heterogeneity in Epa1 Expression is observed at the <i>C. glabrata</i> Cell Surface and appears to depend upon Strain Background	110
4.2.1 Confirmation of EPA1 Expression Heterogeneity	110
4.2.2 Heterogeneity of Epa1 Protein Expression at the Cell Surface	112
4.2.3 Construction of CG2001-Epa1-HA	112
4.2.4 Heterogeneity of Epa1 Expression at the Cell Surface appears to be Strain Dependent	114
4.3 Heterogeneity and Expression of Epa1-HA Varies During Growth in Batch Culture	117
4.4 Inheritance of Epa1	119
4.4.1 Epa1-HA Expression in Daughter Cells represents De Novo Synthesis of Epa1	119
4.4.2 Newly Budded Cells Exhibit a Variety of Expression States	121
4.4.3 Cell Surface Epa1-HA Expression State may be partially Inherited	123
4.5 Discussion	125
Chapter 5 - Regulation of Epa1 Expression in <i>Candida glabrata</i>	129
5.1 Introduction	130
5.2 Impact of Virulence Related Environmental Conditions on Epa1 Expression and Heterogeneity	134
5.2.1 Effect of Temperature	134
5.2.2 Response to Nitrogen Limitation	135
5.2.3 Response to pH Level	139
5.3 Transcriptional Silencing affects EPA1/Epa1 Expression and Heterogeneity	144
5.3.1 Sir3-Dependent EPA1 Transcription in a BG2 Strain Background	144
5.3.2 Sir3-Dependent Transcriptional Silencing in CG2001-Epa1-HA	146

5.3.3 Corroboration of Strain Dependent Sir-Mediated Transcriptional Silencing of Epa1-HA	148
5.3.3.1 Inhibition of Silencing in CG2001-Epa1-HA and BG2-Epa1-HA by Nicotinic Acid Limitation	150
5.3.3.2 – Analysis of Cell Surface Epa1 Expression in sir3Δ Mutant Cells via an Anti-Epa1 Antibody	152
5.3.4 The Effect of Transcriptional Silencing on EPA1 Transcript Levels also depends on Strain Background	155
5.3.5 Sir3 Mediated Silencing appears to be Less Efficient in a CG2001-EPA1-HA Background.....	158
5.3.5.1 Addition of a Second SIR3 Copy Increases Heterogeneity in CG2001-Epa1-HA	158
5.3.5.2 SIR3 Transcript Level appears not to Contribute to the Weakened EPA1 Silencing Observed in CG2001HTUΔ	160
5.3.6 Analysis of NA-Limitation and EPA1 Expression in a Range of Clinical <i>C. glabrata</i> Isolates	160
5.3.6.1 The Extent of EPA1 Silencing Correlates with Cell Surface Epa1 Heterogeneity in Clinical <i>C. glabrata</i> Isolates.....	163
5.4 Variation in EPA1 Distance from the Chromosome End is not a Likely Cause of Strain Dependent Sir-Regulation.....	165
5.4.1 Strategy to look for Differences in the Distance of EPA1 from the Chromosome End in Two Strain Backgrounds	167
5.4.2 Distance of EPA1 from the Chromosome End does not appear to Differ between Strains	167
5.5 Contribution of Additional Post-Translational Factors to Epa1 Heterogeneity.....	171
5.5.1 Lipid Raft Heterogeneity does not contribute to Epa1 Heterogeneity	171
5.5.1.1 Inhibition of Sphingolipid Biosynthesis to Disrupt Lipid Raft Formation.....	173
5.5.1.2 Inhibition of Sterol Biosynthesis to disrupt Lipid Raft Formation.....	175
5.5.1.3 Inhibition of both Sphingolipid and Sterol Biosynthesis simultaneously caused increased Epa1-HA Expression	175
5.5.1.4 Inhibition of Lipid Rafts does not release the Patchy Expression Pattern Exhibited by Epa1-HA	177
5.5.1.5 Epa1-HA Fluorescence does not Co-localise with Filipin Staining in <i>C. glabrata</i>	177
5.5.2 Epa1-HA Localisation does not appear Dependent on the Actin Cytoskeleton.....	181
5.5.3 Removal of Epa1 from the Cell Surface via Yps Proteases does not appear to have a Role in Heterogeneity	183
5.5.3.1 The Yps Proteins do not appear to have a Role in Controlling Epa1 Heterogeneity	183

5.5.4 Heterogeneity in <i>Epa1</i> Expression Occurs Independently of Total Manno-Protein Level at the Cell Surface	186
5.5.4.1 Visualisation of Total Mannoprotein Levels and Comparison with <i>Epa1</i> -HA Expression	186
5.6 Heterogeneity of <i>Epa1</i> Expression is Primarily Determined at the mRNA Level	188
5.6.1 <i>Epa1</i> Cell Surface Expression Level Correlates with <i>EPA1</i> Transcript Level	188
5.7 Analysis of the <i>EPA1</i> Promoter	190
5.7.1 The <i>EPA1</i> Predicted Promoter Region Contains an Alpha2-Repressor Consensus Sequence	190
5.7.2 Alpha2 Repressor Level appears not to Control <i>EPA1</i> Expression	191
5.8 Alignments of <i>EPA1</i> Sequence from Two Strain Backgrounds	193
5.9 Regulation of Other <i>EPA</i> Genes Relative to <i>Epa1</i> -HA	195
5.9.1 <i>EPA6</i> and <i>EPA7</i> mRNA Levels are Correlated with Cell Surface <i>Epa1</i> -HA Expression	195
5.9.2 Sir-Regulated Transcriptional Silencing of Additional <i>EPA</i> Genes	197
5.10 Discussion	200
Chapter 6 - Concluding Remarks	208
6.1 Concluding Remarks	209
References	214
List of Figures.....	230
List of Tables	234

Chapter 1 - Introduction

1.1 Introduction

Conventional studies which involve the analysis of data averaged across whole populations of cells generally mask any variation occurring at the single cell level. Marked cell-to-cell variation is known to exist between cells derived from genetically identical populations, a phenomenon termed phenotypic heterogeneity. This study aimed to investigate this process through the use of two yeast models of cell heterogeneity. The first of these was investigation into bimodal expression of the *S. cerevisiae* ubiquitin conjugating enzyme Rad6. The primary role of this protein is to facilitate DNA damage tolerance and as such the processes involved in this will be introduced. Secondly, and forming a larger part of the project, adhesin expression heterogeneity was studied in the opportunistic yeast pathogen *C. glabrata*, which represents the most prevalent non-albicans *Candida* species causing infection in humans. This pathogen demonstrates an inherent resistance to azole antifungals which is accompanied by relatively high crude mortality (Wisplinghoff et al., 2004, Kaur et al., 2005). Adhesion to host tissues constitutes an important step in the establishment of infection, heterogeneity in adhesin expression may therefore have important implications for virulence, particularly given that in theory just one virulent cell from a larger avirulent population may be sufficient to establish infection. *C. glabrata* encodes a large family of glycosylphosphatidylinositol-anchored cell wall proteins (GPI-CWPs) that function as adhesins. These adhesins, termed epithelial adhesins (Epa adhesins), occupy subtelomeric positions in the genome. It is unsurprising then that position dependent telomeric silencing has been demonstrated as having a role in controlling the expression of EPA adhesins (De Las Penas et al., 2003, Castano et al., 2005, Rosas-Hernandez et al., 2008). In addition to providing a general background to *C. glabrata*, this introduction aims to discuss the fungal cell wall with particular emphasis on the GPI-anchored proteins that reside there. Furthermore owing to the subtelomeric location of these adhesin genes the mechanism of telomeric silencing will be addressed before tackling the subject of cell individuality.

1.2 Classification of Fungi and the Yeasts

The concept of grouping organisms into specific groups has existed since Linnaeus' theory of classification in the early eighteenth century, however it was not until 1949 that the concept of fungi was first introduced and finally advanced into the 5 kingdom system of classification, which

recognises the Fungi as a separate group alongside the Monera, Protista, Plantae, and Animalia (Whittaker, 1959, Whittaker, 1969, Hibbett et al., 2007). Typically known fungal species have been divided into five phyla consisting of; Ascomycota, Basidiomycota, Glomeromycota, Zygomycota, and Chytridomycota (Hedges, 2002, Scannell et al., 2007). In the last few years, however, a comprehensive phylogenetic classification of the fungal kingdom has been proposed which includes a number of changes in the 'basal fungal lineages' and describes one kingdom, one subkingdom and seven phyla. This included the recognition of 3 additional phyla; the Blastocladiomycota, the Neocallimastigomycota, and the Microsporidia along with loss of the Zygomycota (Hibbett et al., 2007).

The yeasts reside within the largest fungal phylum; the Ascomycota, which diverged from the Basidiomycota around 741-1195 million years ago. Almost 50% of all known fungal species and 80% of pathogenic and opportunistic species are contained within this phylum. Shortly after the initial split this phylum further diverged into 2 classes; the Pezizomycotina, including filamentous fungi such as *Neurospora crassa*, and the Saccharomycotina (sometimes referred to as the hemiascomycetes), which includes budding yeasts such as *S. cerevisiae*. Recent molecular evidence, however, has raised calls for a third Ascomycete class; the Archiascomycotina (Taphrinomycotina), in order to accommodate *Schizosaccharomyces pombe* which has been revealed as an out-group to the two existing taxa (Guarro et al., 1999, Hedges, 2002, Hedges et al., 2004, Scannell et al., 2007). The yeasts considered within the scope of this thesis occupy the Saccharomycotina within which over 1000 species have been described. Thus far all sequenced Saccharomycotina genomes fall into 3 clusters; the first of which, termed the 'Saccharomyces complex', is primarily composed of species from the genera *Saccharomyces* and *Kluyveromyces*. Within this cluster the major phylogenetic divergence exists between those yeasts whose common ancestor underwent a whole genome duplication (WGD) event and those that diverged prior to this. The CTG clade forms the second cluster and consists of species which translate CTG codons as serine rather than leucine, a reassignment proposed to have occurred ~170 million years ago, and includes many *Candida* species. There has been a suggestion that this clade could be further diverged into 2 groups relating to sexual status, thus separating the fully sexual species from others which at best have a cryptic sexual cycle (Fitzpatrick et al., 2006, Scannell et al., 2007). Finally

Yarrowia lipolytica is the only sequenced member of the final cluster (Fig. 1) (Scannell et al., 2007).

1.3 *Candida glabrata*

C. glabrata is a pathogenic yeast that along with other budding, including pathogenic, yeasts resides within the Saccharomycotina subphylum of the Ascomycota. Interestingly, however, this pathogenic yeast exists separately from the majority of other *Candida* species (Fig. 1), which are commonly found within the CTG clade, and can instead be found within the WGD portion of the *Saccharomyces* complex along with *S. cerevisiae* (Scannell et al., 2007). Historically *C. glabrata* was classified into the genus *Torulopsis* due to its lack of pseudohyphal growth. It was later determined however, that the ability to produce pseudohyphae was not a reliable distinguishing factor for members of the *Candida* genus and in 1978 it was proposed that *T. glabrata* be reclassified into this genus. Thus the description relating to filamentous growth for the *Candida* genus was altered from "pseudomycelial" to "pseudohyphae: absent, rudimentary, or well developed" (Fidel et al., 1999). Pseudohyphal growth has in fact now been observed in *C. glabrata* under *in vitro* conditions of nitrogen starvation (Fig. 2) (Csank and Haynes, 2000). This process appears to be dependent upon the transcriptional regulator Ste12, however, unlike the case in *Candida albicans*, such filamentous growth is not believed to be important for virulence (Calcagno et al., 2003). Indeed, to date there is no description of *C. glabrata* growing *in vivo* as anything other than budding yeast blastoconidia, typically 1-4 μ M in size (Fidel et al., 1999, Csank and Haynes, 2000). This is in stark contrast to the morphological variation demonstrated *in vivo* by *C. albicans* which is able to switch between yeast blastoconidia of ~4-6 μ M, and two forms of filamentous growth; pseudohyphae and hyphae (Fig. 3) (Fidel et al., 1999, Sudbery et al., 2004); a trait that is widely considered a virulence determinant in this organism (Lo et al., 1997). This difference may not be surprising given the phylogenetically distinct positions of these two pathogens, which suggests that the ability of *C. glabrata* to become associated with the mammalian host evolved independently from *C. albicans*, and indeed other *Candida* species. *C. glabrata* is in-fact more closely related to the non-pathogenic *S. cerevisiae* (Fig. 1) (Kaur et al., 2005, Roetzer et al., 2011). An independent evolutionary route for *C. glabrata* is highlighted by its clear

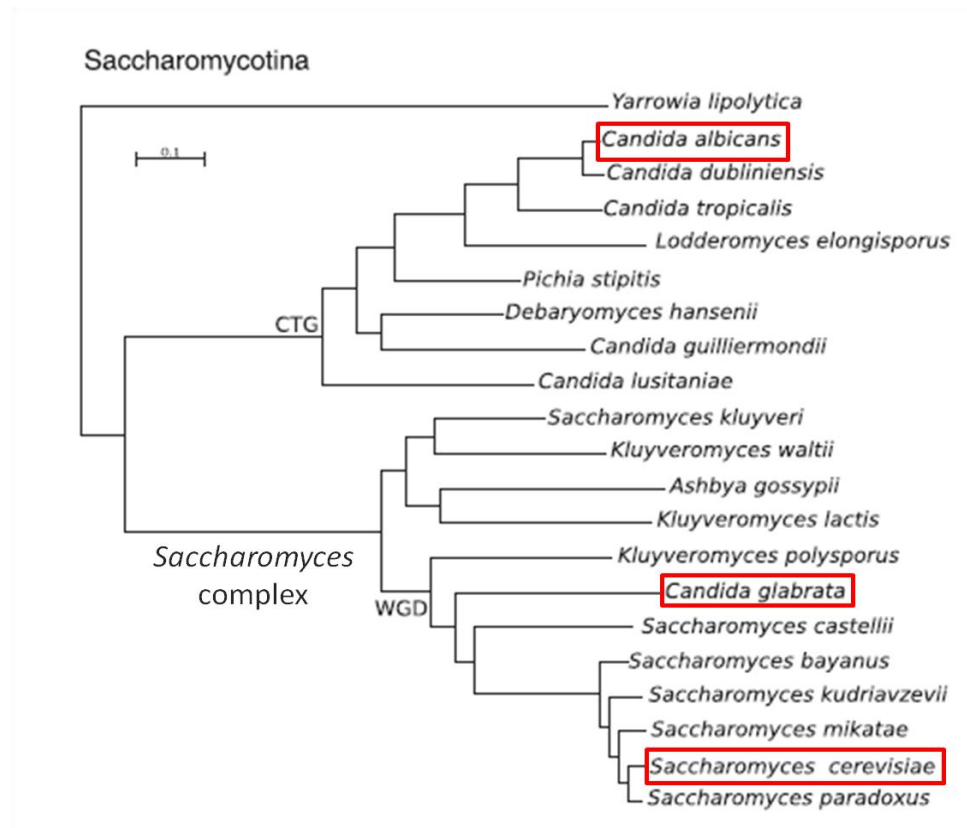


Figure 1 – Phylogenetic tree representing evolution of the Saccharomycotina. *C. glabrata* is identified within the same cluster as *S. cerevisiae* while *C. albicans* is phylogenetically distinct from these 2 organisms and is located within the CTG clade. Slightly modified from (Roetzer et al., 2011).

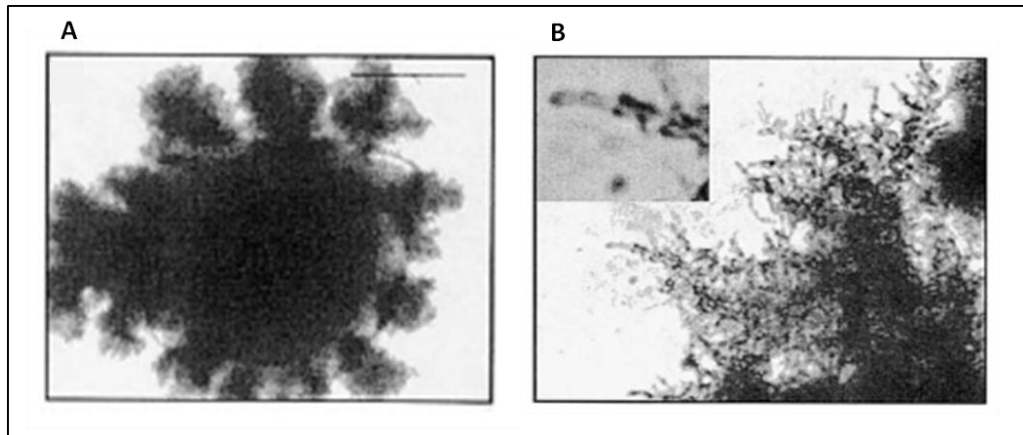


Figure 2 – Demonstration of *C. glabrata* pseudohyphal formation following growth on nitrogen starvation solid medium (SLAD). **(A)** Illustrates a polarized colony, **(B)** Pseudohyphal chains from the perimeter of the colony seen in (A). Taken from (Csank and Haynes, 2000)

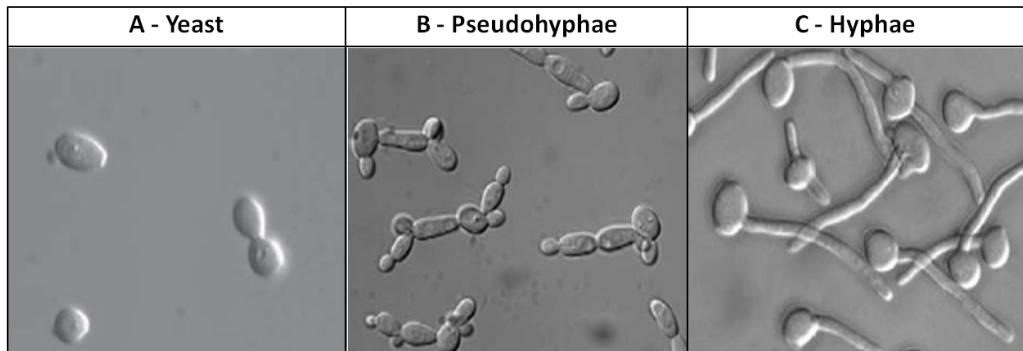


Figure 3 – Yeast **(A)**, pseudohyphal **(B)**, and hyphal **(C)** morphologies exhibited by *C. albicans*. Taken from (Sudbery et al., 2004).

separation from the CTG clade within which many other *Candida* species reside.

1.3.1 The Genomics of *C. glabrata*

The *C. glabrata* type strain CBS138/ATCC2001, which was originally isolated from human faeces, has been sequenced as part of the genolevures project (<http://www.genolevures.org/cagl.html>) to provide subtelomere-to-subtelomere data for all 13 chromosomes (A-M). Upon exclusion of rDNA, which is organised into two distinct loci on chromosomes 12 and 13, this haploid genome totals 12.3Mb, encoding approximately 5283 coding genes and 207 tRNA genes (Sherman et al., 2006). The *C. glabrata* genome shows a high degree of similarity with *S. cerevisiae*, sharing on average 65% amino acid identity between protein orthologues. Nevertheless, and likely due to its close association with the mammalian host, *C. glabrata* demonstrates a significantly greater degree of gene loss compared to *S. cerevisiae* resulting in regressive evolution. For instance, *C. glabrata* has streamlined its metabolic capacity with the loss of genes involved in galactose and sucrose assimilation, phosphate, nitrogen and sulphur metabolism and, thiamine, pyridoxine and nicotinic acid biosynthesis (Domergue et al., 2005, Kaur et al., 2005, Sherman et al., 2006).

Although no sexual cycle has been observed in *C. glabrata* the genome has been shown to encode, like *S. cerevisiae*, three mating type-like loci (MTL); *MTL1*, *MTL2*, and *MTL3*, in addition to many of the genes required for mating, meiosis and sporulation (Srikantha et al., 2003, Ramirez-Zavaleta et al., 2010). Interestingly, unlike *S. cerevisiae*, the three loci do not exist on the same chromosome. Rather, *MTL1* resides at an internal location on chromosome B (II) with *MTL3* 10.5kb from the left end of this chromosome. *MTL2* however is located 29.4kb from the left end of chromosome E (V). In further contrast to *S. cerevisiae*, only one locus, *MTL3*, is subject to silencing, this requires Sir2 to -4, yKu70, yKu80, and Rif1, while both the *MTL1* and *MTL2* loci are transcriptionally active (Muller et al., 2008, Ramirez-Zavaleta et al., 2010). Nevertheless *C. glabrata* is able to maintain distinct a- and alpha- haploid mating types with *MTL1* thought to function as equivalent to the *S. cerevisiae* *MAT* locus. Both the *alpha-1* and *alpha-2* genes have been found to be expressed in a mating type specific manner, however, the *a1* gene can be detected in strains of each mating type. Further analysis of the *a1* gene led to the proposition that mating type identity is maintained to some extent by incomplete

splicing of the transcript (Muller et al., 2008). Such *a1* splicing is locus specific, fully processed *a1* transcript is undetectable when expressed from *MTL2*, while both functional processed and non-functional unprocessed, in addition to partially processed forms can be detected following expression from *MTL1* (Ramirez-Zavaleta et al., 2010). Despite apparently maintaining a mating type identity, genes determined as either a-, alpha-, or haploid-specific based on their expression in *S. cerevisiae* are expressed irrespective of mating type information in *C. glabrata*. Thus cell-type specific genes are not regulated in the same way that *S. cerevisiae* regulates such genes and this likely leads to a lack of cell type identity in *C. glabrata*. Moreover it is not known if the *a1*, *alpha1*, and *alpha2* proteins are actually functional in *C. glabrata*. It has been suggested that *C. glabrata* may have undergone a rewiring of these mating type regulators such that they do not control sexual reproduction or the cell-type identity genes at all. Rather they may control processes important for survival within the mammalian host such as the pheromone response pathway which is known to play a role in *C. glabrata* virulence (Ramirez-Zavaleta et al., 2010). Interestingly mating type switching from a- to alpha- has been reported to occur *in vivo* for this pathogen (Muller et al., 2008) further suggesting that there may be a role for these genes in virulence.

Finally *C. glabrata* exhibits significant genome plasticity with marked variations in chromosome structure evident upon karyotype analysis of different isolates. Large chromosomal size polymorphisms were identified and have been associated with both reciprocal and non-reciprocal translocations of chromosome arms, and the translocation of interchromosomal duplications ranging from 40-700kb in size (Polakova et al., 2009). Furthermore minisatellites, including unusually long elements termed megasatellites, have been identified in the genome and are largely found in genes regulating cell-to-cell adhesion. The presence and length of such repeated motifs has been shown to differ between *C. glabrata* strains (Frieman et al., 2002, Thierry et al., 2008). Another effect of this genome plasticity is the formation of small novel chromosomes composed of large 120- to 200kb segmental duplications that include a centromere region and which have acquired telomeres. In addition chimeric chromosome fusions have been identified (Muller et al., 2009, Polakova et al., 2009). Aneuploidy in *S. cerevisiae* is associated with a proliferative disadvantage (Torres et al., 2007). This and other changes in chromosome structure are generally associated with pathological events in other eukaryotes and are

not compatible with a sexual lifecycle (Delneri et al., 2003, Polakova et al., 2009). Elevated chromosome dynamics may however be beneficial for adaptation to changing environments such that may be encountered by *C. glabrata* during host infection with the suggestion that a sexual cycle has been "sacrificed" to better tolerate such genome alterations (Polakova et al., 2009).

1.3.2 Clinical Relevance and Incidence of *C. glabrata* Infections

Several *Candida* species, including *C. albicans* and *C. glabrata* generally exist as harmless commensals of the gastrointestinal and genitourinary tracts and can be isolated from the mucosa of normally healthy asymptomatic individuals (Kaur et al., 2005). Indeed, *C. glabrata* infections are frequently thought to arise from the hosts endogenous microflora in response to illness or a reduction in immune defences (Fidel et al., 1999, Safdar et al., 2002). Despite being phylogenetically distinct, as discussed section in 1.1, both pathogens cause a similar range of painful superficial mucosal infections such as vaginitis in otherwise healthy women, and more severe surface oropharyngeal and esophageal candidiasis in HIV patients. Upon entering the bloodstream more life threatening systemic infections occur especially among vulnerable intensive care patients, particularly those undergoing cancer chemotherapy or immunosuppressive therapy following bone marrow or organ transplantation (Fidel et al., 1999, Sudbery et al., 2004, Kaur et al., 2005). Furthermore, many *Candida* infections involve the formation of biofilms on implanted devices such as prosthetic heart valves and particularly indwelling catheters, and are thus almost certainly agents of nosocomial infection (Fig. 4). Importantly biofilms are less susceptible to anti-fungal agents, primarily by limiting substance penetration through the biofilm matrix. Thus implant infections are notoriously difficult to treat and eradicate without removal of the device (Douglas, 2003, Iraqui et al., 2005, Silva et al., 2011).

Together *Candida* species are currently considered to be the fourth leading cause of nosocomial bloodstream infections in the USA, estimated to account for 8-10% of such infections, and are associated with a crude mortality rate of ~39% (Pfaller and Diekema, 2004, Wisplinghoff et al., 2004, Choi et al., 2009, Horn et al., 2009). In fact in the USA alone it is estimated that *Candida* infections are responsible for ~10,000 deaths a

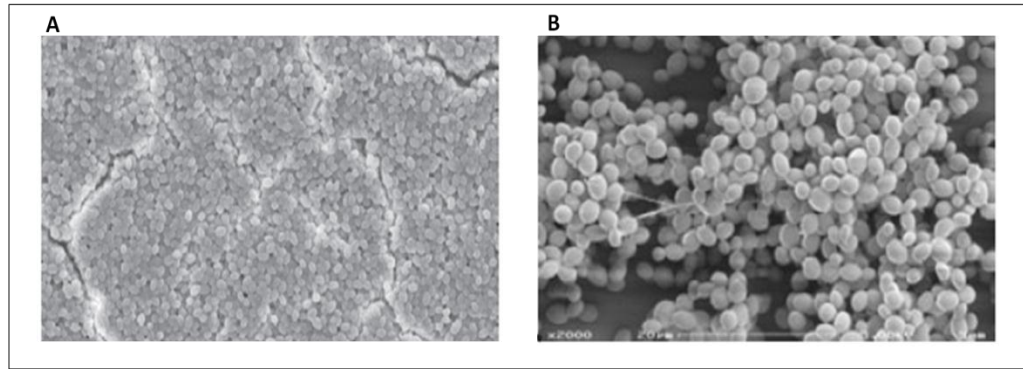


Figure 4 – Both **(A)**, taken from (Silva et al., 2011) and **(B)**, taken from (Iraqi et al., 2005) illustrate *C. glabrata* biofilms.

year with Medicare costs exceeding \$1 billion (Miller et al., 2001, Sudbery et al., 2004). Thus, *Candida* infections clearly constitute a major public health concern. *C. albicans* is known to be the predominant cause of candidemia worldwide, as demonstrated by a study of 6082 bloodstream infection (BSI) isolates of *Candida* spp over a 10 year period (Pfaller and Diekema, 2004). Nevertheless non-*albicans Candida* spp are often isolated from infected individuals (Haynes, 2001). Indeed, recent analysis of isolates from 2019 patients with proven candidemia demonstrated that together the non-*albicans Candida* spp were more frequently isolated than *C. albicans* accounting for 54.4% of infection collectively (Horn et al., 2009). Such non-*albicans Candida* spp include *C. parapsilosis*, *C. tropicalis*, and *C. krusei*. *C. glabrata*, however, has emerged as the most prevalent non-*albicans* yeast pathogen in humans (Pfaller and Diekema, 2004, Wisplinghoff et al., 2004, Horn et al., 2009), being responsible for roughly 26% of *Candida* bloodstream infections in the USA (Horn et al., 2009). In addition the frequency of *C. glabrata* BSI's has been seen to increase from 13% to 24%, from 11% to 13%, and from 14% to 18% in Canada, Europe, and the USA respectively over a 10 year period (Pfaller and Diekema, 2004). *C. glabrata* BSI's also demonstrate a strikingly high crude mortality rate of 50.1% compared with the 36.6% that is observed for *C. albicans* (Wisplinghoff et al., 2004). Inherent resistance to a number of antifungals may contribute to the increased prevalence and higher mortality rates seen for *C. glabrata* (Kaur et al., 2005).

1.3.3 Treatment and Azole Resistance of Candida glabrata Infections

Candidemic patients that remain untreated have been shown to demonstrate significantly higher mortality rates; 61% and 50% in adults and children respectively, versus those undergoing antifungal therapy, leading to the recommendation that all such patients receive antifungal therapy (Pappas et al., 2003). Consequently this has been accompanied by increased demand for existing and novel antifungal agents with the triazoles becoming the primary mode of treating *Candida* infections (Grant and Clissold, 1990, Pfaller and Diekema, 2004). Prior to the discovery of azoles the polyene antifungal amphotericin B (AmpB) was considered the "gold standard" in treatment of systemic *Candida* infections (Wingard, 1994). AmpB is thought to act by creating pores in the yeast cell membrane due to formation of an AmpB-ergosterol complex, this causes leakage of vital cytoplasmic components and ultimately leads to cell death.

It has been suggested however that a poor ability of AmpB to effectively differentiate between yeast ergosterol and mammalian cholesterol may lead to drug toxicity (Ghannoum and Rice, 1999). Renal toxicity has been described as a major drawback of AmpB therapy (Chen et al., 2011). Such toxicity problems have undoubtedly contributed to the triazoles becoming increasingly utilised against fungal infections, although, drug-drug interaction and hepatotoxicity problems have been reported for some of the newer azoles (Chen et al., 2011). Triazoles act by targeting the cytochrome P-450-dependent C14 lanosterol demethylase, encoded by *ERG11*, which is an essential enzyme in the fungal ergosterol biosynthesis pathway. Inhibition of this enzyme is proposed to induce both depletion of plasma membrane ergosterol along with intracellular accumulation of toxic 14 α -methylated intermediates. Ultimately this results in growth arrest but not cell death; azole antifungals are generally considered to be fungistatic rather than fungicidal (Henry et al., 2000, Kaur et al., 2004). Fluconazole has emerged as the most commonly prescribed triazole likely owing to its oral availability, high efficiency, and low toxicity (Grant and Clissold, 1990, Pappas et al., 2003).

During such treatment *C. glabrata* has emerged as being of particular concern due to an innate resistance to azole antifungals (Kaur et al., 2005). In addition azole susceptible *C. glabrata* isolates can generate azole-resistance clones at a surprisingly high frequency upon exposure to fluconazole *in vitro* (Sanglard et al., 2001). Both factors likely contribute to the increased prevalence of *C. glabrata* infections in countries with high fluconazole use (Kaur et al., 2005), and to the relatively high mortality rate observed for this yeast. Indeed the introduction and widespread use of fluconazole has coincided with a significant decrease in the incidence of *C. albicans* BSI's, while *C. glabrata* BSI's notably increased during the same 10 year period (1989-1999) in the USA (Trick et al., 2002). Furthermore $\geq 10\%$ of *C. glabrata* BSI isolates may be highly resistant to fluconazole (Pfaller and Diekema, 2004), and it is often isolated as a replacement species in individuals undergoing fluconazole treatment (Kaur et al., 2004). A number of factors have been implicated in fluconazole resistance including; up-regulation of the multidrug transporters *CDR1* and *CDR2* (Sanglard et al., 2001, Kaur et al., 2005), calcium uptake and signalling (Kaur et al., 2004), up-regulation of the *ERG11* encoded target enzyme (Henry et al., 2000), mitochondrial competence or loss (Sanglard et al.,

2001, Kaur et al., 2004), and the presence of a novel minichromosome (Polakova et al., 2009).

In recent years the echinocandins, including caspofungin, micafungin and anidulafungin, have become a first-line treatment for many cases of mucosal and systemic *Candida* infections. These drugs inhibit 1,3- β -D-glucan synthase and thus prevent synthesis of the essential cell wall component 1,3- β -glucan. Importantly they exhibit potent *in vitro* and *in vivo* fungicidal activity against *Candida* spp including those that demonstrate azole resistance such as *C. glabrata*. Moreover adverse effects and drug-drug interactions appear to be minimal. Anidulafungin may be particularly relevant in the treatment of *C. glabrata* infections as there has been some indication that the minimum inhibitory concentration (MIC) required is especially low (Chen et al., 2011). In addition all three echinocandins have been shown to be effective against *Candida* biofilms (Morace et al., 2009, Chen et al., 2011). Clinical resistance to the echinocandins does appear to be rare, although a number of case reports have identified caspofungin resistance in several *Candida* spp including *C. glabrata*. Resistance has been associated with mutations in *FKS1* and its homologue *FKS2*, which encode subunits of 1,3- β -D-glucan synthase (Kroggh-Madsen et al., 2006, Thompson et al., 2008, Chen et al., 2011).

The relative resistance of *C. glabrata* to antifungals, in particular fluconazole, along with the rising incidence of infection has important implications for therapy. Although the introduction of echinocandins has provided promising results, with resistance rare, resistance has nevertheless been reported in clinical isolates of *C. glabrata*. This, alongside the demonstrated genome plasticity, and subsequent implications for virulence, of this pathogen highlight the need for continuous development of novel antifungals and drug targets.

1.4 The Fungal Cell Wall

The fungal cell wall is an essential and highly dynamic structure that provides shape and physical strength to the fungal cell while allowing enough elasticity to stabilise internal osmotic conditions without rupture of the plasma membrane. In addition, stress-bearing cell wall polysaccharides function as a skeletal scaffold to an external layer of glycoproteins. Collectively such glycoproteins, in particular their N-linked carbohydrate side chains, are important for limiting permeability and therefore protect

the skeletal polysaccharides from hostile degrading enzymes present in the environment. Similarly this protein scaffold may limit the escape of soluble cell wall intermediates and function in the retention of periplasmic proteins (Klis et al., 2006, de Groot et al., 2008). Further to these more general cell wall functions additional functions are conferred via the specific activities of individual cell wall proteins (CWP's). CWP's allow yeast cells to flocculate and adhere either to each other or to a surface. Indeed, being the first point of host-pathogen contact, the cell wall has an important role in numerous host-fungus interactions during the establishment of infection. For instance, cell wall components not only mediate adherence but also, tissue invasion and subsequent proteolytic damage, they provide protection against host defence mechanisms, are involved in biofilm formation, trigger the host immune response, and may also confer resistance to antifungal drugs. In addition they enable recognition of mating partners, offer protection against oxidative stress, facilitate iron acquisition and aid sterol uptake. (Klis et al., 2006, de Groot et al., 2008, Yin et al., 2008, Levitz, 2010).

1.4.1 Cell Wall Structure

Cell wall construction is a tightly controlled process coordinated with the cell cycle and dependent upon environmental conditions (Klis et al., 2006, Lesage and Bussey, 2006). The major components of the fungal cell wall, based on studies in a number of yeasts including *S. cerevisiae*, *C. albicans*, and *C. glabrata*, are the polysaccharides 1,3 β -glucan, 1,6 β -glucan, and chitin and covalently incorporated cell wall glycoproteins (Fig. 5A). All three organisms conform to the same bi-layered architectural model with the various proteins and polysaccharides being localised to the same regions via the same linkages (Fig. 5A and B) (de Groot et al., 2004, Weig et al., 2004, de Groot et al., 2008, Klis et al., 2010). Nevertheless, there are specific differences in the contribution of the individual components (Table. 1) (de Groot et al., 2004, Weig et al., 2004, de Groot et al., 2008). A great deal of metabolic energy is likely invested in cell wall biosynthesis since both *S. cerevisiae* and *C. glabrata* cell walls, typically 100-200nm in thickness, account for roughly 20% of the cells' dry weight (de Groot et al., 2008, Klis et al., 2010). The highly elastic and load bearing inner portion of the cell wall is constructed from a continuous network of 1,3 β -glucan created through the interaction of side chains via hydrogen bonds. The flexible helical structure of 1,3 β -glucan molecules, which can exist at various stages of extension, aids in creating such

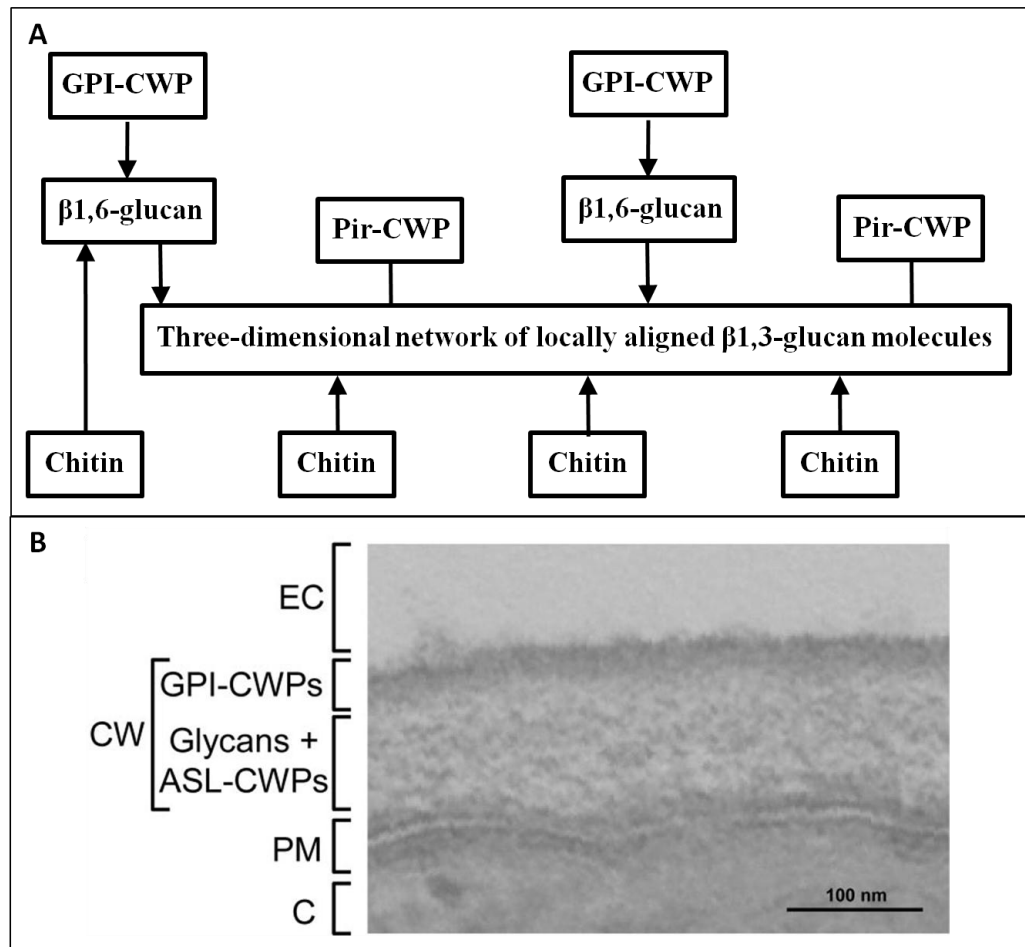


Figure 5 – (A) Schematic representation of cell wall molecular architecture for *S. cerevisiae*, *C. albicans*, and *C. glabrata* (Kapteyn et al., 2000). **(B)** Lateral view of the *C. glabrata* cell wall. CW, cell wall; ASL, alkali sensitive linkage; EC, extracellular environment; PM, plasma membrane; C, cytosol (de Groot et al., 2008).

Species	Protein (%)	Cell Wall Content ^a				Alkali-insoluble glucan (%) ^b	
		Chitin (%)	Man (%)	Glu (%)	M/G	1,6-β	1,3-β
<i>C. glabrata</i>	6.4±0.1	1.2±0.1	43.8±0.5	54.0±0.2	0.81	4.2±0.1	16.7±1.7
<i>S. cerevisiae</i>	4.0±0.1	1.4±0.2	34.2±1.6	60.3±2.5	0.57	7.1±0.2	26.8±0.9
<i>C. albicans</i>	3.5±0.2	4.2±0.1	26.6±2.3	64.0±4.9	0.42	10.6±0.6	26.2±1.1

^a Values are from exponentially growing cells (in YEPD), are the means and standard deviations for two independent samples measured in duplicate, and are expressed as percentages of freeze-dried cell walls. Man, mannose; Glu, glucose; M/G, ratio of mannose to glucose.
^b Enzymatically released with 1,6-β-glucanase or 1,3-β-glucanase.

Table 1 – Cell wall composition of *C. glabrata* in comparison to *S. cerevisiae* and *C. albicans* (de Groot et al., 2008)

elasticity. As alluded to earlier, this allows the inner network to become considerably extended and aids in the prevention of cell rupture when surrounded by hypotonic conditions. Equally it enables the cell, which can lose up to 60% of its volume when placed in hypertonic solutions, to shrink reversibly (Klis et al., 2006).

The non-reducing ends of 1,3 β -glucan molecules can act as sites for the covalent attachment of additional polysaccharides (Fig. 5A). Internal to the 1,3 β -glucan layer these covalent interactions result in attachment of chitin chains and extension of the inner wall. By contrast the 1,3 β -glucan layer is extended towards the cells external face by chains of highly branched 1,6 β -glucan. These branched chains are often covalently attached to GPI-anchored cell wall mannoproteins, chitin can also become attached to 1,6 β -glucan. Additionally a smaller group of cell wall proteins containing internal repeats, the Pir protein family, can be directly linked to the 1,3 β -glucan network via an alkali sensitive linkage (ASL) and are distributed throughout the cell wall (de Groot et al., 2004, Weig et al., 2004, Klis et al., 2006, de Groot et al., 2008).

There has been suggestion that the consensus sequence (DGQJQ) within such Pir internal repeats is involved in direct attachment to 1,3 β -glucan. Consequently it is thought conceivable that Pir-CWP's may act to interconnect several 1,3 β -glucan molecules thus adding considerable strength to the wall (Klis et al., 2006). Consistent with this a strong up-regulation of *PIR* genes upon cell wall stress is observed. It was thought this may also go some way to explaining the apparent essentiality of the only protein to contain Pir repeats in *C. albicans*, Pir1 (Klis et al., 2010), however, this protein has now been successfully deleted (Noble et al., 2010). Proteins can also become attached to the wall in a reducing agent sensitive manner, often via disulphide bridges to other proteins (de Groot et al., 2004, Klis et al., 2006, Ruiz-Herrera et al., 2006), or via non-covalent ionic bonds due to the many negative charges present at the cell wall (Yin et al., 2008).

Estimations based upon exponentially growing *S. cerevisiae* cells in rich medium suggest that the number of covalently linked proteins per cell is ~ 3.1 million with a protein density of 52000 molecules/ μm^2 (Klis et al., 2010). Interestingly this number is likely increased in *C. glabrata* which has been identified as having 50% higher mannoprotein content than either *S. cerevisiae* or *C. albicans*. This is accompanied, as expected, by a higher cell wall mannan component, as such the relative level of glucan is decreased

and the mannose: glucose ratio is seen to increase. Furthermore lower levels of alkali-insoluble glucans, relative to both total wall mass and total glucan, compared to *S. cerevisiae* and *C. albicans* suggests that fewer cross-links between glucan and chitin exist in the cell wall of this pathogen (Table. 1). There is some suggestion that a mannoprotein dense outer layer may aid in masking β -glucans, known to be potent proinflammatory molecules, from host immune recognition more effectively than is observed for *C. albicans*. This may increase the propensity of the pathogen to cause disease (Wheeler and Fink, 2006, de Groot et al., 2008).

As an essential structure, constructed of components largely absent from mammalian cells, fungal cell walls provide an excellent reservoir for the detection of potential drug targets and the development of novel antifungals. The identification of fungal constituents to serve as new drug targets may in future go some way to aid the emerging problem of antifungal resistance in *C. glabrata* clinical isolates.

1.4.2 GPI-Anchored Cell Wall Proteins

Covalently linked CWPs have been identified in numerous fungi and the cell walls of *S. cerevisiae*, *C. albicans* and *C. glabrata* can contain > 20 different types of these CWPs of differing functions at any time. As discussed earlier, the cell wall mannoproteins can be divided into two groups the largest of which comprises proteins that are modified by addition of a GPI anchor and can be specifically released from the cell wall by treatment with HF-pyridine (de Groot et al., 2008, Klis et al., 2010). *S. cerevisiae*, *C. albicans*, and *C. glabrata* have been found to contain 66, 115, and 106 putative GPI proteins respectively (De Groot et al., 2003, Richard and Plaine, 2007, de Groot et al., 2008, Klis et al., 2009). GPI-anchored cell wall proteins undergo a maturation process involving a number of post-translational modifications during which the proteins become fully glycosylated (Klis et al., 2010). Such GPI modifications can be identified in roughly ~0.5% of all eukaryotic proteins (Eisenhaber et al., 2001). Proteins destined for GPI-anchor addition share a number of conserved features including an N-terminal hydrophobic signal sequence, which targets the nascent polypeptide to the endoplasmic reticulum (ER), and a C-terminal GPI anchor addition signal sequence which is replaced by a GPI anchor during the maturation process (Fig. 6). The two signal peptides are separated by a functional domain and a ser/thr rich spacer domain (De Groot et al., 2005, Klis et al., 2006, Klis et al., 2009).

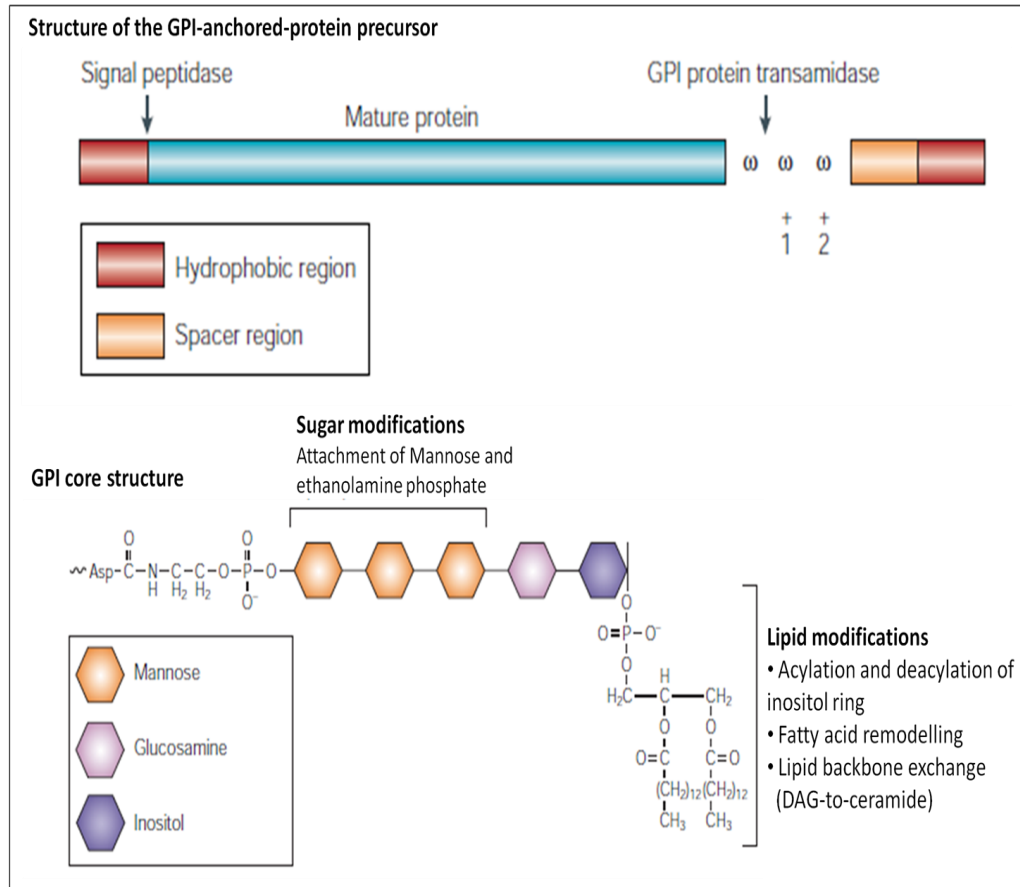


Figure 6 – Structure of the GPI-anchored protein precursor demonstrating the hydrophobic cleavable signal sequences and the enzymes involved, the GPI addition site and spacer sequence. The GPI-anchor core structure is also shown illustrating the components and sites at which further modification can occur, DAG-diacylglycerol (Mayor and Riezman, 2004).

Following targeting to the ER, the entry point to the secretory pathway for newly synthesised proteins, the N-terminal signal peptide is removed by a signal peptidase complex. Similarly, via the action of a GPI transamidase, the C-terminal signal sequence is recognised and cleaved before attachment of a preassembled GPI anchor at the C-terminal GPI-anchor attachment site (ω -site) (Ikezawa, 2002, Mayor and Riezman, 2004, Pittet and Conzelmann, 2007, Klis et al., 2009). Amino acid residues N-terminal to the ω -site are termed ω -minus whilst those C-terminal to the attachment site are designated ω -plus. Studies into this region have been predominately undertaken using *S. cerevisiae* and the GPI-anchor signal sequence is known to have a number of general features. These begin with a stretch of ~ 10 polar amino acids ($\omega-10$ to $\omega-1$) which forms a flexible linker region. The GPI attachment site itself is the first of three contiguous amino acids that precede a moderately polar spacer sequence ($\omega+3$ -to- $\omega+9$), which is finally followed by a hydrophobic sequence of variable length up to the C-terminal end (Fig. 6) (Mayor and Riezman, 2004, Orlean and Menon, 2007, Pittet and Conzelmann, 2007). The anchored protein is rapidly attached to the ER membrane where it exists as a tail-anchored membrane glycoprotein (de Groot et al., 2008, Klis et al., 2010).

The structure of the GPI anchor is common amongst all species and consists of ethanolamine phosphate, through which an amide bond is created with the newly generated carboxyl group at the ω -site following protein cleavage, a trimannosyl core, glucosamine and phosphatidylinositol (Fig. 6). An acyl-chain present on the inositol ring is thought to be required for efficient biosynthesis and attachment of the anchor. Yeast also contains an essential fourth mannose (Man) residue attached to the core trimannoside via Man-3. This fourth mannose is necessary for the addition of the Man-3 ethanolamine phosphate which subsequently becomes protein linked. Man-1 and Man-2 initially contain ethanolamine side chains, however, it is unclear if these side chains are retained by fully mature GPI-anchored proteins at the cell surface (Orlean and Menon, 2007, Pittet and Conzelmann, 2007, Fujita and Kinoshita, 2010). Indeed following addition to the protein the GPI anchor is subject to various modifications within the ER and Golgi during transport to its final destination. Such modifications include inositol deacylation and remodelling of the glycan and lipid components (Fujita and Kinoshita, 2010). Interestingly, in *S. cerevisiae*, newly synthesised GPI-anchored proteins are separated from other secretory transmembrane proteins upon exit from the ER, this is in stark

contrast to the lack of segregation observed for mammalian GPI-anchored proteins. The proteins are then transported to the Golgi in coat protein complex II (COPII) coated vesicles and continue their maturation process (Muniz et al., 2001, Castillon et al., 2009, Rivier et al., 2010).

Fungal GPI proteins follow the secretory pathway until they reach the plasma membrane where some are retained and termed GPI plasma membrane proteins (PMPs) whilst others continue on and are incorporated into the cell wall (GPI-CWPs). Nevertheless other mature GPI proteins have been identified in substantial amounts at both locations and it seem likely that this is the case for both *S. cerevisiae* and *C. albicans* (Mao et al., 2008, Klis et al., 2009). The sequences immediately before the ω -site are known to be important for determining the final destination of such fungal GPI proteins. Particularly a dibasic motif at ω -1 and ω -2 has been implicated in directing a greater proportion of protein to the membrane. CWPs lack this dibasic motif and rather hydrophobic residues at ω -4 and ω -5 are more influential in directing a greater amount of protein to the cell wall. Furthermore all wall-directed proteins contain a substantial hydrophobic region of four to eight residues N-terminal to the ω -site. By contrast proteins destined for the membrane demonstrate a hydrophobic residue exclusion zone within \sim 20 residues of the ω -site. Additionally the characteristic ser/thr rich domains of the proteins are thought to favour cell wall targeting to such an extent that the membrane retaining effect of the dibasic motif may be overridden (Frieman and Cormack, 2004, Dranginis et al., 2007, Mao et al., 2008). Cell wall attachment in ascomycetous yeast is known to require processing of the GPI-anchor, (De Groot et al., 2005). Arriving at the plasma membrane the lipid moiety of the GPI anchor is removed and the proteins become tail anchored to 1,6 β -glucan in the cell wall via a trimmed GPI structure (GPI_t). Consequently the N-terminal region extends out into the external environment (Klis et al., 2010).

1.4.2.1 GPI-Anchored Adhesins

The cell walls of human pathogens act as the first point of contact with the human host and thus govern the initial host-pathogen interactions that underlie the establishment of fungal infections. Adhesion is one of the first such interactions to occur and is an important initial step in the infection process. Thus the proteins often referred to collectively as adhesins, that mediate these interactions are of interest as virulence factors. *Candida* adhesins tend to be grouped into large gene families which include the eight-member *ALS* (agglutinin-like sequence) gene family

in *C. albicans*, (Zhao et al., 2004, Hoyer et al., 2008), and the EPA (epithelial adhesin) family in *C. glabrata* of which there are at least 17 members in the sequenced CBS138 strain (Kaur et al., 2005). When expressed heterologously in *S. cerevisiae*, members of both adhesin families enable this normally non-adherent organism to adhere to mammalian cells (Cormack et al., 1999, Frieman et al., 2002, Sheppard et al., 2004). *S. cerevisiae* itself encodes the FLO (flocculin) family of adhesins which confer adherence to agar, plastics and other yeast cells (Halme et al., 2004). *C. glabrata* has been reported to contain 106 putative GPI proteins, around 50% of which have adhesin like properties and can thus be potentially implicated in fungal-host interactions or biofilm formation during the development of infection (Weig et al., 2004). Further investigation, using a direct cell wall "shaving" method and tandem mass spectrometry, however, identified just 23 proteins to be covalently incorporated into the cell wall (de Groot et al., 2008). Adhesin structure and maturation conforms to that observed for other GPI-anchored proteins (1.4.2), with the N-terminal functional domain being involved in ligand binding and projected from the wall surface by the ser/thr rich region (Frieman et al., 2002, Dranginis et al., 2007). Analysis of the glycan specificity of the *C. glabrata* EPA adhesin family members; Epa1, Epa6, and Epa7, revealed that all three bind to glycans containing a terminal galactose residue. Glycan specificity, however, does vary with Epa6 having a broader substrate range than either Epa1 or Epa7. Interestingly, other pathogenic organisms are known to bind to the same galactosides as have been identified for the Epa proteins (Zupancic et al., 2008). The difference in Epa specificity has been attributed to a 5-amino acid hypervariable region within a surface loop of the PA14 (anthrax toxin protective antigen) domain in the N-terminus (Zupancic et al., 2008). An additional hypervariable region within the PA14 domain corresponds to an adjacent surface loop and has also been implicated in ligand binding (Fig. 7) (Zupancic et al., 2008). The PA14 domain has previously been suggested to contribute to carbohydrate binding (Rigden et al., 2004) and can also be identified in all additional currently known members of the *C. glabrata* Epa family and within the Flo family of *S. cerevisiae*. The Als adhesins of *C. albicans* do not display the lectin-like properties of the Epa and Flo families, and instead are known to bind peptides. Consistent with this, the PA14 domain has not been identified in these proteins (Dranginis et al., 2007, de Groot and Klis, 2008).

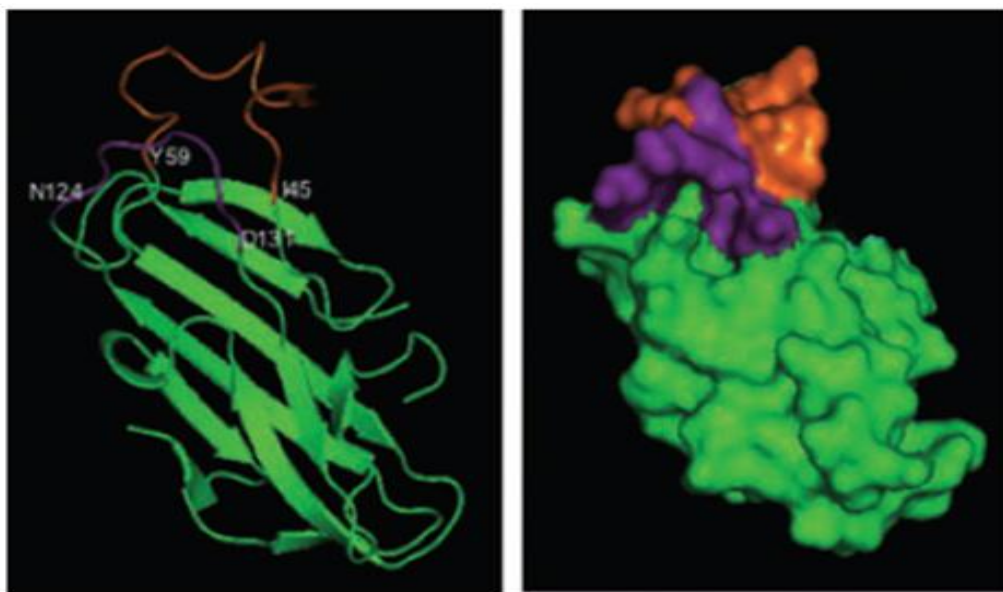


Figure 7 – Cartoon and space filling model of the PA14 domain taken from (Zupancic et al., 2008). The 5 amino acid hypervariable region that determines sugar specificity is shown in purple while the additional hypervariable region also implicated in ligand binding is highlighted in orange.

Given the important role of adhesins in host-pathogen interactions and in the establishment of infection, further investigation into such molecules may be important to advance understanding of host colonization by pathogenic yeasts. Furthermore the pathways responsible for their expression, biosynthesis, and cell wall assembly may provide a potential reservoir of new drug targets. Interestingly members of both the *C. glabrata* EPA and *S. cerevisiae* FLO adhesin families are predominantly located in subtelomeric regions. Consequently these adhesin families are known to be subjects of transcriptional silencing (De Las Penas et al., 2003, Halme et al., 2004, Castano et al., 2005, Rosas-Hernandez et al., 2008). Moreover, transcriptional silencing appears to have an important role in controlling gene expression variation between individual cells (Halme et al., 2004, Verstrepen and Fink, 2009), and may thus be of importance during the investigation into EPA heterogeneity during this study.

1.5 Sir-Dependent Transcriptional Silencing in Yeasts

One of the best studied examples of transcriptional silencing can be found in *S. cerevisiae* where silencing occurs at telomeres, the silent mating type loci and within the ribosomal DNA (rDNA) repeats (Rusche et al., 2003). As such, and owing to the close relationship between *S. cerevisiae* and *C. glabrata*, information obtained from this well researched budding yeast will provide the basis of this section. Despite different mechanisms, the behaviour of silent chromatin and the pathways that assemble it appear to be strikingly similar in the fission yeast *S. pombe* and involve orchestrated changes in chromatin modifications (Rusche et al., 2003, Buhler and Gasser, 2009). Transcriptional silencing involves the establishment of a specialised chromatin structure, similar to the heterochromatin of higher organisms, which is less accessible to restriction enzymes and DNA methylases, and exhibits repressed gene expression within the silenced domain. A major factor underlying the regulation of such silencing is histone modification which includes processes such as acetylation, methylation and monoubiquitination. Acetylation is probably the best understood of these modifications, however the role of methylation is also becoming more prominent. Indeed active regions of chromatin are associated with both acetylation and methylation whereas deacetylated and demethylated histones are associated with silenced regions (Rusche et al., 2003, Shilatifard, 2006, Shahbazian and Grunstein,

2007, Yang et al., 2008, Verzijlbergen et al., 2009, Takahashi et al., 2011). Silent information regulator (Sir) proteins are important regulators of this silencing, with chromatin immunoprecipitation studies revealing them to be spread inward from telomeres and distributed throughout the *HMR* and *HML* loci to form a distinct chromatin structure (Rusche et al., 2003). The Sir2 protein of *S. cerevisiae* was the first discovered member of the class III histone deacetylases (HDACs), also referred to as sirtuins. The class III HDAC's are found in organisms ranging from bacteria to humans and are orthologs of the yeast transcriptional repressor Sir2 (North and Verdin, 2004, Tong and Denu, 2010, McGuinness et al., 2011). By contrast class I and II HDACs are orthologs of the yeast deacetylases Rpd3 and Hda1 respectively and demonstrate no sequence similarity to the class III HDACs. They do however share significant similarity to each other in their catalytic cores (de Ruijter et al., 2003, Verdin et al., 2003).

Sir2 catalyses NAD⁺-dependent deacetylation of histone tail lysines, and is essential, but not sufficient, for transcriptional silencing at all sites in yeast with deacetylation of histone H4 Lys-16 appearing to be of particular importance. Although Sir2 is required at all silenced regions different multiprotein complexes are utilised at these different genomic sites. Silencing at both telomeres and the mating type loci is regulated by the Sir complex which consists of Sir2, Sir3 and Sir4, whereas Sir2-dependent silencing at rDNA is mediated by the regulator of nucleolar silencing and telophase exit (RENT) complex, containing Sir2, Net1, and the telophase-regulating phosphatase Cdc14 (Rusche et al., 2003, North and Verdin, 2004, Shahbazian and Grunstein, 2007, Tong and Denu, 2010). The enzymatic activity initially associated with sirtuins was ADP-ribosyltransferase requiring NAD⁺, and indeed some sirtuins may mediate such a process, however histone deacetylation was later revealed as the primary activity. This efficient histone deacetylation reaction is coupled to formation of the novel acetyl-ADP ribose product *O*-acetyl-ADP ribose (OAADPr). During the reaction one molecule NAD⁺ and acetyl-lysine are readily converted to one molecule of deacetylated lysine, nicotinamide, and OAADPr in particular the 2'-*O*-acetyl-ADP ribose isomer. Ultimately this occurs by transfer of the removed acetyl group to the ADP-ribose moiety of NAD⁺ (Fig. 8) (Smith et al., 2008, Tong and Denu, 2010). Deacetylation of histone H4 Lys-16 via the action of Sir2 as mentioned earlier is of particular importance in gene silencing, however Hos2 mediated deacetylation of this same residue actually has a role in gene activation. It

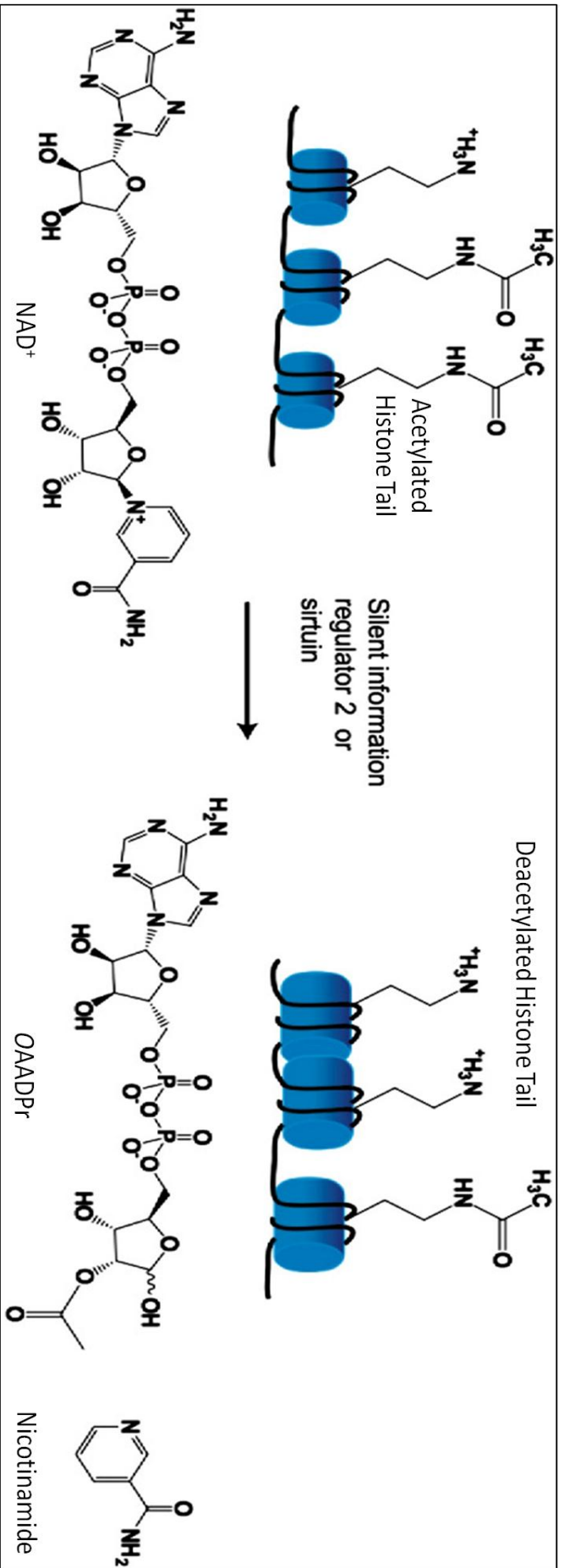


Figure 8 – NAD⁺-dependent histone deacetylation catalysed by the activity of Sir2. The reaction leads to deacetylation of the histone tail along with formation of nicotinamide and the novel metabolite OAADPr. Taken from (Tong and Denu, 2010).

is thought such differing roles for the same modification may be due to the context of histone acetylation of surrounding residues. Deacetylation of H4 Lys-16 with acetylation at other sites is important for activation, while in the context of other unacetylated residues, as found at heterochromatin, the modification is important for the establishment of transcriptional silencing (Rusche et al., 2003, Shahbazian and Grunstein, 2007, Buhler and Gasser, 2009). It is interesting to note that the class I and II deacetylases have lost this energetically expensive mechanism and do not require NAD⁺ as a cofactor. Accumulating evidence implicating OAADPr in numerous downstream cellular functions, including the ability to synergize or antagonize sirtuin biological activity may go some way to explain retention of the process (Tong and Denu, 2010).

1.5.1 Telomeric Silencing

Telomeres were first identified by the observation that x-ray induced chromosomal rearrangements never included loss of the terminal chromosome regions. This was in contrast to the terminal region loss seen at chromosomal breaks. Consequently telomeres were identified as non-nucleosomal structures that function as 'caps' protecting the ends of chromosomes from DNA repair and degradation. More recently, however, a number of additional properties of the chromosome ends have been identified including roles in aging and senescence, transcriptional silencing and chromatin structure, segregation, cell cycle control, chromosome movement, and nuclear architecture (Pryde and Louis, 1997, Louis and Vershinin, 2005).

Telomeric DNA sequences are strongly conserved between a number of divergent species and generally exhibit a single stranded G-rich 3' overhang and double stranded telomeric repeats transitioning into the sub-telomere (Louis and Vershinin, 2005, Buhler and Gasser, 2009). The telomere sequences of *S. cerevisiae* consist of a variable repeat of TG₁₋₃ that can extend to ~300bp in length (Buhler and Gasser, 2009). The size of such repeat regions exhibit remarkable variation between species, ranging from 20bp in the ciliate *Oxytricha* to ~150kb per telomere in laboratory mouse strains, tobacco and wheat (Louis and Vershinin, 2005). The telomeric repeats of *C. glabrata* are suggested to range from 400-700bp (Kachouri-Lafond et al., 2009). Specific synthesis of these telomeric repeats and thus maintenance of the telomere is ensured by the enzyme telomerase, with telomerase deficient mutants demonstrating a progressive

telomere shortening in the so called “ever shorter telomere” phenotype (Pryde and Louis, 1997, Kachouri-Lafond et al., 2009).

Moving away from the chromosome ends, subtelomeric regions follow on from the telomeres and in *S. cerevisiae* are composed of a number of subtelomeric elements that can vary between ends and strains. At many ends this includes the highly conserved Y' element, of which there can be up to four copies. All ends have core X element, most of which contain a core-X repeat, and can range in size from 300bp to 3kb. The core-X is centromere-proximal to the Y' element and the two regions are separated by smaller sequences termed subtelomeric repeats (STR's) (Pryde and Louis, 1999, Louis and Vershinin, 2005, Zhu and Gustafsson, 2009). In contrast to the telomeres themselves, subtelomeres are known to encode several gene families including the *S. cerevisiae* *FLO* family of adhesins (Halme et al., 2004), and the *EPA* family of adhesins in *C. glabrata*, which constitute the major focus of this study. Consequently both adhesins families are subject to telomeric silencing (De Las Penas et al., 2003, Halme et al., 2004, Castano et al., 2005, Rosas-Hernandez et al., 2008).

1.5.1.1 Assembly and Propagation of the Telomeric Sir Complex

In *S. cerevisiae*, assembly of the Sir complex at telomeric regions begins by an initial interaction of Rap1, a sequence-specific DNA binding protein also involved in the regulation of telomere length, with telomeric repeats (Conrad et al., 1990, Pryde and Louis, 1997, Castano et al., 2005, Buhler and Gasser, 2009). Rap1 binding sites exist roughly every 20bp in the telomeric repeat sequences (Pryde and Louis, 1997). The observation that Sir4 is able to bind Rap1 independently of other silencing factors at regions close to the telomeres of *S. cerevisiae*, while all silencing factors are required for the same interaction at telomere distal regions (0.5kb and beyond) (Luo et al., 2002) led to the following model for Sir complex assembly and propagation. After binding to the telomeric repeats Rap1 recruits Sir4 to the telomere, an interaction that initiates further sequential recruitment of additional Sir proteins. Sir2 associates via interaction with both Sir4 and histone H4 at the nucleosome adjacent to the Rap1 binding sites. Sir2-mediated deacetylation, particularly at histone H4 Lys-16, then enables Sir3 and Sir4 binding to histone tails (Fig. 9) (Luo et al., 2002, Liou et al., 2005, Talbert and Henikoff, 2006). The yKu70/yKu80 hetero-

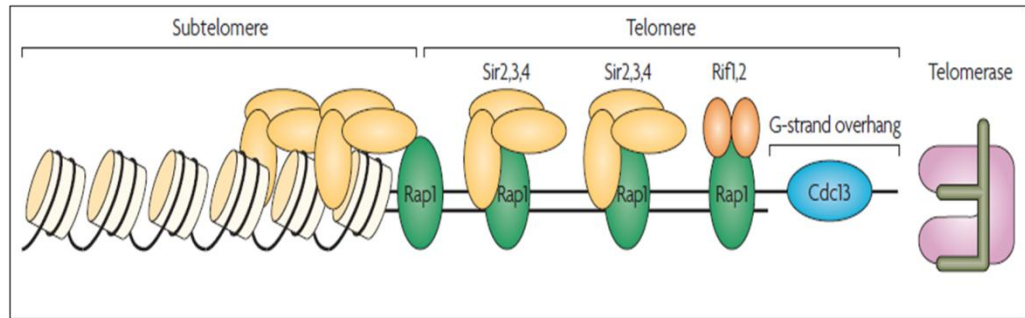


Figure 9 - Representation of Sir complex assembly at the telomeres of budding yeast. Taken from (Blasco, 2007). Rap1 binds to double stranded telomeric repeats and subsequently recruits Sir2, Sir3, and Sir4 in addition to the Rif proteins which compete with the Sir complex for binding. Subsequent histone deacetylation enables further recruitment and spreading of the Sir complex into subtelomeric regions. The G-strand overhang is bound by Cdc13.

dimer is also required for silencing and predominantly associates with telomeres via direct DNA end binding. The heterodimer promotes recruitment of Sir4 to the subtelomere possibly by counteracting the action of Rif1, a Rap1 binding protein that inhibits Rap1-Sir4 association (Mishra and Shore, 1999, Lopez et al., 2011). Interestingly Sir4 appears important in the recruitment of yKu70/yKu80 to the subtelomere likely due to the interaction between yKu80 and Sir4 (Lopez et al., 2011). Spreading of silent chromatin then occurs as Sir3 recruits additional Sir4, which in turn binds Sir2 and allows further deacetylation and binding of more Sir3 and Sir4 to histone tails (Luo et al., 2002, Liou et al., 2005, Talbert and Henikoff, 2006).

More recent studies have increasingly identified methylation as having an important role in the maintenance of silent chromatin with levels of this modification being reduced in silent regions. In particular Dot1 dependent methylation at histone H3 Lys79 and Set1 dependent methylation of H3 Lys4 have been proposed to act as boundary elements, efficiently targeting silencing components to unmethylated heterochromatin. Loss of methylation at these residues does indeed lead to redistribution of Sir proteins across the genome and silencing defects. Histone acetylation appears to have a similar role and such observations demonstrate the ability of histone modifiers to make positive and negative contributions to heterochromatin formation (Verzijlbergen et al., 2009, Norris and Boeke, 2010, Takahashi et al., 2011). Consequently heterochromatin formation and spreading is proposed to be determined by competition between binding of the Sir complex and the action of histone modifying enzymes. For instance Sir3 and Dot1 are thought to compete for the methylation state of H3 Lys-79 while Sir2 competes with the acetyltransferase Sas2 for the acetylation state of histone H4 Lys-16 (Verzijlbergen et al., 2009, Norris and Boeke, 2010).

Transcriptional silencing can be propagated to distances of 4- to 8-kb within the subtelomeric regions of *S. cerevisiae*. By contrast, 20- to 25-kb of the subtelomeric region within *C. glabrata* can be subject to this so called telomere position effect (TPE) gene silencing (Rosas-Hernandez et al., 2008). In each instance, however, the strength of silencing has generally been demonstrated to decrease with increased distance from the telomere (Renauld et al., 1993, De Las Penas et al., 2003, Castano et al., 2005, Rosas-Hernandez et al., 2008). Promoter weakening, the presence of a 6.7kb subtelomeric Y' element and overexpression of Sir3 extend the

distance across which silencing can occur (Renauld et al., 1993), the latter being associated with increased propagation of Sir3 from the telomeric regions into adjacent chromatin. Interestingly, the detection of both Sir2 and Sir4 is decreased at such regions suggesting that Sir3 can function independently (Renauld et al., 1993, Hecht et al., 1996, Strahl-Bolsinger et al., 1997). Indeed incubation of purified full length Sir3 with naked DNA, nucleosome core particles, or defined nucleosomal arrays created condensed chromatin fibers (McBryant et al., 2008).

Initial ideas of repression spreading continuously from the telomere and ever diminishing in strength (Renauld et al., 1993) may be rather too simplistic, particularly with the observation that silencing at the native ends of *S. cerevisiae* chromosomes is actually discontinuous and can vary significantly in intensity between ends (Pryde and Louis, 1999, Zhu and Gustafsson, 2009). Y' elements are highly enriched in nucleosomes and resistant to silencing along the majority of their length. Consistent with active chromatin they lack the classical hallmarks of heterochromatin such as low H4 Lys-16 acetylation, and high Sir3 and Rap1 occupancy. Maximal repression is actually observed within the centromere-proximal subtelomeric core X element which is devoid of nucleosomes and bound by Rap1 and Sir3 (Zhu and Gustafsson, 2009). Repression peaks at a site adjacent to the ARS consensus sequence within core X, before decreasing precipitously towards the centromere (Fig. 10). Such X element repression requires proximity to the telomere and remains dependent upon the Sir and Ku proteins (Pryde and Louis, 1999, Louis and Vershinin, 2005, Zhu and Gustafsson, 2009). Resistance of the Y' element to silencing is suggested to be due to looping out of the Y' element following interaction between the terminus and the core X element, possibly due to the interaction of Rap1 and Sir proteins at the TG₁₋₃ repeats with the Rap1/Sir protein structure at core X (Fig. 10) (Pryde and Louis, 1999, Zhu and Gustafsson, 2009). Alternatively the presence of subtelomeric anti-silencing regions (STARs) and relay elements within X and Y' elements may discontinuously impede and re-establish silencing respectively (Fourel et al., 1999, Louis and Vershinin, 2005). Either way these observations illustrate that repressive chromatin can assemble centromere-proximal to a region that is expressed and indicate that transcriptional silencing does not depend on exact distance to the chromosome end. The precise locations of X and Y' elements are important in determining chromosome specific sub-

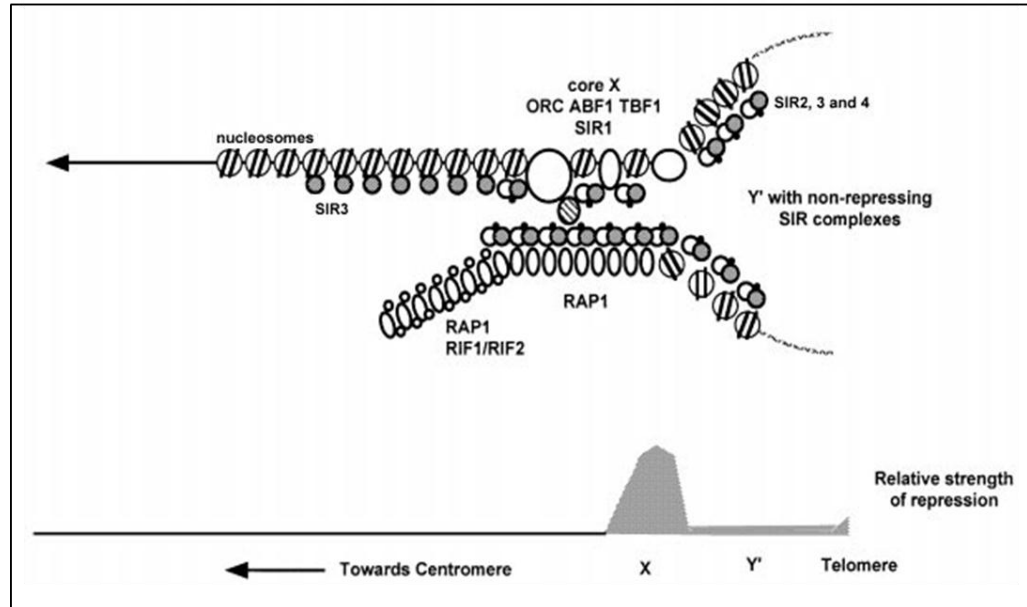


Figure 10 – The looping model of discontinuous telomeric silencing during which the Y' element is protected from silencing with maximal repression occurring within the core X element. Taken from (Pryde and Louis, 1999), the core X element has subsequently been found to be histone deficient.

telomere organisation and indeed silencing at individual chromosome ends (Zhu and Gustafsson, 2009).

The influence of subtelomeric Y' elements on transcriptional silencing is not likely a factor that requires consideration within the *C. glabrata* portion of this study as the pathogenic yeast lacks conserved Y' elements within subtelomeres (Kachouri-Lafond et al., 2009). Even so, silencing in *C. glabrata* is not thought to purely be a product of distance from the telomere. Furthermore, the telomeres of this pathogen are not equivalent, with silencing requirements differing between ends. Position dependent silencer elements have been implicated in this. Variation in TPE between different telomeres is an observation mirrored in *S. cerevisiae* (Rosas-Hernandez et al., 2008). Additional factors, such as the negative regulators of sirtuin activity recently identified in *S. cerevisiae*, may also contribute to differences in telomeric silencing observed between different ends (Raisner and Madhani, 2008).

Ultimately, telomeric silencing appears to be an extremely complex process with various possible modes of regulation. Further understanding of the process will be of particular use in the study of subtelomeric gene families, many of which encode pathogenic virulence factors and have important implications for host infection.

1.6 DNA Damage Tolerance in Yeast

Genetic material contained within cells is constantly subjected to various exogenous and endogenous agents that can lead to a wide variety of different types of DNA damage and/or lesions. The consequences of such damage are, as a result, also extremely diverse and include; obstruction of DNA replication, irreversible mutations contributing to oncogenesis, blockage of transcription and cell death. In reaction to the broad spectrum of DNA damage that can occur cells have developed a number of repair mechanisms. Although no single repair system can cope with all types of DNA damage, together they counter most types of oxidative and spontaneous DNA damage (Hoeijmakers, 2001, Ulrich, 2005), and have overlapping roles (Doetsch et al., 2001). Most repair mechanisms rely on the excision of damaged DNA regions followed by subsequent resynthesis based on information encoded by the complementary strand. A requirement for the complementary strand renders these excision repair systems unable to act on regions of damaged single stranded DNA as these arise during genome replication.

(Hoeijmakers, 2001, Salmon et al., 2004, Ulrich, 2005). Replication of cellular DNA is often blocked by such damage causing replication forks to stall, thus risking their collapse. The resulting cell cycle arrest would eventually lead to cell death. Consequently DNA damage tolerance, which enables bypass of such DNA lesions without actually removing the damage, has evolved to enable completion of replication under such circumstances (Fig. 11). These processes play an integral role in cell survival following exposure to genotoxic agents (Ulrich, 2005, Branzei and Foiani, 2007, Andersen et al., 2008). Two pathways of DNA damage tolerance exist and have been termed the error free pathway and the error prone or translesion synthesis pathway (TLS) (Fig. 11). Both pathways are induced by DNA damage or replication stress and, although they perform damage tolerance through two different mechanisms, they both require the ubiquitin conjugating enzyme (E2) Rad6 and its binding partner, the ubiquitin ligase (E3) Rad18, the former of which will be discussed further in chapter 3. The DNA polymerase processivity clamp, proliferating cell nuclear antigen (PCNA), acts as the ubiquitination target for both damage tolerance pathways (Ulrich, 2005, Ulrich, 2009).

1.6.1 Translesion Synthesis

As alluded to above, TLS is a major damage tolerance pathway allowing DNA replication to continue at damaged templates via bypass of DNA damage lesions (Fig. 11). As a result TLS provides resistance to DNA-damaging agents, and the ability to restart stalled replication forks or to fill ssDNA gaps containing lesions following DNA damage (Waters et al., 2009). The classical replicative polymerases, consisting of Pol1(α), Pol2(ϵ), and Pol3(δ) in yeast, are highly accurate and specific to an unperturbed template and primer terminus. Advancing replication is generally stalled at DNA lesions due to an inability of these high fidelity replicative polymerases to accommodate modified nucleotides into their active sites (Hubscher et al., 2002, Andersen et al., 2008, Waters et al., 2009). However, a class of alternative polymerases, termed the TLS polymerases, exist that are able to insert nucleotides opposite a variety of abnormal structures and are utilised during this method of DNA damage tolerance. In eukaryotes TLS is generally thought to occur by the action of two such polymerases, typically one of the Y family polymerases, consisting of Rev1 and Poln in *S. cerevisiae*, and Pol ζ a B family polymerase also present in *S. cerevisiae* and

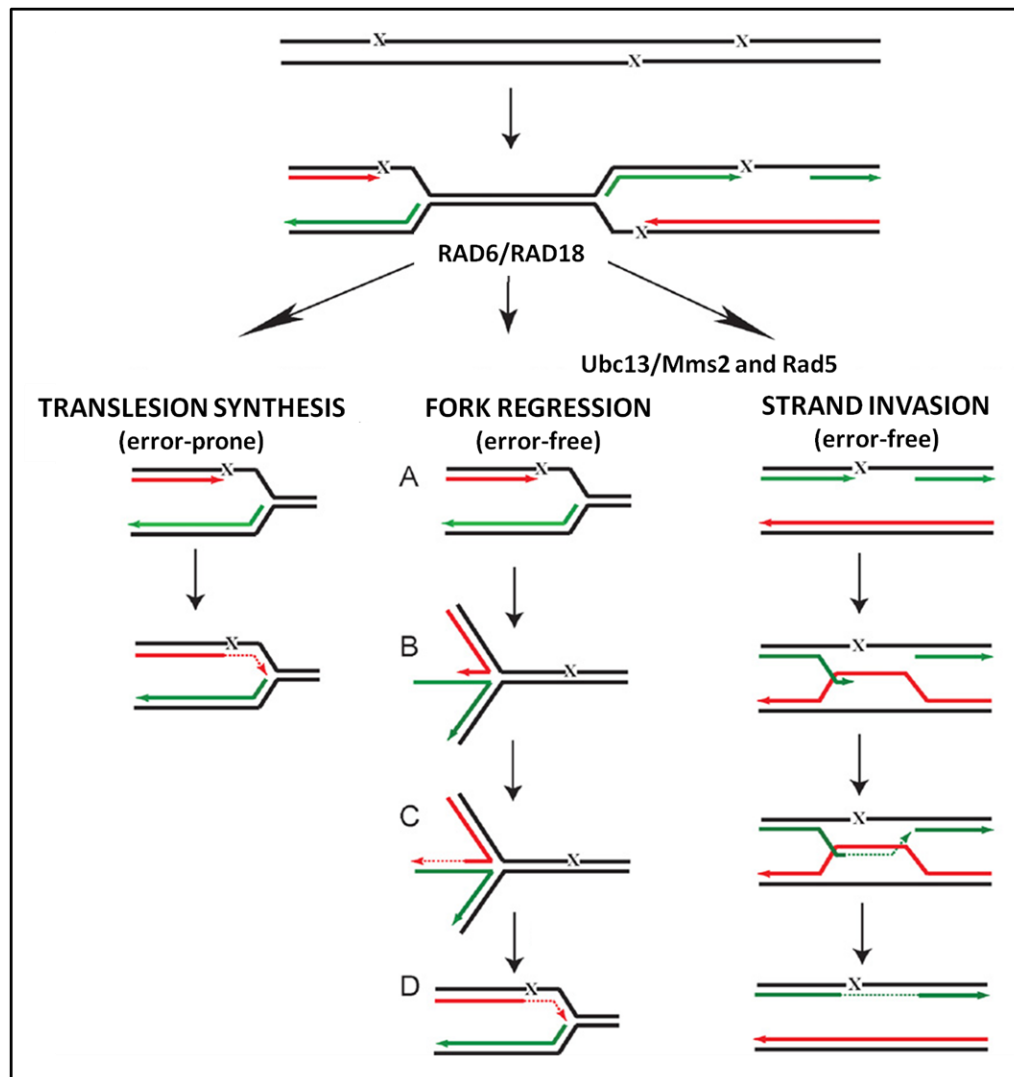


Figure 11 – Mechanisms of DNA damage tolerance. Translesion synthesis (TLS) utilises specialised damage tolerant polymerases to by-pass DNA lesions. Error free damage tolerance is proposed to occur by two mechanisms, replication fork regression or strand invasion. Upon encountering DNA damage **(A)**, template strand switching to the undamaged, newly synthesised sister chromatid occurs **(B)** by either fork regression or strand invasion. Replication takes place utilising genetic information encoded by the sister chromatid to bypass the damage **(C)**, before reversion back to the original template strand **(D)**. Taken from (Unk et al., 2010).

consisting of Rev3 and Rev7 subunits (Ulrich, 2005, Waters et al., 2009, de Groote et al., 2011). Rev1 is notable among the TLS polymerases since its catalytic activity is limited primarily to inserting a dCMP in particular opposite abasic sites and a variety of different adducted guanines. Furthermore the polymerase activity of Rev1 is not essential for the Rev1-mediated bypass of many lesions. Rather a model is proposed whereby Rev1 mediates the majority of its function in TLS by recruiting and coordinating DNA damage tolerance factors to the site of lesions rather than bypassing them directly. Indeed *S. cerevisiae* Rev1 is able to interact with both the Rev3 and Rev7 subunits of Pol ζ and with Poln (Waters et al., 2009). In addition mammalian and yeast Rev1 has been shown to bind to a recessed, 5' phosphorylated primer-template junction and to the 3' OH terminus of the gap (de Groote et al., 2011).

The active site of the TLS polymerases is generally more open compared to the replicative polymerases. This allows better accommodation of bulky adducts present on damaged DNA. Other members have more constrained active sites but even so are specialized to accommodate particular classes of DNA lesions referred to as their cognate lesion (Waters et al., 2009, de Groote et al., 2011). The more relaxed catalytic site, along with lack of a proofreading 5'-to-3' domain and the limited contacts made between the template base and incoming nucleotide, mean the TLS polymerases tend to act with decreased replication fidelity. As such they confer a potentially mutagenic activity within the cell. Indeed most mutations generated by genotoxic agents are believed to be as a result of replication from these damage tolerant polymerases rather than from the actual damage. The process has therefore become known as error prone damage tolerance (Ulrich, 2005, Waters et al., 2009).

To date there is compelling evidence that TLS polymerases act via two models to bypass DNA lesions, these being the polymerase switching model and the gap filling model (Fig. 12). It is likely that TLS polymerases act in a manner consistent with both models when appropriate, for instance, according to the context of the lesion or phase of the cell cycle (Waters et al., 2009). The polymerase switching model is proposed to act at stalled replication forks and involves a switch from the stalled replicative polymerase at the primer-template-terminus to one or more TLS polymerases (Fig. 12A). A final switch then takes place restoring the replicative polymerase and enabling accurate DNA synthesis to resume (Pages and Fuchs, 2002, Waters et al., 2009). Indeed the majority of TLS

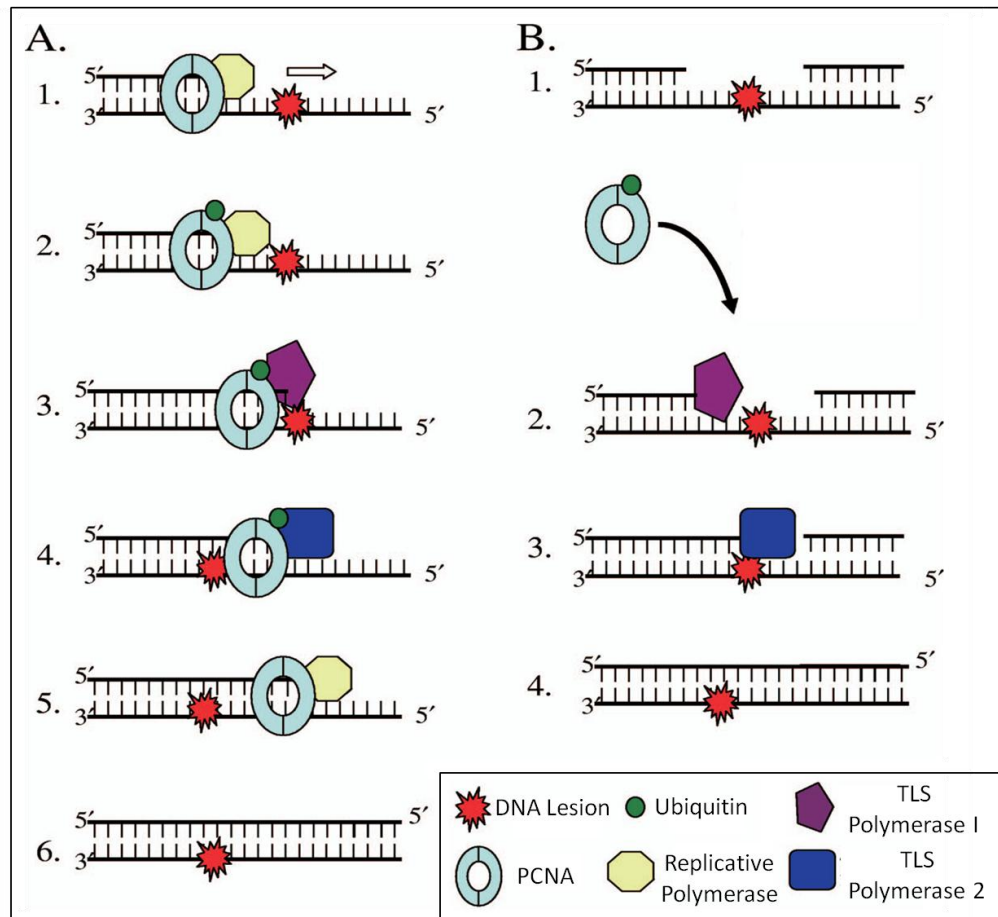


Figure 12 – Bypass of DNA lesions by TLS is proposed to occur by, **(A)** the polymerase switching model, and **(B)** the gap filling model.

polymerases demonstrate very low processivity a factor that may help to minimise the chance of mutation (Ulrich, 2005). Following DNA damage the Rad6/Rad18 heterodimer is recruited to sites of DNA damage. Although Rad18 exhibits DNA binding activity, essential for its *in vivo* role, there is increasing evidence that this recruitment is facilitated by the interaction of Rad18 with the ssDNA binding replication protein A (RPA) in *S. cerevisiae* (Ulrich, 2009). The Rad6/Rad18 heterodimer subsequently monoubiquitinates PCNA at Lys-164, this stage has been shown to be essential for TLS in yeast and is suggested to require PCNA to be loaded onto DNA (Andersen et al., 2008, Pages et al., 2009, Ulrich, 2009, Waters et al., 2009). Although the specific role of PCNA monoubiquitination is not entirely clear the modification directly enhances the affinity of TLS polymerases Rev1 and Pol η for PCNA. This can be attributed to the ubiquitin binding domains of such enzymes. Strengthening of this interaction may then promote the switch between a replicative and a TLS polymerase. Following extension across the lesion a second switch occurs back to the replicative polymerase possibly mediated by the deubiquitination of PCNA (Pages and Fuchs, 2002, Ulrich, 2009, Waters et al., 2009).

The gap filling model is thought to mediate TLS damage bypass at ssDNA gaps outside the context of the replication fork during G₁ or G₂/M phase and likely during late S phase (Lopes et al., 2006, Waters et al., 2009). A recent study does indicate that TLS functions effectively after chromosomal replication, outside of S-phase (Karras and Jentsch, 2010). Gaps can occur due to repriming of the replication machinery downstream from the blocking lesion, processing of closely spaced lesions on opposite DNA strands, or by the processing of interstrand cross-links. Upon identification of the need for lesion bypass the TLS polymerase is thought to be directed to the ssDNA gap by many of the same factors involved in the switching model (Fig. 12B). Handovers between the replicative and TLS polymerases are not thought to play a significant role in the gap filling model however may come into play if the remaining gap following lesion bypass is sufficiently large (Lopes et al., 2006, Waters and Walker, 2006, Waters et al., 2009). Following the completion of replication or filling of ssDNA gaps, via successful TLS, the lesion can be removed by DNA repair pathways possibly before the next round of replication (Waters and Walker, 2006, Waters et al., 2009).

How the most appropriate TLS polymerase is selected to bypass a particular lesion remains one of the most intriguing questions regarding TLS. A trial and error method has been suggested to occur whereby several polymerases may associate at the primer terminus sequentially until the best suited for bypass of the specific lesion is encountered. During such a time, and also possibly in the absence of damage, PCNA may act as a tether for several polymerases thus enabling rapid switching. It is likely, however, that numerous factors play a role in determining which polymerases have access to the primer terminus. For instance, the apparent cell cycle regulation of Rev1, and the ubiquitin state of PCNA and the polymerases themselves (Pages and Fuchs, 2002, Waters et al., 2009).

1.6.2 Error Free Damage Tolerance

An alternative pathway of DNA damage tolerance also exists. This additional pathway does not utilise the damaged region of DNA as a template and is thus deemed error free. Rad6/Rad18 mediated monoubiquitination of PCNA at Lys-164 can be extended by the Ubc13/Mms2 ubiquitin conjugating complex, in cooperation with the ubiquitin ligase Rad5, to a Lys-63-linked polyubiquitin chain. This polyubiquitination of PCNA is a requirement for error free DNA damage tolerance. The mechanism behind how error free lesion bypass is achieved remains to be fully established but is thought to, temporarily, utilise the newly synthesised, undamaged, sister chromatid as a template (Andersen et al., 2008, Ulrich, 2009). At ssDNA gaps this has been suggested to occur via a template strand switch, via strand invasion, leading to the formation of a sister chromatin junction (SCJ) intermediate, in a manner similar to a homologous recombination reaction (Fig. 11) (Andersen et al., 2008, Branzei et al., 2008). This process seems to require SUMOylation of PCNA and may cooperate with Rad51-dependent homologous recombination events. Indeed in the absence of PCNA SUMOylation, SCJ formation can occur and requires Rad51-dependent homologous recombination events which act independently of Rad18 (Branzei et al., 2008). It is suggested that PCNA SUMOylation acts to suppress SCJs occurring by homologous recombination alone. This may be achieved through the interaction of SUMOylated PCNA with the Srs2 helicase which seems to prevent unscheduled recombination events at replication forks (Branzei et al., 2008, Ulrich, 2009).

An alternative model of error free damage tolerance has been suggested, this involves reversion of the replication fork as facilitated by the helicase activity of Rad5 (Fig. 11). It has been proposed that regression of the replication fork is accompanied by pairing of the two nascent strands while the original template strands re-anneal creating a chicken foot structure. Elongation can then continue from the stalled primer terminus using the nascent sister chromatid as a template (Zhang and Lawrence, 2005, Andersen et al., 2008). By contrast it has been suggested that the DNA damage checkpoint acts to prevent regression of the replication fork while error free DNA damage tolerance occurs by the template switching model discussed above (Andersen et al., 2008). Ultimately debate still exists as to the mechanism by which the error free damage tolerance pathway exerts its effect.

1.6.3 Conservation of DNA Damage Tolerance from Yeast to Humans

The above two pathways of DNA damage tolerance are highly conserved in eukaryotes, ranging from yeast to humans, in terms of both the components and the proposed mechanisms utilised (Andersen et al., 2008, Ulrich, 2009, Waters et al., 2009). This includes monoubiquitination of PCNA by Rad6/Rad18 which occurs at the same Lys-164 residue in yeasts and higher eukaryotes, including humans (Hoegge et al., 2002). Indeed the ability of this modification to enhance affinity of TLS polymerases for PCNA and thus promote switching between was first identified for human Pol η (Ulrich, 2009). Although slightly more controversial, Lys-63 linked PCNA polyubiquitination has now been shown to occur in a number of separate human cell lines, following UV irradiation, to promote the error free pathway. This is dependent upon both Rad18, suggesting that monoubiquitination is first required, and Ubc13. In addition Mms2 along with two Rad5 homologues, SHPRH and HLTF, have been identified in human cells (Chiu et al., 2006, Langie et al., 2007, Unk et al., 2010). Both human Rad5 homologues exhibit ubiquitin ligase activity for Ubc13/Mms2 dependent Lys-63 linked polyubiquitination of PCNA and HLTF in particular has been implicated as having a Rad5-like role in damage tolerance (Unk et al., 2010). Unlike in yeast, however, Mms2 appears to serve a redundant role suggesting the presence of an alternative Mms2 variant or complex that can compensate for its loss (Brun et al., 2008).

The significance of DNA damage tolerance in maintaining genomic stability along with such conservation highlights how the study of such pathways may have important implications in the development of novel strategies to combat cancer (Ulrich, 2005, Andersen et al., 2008, Waters et al., 2009). The mutagenic nature of error prone DNA damage tolerance may in itself create detrimental changes in genetic information and must therefore be maintained under tight control (Ulrich, 2005, Andersen et al., 2008). Indeed, yeast cells defective for error free damage tolerance can demonstrate spontaneous mutation rates elevated by 30-fold (Andersen et al., 2008). Furthermore, the Rad5 homologues, HLTf and SHPRH, proposed to function in the error free pathway of damage tolerance, have been implicated in tumour suppression, however further studies are required to clarify their specific roles (Unk et al., 2010).

The majority of current cancer treatments involve the selective killing of malignant cells through the use of radiation or cytotoxic chemicals that interfere with DNA replication, either by the introduction of lesions or interfering with enzymes involved in DNA metabolism. Elimination of damage tolerance pathways, which aid survival under such conditions, should increase the efficiency of such treatments (Ulrich, 2005). In addition, the development of secondary tumours due to DNA damage created by conventional cancer treatments represents one of their greatest risks. Suppression of damage bypass polymerases that enable mutagenic lesion bypass may help to minimize these detrimental consequences (Ulrich, 2005). Ultimately more research is required to establish the roles of DNA damage tolerance in tumorigenesis and carcinogenesis.

1.7 Microbial Cell Individuality

Individual cells from clonal microbial populations are known to exhibit marked phenotypic heterogeneity in a wide variety of functions that are often vital for survival and development. These have been shown to include, for example, variable degrees of virulence in pathogenic microorganisms, different levels of resistance to environmental stressors and variation in cellular and colony morphology (Avery, 2006). Phenotypic heterogeneity at the single cell level is generally masked by conventional studies which use population averaged data often from across thousands or millions of cells. Increased appreciation for the importance of cellular heterogeneity, along with a surge of interest in the processes that govern such cell-to-cell variability, has driven the development of new tools and

techniques to study individual cells and brought the issue of cell individuality to the fore in recent years.

The term 'bet hedging', first introduced by Slatkin in 1974, is often used to describe phenotypic heterogeneity as a risk-spreading strategy that may help to ensure survival of at least a subset of the isogenic population in whichever environmental condition is encountered (de Jong et al., 2011). Indeed, it is generally considered that phenotypic heterogeneity provides a dynamic source of diversity in addition to the heritable genotypic variation created by sequence changes such as mutation and genome rearrangements. Microbial populations are proposed to benefit from the existence of phenotypic heterogeneity due to the creation of variant subpopulations that are pre-equipped to persist better during times of stress and exploit new niches, thus aiding survival during times of environmental fluctuation (Avery, 2006). In support of this, heterogeneous populations can demonstrate increased fitness and, under high states of stress, out-survive a more homogeneous microbial community likely due to the availability of alternative adaptive strategies (Bishop et al., 2007, Smith et al., 2007, Acar et al., 2008). Importantly, and in contrast to variation created by sequence changes, phenotypic heterogeneity does not result in an irreversible commitment to the new cell state, rather individual cells can rapidly revert to their original status if required (Avery, 2006). Representations of this non-genotypic cell-cell heterogeneity exist throughout the microbial world and include such examples as; pili switching in *Escherichia coli* (Wolf and Arkin, 2002), morphology switching in pathogenic *Candida* species, and the presence of dormant persister cells within bacterial populations (Lewis, 2007).

In principle, the initiation of an infection may require just a few variant virulent cells from within a larger avirulent population. Consequently phenotypic heterogeneity may be of particular importance for virulence, enabling pathogens to survive the changing environments that may be encountered during infection of a mammalian host and colonisation of various niches. Indeed genome rearrangement-driven variation in the expression of virulence genes has been linked to pathogenesis in certain protozoa and bacteria (Scherf et al., 2008, Bayliss, 2009). It is possible to link heterogeneity to stochastic fluctuations, at the molecular level, in the processes that control transcription and translation with subsequent mRNA and protein degradation also subject to similar molecular noise. Such processes result from binding events, such as transcription factor binding

to a promoter, which occur randomly and are therefore inherently stochastic. Even small fluctuations of this type can lead to substantial differences as the effect is amplified through subsequent stages (Kaern et al., 2005, Avery, 2006, Kaufmann and van Oudenaarden, 2007). The stochastic process of transcriptional bursting is known to generate increased cell-to-cell variability and can confer advantages in the face of environmental stress (Blake et al., 2006). In addition to the contribution of stochastic gene expression, various other generic drivers of heterogeneity in microbial populations have been uncovered. These include; progression through the cell cycle and oscillatory changes in the physiological state of the cell that may accompany this (biological rhythms), aging, metastably inherited epigenetic modifications, mitochondrial activity, and individual cell growth rates (Avery, 2006). For instance, the cell cycle- and age-dependent activity of Sod1 (Sumner et al., 2003), as well as metabolic oscillations (ultradian rhythms) which modulate single cell redox status (Smith et al., 2007) are implicated in the stress resistance of individual yeast cells. Epigenetic regulation of gene expression also appears to have a particularly prominent role in the induction of cell-to-cell variability. Indeed epigenetic silencing effects due to changes in chromatin structure near telomeres constitute a major source of variation in the expression of genes located in the subtelomere, many of which encode cell surface proteins and adhesins (Halme et al., 2004, Verstrepen and Fink, 2009). To date, the relevance of cell-to-cell gene expression heterogeneity to virulence of yeast pathogens, such as *Candida* spp, has not been examined.

1.7.1 Cell Surface Variation

Many microorganisms have developed mechanisms to generate variability at their cell surface thus producing differential adherence, evasion of the immune system and environmental adaptation strategies (Verstrepen and Fink, 2009). In both yeast and protozoa much of this variation is reliant upon epigenetically regulated processes including transcriptional silencing and differential gene expression (Avery, 2006, Verstrepen and Fink, 2009).

1.7.1.1 Protozoan Cell Surface Variation

Some of the best studied examples of cell surface variation can be found within protozoan parasites, such as the trypanosomes, and the malaria parasite *Plasmodium falciparum*. The African trypanosome

Trypanosoma brucei is well known for its antigenic variation at the cell surface. *T. brucei* is an extracellular parasite carried in the bloodstream of infected hosts and is responsible for African sleeping sickness with transmission occurring via the tsetse fly. The extracellular nature of this parasite renders it fully exposed to the host's immune response, against which a dense glycoprotein coat provides protection and masks other potentially immunogenic cell surface proteins (Barrett et al., 2003, Verstrepen and Fink, 2009). Continual evasion of the immune response is achieved by switching the composition of this outer coat to antigenically distinct glycoproteins from a large repertoire of >1500 so called variant surface glycoprotein (VSG) genes and pseudogenes which are largely located in the subtelomeres (Horn and Barry, 2005, Avery, 2006, Horn and McCulloch, 2010). Each cell expresses only one VSG at a time, a process to which a number of mechanisms may contribute (Fig. 13) and that can create cell- to-cell variation. Firstly and indeed the prominent mechanism from which antigenic variation originates involves duplication of a silent VSG gene into a single active expression site and deletion of the previous VSG resident at that site (Robinson et al., 1999). Such DNA recombination events are believed to be initiated by double strand breaks within the 70bp repeats upstream of the actively transcribed VSG gene (Boothroyd et al., 2009). Secondly, activation of new VSG genes can be achieved by an *in situ* switch involving activation of a silent expression VSG site coupled to repression of the previously active site (Alsford et al., 2009). Reciprocal translocation, including telomere exchange, is also known to be a method of VSG antigenic switching (Boothroyd et al., 2009, Verstrepen and Fink, 2009). Transcriptional silencing is instrumental in maintaining monoallelic VSG expression from among the 10-20 telomeric expression sites that exist and as such protects the integrity of the evasion strategy (Horn and McCulloch, 2010). A direct role for telomeric silencing in the form of telomere position effect however remains controversial. Additional factors suggested to influence such monoallelic expression include chromatin remodelling, DNA modification or a unique transcriptional/elongation apparatus (Horn and Barry, 2005). That many VSG's exist as pseudogenes provides another possible source of antigenic variation and the generation of novel combinations. Such pseudogenes must partially recombine with the active VSG resident in order to reconstitute a functional gene thus creating a chimeric product. This ability further aids evasion of the immune system by increasing the potential VSG reservoir (Pays, 2005).

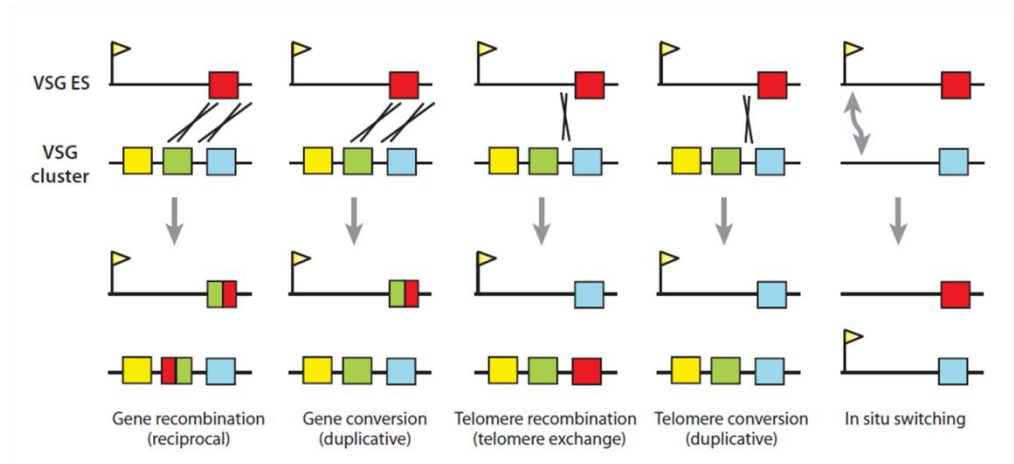


Figure 13 – The mechanisms by which VSG switching of a silent gene or pseudogene in to the VSG active expression site (ES) can occur. The majority of mechanisms involve either reciprocal or duplicative translocations whilst the final mechanism involves an *in situ* switch to a different expression site (ES). Taken from (Verstrepen and Fink, 2009).

A second trypanosome exhibiting cell surface variability is *Trypanosoma cruzi*. This parasite is spread by reduviid bugs and causes Chagas disease, which constitutes the most important parasitic infection in Latin America with many areas being endemic (Barrett et al., 2003, Dias, 2009). The major surface glycoproteins at the cell surface of this parasite are the mucin-like proteins. The mucin coat protects the parasite from host derived defence mechanisms while enabling correct targeting to specific cells or tissues (Buscaglia et al., 2006). The *T. cruzi* genome encodes ~850 members of these mucin-like proteins, within the TcMUC subfamily, the products of which demonstrate many similarities to fungal cell surface adhesins (El-Sayed et al., 2005, Verstrepen and Fink, 2009). A second mucin subfamily is also encoded by the *T. cruzi* genome, TcSMUG, and consists of a small subset of relatively homogenous members that are generally expressed while the parasite resides within its insect vector (El-Sayed et al., 2005, Buscaglia et al., 2006). By contrast the TcMUC family encodes a large number of members which demonstrate substantial variability and dominate expression upon entry to the mammalian host (Buscaglia et al., 2004). Thus, the transition from insect to mammal occupation corresponds with a switch to a different set of mucin genes, the vast majority of which are silenced by an as-yet-unknown mechanism in the insect vector. This results in a switch from a mucin coat of rather homogeneous polypeptide composition to one that is highly heterogeneous. Studies have not yet revealed whether mammal-dwelling mucin variability is due to the expression of multiple mucins on the cell surface of each parasite or if, as has been seen for the *T. brucei* VSG genes, each parasite is able to express a single but different mucin molecule thus generating cell-to-cell variation and ultimately subpopulations of parasites with different TcMUC expression (Buscaglia et al., 2006, Verstrepen and Fink, 2009). In addition, cells rely on post-transcriptional mechanisms such as the control of RNA stability to regulate gene expression making it less straightforward to investigate which mucins are expressed (Verstrepen and Fink, 2009).

The malaria parasite *P. falciparum* also employs an immune response evasion strategy which involves transcriptional switching among members of the highly diverse ~60 member VAR family which encode the PfEMP1 (*P. falciparum* erythrocyte membrane protein 1) surface antigens (Verstrepen and Fink, 2009). The majority of genes of this antigen-encoding family reside at subtelomeric locations in the genome. Individual

parasites within clonal populations generally transcribe only one dominant *VAR* gene thus creating cell-to-cell variation. Furthermore *VAR* switching allows individual parasites within such populations to demonstrate different antigenic and phenotypic characteristics at different times (Ralph and Scherf, 2005). The *VAR* genes can be partitioned into either slow or fast switching phenotypes. This partitioning is suggested to be associated with chromosomal position since genes at more internal locations demonstrate intrinsically slower off rates than those exhibited by their subtelomeric family members (Frank et al., 2007). A model to describe the pattern of switching that occurs in individual parasites has recently been described. This model suggests utilisation of a single-many-single (sms) switching pathway whereby an initial unbiased switch, away from the starting dominant transcript, occurs towards a subset of variants. Each variant in the subset has a high off rate and transcription ultimately becomes biased towards a single new variant within this subset which subsequently gains dominance (Recker et al., 2011). Such a mechanism is believed to have evolved due to the propensity of *P. falciparum* to infect non-naive individuals where discordance between the parasite and the immune repertoire cannot be guaranteed. The initial diversification process may greatly improve the chances of evading pre-existing immune responses since many variants become accessible, while the subsequent contraction protects the remaining repertoire from further exposure. Thus, this mechanism demonstrates a higher level of flexibility than observed for other organisms such as *T. brucei*, where a direct switch is employed, while still remaining structured. It has been suggested that the initial switch occurs to a set of antigenetically similar variants which are then effectively removed by short-lived cross reacting antibody responses, thereby allowing such variants to be recycled at later stages of the infection (Recker et al., 2011).

The above model describes the pattern by which *VAR* gene switching occurs, however the molecular mechanisms that drive such switching and determine the gene to be expressed in individual parasites, ultimately leading to cell-to-cell variation, remain far from being fully understood. To date the process of *VAR* gene switching is known to be under epigenetic control (Recker et al., 2011), DNA rearrangements such as those observed in *T. brucei* are known not to be required (Ralph and Scherf, 2005, Verstrepen and Fink, 2009), which is unsurprising given the proposed sms switching model. Rather, a number of other factors including

changes in intracellular location, chromatin state, and the presence of promoter containing introns have been implicated in the switching mechanism (Verstrepen and Fink, 2009). Position dependent silencing appears to be of particular note and the *P. falciparum* Sir2 homologue (PfSir2) has been shown to bind at regions close to inactive *VAR* genes, an interaction correlated with hypoacetylation and silencing at these regions (Deitsch et al., 1999, Duraisingh et al., 2005, Freitas-Junior et al., 2005, Verstrepen and Fink, 2009). Furthermore subtelomeric *VAR* genes have been observed to occupy different nuclear positions at the nuclear periphery depending on their activation state (Duraisingh et al., 2005, Verstrepen and Fink, 2009). Such organisation into different subnuclear clusters appears to function as another level of epigenetic regulation for these genes. The *P. falciparum* nuclear periphery consists primarily of silent heterochromatin, however, the nucleus of each parasite contains at least one distinct heterochromatin free region at its periphery which may indicate a transcriptionally active zone (Dzikowski and Deitsch, 2009). A model has been proposed whereby silenced subtelomeric *VAR* genes are associated with telomeric clusters at heterochromatin regions of the nuclear periphery. Upon activation, *VAR* genes exit this site to a transcriptionally active region of the nuclear periphery (Fig. 14). It is, however, unknown if transcription at the active site is a consequence of the new nuclear position or if transcriptional activation itself results in positional displacement (Ralph et al., 2005, Dzikowski and Deitsch, 2009). Along with upstream regulatory regions, the promoter-containing intron, present in all but one of the *VAR* genes, has been implicated in silencing at inactive *VAR* loci, additionally these introns are thought to have a role in *VAR* gene recognition by the mechanism that controls mutually exclusive expression (Calderwood et al., 2003, Gannoun-Zaki et al., 2005, Dzikowski and Deitsch, 2009, Verstrepen and Fink, 2009). It has been proposed that *VAR* introns act as heterochromatin boundary elements maintaining repression of adjacent *VAR* genes at the same subtelomere as the active locus, such barrier activity may also require interactions with the nuclear pore complex and may go some way to explaining the nuclear periphery sublocalisation (Ralph and Scherf, 2005, Ralph et al., 2005). In a rare stochastic event intronic promoter activity is able to outcompete the active *VAR* promoter for the transcription initiation complex. This produces a non-coding RNA species that tags the active locus for histone modification,

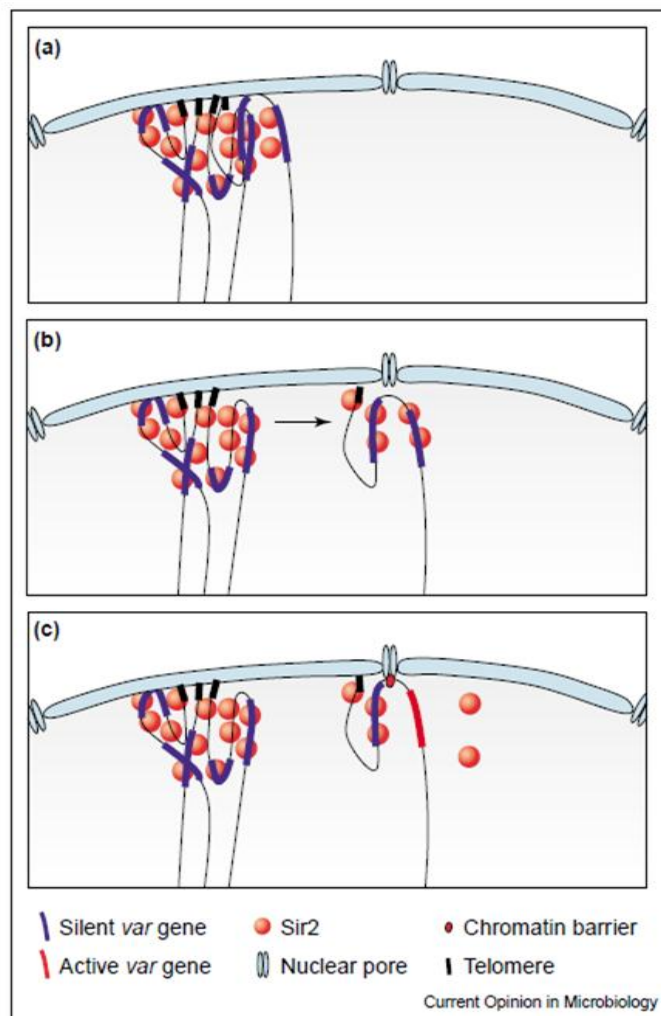


Figure 14 – Model for the activation of *VAR* genes according to nuclear localisation. **(a)** *VAR* genes present in subtelomeric clusters are subject to transcriptional repression due to high levels of silencing factors such as PfSir2. **(b)** The active *VAR* locus then move away from these silenced clusters towards a transcriptionally active region of the nuclear periphery. **(c)** *VAR* gene intron barrier activity, a process that may require interaction with the nuclear pore, preventing the spread of silenced chromatin into the active locus. Taken from (Ralph and Scherf, 2005).

heterochromatin formation and subsequent silencing (Ralph and Scherf, 2005). Activation of a new *VAR* promoter, however, appears sufficient to initiate a switch in cell surface antigenicity (Voss et al., 2006).

1.7.1.2 Yeast Cell Surface Variation

A number of aspects of protozoan cell surface variation discussed above such as subtelomeric location and epigenetic transcriptional silencing may also contribute to adhesin variation at the fungal cell surface. The cell wall adhesins produced by many fungi mediate flocculation, adherence to both inert surfaces and mammalian tissues and biofilm formation (Verstrepen et al., 2004). An important survival strategy for yeast cells is the ability to adapt to new conditions which may often require adhesion to a new substrate or, in the case of pathogenic yeast, to different host tissues in order for infection to occur.

As mentioned briefly in earlier sections the *S. cerevisiae FLO* gene family is a group of adhesins that are able to confer attachment to agar, solid surfaces and other yeast cells (flocculation). There are only five known members of the *FLO* gene family; *FLO1*, *5*, *9*, and *10*, which reside adjacent to their respective telomeres and *FLO11* which is neither adjacent to a telomere or centromere. The subtelomeric *FLO* genes confer varying degrees of flocculation, with *FLO1* providing the strongest level of cell-to-cell adhesion. By contrast expression of *FLO11* is more relevant for adhesion to abiotic surfaces and for haploid invasive or diploid filamentous growth (Guo et al., 2000, Verstrepen et al., 2004, Soares, 2011). However, *FLO10* has been observed to compensate for loss of *FLO11* function and induce filamentation, thus generating phenotypes which overlap those of *FLO1* and *FLO11* (Guo et al., 2000).

Cell-to-cell variation in expression of the *FLO10* and *FLO11* genes is known to have an epigenetic basis (Fig. 15). The propensity of diploid *S. cerevisiae* to filament under conditions of nitrogen starvation has been shown to vary between individual cells. While some cells are seen to grow as filamentous pseudohyphae others, within the same population, remain in the yeast form. This morphological heterogeneity is dependent upon metastable silencing of the *FLO11* gene. This gene is known to be silent while cells reside in the yeast form but is expressed to produce filamentous growth, an expression state that can be inherited for >10 generations. Transcriptional silencing from the *FLO11* promoter is dependent upon its chromosomal position. However, in contrast to conventional telomere

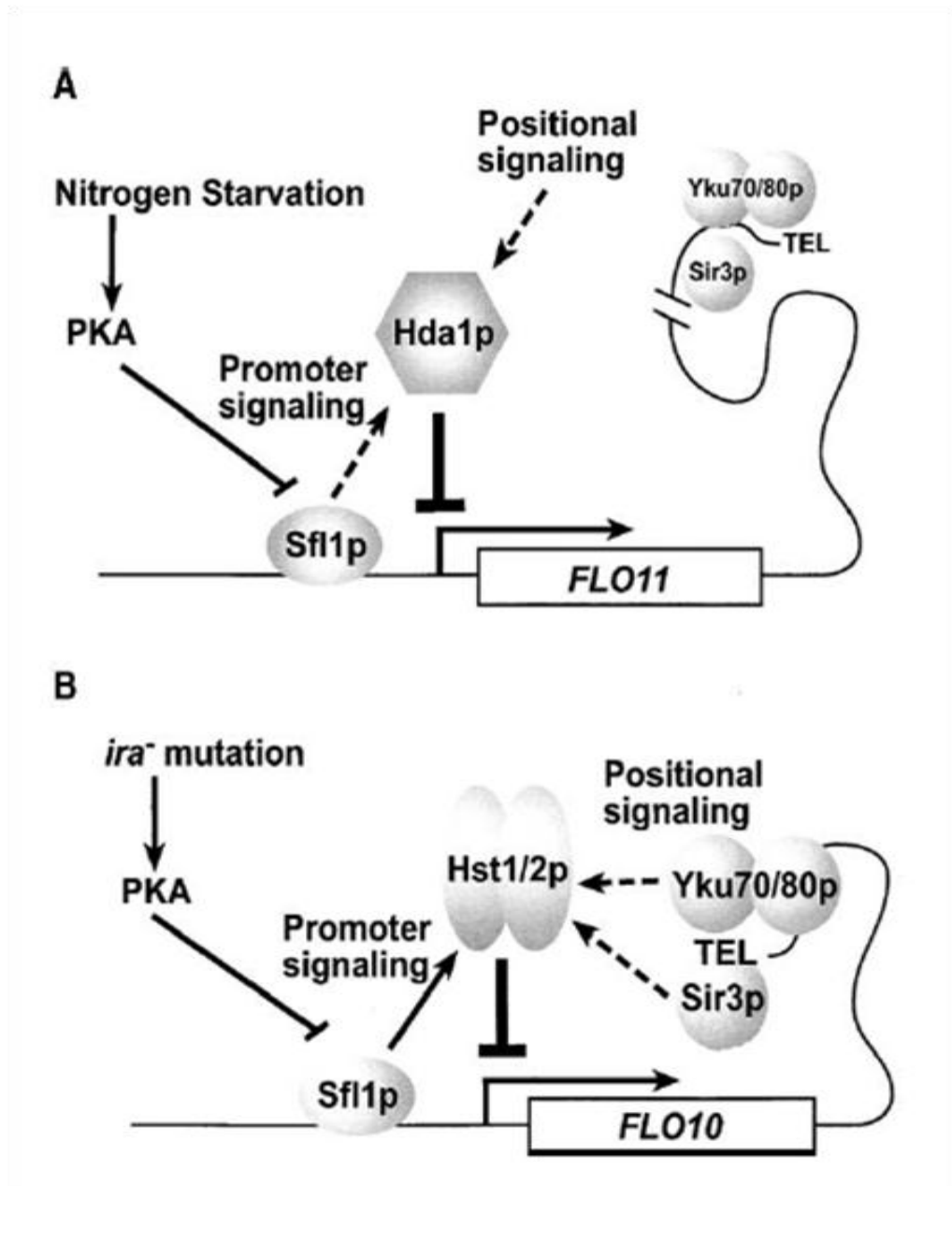


Figure 15 – Schematic representations of the positional- and promoter dependant mechanisms that mediate heterogeneous expression of **(A)** *FLO11* and **(B)** *FLO10*. Taken from (Halme et al., 2004)

silencing, repression of *FLO11* is also promoter specific (Halme et al., 2004). The transcriptional repressor Sfl1, for which DNA binding is inhibited by protein kinase A (PKA) activity, works antagonistically with the Flo8 activator to regulate expression of *FLO11* via a common promoter element (Conlan and Tzamarias, 2001, Pan and Heitman, 2002). As such Sfl1 has been implicated as a possible candidate for regulation of the promoter specific portion of *FLO11* silencing and has indeed been identified as necessary for such repression (Halme et al., 2004). In addition Hda1p is believed to be associated with deacetylation within regions that encompass the *FLO11* locus. Such deacetylation is restricted to specific areas of the genome and is thus believed to be responsible for the position dependent fraction of *FLO11* silencing (Halme et al., 2004). Hda1p is recruited to specific promoters by Tup1 (Wu et al., 2001), which is thought to be recruited to the *FLO11* promoter by Sfl1p (Conlan and Tzamarias, 2001), thus suggesting a strategy by which both promoter dependent and position dependent factors co-operate to silence *FLO11*. Indeed deletion of either regulatory factor (Sfl1p or Hda1p) leads to constitutive expression of *FLO11* and loss of cell-to-cell variability in the expression of this adhesin (Halme et al., 2004). Interestingly, the Sfl1p component of this regulation occurs independently of the *FLO* transcriptional activator Flo8 (Conlan and Tzamarias, 2001). The above strategy therefore provides a novel regulatory pathway for *FLO11* expression.

A subsequent study utilised a dual-reporter assay system to demonstrate the slow transition rates between on and off associated with epigenetic silencing at the *FLO11* promoter. In diploid cells, these switches create four possible expression states: both ON, both OFF, ON/OFF, and OFF/ON. Such independent switching may represent an additional mechanism in the generation of variation. In addition three classes of global *trans* activators including Msn1p, Tec1p, and Flo8p were found to have roles in governing either epigenetic (slow, Class II), conventional (fast, Class I), or both forms (Class III) of regulation, respectively. Distribution in the control of transition rates may enable individual cells within isogenic populations to shape the diversity of *FLO11* expression through the utilisation of various combinations of such regulators (Octavio et al., 2009).

Access to the remaining reservoir of *S. cerevisiae* *FLO* genes is governed by a mutational mechanism involving high frequency mutations ($\sim 10^3$) in the genetically unstable *IRA1* or *IRA2* genes, which encode the

yeast Ras GTPase activation proteins. In haploid cells which do not undergo filamentation, such mutation leads to hyperinvasive growth and increased flocculence. The novel adhesive phenotypes exhibited by such mutants are mainly the result of increased *FLO10* expression. This transcriptional activation is dependent upon both the MAP kinase and cAMP regulated PKA pathways and is suggested to occur due to increased Ras activity in *IRA* mutants. As with *FLO11*, *FLO10* expression was identified as being heterogeneous between individual cells. Such variation is again due to metastable epigenetic silencing, influenced by both promoter and position specific mechanisms by the actions of Sfl1. Sfl1 is thought to inhibit the Flo8 activator and recruit the Sir2 homologues, Hst1 and Hst2, to the *FLO10* promoter. The telomeric Sir3 and Ku proteins are also involved in *FLO10* silencing, although it is unclear whether these proteins act through Hst1 and/or Hst2 or independently (Halme et al., 2004). Such results demonstrate the ability of gene expression to vary between individual cells of a genetically identical population following environmental stimulus. Ultimately this is able to generate subpopulations that vary in their ability to filament, invade and adhere. It seems logical to speculate that should similar events occur within pathogenic yeast, such as *C. glabrata*, there would be important implications for virulence.

1.8 Aims of the Current Work

The pathogenic yeast *C. glabrata* encodes a family of GPI-anchored cell wall adhesins termed the EPA (epithelial adhesin) family. The predominant aim of this study was to investigate the possibility of heterogeneous expression of Epa1 in this pathogenic yeast. Mediating one of the initial host-pathogen interactions to occur during infection, such adhesins play an integral role in the establishment of host infection and are an important virulence factor. It is possible that heterogeneity in the expression of these adhesins is able to confer a selective advantage during host colonization. Consequently further understanding of the mechanisms and regulatory elements involved in controlling cell-to-cell variability will be important in further understanding how this pathogen interacts with its host, possibly pointing to new drug targets. This may be particularly pertinent for *C. glabrata* due to its rising prevalence, high mortality, and antifungal resistance. Such regulatory processes may encompass transcriptional silencing, owing to the subtelomeric nature of these genes. Indeed a number of *EPA* genes are known to be subject to sir-mediated

silencing (De Las Penas et al., 2003, Castano et al., 2005, Rosas-Hernandez et al., 2008). Post-translational effects occurring during the process of GPI-CWP maturation, placement at the cell wall, and subsequent removal must also be considered as possible points at which expression heterogeneity can occur.

A smaller aim of this study was to investigate the regulatory proteins, in particular Sir2 and Swi6, which may control heterogeneous expression of Rad6 in *S. cerevisiae*. Preliminary data from the laboratory prior to this project suggested that expression of Rad6, a protein involved in DNA damage tolerance regulation, was bimodal. Such an observation may have important implications for stress resistance and again aid survival under different environmental conditions.

Chapter 2 - Materials and Methods

2.1 Strains and Plasmids

Candida glabrata BG2 (Cormack et al., 1999) and the type strain derivative CG2001 HTUA (*his3Δtrp1Δura3Δ*) (Kitada et al., 1995), the latter being kindly donated by Ken Haynes (University of Exeter), were the wild type backgrounds from which other strains were derived. *C. glabrata* BG2 and derivatives *ura3Δ* (BG14), *epa1Δ* (BG64) and an *EPA1*-GFP transcriptional fusion strain (BG198), which is also deleted for *URA3* were gifts from Brendan Cormack (Johns Hopkins University). A *yps7Δ* deletion strain in the ATCC2001 background was also kindly provided by Ken Haynes. The triple HA-tagged strain, BG2-Epa1-HA, was constructed prior to the initiation of this study (M.C. Smith), using the *ura3Δ* BG2 derivative, BG14, by the same method described for CG2001-Epa1-HA below. Clinical isolates of *C. glabrata* were provided by Michael Petrou, from the collection at the Department of Medicine, Imperial College London. *C. glabrata* NCYC388 was from the NCYC, Norwich. Single copy *C. glabrata* plasmids, pCgACH-3 and pCgACH-14 (Kitada et al., 1996), were donated by Ken Haynes. Maps of the plasmids discussed and constructed below can be found in (Fig. 16) with the exception of plasmids used in *S. cerevisiae*, which are discussed in chapter 3. Primers (Table. 5) and protocols utilised in the construction of strains and plasmids can be found in the ensuing sections of this chapter.

2.1.1 Construction of CG2001-Epa1-HA

To construct strains expressing hemagglutinin (HA)-tagged *EPA1*, a fragment containing triple HA-tagged *EPA1* under the control of its own promoter and containing extended regions of genomic sequence around *EPA1*(-3HA), together with the internal *URA3* marker, was excised as a ~6.8kb fragment from pMS15 by digestion with *Xba*I and *Pac*I and transformed in to *C. glabrata* using a modified lithium acetate method (Castano et al., 2003). Ura⁺ transformants were selected on YNB plates lacking uracil. Appropriate integration of the transforming fragment was verified with diagnostic PCR using genomic DNA and primers WIEPA1-FWD/HAtag-FWD and EPA1-REV-OSHO. Primers WIEPA1-FWD and EPA1-REV-OSHO indicated successful integration by generation of a ~4.5kb band compared to a ~3.4kb band produced in untagged strains. Primers HAtag-FWD and EPA1-REV-OSHO confirmed the presence of 3HA-EPA1 by generation of a ~5.8kb band while no band was produced in untagged transformants. This is illustrated further in chapter 4 (4.2.3).

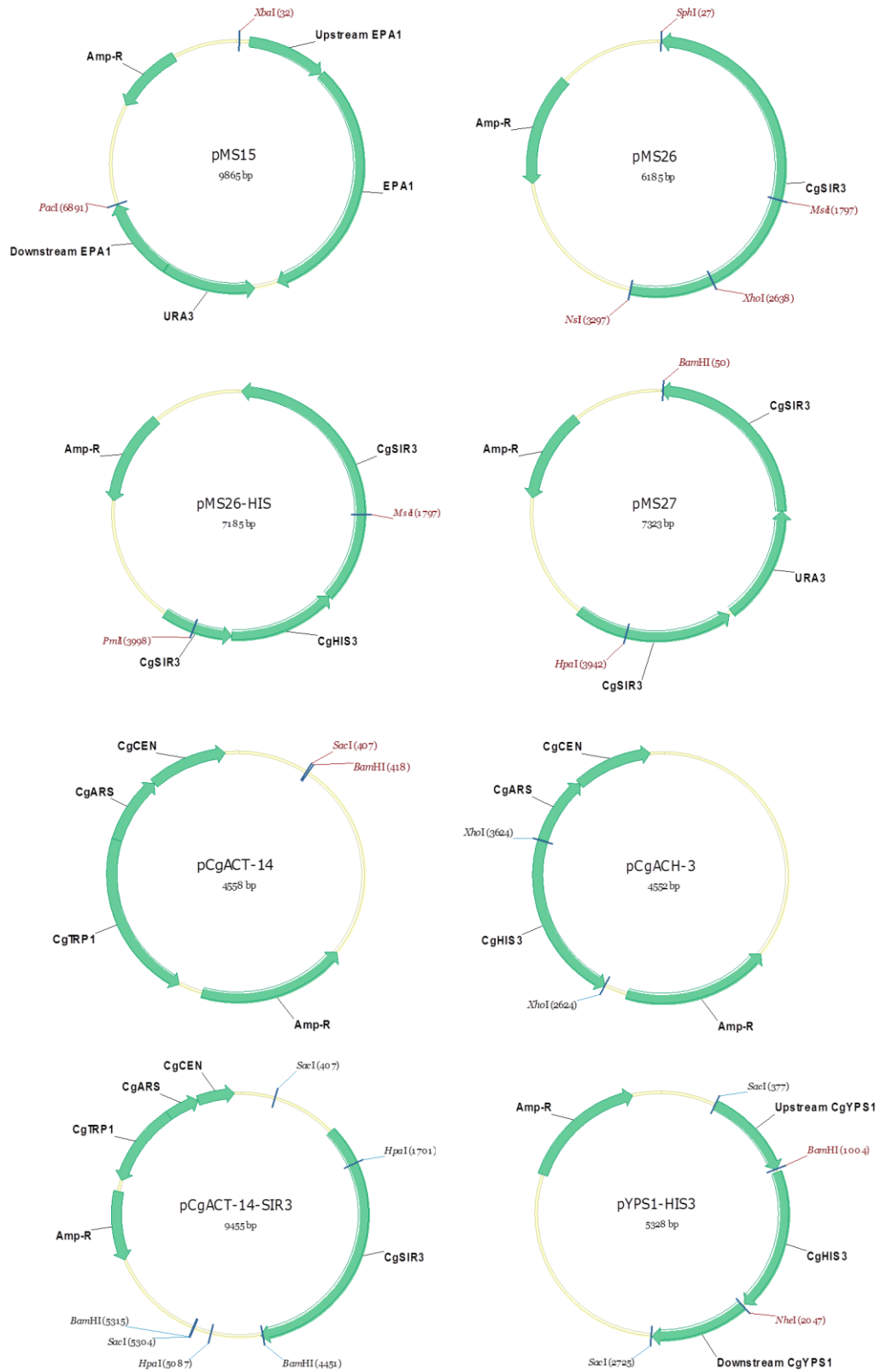


Figure 16 – Maps of plasmids utilised during this study. pMS15, pMS26, and pMS27 were generated prior to the start of this project (M.C. Smith). pCgACH-3, and pCgACT-14 (Kitada et al., 1996), were kindly donated by Ken Haynes (University of Exeter). Plasmids constructed and utilised during this study included pMS26-HIS, pCgACT-14-SIR3, and pYPS1-HIS3.

The plasmid, pMS15, was generated prior to the initiation of this project and contained 3HA-tagged *EPA1* from pBC214 (from B. Cormack) (Frieman et al., 2002) under *EPA1* promoter control due to the presence of ~1kb of upstream *EPA1* sequence. The *URA3* marker (from pHOBST-URA3 (Payne, 2007)) is present after the *EPA1* followed by a ~1kb region of sequence found immediately downstream of the *EPA1* ORF.

2.1.2 Construction of *sir3*Δ Strains

BG2-*sir3*Δ, CG2001-*sir3*Δ, and BG2-*EPA1*-GFP *sir3*Δ strains were constructed in the *ura3*Δ backgrounds of BG14, CG2001 HTUΔ, and *EPA1*-GFP (BG198), respectively, by the same method. This involved the use of plasmid pMS27, which had been constructed prior to the initiation of this study (M.C. Smith). Briefly this had involved amplification of *C. glabrata* *SIR3* from BG2 genomic DNA and subsequent ligation into the *Nsi*I and *Sph*I sites of pGEM7 (Promega) to initially generate pMS26 (M.C. Smith). The *URA3* selection marker (from pMS15) was then ligated into *Msc*I-cut pMS26 in order to disrupt *SIR3* and ultimately generate pMS27 (M.C. Smith). Digestion of pMS27 with *Bam*HI and *Hpa*I released a ~3.8kb *sir3::URA3* fragment which was transformed into the relevant *C. glabrata* strains mentioned above. Ura⁺ transformants were selected for on YNB plates lacking Uracil. Appropriate integration of the transforming fragment was verified by diagnostic PCR with genomic DNA using primers MS-SIR3-FWD and MS-SIR3-REV, both of which recognise regions outside of the transforming fragment. Successful disruption of *SIR3* was confirmed by the generation of a ~4.4kb fragment compared to a ~3.2kb band produced in untransformed cells using these primers.

To disrupt *SIR3* in Ura⁺ CG2001-Epa1-HA cells, a *HIS3* marker excised by *Xho*I digestion of pCgACH-3 (Kitada et al., 1996), was ligated in to the *Xho*I site of pMS26 to disrupt the *SIR3* ORF within this plasmid generating pMS26-*HIS*. Digestion of this plasmid with *Msc*I and *Pml*I released a ~2.2kb *sir3::HIS3* fragment for *SIR3* disruption via homologous recombination. Successful transformants were selected for on YNB plates lacking histidine and further confirmed by diagnostic PCR with genomic DNA, again using primers MS-SIR3-FWD and MS-SIR3-REV which both recognise regions outside of the transforming fragment. Successful integration of the transforming fragment was indicated by a band size of ~4.2kb, by contrast a band of ~3.2kb was obtained from strains containing wild type *SIR3*.

2.1.3 Construction of pCgACT-14-SIR3 Single Copy Plasmid

Expression of *C. glabrata* *SIR3* from a single copy plasmid was achieved by amplification of the *SIR3* ORF, together with ~800bp each of the upstream and downstream genomic sequence, as a ~4.8kb *SacI* fragment using the primers, *SIR3-FWD-SacI* and *SIR3-REV-SacI*. This fragment was subsequently digested with *SacI* and ligated into the similarly digested single copy *C. glabrata* plasmid pCgACT-14 (Kitada et al., 1996), to create pCgACT-14-*SIR3*. Successful ligation was first indicated by diagnostic colony PCR, following transformation into *Escherichia coli* XLI blue and selection on LB ampicillin plates, using primers *SIR3-FWD-SacI* and *SIR3-REV-SacI* to identify the presence of *C. glabrata* *SIR3*. Correct ligation was further confirmed by digestion of plasmid DNA with *BamHI* to produce bands of ~8.5kb and ~0.8kb, and with *HpaI* to produce bands of ~6kb and ~3.3kb. The *BamHI* digestion was also able to indicate the orientation of the ligated fragment owing to the fact that one site resides within the pCgACT-14 vector while the other is in the *SIR3* fragment. Transformation of pCgACT-14-*SIR3* into *C. glabrata* CG2001-Epa1-HA cells followed, with successful transformants selected for on YNB agar lacking tryptophan. Further confirmation was obtained by isolation of plasmid DNA from transformed yeast followed by diagnostic restriction digests as described above.

2.1.4 Construction of *yps7*Δ and *yps1yps7*Δ Mutant Strains

The *yps7*Δ deletion strain in an ATCC2001 background, provided by Ken Haynes, was utilised during the generation of these mutants. A deletion cassette was amplified from this strain as a ~3.2kb fragment, encompassing the *NAT^R* marker together with flanking sequences corresponding to ~1kb upstream and downstream of the *YPS7* ORF, using *YPS7-FWD* and *YPS7-REV* primers. This fragment transformed into CG2001-Epa1-HA cells in order to generate an Epa1-HA tagged strain in which *YPS7* was deleted (CG2001-Epa1-HA *yps7*Δ). Transformants were selected for successful integration by growth on YPD medium supplemented with nourseothricin. Successful integration of the deletion cassette was further confirmed by diagnostic PCR utilising genomic DNA and primers *YPS7-FWD-OSHOM* and *YPS7-REV* which recognise regions outside and within the transforming fragment respectively. Transformants in which *YPS7* was successfully deleted produced a band of ~3.4kb, by contrast wild type *YPS7* generated a band of ~4kb.

To delete *YPS1* in the CG2001-Epa1-HA *yps7Δ* strain, the *YPS1* ORF was amplified, along with 1kb flanking sequences, as a ~3.8kb *SacI* fragment with primers YPS1-FWD-*SacI* and YPS1-REV-*SacI*. The amplified fragment was inserted into the pJET2.1 vector (Fermentas Life Sciences). The *HIS3* marker from pCgACH-3 was amplified as a *BamHI/NheI* fragment using the primers Cg-HIS-FWD-*BamHI* and Cg-HIS-REV-*NheI* and, following appropriate digestion, inserted in to the above plasmid creating pYPS1-HIS3. Digestion of this plasmid with *SacI* released a ~2.3kb fragment for transformation to produce *yps1Δ* cells. Successful transformants were selected for on YNB plates lacking histidine and further confirmed by diagnostic PCR with genomic DNA and primers YPS1-FWD-OSHOM and YPS1-REV-*SacI* which produced a band of ~2.7kb to demonstrate correct integration. By contrast cells containing wild type *YPS1* produce a band of 4.1kb.

2.1.5 *S. cerevisiae* Strains and Plasmids

S. cerevisiae BY4741 (*MATahis3Δleu2Δmet15Δura3Δ*) and a Rad6-GFP translational fusion (*MATaleu2Δmet15Δura3Δ*), in the BY4741 background (Invitrogen) were the wild type backgrounds from which other strains were derived. *S. cerevisiae* strains and plasmids constructed during this study are discussed further in Chapter 3.

A *RAD6*-GFP transcriptional fusion was constructed by amplification of the GFP cassette from pSVA12, which includes the *HIS3* selection marker (Avery et al., 2000), using primers RAD6GFP-TF-FWD and RAD6GFP-TF-REV, which each contain 50bp of flanking *RAD6* homology. The resulting ~2.2kb fragment was transformed in to *S. cerevisiae* BY4741 and selected for on YNB agar lacking histidine, and correct integration confirmed by diagnostic PCR utilising primers RAD6-FWD and RAD6-REV. These diagnostic PCR primers recognise regions outside of the transforming fragment and produce a band of ~3.5kb in *RAD6*-GFP transcriptional fusion strains while untagged *RAD6* results in a band of only ~1.8kb

In order to construct a Rad6-GFP translational fusion the Rad6-GFP cassette was amplified from the Invitrogen Rad6-GFP translational fusion strain using primers, RAD6-TLF-FWD and RAD6-TLF-REV. These primers amplify a region that includes the *HIS3* selection marker and following transformation of the resulting ~2.4kb fragment was transformed into *S. cerevisiae* BY4741 with successful integration being selected for on YNB agar lacking histidine. Further confirmation of integration was achieved via

diagnostic PCR utilising the primers RAD6-FWD and RAD6-REV which recognise regions outside of the transforming fragment produce a band of ~4kb to indicate successful transformation.

Expression of *S. cerevisiae* *SIR2* and *SWI6* from single copy plasmids was achieved by amplification of the *SIR2* and *SWI6* ORFs, along with their own promoters and terminators, from genomic DNA. Primers SIR2-FWD-PstI and SIR2-REV-XbaI amplify *SIR2* along with ~1kb and ~0.25kb upstream and downstream sequences respectively, as a PstI-XbaI fragment (~3.2kb). SWI6-FWD-BamHI and SWI6-REV-SacII enabled amplification of *SWI6* as a BamHI-SacII fragment (~3.2kb), this included ~0.66kb and 0.25kb of upstream and downstream sequence respectively (~3.3kb). These fragments were subsequently digested with the appropriate combination of restriction enzymes and ligated into the similarly digested single copy *S. cerevisiae* plasmid pRS315, to create pRS315-*SIR2* and pRS315-*SWI6*. Following transformation into *Escherichia coli* XLI blue and selection on LB ampicillin plates, successful ligation was further confirmed by digestion of pRS315-*SIR2* plasmid DNA with BamHI to produce bands of ~8.7kb and ~0.5kb. Correct ligation of pRS315-*SWI6* was demonstrated by digestion of plasmid DNA with XhoI to produce bands of ~8.6kb and ~0.7kb. Transformation of pRS315-*SIR2* and pRS315-*SWI6* into Rad6-GFP *sir2* Δ and Rad6-GFP *swi6* Δ , respectively, was followed by selection for successful transformants by growth on YNB agar lacking Leucine. Further confirmation was obtained by isolation of plasmid DNA from transformed yeast and diagnostic restriction digests using BamHI and XhoI as described above.

2.2 Growth Conditions for Experiments and Storage

Organisms were routinely maintained on yeast extract peptone dextrose (YPD) (yeast extract 10gL⁻¹, peptone 20gL⁻¹, 2% glucose, with 16 gL⁻¹ agar for plates), agar and, unless otherwise stated grown, with shaking at 120rev.min⁻¹ and 30°C, overnight to stationary phase in standard YPD broth, before dilution into fresh medium and further growth for 3 hours before experimental use (Holland and Avery, 2009). When growth at 37°C was required, the above culturing steps were performed at the alternate temperature. Synthetic complete (SC) medium was used for experiments involving nicotinic acid (NA) limitation, comprising yeast nitrogen base (YNB) without amino acids and NA (Formedium), and supplemented with SC amino acid mixture (Formedium) and 2% glucose.

The medium was supplemented with 5% (0.167 μ M) or 100% (3.25 μ M) of the normal SC nicotinic acid concentration. Cultures grown overnight at 5% or 100% NA were diluted in the same medium and grown for a further 3 hours. For experiments where nitrogen was limited, SC medium comprised of YNB without amino acids and ammonium sulphate ((NH₄)₂SO₄) (Formedium), supplemented with SC amino acid mixture and 2% glucose was used. The medium was supplemented with 5% (1.9mM) or 100% (37.8mM) of the normal SC (NH₄)₂SO₄ concentration. Cultures grown overnight at 5% or 100% (NH₄)₂SO₄ were diluted in the same medium and grown for a further 3 hours. *C. glabrata* cells were grown at different ambient pH's in Pan Fungal Medium (PFM) which was buffered to pH7.4 or pH8 with 100mM Tris-HCL, or to pH4 with 100mM glycolic acid (Schmidt et al., 2008). Cells were grown overnight at the pH of interest before dilution into the same medium and growth for a further 3 hours. Myriocin and ketoconazole (Sigma) were dissolved in methanol and added to YPD at final concentrations of 2 μ M and 100 μ M respectively. Phytosphingosine (Sigma) was dissolved in ethanol and added to YPD at a final concentration of 30 μ M (Martin and Konopka, 2004). In all cases cells were grown overnight in YPD broth supplemented with the appropriate combination of myriocin, ketoconazole, or phytosphingosine before dilution into similarly prepared YPD medium and growth for a further 3 hours.

Selection of yeast colonies following transformation (2.9.1) was performed on YPD agar supplemented with nourseothricin (Shen et al., 2005, Ferrari et al., 2009), or when required hygromycin (Table. 2). Alternately colonies were selected on YNB without amino acids (Formedium) agar (16 gL⁻¹ agar) supplemented with, the appropriate amino acids (Table. 2) and 2% glucose. If 5-FOA selection was required SC agar was supplemented with 5-FOA at a final concentration of 400 μ g ml⁻¹. Maintenance of the transformed plasmid, pCgACT-14-*SIR3*, by cells was insured through the use of YNB (without amino acids) agar and broth supplemented with 2% glucose and the appropriate amino acids, but lacking tryptophan.

In all cases *E. coli* XLI blue strains were maintained on Luria Bertani (LB) (Bertani, 1951) (10gL⁻¹ tryptone, 5 gL⁻¹ yeast extract, 10 gL⁻¹ NaCl, pH7, with 15 gL⁻¹ agar for plates), agar supplemented with ampicillin (Table. 2) and grown with shaking at 200rev.min⁻¹, 37°C, overnight in LB broth, supplemented with ampicillin (Table. 2), prior to experimental use.

In order to create electro-competent (2.9.2.1) *E. coli* XLI blue was grown in LB broth supplemented with tetracycline (Table. 2).

Short term storage of all yeast and bacterial strains took place at 4°C on the appropriate agar plates. For long term storage glycerol stocks were produced with 25% glycerol and kept at -80°C.

Table 2 - Amino Acid and Antibiotic Concentrations

Amino Acid or Antibiotic	Stock Concentration (mg ml ⁻¹)*	<i>C. glabrata</i> Working Concentration (µg ml ⁻¹)	<i>E. coli</i> Working Concentration (µg ml ⁻¹)
Histidine	10	20	-
Tryptophan	10	20	-
Uracil	2	20	-
Ampicillin	50	-	50
Tetracycline	5	-	50
Nourseothricin	200	200	-
Hygromycin	50	500	-

* Tetracycline stock solution was made in ethanol. In all other cases, stock solutions were made to the concentrations indicated in dH₂O and filter sterilised. Amino acid stock solutions were stored at 4°C and antibiotic stock solutions were stored at -20°C with the exception of hygromycin which was kept at 4°C.

2.3 Isolation of DNA

In all cases isolated genomic and plasmid DNA was stored at -20°C

2.3.1 Genomic DNA Isolation from Yeast

Yeast were grown overnight at 30°C. 1.5ml of culture was pelleted and resuspended in 250µl 0.5M sorbitol containing 100µg RNase A and 100U lyticase (L4025 Sigma). Samples were incubated for 1.5h at 37°C, with a gentle inversion at 45 minutes to remix the solution. SDS (25µl of 10% (w/v)) was added and samples were mixed gently by pipetting before incubation at 65°C for 20 min. A 200µl aliquot of 5M potassium acetate was added to the mixture, tubes were inverted to mix and incubated on ice for 10 min. Cell debris was pelleted by centrifugation at 13000g for 10 min, 450µl of the supernatant was then transferred to a new 1.5ml microfuge tube containing 450µl isopropanol. Samples were incubated on ice for 5

min followed by a second 10 minute centrifugation at 13000g. The supernatant was removed and discarded and the remaining pellet washed in 200µl of (v/v) 70% ethanol by centrifugation for 1 min at 13000g. Ethanol was removed and the pellet allowed to air dry for 5-10 min. The pellet was resuspended in 100µl dH₂O and incubated at 65°C for 5 min in order to dissolve the DNA.

2.3.2 Plasmid Isolation from E. coli

E. coli plasmid DNA was isolated from overnight liquid cultures in LB broth containing ampicillin for plasmid selection (Table. 2). Mini preparations of plasmid DNA were with the Zyppy™ Plasmid Miniprep Kit (Zymo Research Corp) as follows: Lysis Buffer (100µl) was added directly to 600µl of overnight culture or alternatively to 600µl of cells resuspended in sterile dH₂O following centrifugation (1 min, 13000g) of up to 3ml bacterial culture. Samples were mixed by inversion four-six times at which point the colour should change from opaque to clear blue indicating complete lysis. An aliquot (350µl) of cold Neutralization Buffer was added and samples mixed by inversion, resulting in a colour change to yellow and formation of a yellow precipitate. Samples were inverted a further two-three times to ensure complete neutralisation followed by centrifugation at 13000g for 4 min. The supernatant, (~900µl), was carefully transferred to a Zymo-Spin™ IIN column. The column was placed in a collection tube and centrifuged for 15 sec at 13000g, the flow through was discarded and the column placed back in the same collection tube. Endo-Wash Buffer (200 µl) was added to the column. Samples were centrifuged at 13000g for 15 sec followed by the addition of 400µl Zyppy™ Wash Buffer. A slightly longer 30 sec centrifugation at 13000g was then performed to ensure complete removal of ethanol from the column. Columns were transferred to new 1.5ml microfuge tubes and plasmid DNA was eluted by adding 30µl of Zyppy™ Elution Buffer directly to the column matrix. Samples were allowed to stand at room temperature for 1 min, and finally centrifuged at 13000g for 15 seconds.

2.3.3 Plasmid Isolation from C. glabrata and S. cerevisiae

Yeast colonies were picked into a 5ml sterile tubes containing 500µl of the appropriate YNB selection medium and vortexed for 1 min. Cultures were left to grow overnight at 30°C, 120rev.min⁻¹ before cells were transferred to 1.5ml microfuge tubes and pelleted by centrifugation at 13000g for 5 min. The supernatant was removed by pouring and the pellet

resuspended in the residual liquid, ~50 μ l. Lyticase (10 μ l at 5U/ μ l) was added and the samples mixed thoroughly by pipetting before being incubated at 37°C, 200rev.min⁻¹ for 1h. Sodium dodecyl sulfate (SDS) (20 μ l of 10% (w/v)) was added to the samples which were then vortexed for 1 min and frozen at -20°C. Samples were thawed and made up to 600 μ l with sterile dH₂O. The protocol for plasmid isolation from *E. coli* (2.3.2) was then followed from the point of adding Lysis Buffer (100 μ l).

2.4 Polymerase Chain Reaction (PCR)

PCR reactions were performed using a Techhne TC-512 gradient thermal cycler with Phusion[®] high-fidelity polymerase (Finzymes) (2.4.1, Table. 3) when high accuracy was required or Taq DNA polymerase (New England Biolabs Inc) (2.4.2, Table. 4) for diagnostic PCR reactions. PCR reactions using genomic/plasmid DNA and colony PCR (2.4.3, 2.4.4) reactions were carried out in a total volume of 50 μ l in 0.2ml PCR tubes (Star Lab). The amplification products were analysed by agarose gel electrophoresis (2.6) in the appropriate strength gel. Any PCR products required for additional use were excised from the gel and the DNA was purified by gel extraction (2.7).

2.4.1 Phusion[®] High-Fidelity Polymerase PCR Reaction

The standard reaction mixture for PCR reactions utilising Phusion[®] high-fidelity polymerase is detailed in (Table. 3). Cycling conditions for these reactions were: initial denaturation at 98°C for 30 sec, followed by 30 cycles of 10 sec at 98°C, 30 sec at (*)°C, and 30 sec kb⁻¹ of the desired product at 72°C; the 30 cycles were followed by a 10 min extension at 72°C before a final hold at 4°C

* T_m values were calculated using the nearest neighbor method. Primers >20nt were annealed at a temperature +3°C of the lower T_m primer. For primers ≤20nt an annealing temperature equal to the T_m of the lower T_m primer was used.

Table 3 - Phusion[®] High-Fidelity Polymerase PCR Reaction Mixture

Component	50 μ l Reaction
5x Phusion [®] HF Buffer	10 μ l (1x)
10mM dNTPs	1 μ l (200 μ M final conc.)
Forward Primer	0.5 μ M
Reverse Primer	0.5 μ M
Template DNA	50-250ng
DMSO (100%)	1.5 μ l
Phusion [®] DNA Polymerase	1 unit
dH ₂ O	Make up to 50 μ l final volume

2.4.2 Taq DNA Polymerase PCR Reaction

The standard reaction mixture for PCR reactions utilising Taq DNA polymerase is detailed in (Table. 4). Cycling conditions for these reactions were: initial denaturation at 95°C for 30 sec, followed by 30 cycles of 15 sec at 95°C, 30 sec at (*)°C, and 1 min kb⁻¹ of the desired product at 68°C; the 30 cycles were followed by a 10 min extension at 68°C before a final hold at 4°C

* T_m values were calculated using the nearest neighbor method. Primers >20nt were annealed at a temperature +3°C of the lower T_m primer. For primers ≤20nt an annealing temperature equal to the T_m of the lower T_m primer was used.

Table 4 - Taq DNA Polymerase PCR Reaction Mixture

Component	50 μ l Reaction
10x Standard Taq or ThermoPol Buffer	5 μ l (1x)
10mM dNTPs	1 μ l (200 μ l final conc.)
Forward Primer	0.5 μ M
Reverse Primer	0.5 μ M
Template DNA	50-500ng
Taq DNA Polymerase	1.25 units
dH ₂ O	Make up to 50 μ l final volume

2.4.3 Yeast Colony PCR

A stock solution of lyticase was diluted to 5U μ l⁻¹ and aliquoted in to 50 μ l quantities. *C. glabrata* or *S. cerevisiae* colonies were picked using either, a sterile wooden cocktail stick or pipette tip and added to the 50 μ l lyticase aliquots (1 colony per aliquot). Samples were then agitated by pipetting and incubated at 30°C for 30 min. After incubation at 95°C for 10 min, 5 μ l of each sample was used as template in a 50 μ l Taq DNA polymerase PCR reaction (2.4.2, Table. 4).

2.4.4 Bacterial Colony PCR

Colonies were picked as in (2.4.3) and added to 5 μ l dH₂O. Samples were incubated at 95°C for 10 min, and then tubes were briefly spun to collect any condensation. The whole 5 μ l was then used as template in a 50 μ l Taq DNA polymerase PCR reaction (2.4.2, Table. 4).

Table 5 – PCR Primers

Primer Name	Sequence (5'-3')
WIEPA1-FWD	GTCTTACATCGTATTCTATCTCTC
HAtag-FWD	CCGGACTATGCAGGATCCTATC
EPA1-REV-OSHOM	GATATATACTGCTTTACTGAATATCAATC
MS-SIR3-FWD	CTGAGCTTATAAAAGACCTGGAAGG
MS-SIR3-REV	TCTATTCGGTGAGACACGATTGGATCC
SIR3-FWD-SacI	GATC <u>GAGCT</u> CCCAGGATCGATACTCGCAGTAG
SIR3-FWD-SacI	GATC <u>GAGCT</u> CGGAATGCAATTCTGAAAAACAACC
YPS7-FWD	CGCGTATGAGGTGCTGGTGG
YPS7-REV	CGTCTAGCTTGTTCGATGGTATCC
YPS7-FWD-OSHOM	GCGTTGACGTTGTGCTGCTG
YPS1-FWD-SacI	AAAAG <u>GAGCT</u> CGTGGATCGTCGATCTGCGCAAG
YPS1-REV-SacI	AAAAG <u>GAGCT</u> CCGTGTCCTACCTCTATCTGGG
Cg-HIS-FWD-BamHI	GATC <u>GGATC</u> CGTGCCACCTGACGTCCTCGAG
Cg-HIS-REV-NheI	GATC <u>GCTAG</u> CGTGCCACCTGACGTCCTCGAG
YPS1-FWD-OSHOM	GCCATTACATATCATGTTTGTATAAG
RAD6GFP-TF-FWD	GAATTCAAAGATTATTTTTAGGCAGACAGAGACTAAA AGATAAAGCGTCATGTCTAAAGGTGAAGAATTATTC *
RAD6GFP-TF-REV	CGAATTCATAATATCGGCTCGGCATTCATCATTAAAGAT TCTTTTGATTTTTCTTAAACTGGATGGCGGCGTTAG *
RAD6-FWD	AGCCAGTGAGGAATCTCAAAAATTTATCC
RAD6-REV	AAGATACGGGTATCGGCAGTTATAACCG
ADH1-term-REV	GTGTGGTCAATAAGAGCGAC
RAD6-TLF-FWD	GGACGATATGGACGATGATGATGATGATGATGACGAC GACGACGACGACGAAGCAGAC
RAD6-TLF-REV	GTAATCGAATTCATAATATCGGCTCGGCATTCATCATT AAGATTCTTTTGATTTTTTC
SIR2-FWD-PstI	AAA <u>ACTGCAG</u> CGAAGATGACCAGTTGGATTTCCATTCA TACTGTATG
SIR2-REV-XbaI	CTAGT <u>CTAG</u> AGATTTGAATTTGCTGTTCCACCTGCCCT TCTTACATTAAG
SWI6-FWD-BamHI	AAA <u>AGGATC</u> CGTAAAATGCATGAAAATAAATCAATACA ACACCAAAG
SWI6-REV-SacII	AAA <u>ACCG</u> GGGCTTAAGATCTTGTAGAAGGACACATA ACAATATTTTTGG

Underlined sequence corresponds to restriction sites.

**Italics* correspond to homology to the GFP cassette from pSVA12

2.5 DNA Sequencing

High sensitivity DNA sequencing reactions were performed by the University of Nottingham, Medical School Sequencing laboratory, utilising BigDye v3.1. Analysis was performed using a 3130x1 PRISM Genetic Analyser. Primers used for sequencing are shown in (Table. 6)

Table 6 – Sequencing Primers

Primer	Sequence (5'-3')
RAD6-SEQ1	CAATTAGATAAAGTGTGAGC
RAD6-SEQ2	GATGATGATGACGACGACGAC
RAD6-SEQ3	CTATATTTTTCAAGATGAC
RAD6-SEQ4	GCGAATTTCTTATGATTTATG

2.6 Digestion of DNA with Restriction Enzymes

Restriction enzymes, were purchased from New England Biolabs Inc, and used in accordance with manufacturer's instructions. All restriction digestion reactions were performed in a total volume of 50µl. Digestion products were separated by electrophoresis on the appropriate percentage agarose gel (2.7). Where specific digestion products were required for further use (e.g. cloning) the corresponding band was excised from the gel and the DNA purified by gel extraction (2.8).

2.7 Agarose Gel Electrophoresis

Nucleic acids were separated out according to size by electrophoresis using high melting temperature agarose gels. Gels of various concentrations, typically between 0.8-1.5% (w/v) were used depending on the size of nucleic acid fragments to be resolved. Gels were routinely prepared using the appropriate amount of agarose (Seakem® LE Agarose) in 1x TAE buffer followed by heating in a microwave until the agarose had dissolved. The solution was left to cool for approximately 10 minutes at which point ethidium bromide was added to a final concentration of 0.5µg ml⁻¹ to allow visualisation of separated DNA. The solution was then poured into a mould and allowed to set for ~20 min to form a solid gel. Gels were placed into the appropriate size electrophoresis tank filled with 1x TAE buffer. Bromophenol blue DNA loading dye was

added to samples at a final concentration of 1x and they were loaded onto the gel along with either a 1kb or 100bp DNA ladder (NEB UK) (Fig. 17). Gels were run for 30-60 minutes at 80-100V using a Biorad Power-Pac 300. Following electrophoresis, separated DNA was visualised using a Biorad Gel Doc 2000.

2.8 Purification of DNA from Agarose Gels

Gel extractions were performed using the Geneflow Q-Spin gel Extraction/PCR Purification Kit (GENEFLOW). For DNA extraction from agarose gels, the appropriate fragment was excised and transferred to a 1.5ml microfuge tube. The gel fragment was weighed and an equivalent (w/v) amount of Binding Buffer was added. For agarose gels above 1.5% (w/v) twice the volume of Binding Buffer was used. Samples were incubated at 50°C with occasional vortexing until the gel had completely dissolved. The resulting solution was transferred to a spin column and allowed to stand at room temperature for 2 min. Spin columns were centrifuged for 1 min at 11000g and flow through in the collecting tube discarded. Wash Solution I (500µl) was added to each column before centrifugation for 15 sec at 11000g and the flow through discarded. This wash step was then repeated. A longer centrifugation step of 1 min at 11000g removed any residual Wash Solution I. Columns were then transferred to new 1.5ml collection tubes and 30-50µl of Elution Buffer added directly to the spin column membrane. Columns were allowed to stand at room temperature for 2 min before DNA was eluted by centrifugation for 1 min at 11000g. All DNA purified in this way was stored at -20°C.

2.9 DNA Ligations

Prior to ligation, DNA fragments were purified from their either PCR (2.4) or restriction digest (2.6) enzymatic reactions. The CloneJET™ PCR Cloning Kit (K1231 Fermentas Life Sciences) was used for cloning of blunt ended Phusion® high-fidelity polymerase (Finzymes) PCR products into the pJET1.2 blunt cloning vector. For this, 50ng of pJET1.2 blunt cloning vector were used per ligation reaction. Ligations not involving pJET1.2 were performed using 100-200ng of the appropriate vector per ligation reaction. All DNA was quantified using a Nano-Drop spectrophotometer (NanoDrop Technologies). When required, vector DNA was treated with Antarctic

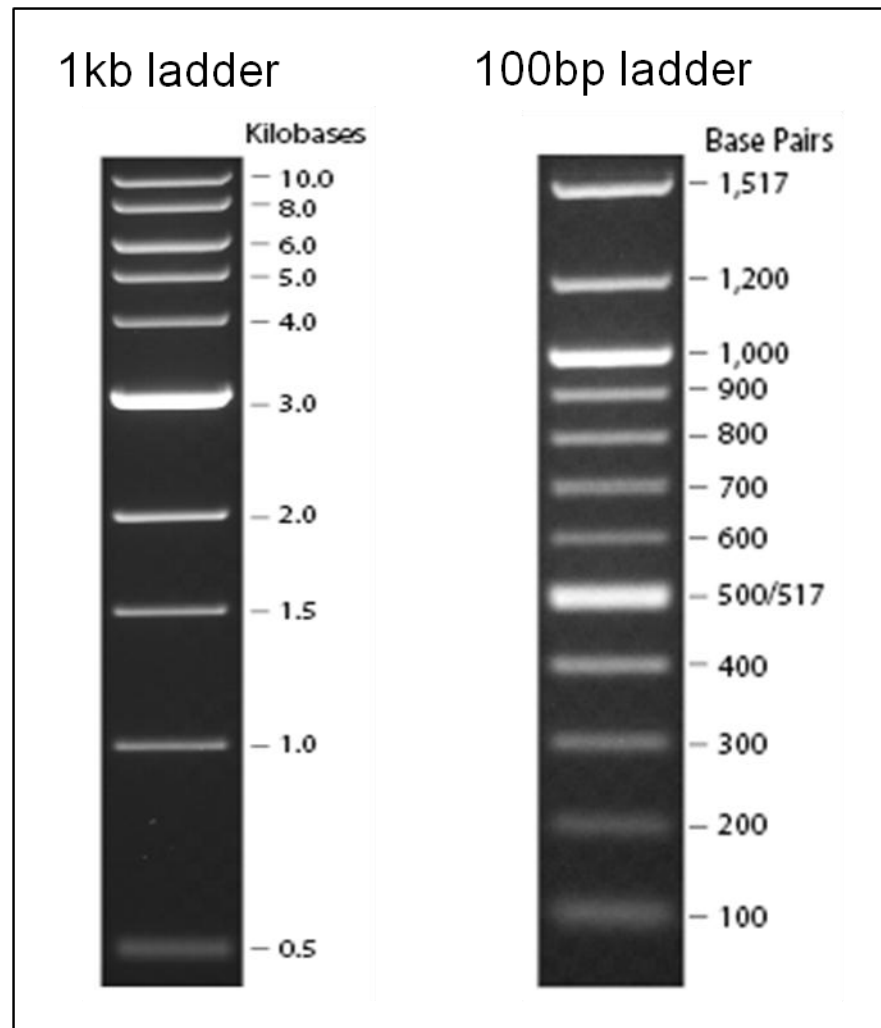


Figure 17 – 1kb and 100bp DNA ladders used in agarose gel electrophoresis

phosphatase (M0289S NEB UK) prior to ligation. All DNA ligations were performed at room temperature using T4 DNA Ligase (M0202S NEB UK or supplied with the CloneJET™) after which ligated DNA was prepared for transformation (2.10) by ethanol precipitation (2.9.1). All enzymes were used in accordance with the manufacturer's instructions. A total volume no greater than 30µl and an insert to vector fragment ratio of 3:1 was used in all cases. In order to calculate the appropriate amount of insert to include in the ligation reaction the following equation was used;

$$\text{ng Insert} = \frac{\text{ng Vector} \times \text{kb Size of Insert}}{\text{kb Size of Vector}} \times \text{Insert:Vector Molar Ratio}$$

2.9.1 Ethanol Precipitation

Ethanol precipitation was performed on ligated DNA, in microfuge tubes, prior to transformation. Initially 3M sodium acetate was added at 1/10 the volume of the sample being treated followed by 3x the sample volume of 100% (v/v) ethanol. Samples were then mixed by inversion and centrifuged at 13000g for 10 min creating a DNA pellet. The Supernatant was carefully removed so as not to disturb the pellet which was then washed with 70% (v/v) ethanol by centrifugation at 13000g for 1 min. Ethanol was removed and DNA pellets air-dried, before being resuspended in 10µl dH₂O. All samples were stored at -20°C.

2.10 Transformations

2.10.1 Yeast Transformation

A slightly modified version of the traditional lithium acetate (LiAc) method was used for all *C. glabrata* and *S. cerevisiae* transformations (Castano et al., 2003). Cells were grown to OD₆₀₀~1 in 50ml YPD medium (2.2), harvested and washed with the same volume (50ml) of dH₂O. Cells were resuspended in 500µl of 100mM LiAc and 50µl aliquots, each containing roughly 5x10⁷ cells, were used for each transformation. To each 50µl sample a transformation mix containing 240µl 50% polyethylene glycol 3350 (PEG), 36µl of 1M LiAc, 50ug of heat-denatured salmon sperm DNA (Sigma) and the DNA to be transformed dissolved in 50µl of sterile dH₂O. Typically 5-10ug of transforming DNA, quantified using a Nano-Drop spectrophotometer (NanoDrop Technologies), was used. Once all

components had been added the sample was mixed by pipetting and incubated at 30°C for 30 min. Subsequently, 45µl of DMSO was added and samples were mixed by inversion and immediately heat shocked at 42°C for 15 min. For selection using an auxotrophic marker the transformation mix was centrifuged at 5000g for 20 sec to pellet the cells. Cells were resuspended in 1ml of sterile dH₂O and allowed to recover for 5 min at room temperature before plating on selective YNB medium (2.2). For selection with antibiotic cells were allowed to recover in 5ml YPD for 1h at 30°C with shaking at 120 rev min⁻¹, after which they were pelleted and resuspended in 1ml sterile dH₂O before plating on antibiotic supplemented YPD agar (2.2).

2.10.2 Bacterial Transformation

All bacterial transformations were performed by electroporation of XL-1 blue *E. coli* cells. Electro-competent XLI blue cells (50µl) (see below 2.10.2.1) were added to transforming DNA dissolved in 10µl sterile dH₂O and gently mixed by pipetting. This mixture was transferred to an electroporation cuvette and the sample electroporated at 1.8kV, 200Ω and 25µF capacitance using a Biorad electroporater. Super optimal broth with catabolite repression (SOC) medium (2% tryptone, 0.5% yeast extract, 10mM NaCl, 2.5mM KCl, 10mM MgCl₂, 10mM MgSO₄, 20mM glucose) (1ml) was then immediately added to the electroporation cuvette and cells resuspended before being transferred to a 20ml sterile tube. Cells were allowed to recover for 1 hour at 37°C with shaking at 200 rev min⁻¹. The transformation mixture was subsequently plated onto LB agar supplemented with ampicillin (50µg ml⁻¹).

2.10.2.1 Preparation of Electro-competent E. coli XLI Blue Cells

E. coli XLI blue cells were grown overnight in 10ml LB broth supplemented with tetracycline (2.2, Table. 2). This culture was then added to 1L LB broth supplemented with tetracycline and grown to an OD₆₀₀ ~0.5-0.8. Cells were transferred to sterile centrifuge tubes and harvested by centrifugation at 8000g, 4°C for 15 min. The supernatant was removed and cells resuspended in 1L of sterile ice-cold 1mM HEPES. Cells were centrifuged at 10000g, 4°C for 15 min and again pellets were resuspended in 1L sterile, ice-cold 1mM HEPES. Resuspendend cells were centrifuged at 10000g, 4°C for 15 min before removal of the supernatant and resuspension in 100ml of sterile, ice-cold 1mM HEPES with 10%

glycerol. A final centrifugation at 10000g, 4°C for 15 min was performed and cells resuspended in 1ml sterile, ice-cold HEPES with 10% glycerol. Aliquots (52µl) of cells were transferred to sterile screw-cap microfuge tubes and frozen on dry ice. Cells were then stored at -80°C until use.

2.11 Cell Staining/Probing

Freshly harvested cells (1.5×10^6) were used for all staining procedures, after 5min incubation at 30°C with 50mM EDTA to prevent cell aggregation. Cells were collected by centrifugation (8000 g, 2 min) and pellets resuspended in 300µl phosphate buffered saline (PBS). The appropriate staining procedure (below) was then applied.

2.11.1 Probing for *Epa1*

Hemagglutinin (HA)-tagged *Epa1* was probed with anti-HA, Alexa Fluor® 488 conjugate (Molecular Probes, Invitrogen) by incubation of 1.5×10^6 with $3.5\mu\text{g ml}^{-1}$ antibody for 30 min at 4°C. Samples were washed twice with 300µl PBS (8000 g, 2 min) before analysis.

An anti-*Epa1* rabbit polyclonal antibody (Kaur et al., 2007), was a gift from Brendan Cormack. To avoid cross-reactivity, the antibody was pre-absorbed against *C. glabrata epa1Δ* cells before use: cultures were grown in SC, 5% NA medium (2.2) to induce *EPA* gene expression (Domergue et al., 2005). Cells (1×10^8) were suspended in 500µl PBS and preabsorption performed through 10 x 1 h incubations on ice with antibody (1/5 dilution), each incubation with a fresh batch of cells. The final supernatant was confirmed to have *Epa1*-specific reactivity by probing wild type and *epa1Δ* cells, grown in SC, 5% NA medium, with analysis by flow cytometry (2.12). This antibody was used to probe *Epa1* by incubating 1.5×10^6 cells for 30 min at 4°C in the presence of antibody (1/5,000 dilution). Cells were washed twice with PBS (8000 g, 2 min) and resuspended in 300µl PBS before incubation with $3.5\mu\text{g ml}^{-1}$ anti-rabbit Alexa Fluor® 488 conjugate secondary antibody (Molecular Probes, Invitrogen). After 20 min at 4°C, cells were washed twice with PBS (8000 g, 2 min) before analysis.

2.11.2 Probing for Mannoprotein

Cells (1.5×10^6) were probed for cell surface mannoprotein by staining with concanavalin A, Alexa Fluor® 647 conjugate (Molecular Probes, Invitrogen). A 5mg ml^{-1} stock solution of the conjugate in 0.1M sodium bicarbonate was added to cell samples to give a final conjugate concentration of $70\mu\text{g ml}^{-1}$. Samples were then incubated for 30 min at 4°C

before being washed twice in 300 μ l PBS (8000 *g*, 2 min) and used for analysis by flow cytometry (2.12).

2.11.3 Filipin Staining

Prior to staining cells were resuspended in 1ml PBS. A filipin stock solution (5mg ml⁻¹ in DMSO) was added at a final concentration of 5 μ g ml⁻¹, samples mixed, and cells analysed by fluorescence microscopy (2.13) within 5 min.

2.11.4 Dual Staining

When dual staining of cells was required with anti-HA, Alexa Fluor[®] 488 conjugate and concanavalin A, Alexa Fluor[®] 647 conjugate staining was performed simultaneously as described above (2.11.1, 2.11.2). For dual staining with anti-HA, Alexa Fluor[®] 488 conjugate and filipin, staining was performed first with anti-HA, Alexa Fluor[®] 488 conjugate (2.11.1) followed by filipin just before analysis (2.11.3).

2.11.5 Actin Staining

Cells were fixed with formaldehyde (4% v/v) with inversion at 30°C for 15 min before being pelleted by centrifugation at 8000*g* for 1 min and resuspended in PBS. Samples were then incubated with 4% (v/v) formaldehyde for a further 1h at room temperature. The fixed cells were washed 5 times in PBS and resuspended in 50 μ l PBS. An 8 μ l aliquot of cells was removed and 2 μ l of Alexa Fluor[®] 488 phalloidin (Invitrogen) added, before incubation in the dark at room temperature with vortexing every 15 min for 90 min. Samples were washed 5 times in PBS prior to analysis.

2.12 Flow Cytometry and Fluorescence Activated Cell Sorting (FACS)

Analysis by flow cytometry was with a BD FACSCanto instrument, equipped with a 488 nm argon-ion laser (BD Biosciences). After staining (2.11) cell samples were suspended in 300 μ l PBS in flow cytometry tubes (BD Biosciences). Alexa Fluor[®] 488 fluorescence was measured via a FITC filter and Alexa Fluor[®] 647 fluorescence via an APC-A filter. Data was recorded for 10,000 cells per sample, at ≤ 5000 cells sec⁻¹. When quantification of fluorescence for dual stained cells was required compensation controls, which take and fluorescence overlap into account, were set for each fluorochrome using single stained cells. Data were stored and analyzed using FACS DIVA (BD Biosciences), with additional analysis

using Weasel software (the Walter and Eliza Hall Institute of Medical Research, Australia). Fluorescence measurements with the FACSCanto were normalized for cell size, by forward scatter (FSC-A) correction. Unless indicated otherwise (Newman et al., 2006), these normalized data were used to determine Coefficients of Variation (CV), excluding the outlying top and bottom 0.1% of data. When an alternate method of CV calculation was utilised this was as described by Newman et al (2006). Cell sorting (FACS) was performed with a Coulter Altra flow cytometer. Similar sized cells, as determined by FSC-A values, were gated into the lowest- or highest- 13% of Epa1-HA fluorescence. Cells from each subpopulation (1×10^6) were sorted directly onto ice prior to RNA extraction (2.15).

2.13 Fluorescence Microscopy

Cells were examined through a 100x objective lens with a Nikon Eclipse Ti microscope equipped with a DS-Qi1 camera and temperature controlled chamber. Image acquisition was with NIS elements Br Software (Nikon). Following staining (2.11), cells were pelleted by centrifugation at 8000g for 2min and resuspended in 10 μ l PBS. An aliquot (1 μ l) of stained cells was added to a microscope slide and covered with a coverslip prior to imaging. Imaging was performed using the bright field filter for all cells. Alexa Fluor[®] 488 fluorescence was imaged using the FITC filter while filipin fluorescence was observed using the DAPI filter. Cell fluorescence was quantified per unit cell area with Image J software, using the region of interest (ROI) tool.

2.13.1 Time Lapse Microscopy

For time lapse studies 5×10^6 freshly harvested cells, incubated for 5min at 30°C with 50mM EDTA to prevent cell aggregation, were used for (HA)-tagged Epa1 probing with anti-HA, Alexa Fluor[®] 488 conjugate (2.11). Stained cells were resuspended in 1ml PBS and added to glass chambers (WAKI), pre-coated with 1 mg ml⁻¹ concanavalin-A and air dried, where they were allowed to adhere for 20 min at 4°C. The supernatant above adhered cells was removed and the chamber washed gently with 1 ml PBS to remove nonadherent cells, before adding 1ml of pre-warmed (30°C) YNB broth with appropriate amino acid supplements (2.2). The time course was started immediately with the temperature controlled chamber pre-heated to 30°C. Bright field and fluorescence images, using the FITC channel, were captured at 10 min intervals.

2.14 Adherence Assay

HEp-2 epithelial cells were grown (5% CO₂, 37°C) to confluence in Dulbecco's Modified Eagles medium (DMEM) supplemented with 10% (v/v) fetal calf serum, 100U ml⁻¹ penicillin, 0.1 mg ml⁻¹ streptomycin, and 2mM L-glutamine before splitting with 0.25% (w/v) trypsin, 0.53mM EDTA. After incubation for 24–48 h in DMEM, 24-well tissue culture plates (Nunclon®) were seeded with 1 x 10⁴ cells ml⁻¹ in DMEM and incubated at 37°C for 2 d. Confluent monolayers were washed twice with Hank's Buffered Salt Solution (HBSS, Sigma) and fixed for 10 min in 4% (v/v) paraformaldehyde, before three 5-min washes with PBS. *C. glabrata* cells grown to exponential phase at 30°C and at 37°C in YPD broth (2.2) were diluted to 2,000 cells ml⁻¹ in HBSS before 1 ml of cells was added to individual wells containing the HEp-2 monolayers. Plates were centrifuged (500 g, 1 min) and incubated at 37°C for 30 min to allow adherence. Supernatant was removed by pipetting, followed by three washes with 500µl HBSS to remove unbound cells. Monolayers and bound *C. glabrata* cells were released by incubation at 37°C for 15 min with 500µl 2% (w/v) trypsin in PBS. After addition of 10µl of 10% (v/v) Triton X-100, 50µl 100mM EDTA and 40µl YEPD broth, released cells were plated in replicate on YEPD agar and incubated at 30°C for at least 2d. Colonies were counted to determine adherent cell numbers.

2.15 RNA Extraction

Total RNA was isolated using an RNeasy® Mini Kit (Qiagen) either from 1 x 10⁶ (after FACS, 2.12) or 1 x 10⁷ cells on all other occasions. This kit utilizes the selective binding properties of a silica based membrane within RNeasy® mini spin columns. If not indicated otherwise all centrifugation steps were performed at room temperature, 8000g. Cell samples were centrifuged for 5 min, 1000g at 4°C. Cell pellets were resuspended in 100µl of freshly prepared buffer Y1 (1M sorbitol, 0.1M EDTA, pH7.4, just before use 0.1% (v/v) β-mercaptoethanol and lyticase (50U per 1x10⁷ cells) were added), containing 50U of lyticase and incubated for 10 min at 30°C with gentle shaking to generate spheroplasts. Buffer RLT (350µl) was added and the samples vortexed vigorously to lyse the spheroplasts, after which 250µl of 100% ethanol was added and mixed by pipetting. The homogenized lysate was transferred to an RNeasy® mini spin column, placed in a 2ml collection tube, and centrifuged for 15 sec. Flow-through was discarded and 700µl Buffer RW1 added before spinning

for 15 sec. The flow through was again discarded and the column washed with 500µl Buffer RPE by centrifugation for 15 sec. This step was repeated with centrifugation for 2 min. An additional centrifugation step at 13000g for 1 min ensured complete removal of Buffer RPE. The columns were transferred to new 1.5ml collection tubes and 30-50µl of RNase free water, added to the spin column membrane. RNA was finally eluted by centrifugation for 1 min and stored at -20°C. All RNA was quantified using a Nano-Drop spectrophotometer (NanoDrop Technologies)

2.16 Reverse Transcription

Reverse transcription was performed using SuperScript™ III Reverse Transcriptase (RT), and Oligo(dT)₂₀ Primer (Invitrogen) according to the manufacturer's instructions. RNase free conditions were maintained with RNaseOUT™ Recombinant RNase Inhibitor (Invitrogen) and nuclease-free microcentrifuge tubes were used throughout. Initially 1µl of oligo(dT)₂₀ (50µM) was added to a microfuge tube, this was followed by 10pg-5µg total RNA and 1µl of 10mM dNTP mix. If required sterile dH₂O was added up to a volume of 13µl. Samples were heated to 65°C for 5 min followed by at least a 1 min incubation on ice. The contents of the microfuge tubes were collected by a brief centrifugation before addition of; 4µl 5X First Strand Buffer, 1µl of 0.1M dithiothreitol (DTT), 1µl of RNaseOUT™ Recombinant RNase Inhibitor, and 1µl of SuperScript™ III RT (200U/µl). The samples were mixed by gentle pipetting and incubated at 50°C for 1h after which the reaction was inactivated by heating to 70°C for 15 min. The resulting cDNA was then prepared by PCR purification using the Geneflow Q-Spin gel Extraction/PCR Purification Kit (GENEFLOW). In this instance an equivalent volume of Binding Buffer was added to cDNA samples and the solutions mixed. Samples were then incubated at room temperature for 1 min before being transferred to a spin column after which all steps were performed as described for gel extraction in (2.8). All cDNA purified in this way was quantified with a Nano-Drop spectrophotometer (NanoDrop Technologies) and subsequently used for quantitative RT-PCR (qRT-PCR) (2.17). Samples were stored at -20°C.

2.17 Quantitative RT-PCR (qRT-PCR)

qRT-PCR was performed in triplicate reactions, each comprising 30ng cDNA, 100nM of each gene specific primer (Table. 7), and 1X Fast

SYBR[®] Green master mix (Applied Biosystems), made up to 10µl with RNase free water. Reactions were performed in sealed 96-well plates and monitored with a 7500 Fast Real Time PCR System (Applied Biosystems) using 7500 software v2.0.4 (Applied Biosystems). The most appropriate annealing temperatures were chosen based on gradient PCR reactions using Taq DNA polymerase (2.4.2), and the relevant primers with genomic DNA and were as follows: 56°C for *EPA1*, *EPA6*, and *EPA7*; 59°C for *α2*, 58°C for *ACT1*, and 67°C for *SIR3*. For annealing temperatures below 60°C a three-step 40 cycle protocol of, 3 sec at 95°C, 30 sec at the appropriate annealing temperature, 30 sec at 60°C. When annealing temperatures were above 60°C a two-step protocol was utilised with reactions being run for 40 cycles of 3 sec at 95°C, 30 sec at the appropriate annealing temperature. In all cases a melt curve was included after the amplification stage to check for the detection of just one product. Amplification was quantified from a standard curve constructed from reactions with defined copy number of the expected PCR product (2.17.1). Results were analysed with 7500 software v2.0.4.

2.17.1 Calculation of DNA Copy Number for qRT-PCR Standard Curves

Determination of copy number for the PCR products to be used in the construction of standard curves was achieved by calculation of the molecular weight (MW) (g mol^{-1}) of dsDNA PCR products and subsequent determination of the number of molecules in 1ng of DNA. The MW of dsDNA PCR products for use in standard curve reactions were calculated using the following equation:

$$MW (\text{g mol}^{-1}) = (\text{Size of DNA (bp)} \times 607.4) + 157.9$$

The resulting MW (g mol^{-1}) value was used to determine the number of moles present in 1g of material. Using Avogadro's number (6.022×10^{23} molecules mole^{-1}), the number of template molecules g^{-1} can be calculated:

$$\text{Molecules } \text{g}^{-1} = \text{moles } \text{g}^{-1} \times \text{Avogadro's number (molecules } \text{mole}^{-1})$$

The resulting values can be converted to ng to give the number of molecules (copy number) in 1ng of template DNA.

The template PCR products were quantified using a Nano-Drop spectrophotometer (NanoDrop Technologies) and diluted to 1ng ml^{-1} before four further serial 10-fold dilutions, 1µl of each dilution was utilised in

standard curve reactions. Consequently a standard curve could be constructed from reactions with defined copy number of the expected PCR product.

Table 7 – qRT-PCR Primers

Primer Name	Sequence (5'-3')
EPA1-RT-FWD	GGGCTCAAAAACAGCTAAAG
EPA1-RT-REV	TAACAGTGTTTTCGTTTGAT
EPA6-RT-FWD	GGGTTCTCAAACAGCTAAGG
EPA6-RT-REV	GTACTIONCGCTGTTTGATACA
EPA7-RT-FWD	TACGGAAGAATGGTTCGTAC
EPA7-RT-REV	GCTTGCCGGTAAATGATCT
α 2-RT-FWD	GAAATCAAGAATTAGTATTACGCATC
α 2-RT-REV	GGGTAAACTGGAACACAATGATATAAGT
ACT1-RT-FWD	CGCCGGTGACGATGCTCC
ACT1-RT-REV	CTTGGATTGAGCTTCGTC
SIR3-RT-FWD	CGGTCTGCTCGCGATTTTGAG
SIR3-RT-REV	TTACAGTATTGTCGGTATCCTCAGCC

2.18 Digestion, Separation and Probing of *EPA1*-containing High Molecular Weight DNA

2.18.1 Isolation of High Molecular Weight DNA in Agarose Plugs

To preserve high molecular weight DNA fragments, genomic DNA was isolated in low melting temperature agarose plugs. *C. glabrata* cultures were grown overnight in YPD at 30°C (2.2), pelleted by centrifugation for 5 min at 3000g and resuspended in 200 μ l cold EDTA (50mM). All remaining steps were performed in a fume hood. Cells were transferred to 1.5ml microfuge tubes before adding 100 μ l of 1 M sorbitol, 0.1 M sodium citrate, 50mM EDTA pH 5.8, 25 μ l ml⁻¹ β -mercaptoethanol, 3mg ml⁻¹ Zymolase 20T. This was mixed with 500 μ l of warm 1% (w/v) low melting point agarose, made up with 0.125M EDTA and heated in a microwave until dissolved. Agarose aliquots (~100 μ l) were added to pre-sealed and cooled plug moulds (Biorad) and allowed to set for 1h. Set plugs were removed from the moulds and incubated overnight at 37°C with 500 μ l of 0.45M

EDTA, 0.1M Tris, 5µl ml⁻¹ β-mercaptoethanol, in 1.5ml microfuge tubes covered with Saran wrap. The solution was removed and the plugs overlaid with 500µl of 1% (w/v) Sarkosyl, 0.4M EDTA, 1mg ml⁻¹ Proteinase K, 0.1mg ml⁻¹ RNase, before a further overnight incubation at 37°C. Plugs were cooled to room temperature and the solution overlay removed. This was followed by rinsing the plugs with 500µl of 0.5 M cold EDTA, which was removed before the plugs were overlaid with 500µl of 0.45 M EDTA, 0.1 M Tris. Plugs were stored at 4°C until use in restriction digest reactions.

2.18.2 Digestion of DNA Isolated in Agarose Plugs

Approximately one third of a plug (2.18.1) was used for each digestion. Each plug was equilibrated in 500µl 1x Tris-EDTA (TE) buffer (10mM Tris pH7.5, 1mM EDTA pH8) for 3 x 1h incubations at 37°C. This was followed by 3 x 1h incubations in 500µl of a buffer comprising 50mM potassium acetate, 20mM Trizma acetate, 1mM (DTT), 0.1 mg ml⁻¹ bovine serum albumin (BSA), pH 7.9. Samples were placed on ice before transfer to an equivalent volume of fresh buffer and addition of 60U *PmeI* or *StuI*. After 1h on ice, the volume was made up to 500µl with the same buffer including a final concentration of 10mM magnesium acetate and incubated overnight at 37°C. Digested plugs were rinsed with TE buffer and then stored in 500µl TE buffer at 4°C prior to separation of DNA by field inversion gel electrophoresis (FIGE).

2.18.3 Field Inversion Gel Electrophoresis (FIGE)

Conventional electrophoresis can effectively separate DNA fragments up to 20 kb. Pulsed field gel electrophoresis (PFGE) can resolve larger fragments by alternating the electrical field between spatially distinct pairs of electrodes. During field inversion gel electrophoresis (FIGE) the electrical field is fixed at 180° and inverted in the forward and reverse directions enabling sample resolution in the 0.1-250 kb size range. Agarose plugs were loaded into individual wells of a 1% (w/v) agarose gel (2.7) made up with 0.5% TBE buffer. MidRange PFG marker I (NEB UK) (Fig. 18) was also added to a well. Digested-DNA was separated by FIGE, using 0.5% (w/v) TBE as running buffer and a Biorad FIGE mapper programmed to resolve fragments of 20-50 kb. Digested DNA was visualised by staining the gel in 0.5µg ml⁻¹ ethidium bromide (in dH₂O) for 30 min and photographed using a Biorad Gel Doc 2000.

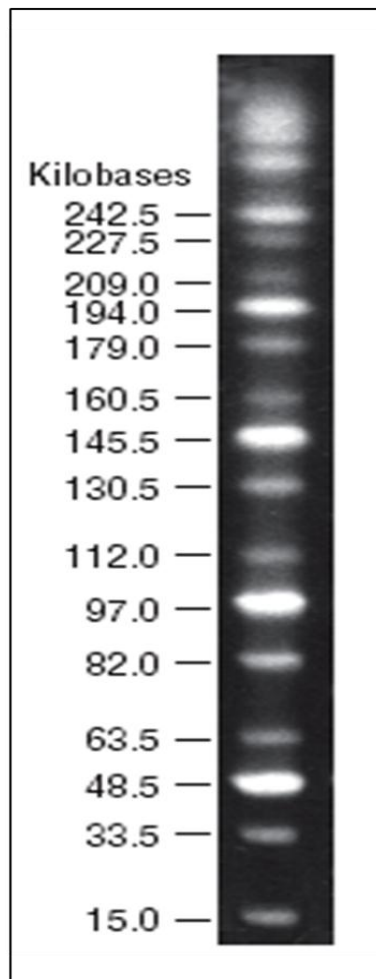


Figure 18 – MidRange PFG Marker I (NEB UK)

2.18.4 Southern Transfer and Probing for *EPA1*

Southern transfer was performed according to the standard capillary action protocol whereby DNA molecules are transferred from the gel to a porous nylon membrane (Biorad zeta-probe GT membrane) using absorbent paper to draw solution through the gel and the membrane (Southern, 2006).

Bands of interest were detected using a 416bp probe specific to *EPA1*, amplified by PCR from genomic DNA using Phusion[®] high-fidelity polymerase (2.4.1) and primers 5'-GTTTCGTTCAACACTTCCTTCATCAGCAGGC-3' and 5'-CTTTGTGATAAGCTGGTCATGATAATGCCTGC-3' and labelled with dCT³²P using a HighPrime labelling kit (Roche) according to the manufacturers' instructions. Prior to probe hybridisation the nylon membrane containing transferred DNA was neutralised for 5 min in 500ml 2x SSPE before being placed in a hybridisation tube and prehybridised for >3h at 65°C in the presence of 40ml prehybridisation solution (Table. 8). The dCT³²P-labelled probe was added to 450µl denatured fish DNA (10mg ml⁻¹) and the solution boiled for 4 min before being chilled on ice and added to 30ml of hybridisation solution (Table. 8). This hybridisation solution was added to the hybridisation tube immediately after removal of the prehybridisation solution and incubated overnight at 65°C. Hybridisation solution was removed and the membrane washed, with incubation at 65°C, by the addition of 50ml wash solution I (Table. 8) for 10 min. A second wash with the same solution was performed for 30 min, followed by 2x 30 min washes with 50ml of wash solution II (Table. 8). Finally the membrane was removed from the hybridisation tube and excess liquid blotted off before imaging electronically (Biorad Developer) to detect dCT³²P-labelled probe binding. Resulting bands were sized against a standard curve constructed in Excel, according to the distances migrated by DNA ladder fragments of known size.

Table 8 – Solutions for dCT³²P-Labelled Probe Hybridisation

Components for the solutions described below were obtained from Sigma.

Solution	Components
20x SSPE	NaCl - 175.3g NaH ₂ PO ₄ -H ₂ O - 27.6g EDTA 7.4g pH 7.4 Make up to 1L with dH ₂ O Autoclave
100x Denhardt's	Ficoll [®] 400 - 1g Polyvinylpyrrolidone (PVP360) - 1g BSA (fraction V) - 1g Make up to 50ml with dH ₂ O Filter sterilize Store at -20°C
Prehybridisation Solution	SSPE - 6x (above) SDS - 1% Denhardt's - 5x (above) Denatured Fish DNA* - 200µg ml ⁻¹ Make up to 40ml with dH ₂ O heated to 50°C
Hybridisation Solution	Dextran Sulphate - 1.5g SSPE - 6x (above) SDS - 1% Make up to 30ml with dH ₂ O heated to 50°C
Wash Solution I	SSPE - 2x SDS - 0.5%
Wash Solution II	SSPE - 0.2x SDS - 0.5%

*Fish DNA (10mg ml⁻¹) was denatured by boiling for 5 min before being chilled on ice.

2.19 Statistical Analysis

Statistical analysis of data was performed by Student's t-test using excel order to indicate if observed differences were statistically significant. Statistical significance was inferred when resulting *p* values were below 0.05 (*p* < 0.05) while *p* > 0.05 indicated a lack of significance.

Chapter 3 - Heterogeneity in Rad6 Expression

3.1 Introduction

The genes responsible for DNA damage tolerance in *S. cerevisiae* are grouped into the *RAD6* pathway, named after its founding and most prominent member. Members of this pathway have been classified into either the TLS branch, also known as the error prone pathway, or the error free branch of damage tolerance, both of which have been discussed more fully in the introduction to this thesis (1.6). Briefly, however, these pathways enable DNA lesions occurring at ssDNA to be bypassed without the need for lesion removal. The majority of repair mechanisms act via excision of the damaged region followed by resynthesis based on sequence information from the complementary strand. Consequently DNA damage bypass is important at regions of ssDNA, such as those found at the replication fork, where no complementary strand exists to allow resynthesis of an excised region. The DNA damage tolerance pathways therefore allow DNA replication to be completed and ssDNA gaps to be filled in the presence of damage (Ulrich, 2005, Andersen et al., 2008, Ulrich, 2009, Waters et al., 2009). Despite their different mechanisms, initiation of both damage tolerance pathways requires the Rad6 ubiquitin conjugating enzyme (E2) and the ubiquitin ligase (E3) Rad18. The two proteins form a heterodimeric complex which is recruited to sites of ssDNA damage, likely through the ssDNA binding activity of Rad18, and acts to monoubiquitinate PCNA (Andersen et al., 2008, Ulrich, 2009). Such monoubiquitinated PCNA promotes the TLS pathway of damage tolerance which is proposed to act via a polymerase switching model making use of one of more damage tolerant TLS polymerases (Ulrich, 2009, Waters et al., 2009). Further polyubiquitination of PCNA by Mms2-Ubc13-Rad5 activates error free lesion bypass which is thought to occur by a template switching model (Andersen et al., 2008, Branzei et al., 2008, Ulrich, 2009).

DNA damage tolerance constitutes the central and best characterised role of *S. cerevisiae* Rad6, however, the protein appears to be a multifunctional ubiquitin conjugating enzyme and is known to interact with two additional ubiquitin ligases, Bre1 and Ubr1 (Andersen et al., 2008, Game and Chernikova, 2009). The Rad6-Bre1 heterodimer acts to monoubiquitinate histone H2B at the Lys-123 residue. This modification facilitates histone H3 di- and tri-methylation at Lys-4 and Lys-79 (Game and Chernikova, 2009), which subsequently affects numerous cellular functions including transcriptional regulation and silencing as discussed in the introduction to this thesis (1.5) (Verzijlbergen et al., 2009, Norris and

Boeke, 2010, Takahashi et al., 2011). Indeed *RAD6* mutant strains have been identified to exhibit deficiency for Sir-dependent silencing (Huang et al., 1997). In addition the Rad6-Bre1 complex is involved in a less well known aspect of Rad6-mediated DNA repair as H3 methylation, particularly at Lys-70, can substantially influence DNA damage checkpoint activation and repair. In *S. cerevisiae* this pathway is required for G1 checkpoint activation and contributes to the homologous recombination pathway of DNA repair in G2 cells (Game and Chernikova, 2009). The interaction of Rad6 with Ubr1, on the other hand, is required for Rad6-mediated N-end rule ubiquitination and protein degradation (Ulrich, 2002, Andersen et al., 2008, Game and Chernikova, 2009).

Previous work in the Avery lab indicated, through the use of an *S. cerevisiae* strain expressing a Rad6-GFP translational fusion (Invitrogen) and subsequent analysis by flow cytometry, that Rad6 protein expression was bimodal: apparent high- and low-expressing subpopulations were distinguishable. This observation seemed independent of cell size since normalization of GFP fluorescence by forward scatter (FSC), which provides a measure of cell size, did not result in loss of the two subpopulations (Fig. 19). In contrast, deletion of either *SIR2* or *SWI6* did abolish the two subpopulations which were replaced with one high expressing population (Fig. 19). Deletion of *SIR2* is known to cause loss of transcriptional silencing (Huang, 2002, Liou et al., 2005) suggesting that the different Rad6 expression levels could reflect differing silencing capacities of individual cells. Furthermore Rad6, along with the Sir proteins, is required for silencing at both telomeres and the *HM* loci in budding yeast, (Huang et al., 1997), thus raising the question of whether Rad6 may regulate its own expression. Sir2 function impacts a number of processes including cell aging, cell cycle progression and, interestingly, regulation of cellular response to DNA damage (North and Verdin, 2004) which could be related to the observed induction of Rad6 in the *sir2Δ* mutant.

Swi6 on the other hand was initially targeted for study here due to its role in *S. pombe*, where the protein binds histone H3 and is a crucial silencing component with silencing being predominately mediated by Swi6 containing complexes (Bannister et al., 2001, Huang, 2002, Buhler and Gasser, 2009). By contrast *S. cerevisiae* Swi6 acts as a transcription cofactor that does not bind DNA directly but rather forms the SBF and MBF complexes via interaction with either Swi4p or Mbp1p, respectively. The

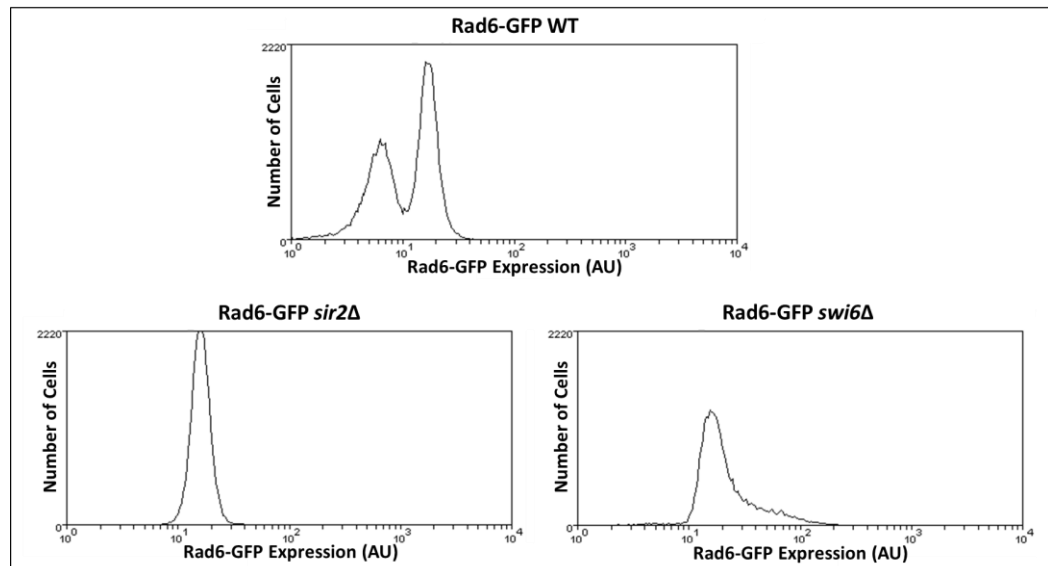


Figure 19 – Analysis of Rad6 expression (AU=arbitrary units) by flow cytometry through use of a Rad6-GFP translational fusion containing strain in wild type (WT), *sir2*Δ and *swi6*Δ cells, (Data from A. L. Bishop).

transcription factor complexes activate transcription maximally in late G1, with down-regulation occurring during G2 and M phases, both actions appearing to require *SWI6* (Lowndes et al., 1992, Sedgwick et al., 1998, Breeden, 2003). The SBF complex may have an additional role in the transcriptional response to cell wall stress (Kim et al., 2010). Swi6 is known to contain at least four ankyrin repeat (ANK) motifs which have been shown to have an antagonistic effect on transcription. Such transcriptional attenuation may have a role in modulating the periodic transcriptional activation mediated by Swi6 during the cell cycle (Sedgwick et al., 1998). One possible explanation for the Rad6 results could be that Swi6 exerts some partial repression on Rad6 expression, which is subsequently lost upon deletion of the genes. Alternatively, *SWI6* deletion may affect Rad6 expression indirectly.

This chapter set out to corroborate the above observations through complementation of both the *SIR2* and *SWI6* deletions and to elucidate further the basis for the apparent heterogeneity in Rad6 expression.

3.2 Complementation of the *sir2* Δ and *swi6* Δ Deletions in Rad6-GFP Expressing Cells

In order to corroborate that loss of the two Rad6-GFP expression subpopulations following deletion of either *SIR2* or *SWI6* (see introduction to this chapter) genuinely resulted from loss of either gene, these deletions were complemented. The complementation strategy required construction of single copy plasmids containing the genes expressed under the control of their respective promoters and terminators.

3.2.1 Construction of *SIR2* and *SWI6* Single Copy Plasmids

Both *SIR2* and *SWI6* were initially amplified from genomic DNA from *S. cerevisiae* BY4741 utilising primers SIR2-FWD-PstI/SIR2-REV-XbaI and Swi6-Fwd-BamHI/Swi6-Rev-SacII (Materials and Methods) to generate PstI/XbaI and BamHI/SacII fragments respectively. These fragments encompassed sufficient upstream and downstream sequence to include both native promoters and terminators. The amplified PCR fragments were ligated into appropriately digested yeast single copy vector pRS315 to create pRS315-*SIR2* and pRS315-*SWI6* (Fig. 20).

3.2.2 Complementation of Rad6-GFP *sir2* Δ and Rad6-GFP *swi6* Δ Strains does not restore Bimodal Rad6-GFP Expression

In order to complement Rad6-GFP *sir2* Δ and *swi6* Δ deletion strains pRS315-*SIR2* or pRS315-*SWI6* were transformed into the appropriate strain to reintroduce the relevant wild type gene. As discussed earlier, these deletion strains exhibit loss of one of the Rad6-GFP subpopulations previously identified in wild type cells. Assuming that such a phenotype is genuinely attributable to loss of either *SIR2* or *SWI6*, reintroduction of these genes would be expected to restore bimodal Rad6-GFP expression. However, introduction of pRS315-*SIR2* or pRS315-*SWI6* did not accomplish this, as demonstrated by flow cytometry (Fig. 21A, B), although reintroduction of *SWI6* did induce a slight decrease in Rad6-GFP levels. This lack of complementation argued against a role for Sir2 or Swi6 in the generation of bimodal Rad6-GFP expression. Moreover, in parallel analysis wild type cells were observed not to demonstrate two Rad6-GFP subpopulations, but rather either a high- or low-Rad6-GFP expressing phenotype was seen in different wild type cultures (Fig. 21C). High expressing cultures exhibited similar Rad6-GFP expression to that seen in the *sir2* Δ and *swi6* Δ deletion strains. In the low expressing cultures, many

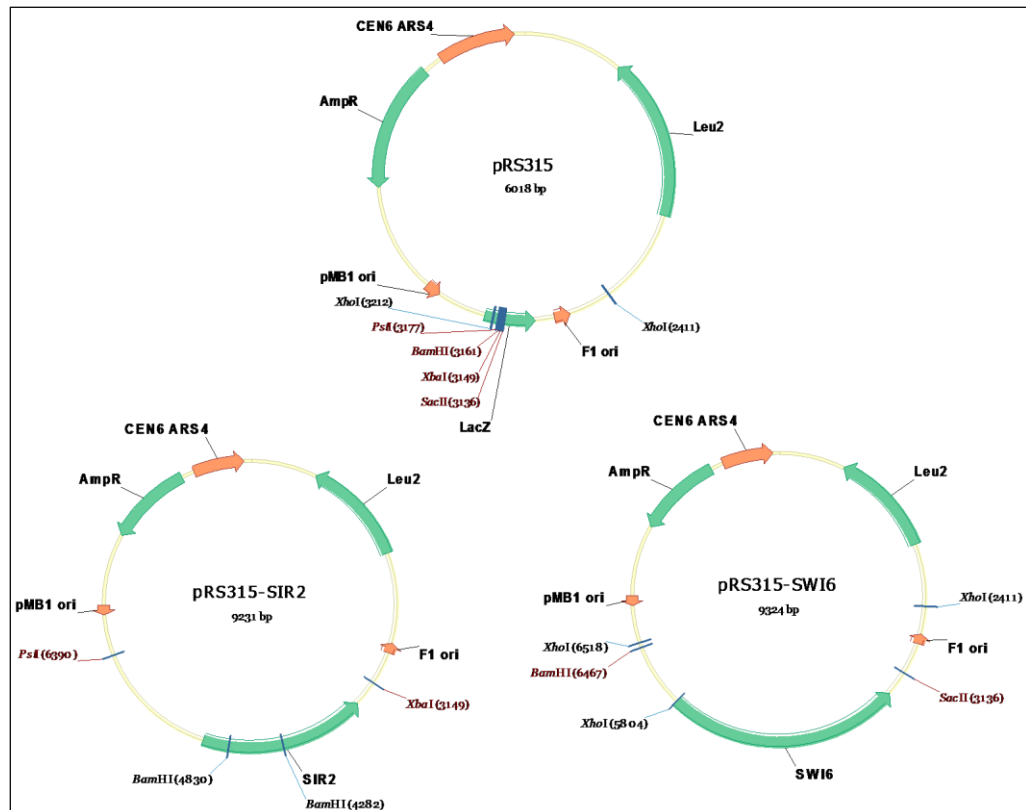


Figure 20 – Single copy plasmids pRS315, pRS315-SIR2 and pRS315-SWI6. Plasmids pRS315-SIR2 and pRS315-SWI6 were used for complementation of Rad6-GFP *sir2* Δ and Rad6-GFP *swi6* Δ respectively.

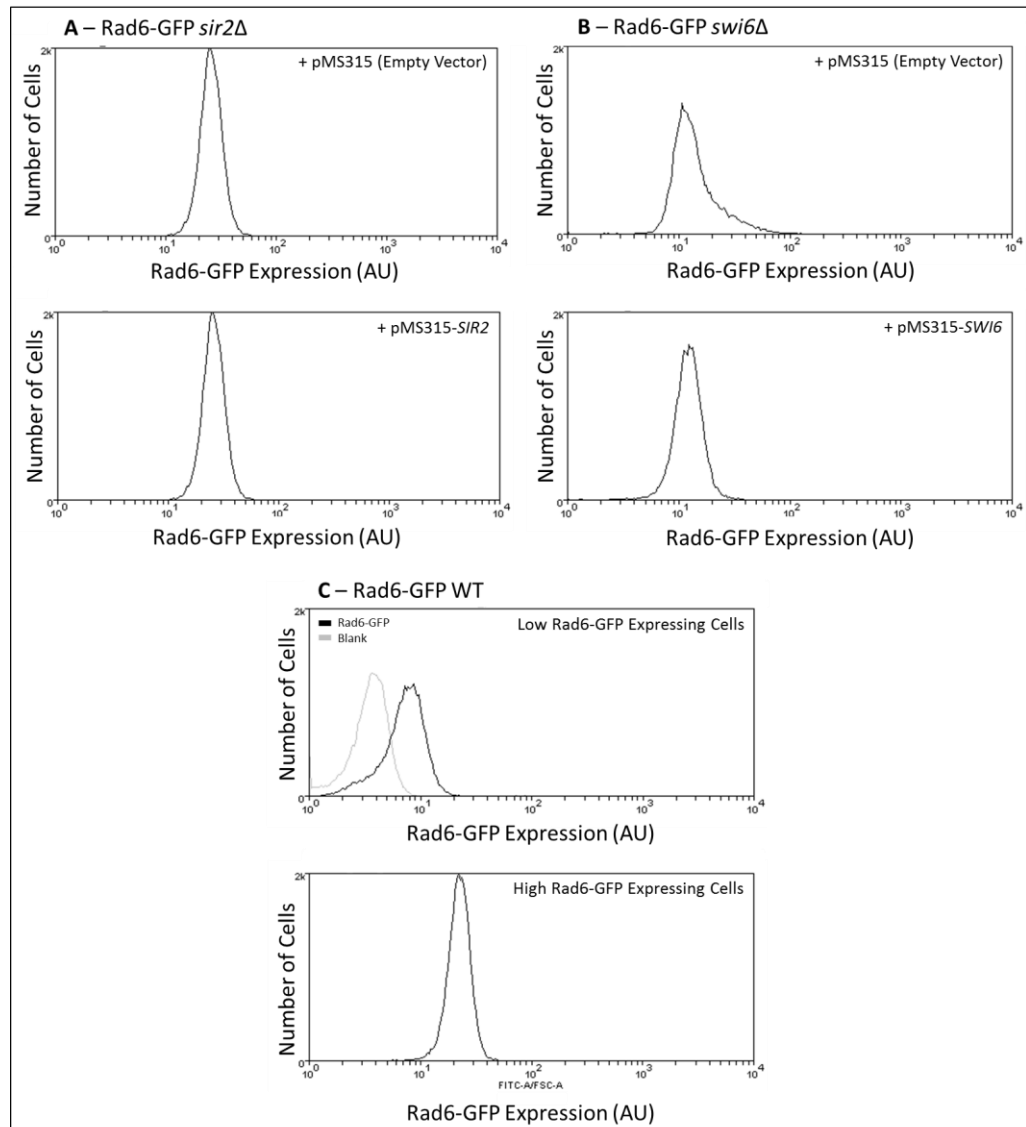


Figure 21 – Flow cytometric analysis of Rad6-GFP expression (AU) in exponential **(A)** Rad6-GFP *sir2Δ* and **(B)** Rad6-GFP *swi6Δ* cells with and without pRS315-*SIR2* or pRS315-*SWI6* respectively and **(C)** wild type Rad6-GFP cells exhibiting **(top)** low- (autofluorescence from unlabelled cells is indicated in grey) and **(bottom)** high-Rad6-GFP expression (AU).

cells fell into the region of autofluorescence exhibited by unlabelled wild type cells, indicating that Rad6-GFP expression within these cells can be considered minimal. The Low-expressing Rad6-GFP phenotype was identified with greater frequency, being seen in ~71% of the 35 cultures tested. These observations suggested that Rad6-GFP expression did not occur as two subpopulations within a culture derived from a single colony, although expression levels can differ markedly between cultures derived from different colonies. It appeared that the previous data (see introduction to this chapter) had been derived from cultures inoculated with cells from mixed colonies.

3.3 Rad6 Expression Levels are Maintained for Many Generations

If the two Rad6-GFP expression levels observed in cultures derived from different colonies is indeed due to some form of epigenetic regulation, rather than genetic mutation, then it is logical to expect cells to switch between the 2 states. In order to identify any switching, three cultures of each expression state were maintained in exponential phase by daily subculture with analysis by flow cytometry at one, four, and ten days (Fig. 22). No switching was observed in any culture up to four days and after ten days only one of three low expressing cultures began to show any signs of switching towards a higher expression state (Fig. 23A). Subsequent analysis revealed high-Rad6 expressing cells to demonstrate a slightly quicker growth rate of ~1.4 hours compared to the ~1.5 hours for equivalent low expressing cells (Fig. 23B). It was thus suggested that the one culture to demonstrate an apparent switching capacity after ten days may have arisen due to initial contamination with some cells of a high expressing colony. It may have taken up to ten days outgrowth for the faster growing contaminant to become detectable by flow cytometry.

Retention of the expression state over such extended periods of time was not indicative of phenotypic heterogeneity that did not have a genotypic basis. Rather it would suggest the existence of inherited genotypic differences between cells demonstrating the 2 expression states.

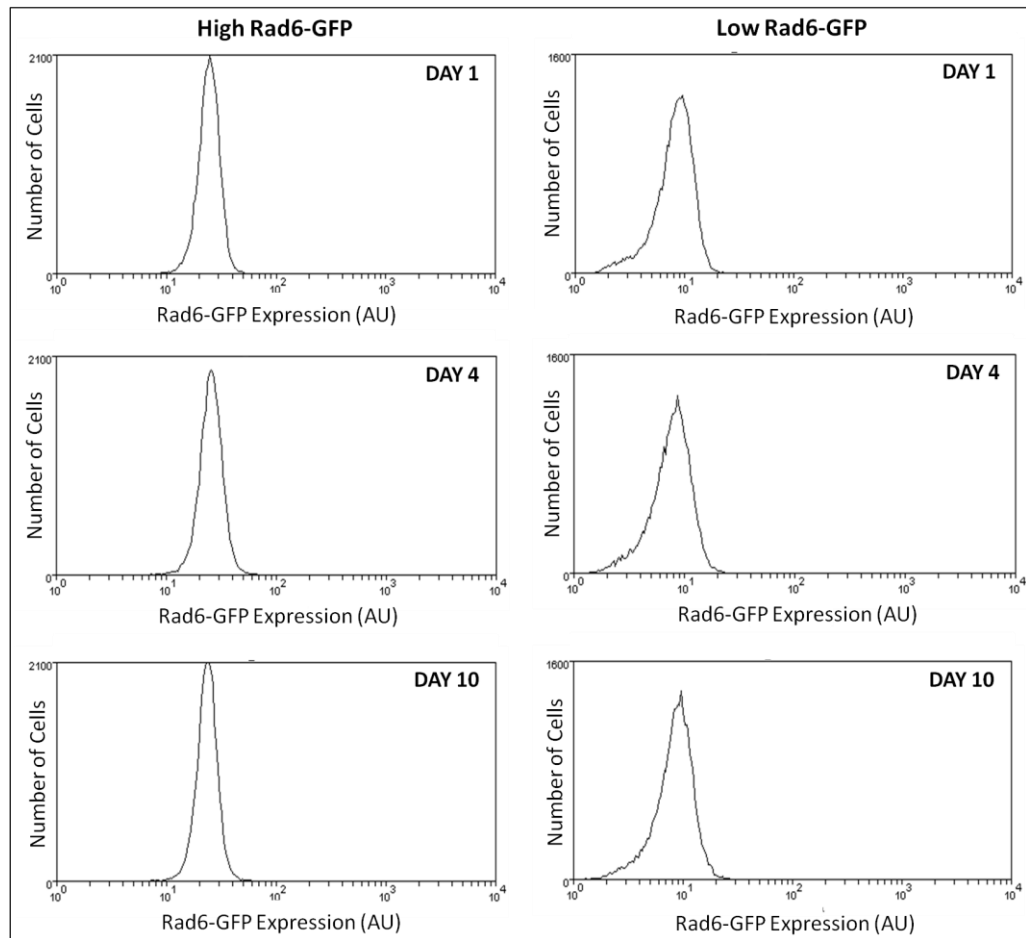


Figure 22 – Flow cytometric analysis of high- and low-expressing Rad6-GFP cells. Three cultures of each expression state were maintained in exponential phase during growth in YPD medium and analysed at one, four, and ten days.

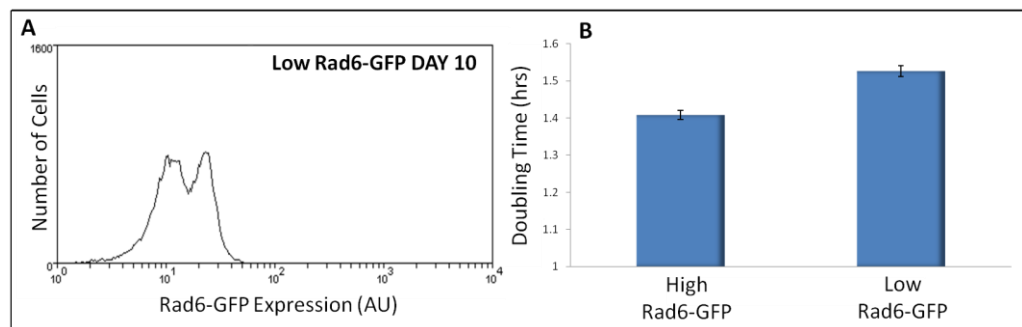


Figure 23 – **(A)** One of three low-Rad6-GFP expressing cultures, maintained in exponential phase in YPD and analysed by flow cytometry, demonstrated an apparent switching capacity after ten days growth. **(B)** Growth rates of high- and low-Rad6-GFP expressing cells. Data indicate the mean of three independent experiments \pm SEM.

3.4 Rad6 Does Not Exhibit Bi-stable Gene or Protein Expression

The observation that individual yeast cultures do not exhibit bi-stable Rad6-GFP expression was in contrast to previous results obtained prior to this study. Rather in this instance cultures were shown to either demonstrate high or low expression, these expression states being inheritable over extended periods of time.

It was decided to confirm that both types of population did indeed contain tagged Rad6 constructs, and that low-expressing cells were not untagged contaminants. The Rad6-GFP cassette in genomic DNA of different clones was detected by PCR using primers RAD6-FWD and ADH1-term-REV (Materials and Methods). Both types of culture did indeed contain the Rad6-GFP construct, evident as a ~2.4kb band that was absent in unlabelled strains (Fig. 24). This indicated the low expressing population does not originate from an unlabelled contaminant. Furthermore, sequencing across the Rad6-GFP region, using primers RAD6-SEQ 1-5 (Materials and Methods) confirmed the presence of an identical Rad6-GFP construct in both high and low cells.

Given that strong inheritance of the Rad6 expression state seems to indicate the occurrence of a genetic difference between high- and low-expressing cells, either around the *RAD6* locus or elsewhere, it was decided to re-construct Rad6-GFP expressing yeast.

3.4.1 Analysis of a RAD6-GFP Transcriptional Fusion

Initially a *RAD6*-GFP transcriptional fusion was constructed by amplification of the GFP cassette from pSVA12 (Avery et al., 2000) using primers Rad6GFP-TF-Fwd and Rad6GFP-TF-Rev (Materials and Methods) which include 50bp regions of homology to either side of the *RAD6* ORF. The resulting fragment was transformed into *S. cerevisiae* BY4741 and successful integration in selected transformants confirmed by diagnostic PCR using primers RAD6-FED and RAD6-REV (Materials and Methods). These primers recognise regions outside of the inserted cassette and produce a ~3.5kb band to indicate correct integration whereas unsuccessful transformants yielded a PCR product of ~1.8kb (Fig. 25).

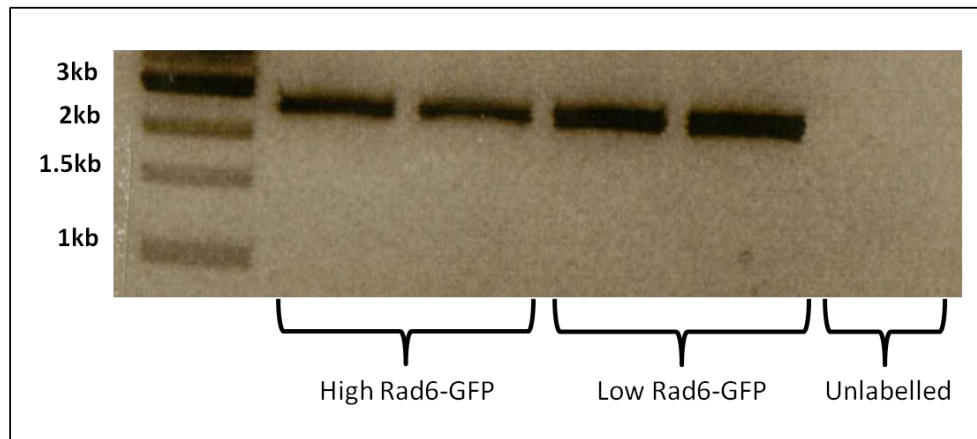


Figure 24 – PCR for the Rad6-GFP construct using DNA isolated from both high and low expressing cells and primers RAD6-FWD and ADH1-term-REV. The presence of the construct is indicated by a PCR product at ~ 2.4 kb

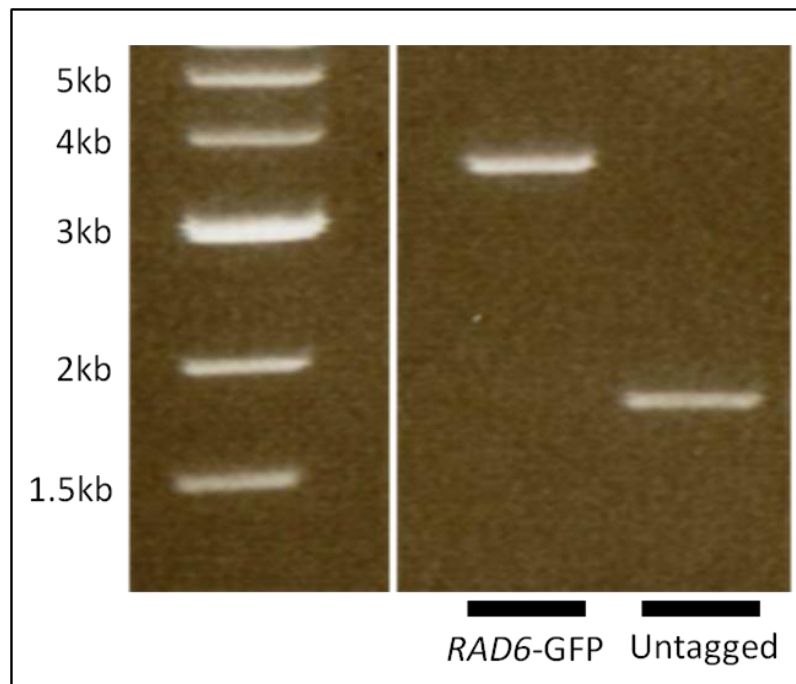


Figure 25 – Diagnostic PCR for successful generation of a *RAD6*-GFP transcriptional fusion using primers RAD6-FWD and RAD6-REV. A PCR product of ~ 3.5 kb indicates the presence of the *RAD6*-GFP constructs whilst untagged strains produced a band at ~ 1.8 kb.

Analysis of the *RAD6*-GFP transcriptional fusion strain, in triplicate experiments, revealed expression of the gene to occur as a single population, similar to the constitutively expressed *ACT1*-GFP used as a control (Fig. 26). To rule out the possibility of colonies being present that give rise to alternative levels of *RAD6* expression, numerous colonies were pooled and analysed together. A similar strategy does indeed reveal the two Rad6-GFP populations identified through flow cytometric analysis of the original translational fusion strain from invitrogen (Fig. 19). This, analysis, however, again revealed only one *RAD6*-GFP expression population as shown for single colony analysis (Fig. 26).

3.4.2 Analysis of a Newly Constructed Rad6-GFP Translational Fusion

In Addition to the *RAD6*-GFP transcriptional fusion described above, a Rad6-GFP translational fusion was remade. Primers RAD6-TLF-FWD and RAD6-TLF-REV (Materials and Methods) were utilised to amplify the Rad6-GFP cassette from the Invitrogen translational fusion strain. This cassette was then transformed into the BY4741 background with appropriate integration being confirmed by diagnostic PCR using primers RAD6-FWD and RAD6-REV (Materials and Methods). These primers recognise regions outside of the inserted cassette, with successful transformants producing a band of ~4kb whereas unsuccessful integration results in a ~1.8kb band. Triplicate successful transformants were analysed by flow cytometry using cells obtained from single colonies. These exhibited an expression level roughly intermediate between the two expression levels previously identified in the Invitrogen translational fusion strain (Fig. 27). In a similar strategy as employed for the transcriptional fusion strain (above), many colonies were pooled and analysed together. This approach did not reveal two different levels of Rad6 expression but rather exhibited an intermediate expression level as seen for single colony analysis (Fig. 27). Thus both the transcriptional and translational fusion strains created during this study are in agreement that only one population of cells could be distinguished according to *RAD6* expression level.

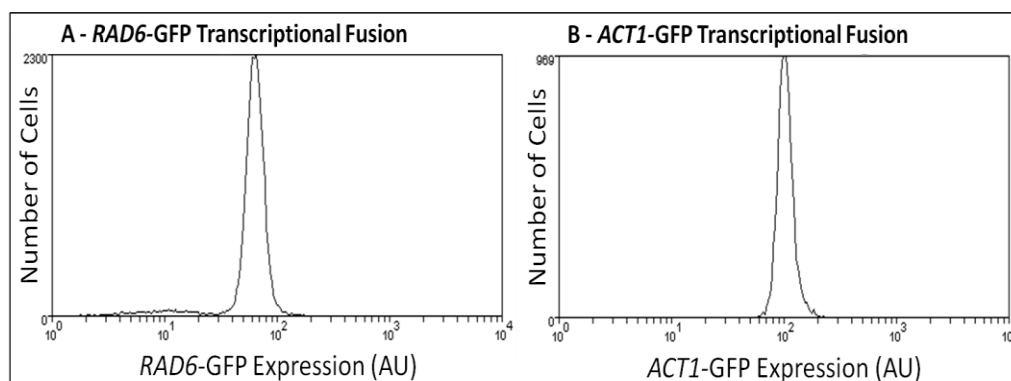


Figure 26 – Exponential cells of a newly generated *RAD6*-GFP transcriptional fusion strain grown in YPD and analysed by flow cytometry. A constitutively expressed *ACT1*-GFP strain grown under the same conditions was analysed for comparison. Histograms are representative of three independent experiments.

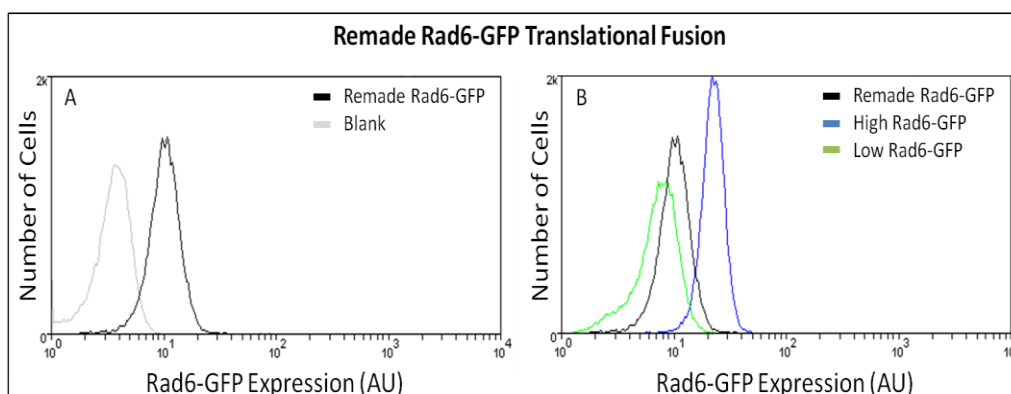


Figure 27 – Flow cytometric analysis of a remade Rad6-GFP translational fusion strain. Cells were grown to exponential phase in YNB prior to analysis. **(A)** Rad6-GFP expression (AU) (black) along with Autofluorescence from an untagged strain (grey). **(B)** Comparison of Rad6-GFP expression (AU) from the remade translational fusion (black) and the high- (blue) and low- (green) expression levels obtained by analysis of the Invitrogen translational fusion. Histograms are representative of three independent flow cytometry experiments utilising the remade Rad6-GFP translational fusion.

3.5 Discussion

This chapter aimed to elucidate further a previous observation in the Avery laboratory that the Rad6 protein of *S. cerevisiae* appeared to exhibit bi-stable expression. Initial results suggested a role for differential transcriptional silencing and regulation between cells, according to the phenotypes obtained via either *SIR2* or *SWI6* deletion. During the course of this study, however, complementation of *sir2* Δ or *swi6* Δ did not re-establish bi-modal Rad6 expression. These observations suggested the apparent roles of Sir2 and Swi6 in controlling bi-stable Rad6 expression to be artifactual. Indeed it is worth noting that the *RAD6* gene does not reside in a subtelomeric location but rather ~400kb from the left end of chromosome VII, supporting the lack of a direct role for Sir2 in controlling Rad6 expression. Additionally, although Swi6 of fission yeast is known to function in transcriptional silencing at centromeres, telomeres and the silent mating type, Swi6 function in *S. cerevisiae* is rather different. Swi6 of *S. cerevisiae* acts as a transcriptional cofactor forming complexes with either Swi4 or Mbp1 to activate and subsequently repress gene expression during cell cycle progression (Lowndes et al., 1992, Sedgwick et al., 1998, Huang, 2002). These points, along with the lack of complementation, add further weight to the likelihood that preliminary conclusions based on the deletion strain phenotypes were not reliable. In addition I was unable to distinguish two subpopulations according to Rad6 expression in cells derived from any single colony in the present study. Rather cultures either exhibited high or low Rad6 expression. Prior identification of two Rad6 expressing subpopulations may have arisen due to inoculation of cultures with more than one colony, thus encompassing cells expressing both high- and low- levels of Rad6-GFP. Inoculation of cultures with many colonies was indeed observed to, in the present study, suggest the occurrence of two Rad6 expressing subpopulations within one culture. It seems logical to suggest that the results obtained prior to this study indicating a role for both Sir2 and Swi6 in regulating Rad6 expression may have resulted from construction of the deletion strains in high-Rad6 expressing variant colonies.

Further analysis of Rad6 expression through the creation of new *RAD6*-GFP transcriptional- and Rad6-GFP translational-fusion strains did not support the observation of two Rad6-GFP expression states with the original Invitrogen strain. The one Rad6 expressing subpopulation identified in the newly generated Rad6-GFP translational fusion strain occupied an

intermediate position between the high and low expression levels identified previously. Considering that both of the original high- and low-Rad6 expressing populations were confirmed to contain identical Rad6-GFP constructs, it seems likely that the two distinct Rad6 expression levels initially observed reflected some genetic heterogeneity elsewhere in the genome, possibly due to a mutation, in the Invitrogen strain. This was substantiated by the fact that different Rad6 expression states were inherited indefinitely consistent with a genotypic basis (Avery, 2006).

The further investigation performed here indicated that initial results suggesting that Rad6 is expressed bi-stably in *S. cerevisiae* were misleading. As the main aim of this thesis was the analysis and further characterisation of heterogeneity in yeasts, it was decided not to take the Rad6 part of the studies any further.

Chapter 4 - *Candida glabrata* exhibits Strain Background-Dependent Heterogeneous Epa1 Expression

4.1 Introduction

Adhesion is an important step in the infection process of any human pathogen. The genome of the pathogenic yeast *C. glabrata* contains sequences that encode a family of GPI-anchored CWPs that function as adhesins. This group of GPI-CWPs is known as the EPA family of adhesins, the majority of which reside in subtelomeric clusters (De Las Penas et al., 2003, Castano et al., 2005, de Groot et al., 2008). The *C. glabrata* genome encodes approximately 67 adhesin-like GPI proteins, with 17 and 23 of these being allocated to the EPA family in two commonly used laboratory strains, ATCC2001 and BG2 respectively (de Groot et al., 2008, Kaur et al., 2005). Despite this large adhesin repertoire *EPA1* remains, to date, the best characterized member of the EPA family. *EPA1*, which itself encodes a Ca²⁺-dependent lectin (Cormack et al., 1999), forms part of a subtelomeric cluster containing three *EPA* genes (*EPA1-3*) adjacent to the right telomere of chromosome E (De Las Penas et al., 2003). As with other GPI-cell wall adhesins the Epa1 protein precursor has been shown to possess an N-terminal signal sequence, C-terminal Ser/Thr rich domain and a C-terminal GPI addition signal. The N-terminal region also contains the ligand binding domain responsible for recognition of host-encoded N-acetyl lactosamine-containing glucoconjugates (Cormack et al., 1999, Frieman et al., 2002). *In vitro* adherence appears to be largely dependent upon Epa1, with deletion of the gene reducing adherence to human epithelial cells by 95% (Cormack et al., 1999). In addition, a chimeric construct of *EPA1* containing the GPI anchor signal of *ScCWP2*, was able to confer adherence of normally non-adherent *S. cerevisiae* to cultured human epithelial cells (Frieman et al., 2002). Interestingly, and likely due to the expression of additional adhesins, deletion of *EPA1* does not result in a significant virulence phenotype in murine models of mucosal infection (Cormack et al., 1999). By contrast deletion of the entire *EPA1* gene cluster (*HYR1/EPA1-3*) does cause a significant reduction in kidney colonization lending support for the importance of additional adhesins *in vivo* (De Las Penas et al., 2003). Further to this two additional *EPA*'s, *EPA6* and *EPA7*, have been implicated as important for kidney colonization (Castano et al., 2005).

It has previously been demonstrated in the Avery laboratory, that *EPA1* exhibits marked variation in its expression levels within a genetically identical population of cells (Fig. 28) (M.C. Smith and S.V. Avery, Unpublished). That result prompted further investigation as to whether variation in *EPA1* expression was able to manifest as variation in adhesion

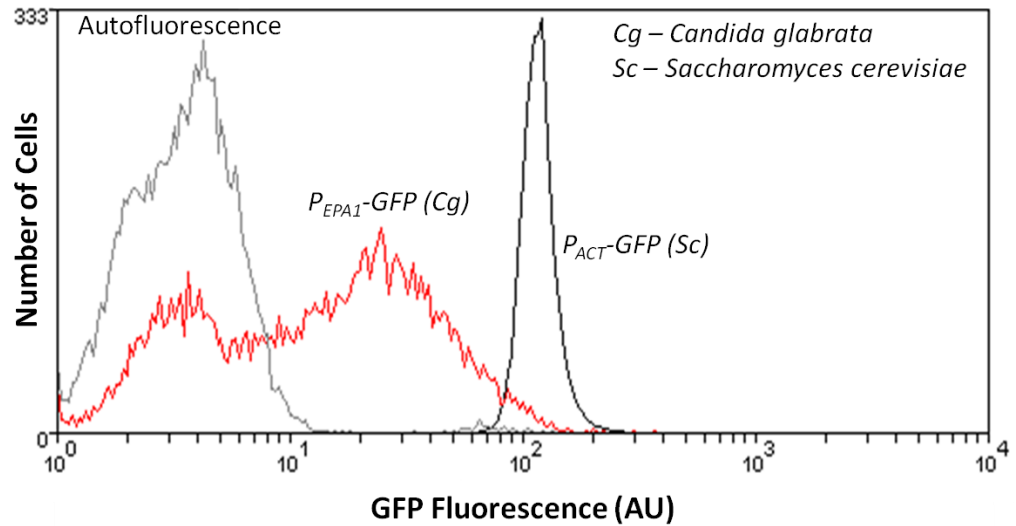


Figure 28 - FACS analysis of *C. glabrata* *EPA1*-GFP transcriptional fusion strain (BG198) shown in red. For comparison a *S. cerevisiae* *ACT1*-GFP construct is shown in black. Autofluorescence from cells containing no GFP construct is shown in grey. The vertical axis demonstrates cell numbers while the horizontal axis represents GFP fluorescence levels.

capacity to cultured epithelial cells. *C. glabrata* strain BG2-Epa1-HA, expressing functional, human influenza hemagglutinin (HA) epitope-tagged, Epa1 enabled cells to be sorted based on their cell surface Epa1-HA expression levels. Subsequent adhesion assays to human Hep2 epithelial cells illustrated that cells expressing high levels of Epa1 exhibited more than threefold greater adherence than observed for the low Epa1 sub-population (Fig. 29A) (M.C. Smith and S.V. Avery, Unpublished). This data indicated a functional consequence of heterogeneity that may be related to the virulence of this yeast pathogen. Additional previous analysis of BG2-Epa1-HA revealed the Epa1 expression level of single cells to be transient and therefore consistent with a non-genotypic rather than a genotypic basis for variation (Fig. 29B). Cells were again sorted to obtain sub-populations of high and low Epa1-HA expressing cells. Sorted cells were sub-cultured into fresh medium and analysed at intervals. In both instances sorted populations reverted back to demonstrate a mixed population of Epa1-HA expression within 20hrs. Such reversion indicates that after a few cell generations no further inheritance of the Epa1-HA expression state is discernible (M.C. Smith and S.V. Avery, Unpublished).

The following chapter aims to confirm the existence of heterogeneity in both *EPA1* transcriptional expression and Epa1-HA cell surface expression. In addition I aimed to generate another Epa1-HA construct in an alternative strain background, CG2001 HTU Δ . This strain would provide a greater variety of possible selection markers for subsequent genetic manipulations in addition to enabling comparison of Epa1-HA expression in two commonly used *C. glabrata* strain backgrounds. In addition I wanted to further analyse inheritance of the Epa1 expression state in single cells through the exploitation of fluorescence microscopy.

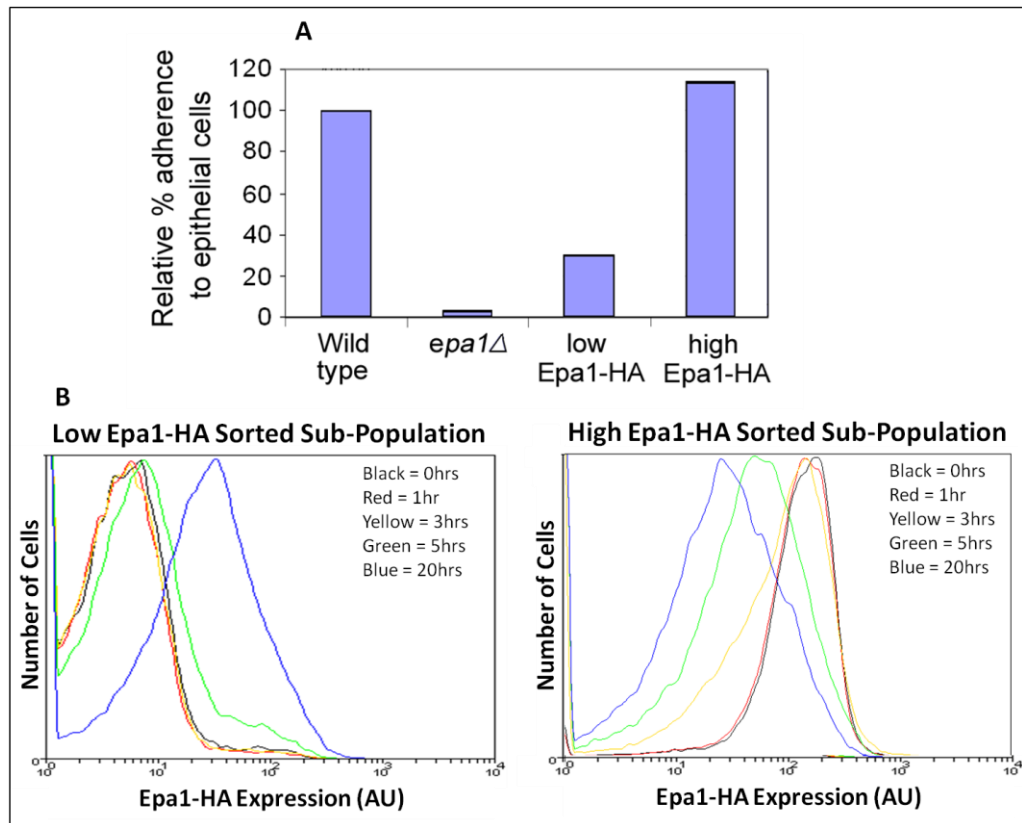


Figure 29 – (A) Adhesion of high and low Epa1-HA subpopulations to human Hep2 epithelial cells. **(B)** Reversion of high and low Epa1-HA cells to a mixed population over time. (M.C. Smith and S.V. Avery, Unpublished).

4.2 Cell-to-Cell Heterogeneity in Epa1 Expression is observed at the *C. glabrata* Cell Surface and appears to depend upon Strain Background

4.2.1 Confirmation of EPA1 Expression Heterogeneity

As described in the introduction to this section, heterogeneity of *EPA1* has previously been demonstrated in the BG2 strain background through use of an *EPA1*-GFP transcriptional fusion. Comparison with the *S. cerevisiae* *ACT1* gene, also through use of a GFP transcriptional fusion to the *ACT1* promoter, indicated a significant difference between the spread of expression levels for the two genes (Fig. 28). Although this comparison was performed between genes of different species, the *S. cerevisiae* and *C. glabrata* genomes are highly related. In fact, of the almost 6000 *S. cerevisiae* ORF's, roughly only 200 have no obvious ortholog in *C. glabrata*, (Domergue et al., 2005). In addition there is an average of 65% amino acid identity between orthologous proteins of these two species, (Kaur et al., 2005). It was thought appropriate here to further substantiate the observed heterogeneity by additional means. This was done by calculation of the Coefficient of Variation (CV) according to the criteria used by Newman et al (2006). Briefly, a circular gate, containing 500 cells, was placed around the forward scatter (FSC) and side scatter (SSC) medians (Fig. 30). Consequently this method enables the analysis of CV from a gated population of cells containing more uniform properties of cell size and granularity. This method generated an *EPA1*-GFP CV value of 106.3, higher than the value obtained for 2,212 other *S. cerevisiae* yeast genes, where CV's ranged from 8.4-77.3. A much lower CV of 13.1 was obtained by this method for *ACT1*-GFP from the present data. The CV obtained for *EPA1*-GFP expression by this accepted method is therefore indicative of a high level of expression heterogeneity for *EPA1*.

An additional method used during CV analysis was division of the fluorescence signal by FSC, which can be used as a measure of cell size, for individual cells. This takes into account the differences in cell size that are encountered during the analysis process and provides a similar CV level (107) as that obtained by the Newman method (106.3) for *EPA1*-GFP. This method has been favoured throughout this study as it encompasses data from a greater proportion of the population rather than such a small subset.

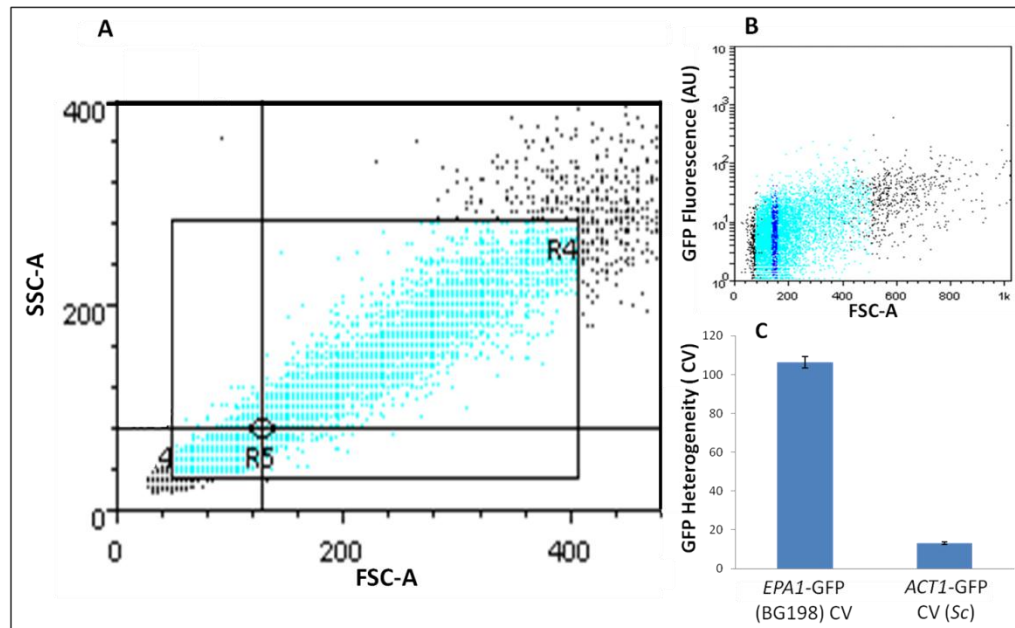


Figure 30 – (A) Gating of 500 cells around the forward scatter (FSC) and side scatter (SSC) medians. The light blue colour within gate R4 illustrates the remaining cell population following removal of the top and bottom 5% FSC and SSC values. The FSC and SSC medians for this population were calculated, demonstrated by the point at which the two lines cross, around which a circular gate, R5, encompassing 500 cells was placed. **(B)** GFP fluorescence from cells within the R5 circular gate in (A) is represented by the dark blue region in (B). CV's of GFP expression were then calculated using only cells from within this region. **(C)** EPA1-GFP CV values, calculated according to the gating described in (A) and (B), error bars are representative of triplicate experiments.

4.2.2 Heterogeneity of Epa1 Protein Expression at the Cell Surface

Analysis of a previously constructed *C. glabrata* strain, BG2-Epa1-HA, enabled visualisation of Epa1 protein expression at the cell surface through use of the HA epitope tag. BG2-Epa1-HA contains a functional triple-HA tagged *EPA1* construct (Frieman et al., 2002), under the control of its native promoter, at the *EPA1* locus in the BG2 *C. glabrata* strain background (Fig. 31A). The HA epitope tag (YPYDVPDYA) is recognised by commercially-available antibodies raised against this sequence. Consequently Epa1-HA protein expression at the cell surface can be measured by staining cells with the anti-HA, Alexa Fluor® 488 conjugate antibody. Analysis by flow cytometry of *C. glabrata* cells stained with this antibody revealed that a high level of heterogeneity, as also seen using the *EPA1*-GFP transcriptional fusion in the same strain background, is also evident at the protein level. This produced a CV of ~94. This is also the same strain background as that used previously to demonstrate that the extent of Epa1 has a functional consequence for adherence, and such variation appears non-genotypic (Fig. 29).

4.2.3 Construction of CG2001-Epa1-HA

The previous experiments, discussed above, utilised *C. glabrata* strain BG2. Although used regularly, the complete sequence for this strain is unavailable. In addition there are limited options for the type and number of available selection markers.

In order to create a strain containing triple-HA tagged *EPA1* along with more selectable marker options it was decided to use *C. glabrata* strain CG2001 HTUΔ, (Kitada et al., 1995). This strain is a derivative of the *C. glabrata* type strain (ATCC2001) for which complete subtelomere-to-subtelomere genome sequence is available (Sherman et al., 2006). In addition this strain provides more flexibility in the choice of selection markers for future genetic manipulations. Triple-HA tagged *EPA1*, under control of its own promoter and contained within pMS15, a plasmid constructed prior to the initiation of this study, was utilised. Digestion of the plasmid with XbaI-PacI released a ~6.8kb *EPA1*-HA fragment, which included *URA3* as a selection marker, targeted to the *EPA1* locus by 1kb regions of flanking homology (Fig. 31A). This provided a strain expressing a functional *EPA*-HA with more selectable marker options and consequently more scope for genetic manipulation. Transformed cells were selected for

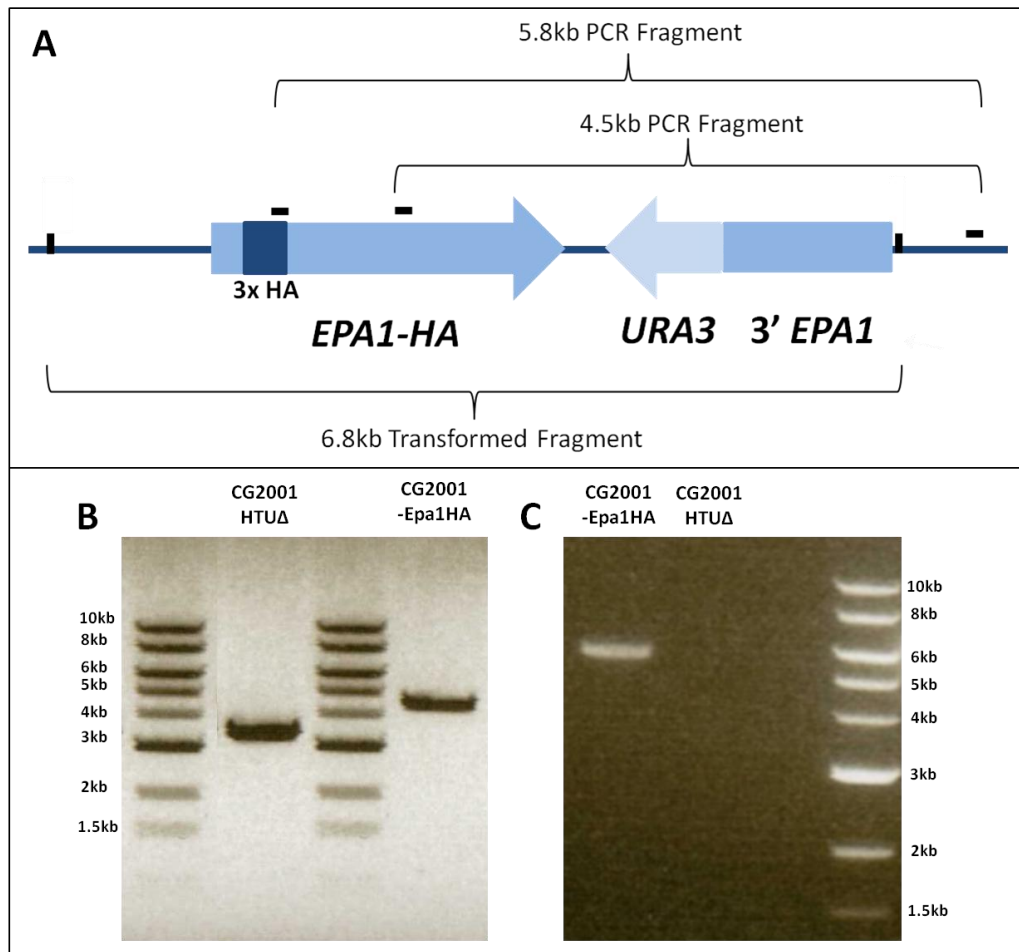


Figure 31 - (A) The 6.8kb fragment containing a triple HA-tagged *EPA1* construct transformed into CG2001 HTUΔ generating CG2001-Epa1-HA. This fragment is also expressed in BG2-Epa1-HA. **(B and C)** Diagnostic PCR products generated from genomic DNA of CG2001 HTUΔ and CG2001-Epa1-HA strains. **(A and B)** Primers WIEPA1-FWD and EPA1-REV-OSHOM produce a band of ~4.5kb demonstrating successful integration of the *EPA1*-HA fragment. By contrast CG2001 HTUΔ containing untagged *EPA1* produces a band of ~3.4kb. **(A and C)** To confirm that homologous recombination of the transforming fragment had occurred in such a way as to include the HA tag diagnostic PCR was performed using the primers HAtag-FWD and EPA1-REV-OSHOM. Successful transformants, generating CG2001-Epa1-HA, produce a band at 5.8kb while CG2001 HTUΔ cells demonstrate no amplification.

on *URA⁻* YNB medium, and confirmed to contain *EPA1*-HA at the correct locus by diagnostic PCR utilising genomic DNA and primers WIEPA1-FWD/HAtag-FWD and EPA1-REV-OSHO which recognise regions within and outside of the transforming fragment respectively (Fig. 31). In addition, through use of anti-HA, Alexa Fluor[®] 488 conjugate, flow cytometry and microscopy were employed to confirm expression of the HA tagged Epa1 protein at the cell surface (Fig. 32). Expression of Epa1-HA is clearly illustrated when compared to an untagged CG2001 HTUΔ control. In addition fluorescence can be identified at the surface of cells analysed by fluorescence microscopy.

4.2.4 Heterogeneity of Epa1 Expression at the Cell Surface appears to be Strain Dependent

Construction of BG2-Epa1-HA and CG2001-Epa1-HA, both of which contain triple-HA tagged *EPA1* (Fig. 31) in BG2 and CG2001 HTUΔ backgrounds respectively, enabled comparison of Epa1 expression and heterogeneity at the cell surface in two separate strain backgrounds. As described earlier, analysis was performed using an anti-HA, Alexa Fluor[®] 488 conjugate antibody followed by flow cytometry. Interestingly this revealed that the level of heterogeneity in Epa1 expression was markedly different between the two strains, with BG2-Epa1-HA exhibiting a CV value of ~94 compared with a value of just ~53 for CG2001-Epa1-HA (Fig. 33). The increased level of heterogeneity was accompanied by a 15.8% decrease in overall population-averaged Epa1 expression level (Fig. 33). Such a decrease can be attributed to an increase in the number of cells expressing lower levels of Epa1. A large proportion of these low expressing Epa1 cells are seen to overlap with the Autofluorescence recorded for unstained cells (Fig. 33). This may suggest that such cells are exhibiting very low and possibly no expression of Epa1 at their surface.

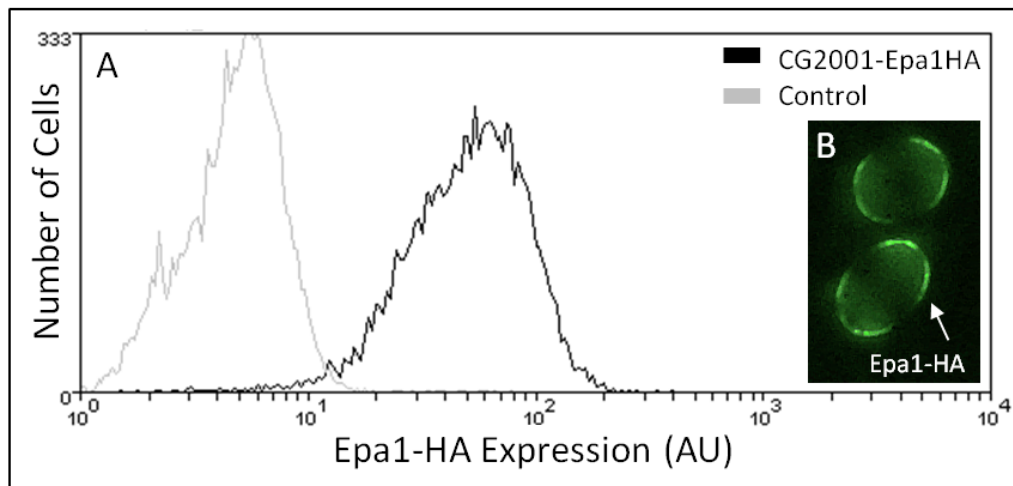


Figure 32 – Following staining with anti-HA, Alexa Fluor[®] 488 conjugate (Materials and Methods) both analysis by **(A)** flow cytometry together with **(B)** fluorescence microscopy confirmed expression of Epa1-HA at the cell surface. (i) Black line, stained CG2001-Epa1-HA cells; grey line CG2001 HTUΔ cells expressing untagged Epa1. Cell number is depicted along the vertical axis while the horizontal axis represents Epa1-HA fluorescence

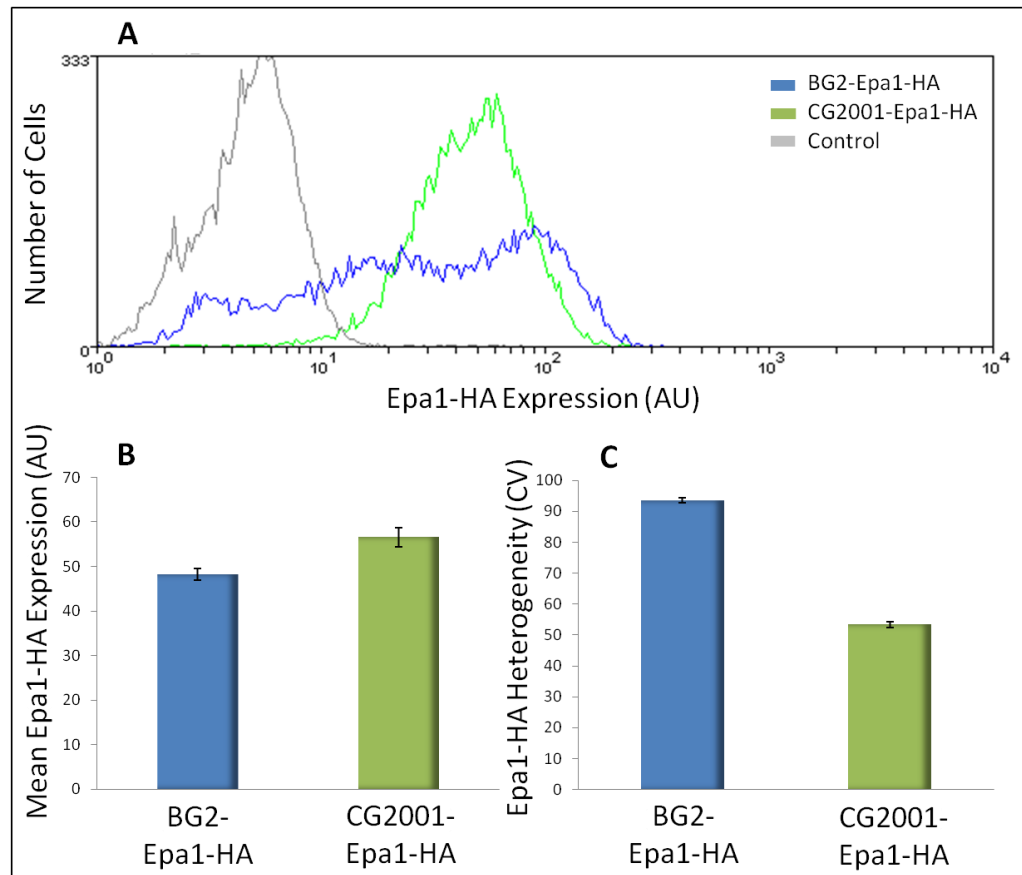


Figure 33 – (A) Histogram depicting Epa1-HA expression differences between the two strains analysed by flow cytometry. BG2-Epa1-HA (blue), CG2001-Epa1-HA (green) and unstained control (grey). Number of cells is represented by the vertical axis while Epa1-HA expression is shown along the horizontal axis. **(B)** Population averaged Epa1-HA expression as calculated by flow cytometric analysis. BG2-Epa1-HA is represented in blue while green represents CG2001-Epa1-HA. **(C)** Epa1-HA CV values, representing cell-to-cell heterogeneity, calculated by flow cytometric analysis. BG2-Epa1-HA and CG2001-Epa1-HA are again depicted by blue and green respectively.

4.3 Heterogeneity and Expression of Epa1-HA Varies During Growth in Batch Culture

In order to determine if Epa1 heterogeneity levels fluctuate during batch culture, time course experiments were performed (Fig. 34). BG2-Epa1-HA and CG2001-Epa1-HA cells were inoculated into fresh medium from stationary phase starter cultures and sampled regularly for a period of 12 hours. Sampled cells were stained with anti-HA, Alexa Fluor[®] 488 and Epa1-HA expression levels analysed by flow cytometry. Previous work in the BG2 strain background utilised a polyclonal antibody raised against the N-terminal domain of Epa1, (Kaur et al., 2007). During this study highest expression levels were identified at 2 hours post inoculation with background levels being reached by 10 hours.

In agreement with the above mentioned study, Epa1-HA levels at the cell surface were found to peak in the hours immediately following inoculation. The highest level of expression in both strains tested was observed at 1hr post inoculation; this high expression also correlated with the lowest level of heterogeneity in both strains. Most variation in expression levels occurred between 1-5 hours following inoculation into fresh medium, with lowest levels being reached between 7-10 hours as cells progress into stationary phase. At this point expression levels appear to remain relatively constant. Epa1 CV values remained higher in BG2-Epa1-HA at every time-point when compared to values at the equivalent time-point for CG2001-Epa1-HA. Interestingly, the highly heterogeneous BG2-Epa1-HA strain also demonstrated marked fluctuation in Epa1-HA CV levels during the course of the experiment. CV values ranged from 51 to almost 126 in BG2-Epa1-HA meaning that the highest heterogeneity level was more than double the lowest heterogeneity value. By contrast, Epa1-HA heterogeneity levels were relatively constant in CG2001-Epa1-HA, suggesting that Epa1 expression may be under tighter control in CG2001-Epa1-HA than in BG2-Epa1-HA during growth in batch culture.

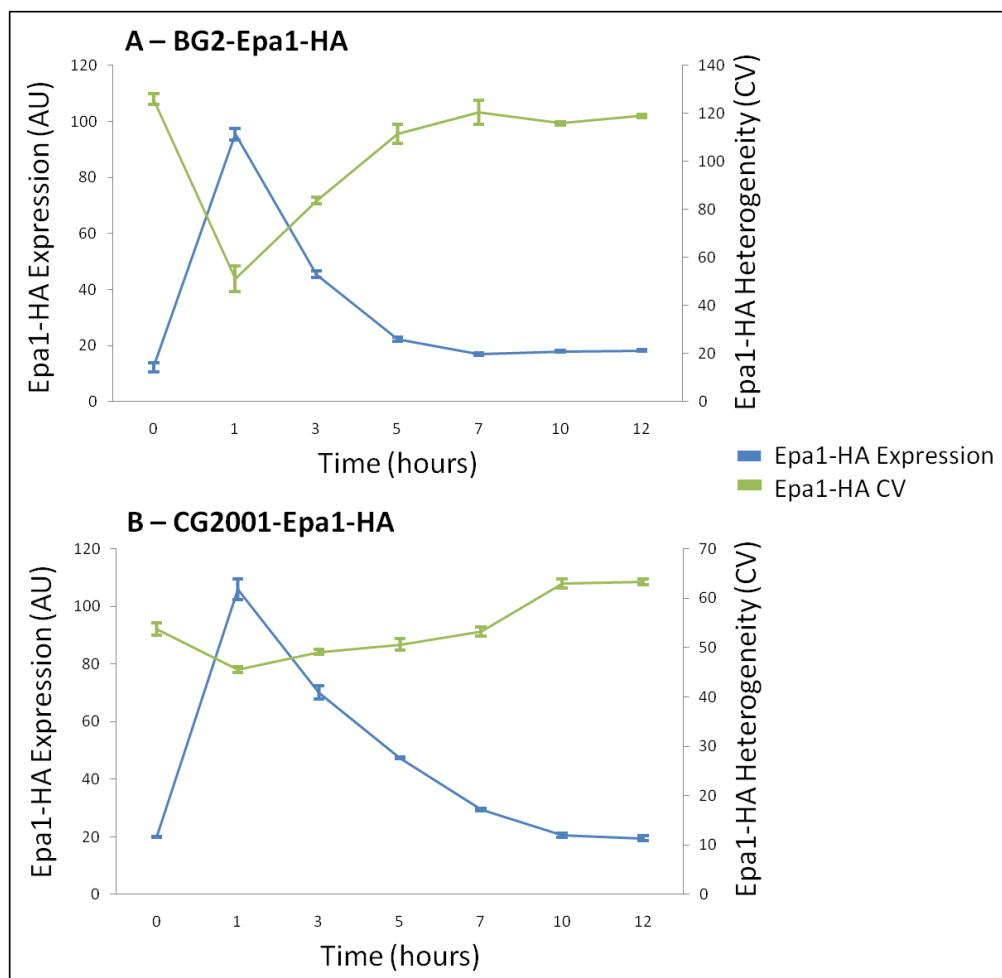


Figure 34 – Time course flow cytometry analysis of Epa1-HA expression (blue) and CV (green) in **(A)** BG2-Epa1-HA and **(B)** CG2001-Epa1-HA over a period of 12 hours during growth in batch culture. In both instances the left vertical axis corresponds to Epa1-HA expression and the right vertical axis corresponds to Epa1-HA CV. Time in hours is depicted along the horizontal x-axis.

4.4 Inheritance of Epa1

A previously performed reversion assay using BG2-Epa1-HA cells sorted according to Epa1-HA expression has been discussed earlier (Fig. 29B). This assay revealed that cells expressing high- or low- levels of Epa1-HA reverted back to mixed levels of expression over a period of 20hrs. This timescale was rather long compared to timescales that are relevant when considering many forms of heterogeneity (e.g. those that are cell cycle or rhythm driven) (Smith et al., 2007, Sumner et al., 2003). Initial time-points suggested a partial inheritance of the Epa1 expression state over a limited time period. This was further tested by analysis of Epa1-HA expression of parent cells and their offspring by fluorescence microscopy, as described below.

4.4.1 *Epa1-HA Expression in Daughter Cells represents De Novo Synthesis of Epa1*

Differential partitioning of molecules during cell division may contribute towards measured fluctuations in protein abundance between cells, (Huh and Paulsson, 2011). Time-lapse fluorescent microscopy was used to determine by what extent, if any, Epa1 levels are dictated by partitioning of already synthesised Epa1 protein from the mother cell to the daughter bud during cell division. Anti-HA, Alexa Fluor[®] 488 antibody stained Epa1-HA cells were followed through the process of cell division by imaging at 10 min intervals for a period of 3 hours. This enabled the fate of pre-synthesised parental Epa1-HA to be tracked. Captured images revealed no partitioning of pre-stained cell wall Epa1 from a mother to a daughter cell (Fig. 35). The observations suggest that pre-synthesised Epa1 protein itself remains associated with the mother cell during division and any subsequent expression in the daughter cell occurs *de novo*. This was found to be true for both the BG2-Epa1-HA and CG2001-Epa1HA strain backgrounds.

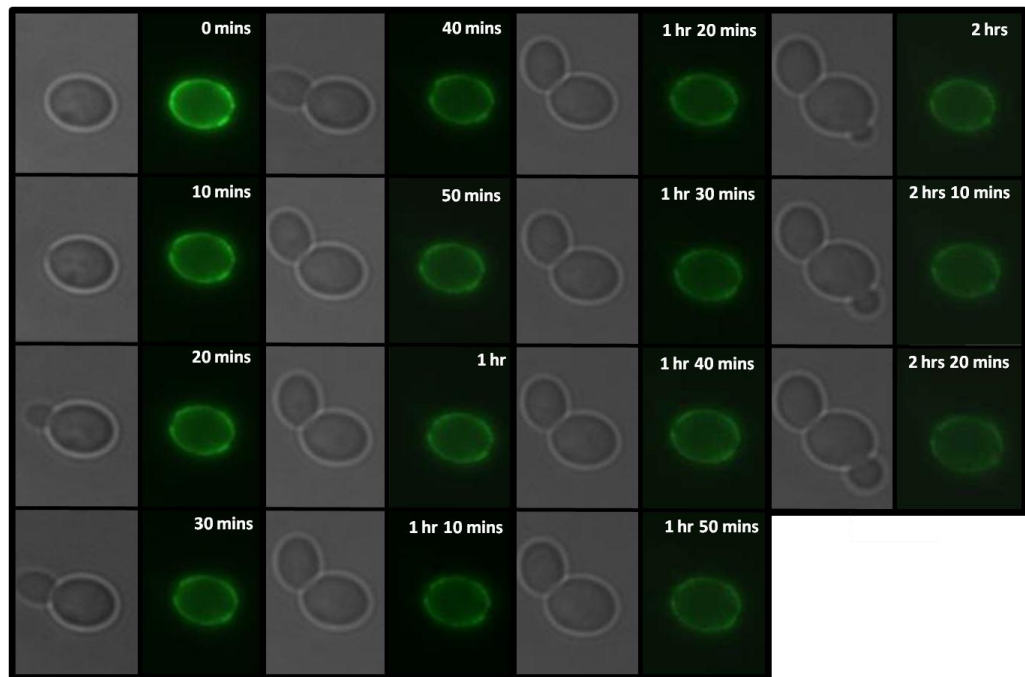


Figure 35 – Time-lapse fluorescence microscopy of anti-HA, Alexa Fluor[®] 488 conjugate stained cells. Brightfield (left) and fluorescent (right) images were captured every 10 minutes in order to follow the process of cell division and any partitioning of parental cell wall Epa1-HA protein.

4.4.2 Newly Budded Cells Exhibit a Variety of Expression States

The above time-lapse microscopy data provides information on the fate of parental Epa1-HA, however it does not provide information on the subsequent bud cell Epa1-HA expression. The observation that Epa1-HA synthesis likely occurs *de novo* in newly budded cells substantiates that antibody probing provides a snapshot of Epa1-HA synthesised in a particular cell. This, along with bud cell size as an indicator of the daughter cell development, can provide information about Epa1-HA expression during cell cycle progression of new cells.

Fluorescence microscopy, in the form of static snapshots, was used to compare the mean Epa1-HA expression of individual budded cells with the corresponding bud cell area for 100 cells (Fig. 36). Analysis of these data revealed low correlation between bud cell size and subsequent Epa1-HA expression level. I was able to show that large and small buds alike demonstrated a variety of Epa1-HA expression levels. Correlation coefficients of bud cell size against Epa1-HA expression were -0.334 and -0.068 for CG2001-Epa1-HA and BG2-Epa1-HA strains respectively, thereby indicating virtually no relationship between the two parameters particularly in the latter strain. CG2001-Epa1-HA cells demonstrate a slightly greater correlation, however, -0.334 is still rather low given that a value of, 0, indicates no correlation while +1/-1 indicate strong positive and negative correlations respectively. Furthermore, a large proportion of small (below 6 μ M) CG2001-Epa1-HA buds can be seen to demonstrate low levels of fluorescence, relative to high expressing buds of an equivalent size, despite this possible correlation. It is also possible that a limited number of small buds with very high expression have skewed results towards suggesting a correlation, this may be rectified by increasing sample size. Such results suggest that Epa1 expression at the cell surface occurs independently of the daughter cell progression through the cycle. Rather, expression occurs at various points or rates, and sometimes not at all, in newly formed *C. glabrata* cells. Such immediate heterogeneity between daughter cells will thereby contribute to heterogeneity in the wider population. It may be interesting to note that BG2-Epa1-HA buds demonstrate both a lower mean Epa1-HA expression (\sim 11.3) and a higher CV (\sim 59.0) than that seen for CG2001-Epa1-HA cells which give values of \sim 21.56 and \sim 44.84, respectively. Such differences between the strains are in general

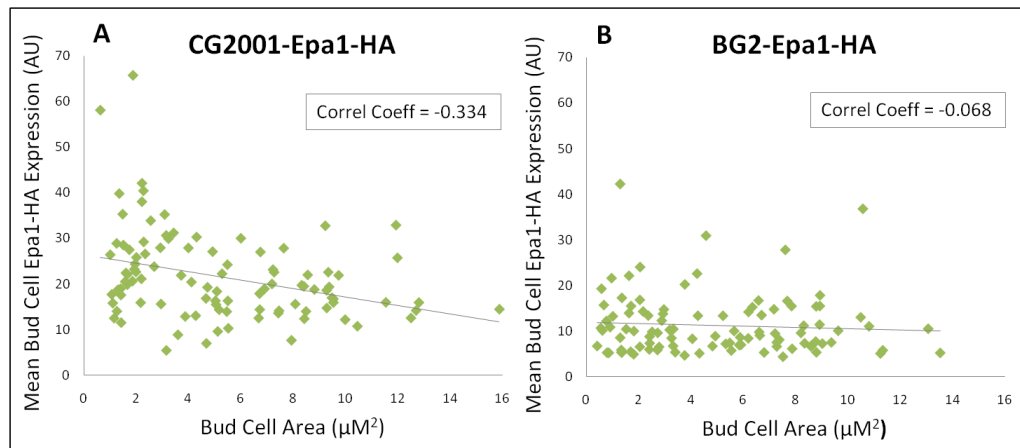


Figure 36 – The relationship between bud cell area (μM^2) and mean Epa1-HA expression (AU) for individual **(A)** CG2001-Epa1-HA and **(B)** BG2-Epa1-HA cells. Scatter graphs demonstrate results for 100 bud cells analysed from static fluorescence image snapshots following staining with anti-HA, Alexa Fluor[®] 488 conjugate. In both instances mean Epa1-HA expression is illustrated by the vertical axis while bud cell area is shown along the horizontal axis. Correlation coefficients are indicated for each strain.

agreement with the trends demonstrated by previous flow cytometry described in this thesis (4.2.4) and (Fig. 33).

4.4.3 Cell Surface Epa1-HA Expression State may be partially Inherited

The method of bud cell analysis described above also enabled Epa1-HA expression to be measured specifically in mother cells. Ultimately this allowed a direct comparison between expression in the mother and the corresponding bud, this was performed for 100 cells. For both strain backgrounds, high and low expressing mothers gave rise to both low expressing and high expressing daughters irrespective of the mothers Epa1-HA expression level (Fig. 37A). This indicated that the level of Epa1-HA expression developed in daughters is not dictated by cell surface Epa1-HA expression in the mother. A correlation coefficient value of 0.12 confirmed the lack of a marked relationship between mother and daughter cell fluorescence in CG2001-Epa1-HA cells (Fig. 37B). Interestingly, however, there was some correlation between mother and daughter cell fluorescence in BG2-Epa1-HA cells, as a correlation coefficient of 0.54 was obtained. The observed ability of BG2-Epa1-HA mother cells to produce daughters of a different Epa1 level does however indicate that daughter cell expression levels are not absolutely governed by the mother. Such results suggest that in this particular strain background there may be at least some partial heritability of the Epa1-HA expression state (Fig. 37C). This method also enabled a comparison of the expression levels of individual mother cells in the two strains. In agreement with previous flow cytometry and microscopy data, BG2-Epa1-HA mother cells demonstrated a higher Epa1-HA CV value (~69) than that seen for equivalent cells of CG2001-Epa1-HA (~44).

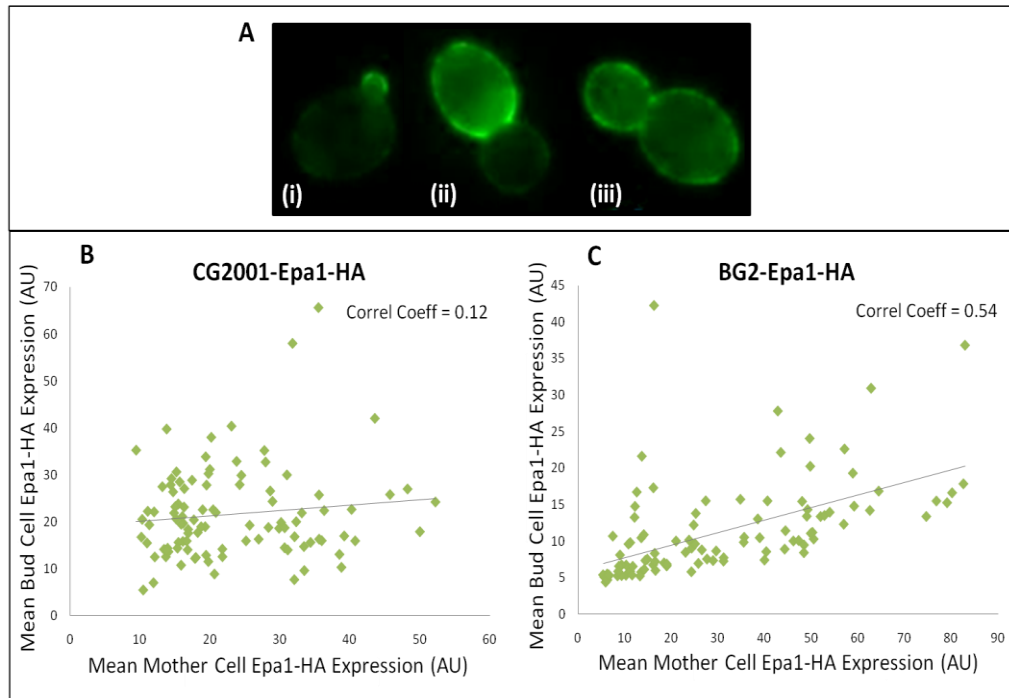


Figure 37 – (Non) heritability of Epa1-HA expression state. **(A)** Fluorescence microscopy images showing examples where a low Epa1-HA expressing mother produces a bright bud (i), or a high Epa1-HA expressing mother gives rise to low (ii) or high (iii) expressing buds. Scatter plots illustrate the relationship between mother and bud mean Epa1-HA expression as analysed by anti-HA, Alexa Fluor[®] 488 staining and fluorescence microscopy of 100 cells for **(B)** CG2001-Epa1-HA and **(C)** BG2-Epa1-HA. Mother cell Epa1-HA expression is represented by the horizontal x-axis while bud cell Epa1-HA expression is demonstrated along the vertical Y-axis. Correlation coefficients are indicated for both strains.

4.5 Discussion

I investigated Epa1 expression at both the transcription and protein levels in order to elucidate the degree of heterogeneity present during expression of this cell wall adhesin. Initial results using an *EPA1*-GFP transcriptional fusion strain enabled confirmation that heterogeneity in expression of this gene does indeed exist. Calculation of the coefficient of variation (CV) according to the method described by Newman et al. (2006) yielded a value for *EPA1*-GFP expression that was higher than the CVs obtained for 2,212 other yeast genes (Newman et al., 2006). Such a result indicated that *EPA1* expression in this pathogenic yeast is indeed highly heterogeneous. The fact that the calculated CV value for *EPA1* however was markedly higher than any of the other yeast genes tested could reflect some difference in heterogeneity regulation between *S. cerevisiae* and *C. glabrata*. However, it should be noted that the Newman study was not comprehensive, and excluded members of the *S. cerevisiae* *FLO* gene family. Like the *C. glabrata* *EPA* family, the *FLO* genes encode a group of GPI-CWPs that confer adhesion to agar, plastic and to other yeast (Guo et al., 2000). Inclusion of these genes in the Newman study would have provided a useful comparison. The *FLO10* and *FLO11* genes, in particular, are known to demonstrate variegated expression due to metastable silencing (Halme et al., 2004, Octavio et al., 2009). It is unlikely that the high level of heterogeneity observed with the *EPA1*-GFP construct is artifactual since subsequent tagging of Epa1 by a separate method, using the HA epitope, in the same strain background also indicated a high CV value.

Subsequent use of two Epa1-HA tagged strains allowed a demonstration that the extent of Epa1 expression heterogeneity appears to be dependent upon strain background. The results provided evidence that strain BG2-Epa1-HA, has a markedly higher level of Epa1-HA expression heterogeneity than CG2001-Epa1-HA. The increased heterogeneity is accompanied by an overall decrease in expression level due to an increase in the proportion of low Epa1-HA expressing cells. Differences pertaining to adhesion capacity of *C. glabrata* according to strain background have been previously identified (de Groot et al., 2008). ATCC2001 was shown to be strongly adherent when compared to cells of the ATCC90876 strain background. This difference was accompanied by increased surface hydrophobicity in ATCC2001, a state that is seen to coincide with incorporation of additional cell surface adhesins not present in ATCC90876

(de Groot et al., 2008). Indeed increased incorporation of hydrophobic cell wall adhesins is likely related to increases in cell surface hydrophobicity (Ishigami et al., 2006, de Groot et al., 2008, Hoyer and Hecht, 2001). The observation of high Epa1-HA expression in an ATCC2001 derivative strain background is consistent with the hydrophobicity and adherence properties of this strain. *In vitro* adhesion to epithelial cells is known to be mediated by Epa1 (Cormack et al., 1999). Therefore, based on the present data, it may be logical to assume that the CG2001-Epa1-HA strain would also demonstrate both increased population-averaged adherence and population averaged hydrophobicity when compared to BG2-Epa1-HA.

In agreement with previously reported data (Kaur et al., 2007) Epa1 was expressed at its highest levels during early stages of growth in both tested strains. This expression decreased as cells progressed through to stationary phase, again in agreement with previous data that suggested *EPA1* expression to be low in stationary phase cells (Castano et al., 2005, De Las Penas et al., 2003). Such experiments also enabled any changes in Epa1 heterogeneity that may be occurring during growth in a batch culture to be tracked. It was interesting to note that strain CG2001-Epa1-HA, which demonstrates lower levels of Epa1 heterogeneity than BG2-Epa1-HA, also exhibited less fluctuation in these heterogeneity levels during growth. Results suggested that Epa1 expression may be under tighter control in the CG2001-Epa1-HA strain.

As cell surface Epa1 protein generated in single cells was retained by those cells during division and not partitioned into an emerging bud, it could be inferred that any Epa1 protein detected at the cell surface had been synthesised *de novo* in that particular cell. Although Epa1 already present in the cell wall is not partitioned into new daughter cells this is not to say that Epa1 protein at other stages of the maturation process, or indeed *EPA1* mRNA, does not undergo differential partitioning (Huh and Paulsson, 2011). Maturation of GPI-anchored CWPs requires a series of post-translational modifications. Initially these proteins are targeted to the endoplasmic reticulum (ER) where addition of the GPI anchor occurs. Newly synthesised GPI-anchored proteins are segregated from other secretory proteins and transported to the Golgi in COPII-coated vesicles. The proteins must move through the Golgi before further transportation to their final destination of the cell wall (Castillon et al., 2009, Doering and Schekman, 1996, Muniz et al., 2001, Rivier et al., 2010, Verstrepen et al., 2004). Such vesicles and the ordered partitioning of the relevant organelles

themselves provide additional means by which protein may be segregated from mother to daughter cells (Shima et al., 1997, Huh and Paulsson, 2011). In addition stochastic partitioning has been shown to contribute to non-genetic heterogeneity (Huh and Paulsson, 2011).

The transcript levels of many *S. cerevisiae* CWP-encoding genes are cell cycle dependent leading to some *S. cerevisiae* CWPs being preferentially incorporated either in small buds or large buds or found in mother cells only. Temporal regulation of CWP incorporation has also been described in *C. albicans*, with the GPI-CWP Csa1 only being observed in growing yeast buds while it is absent from mother cells (Smits et al., 2006, Klis et al., 2009). By contrast, the data presented here, using bud cell size as an indicator of cell cycle progress, revealed very little correlation between bud cell size and Epa1 expression in either tested strain background. Rather Epa1 was found to be incorporated into the cell walls of mother cells and large and small bud cells alike. The results indicated that Epa1 protein expression is regulated independently of the cell cycle. In addition the variation in Epa1 protein arising at the cell surface of new buds resulted in immediate heterogeneous Epa1 expression in the newly formed population of cells.

Incorporation of the *S. cerevisiae* CWPs Tip1 and Cwp2 into mother cells and small/medium bud cells respectively can be determined by the timing of transcription during the cell cycle (Smits et al., 2006). Heterogeneous incorporation of Epa1 protein into bud cells of equivalent size may thus indicate variation in *EPA1* transcription between such cells. Indeed such variation in gene expression between single cells is evident for both *S. cerevisiae* *FLO10* and *FLO11* due to metastable silencing (Halme et al., 2004). Lack of consistent inheritance of the expression state, in either strain background, corroborates a non-genetic mechanism underlying heterogeneous Epa1 expression. Additionally the ability of cells sharing such close proximity to exhibit differential expression indicates that observed Epa1 variation does not result from differing environmental inputs. Nevertheless, a slight relationship between mother and daughter cell fluorescence in BG2-Epa1-HA Epa1 protein expression level was observed. The partial heritability in the BG2-Epa1-HA strain would be consistent with an epigenetic basis for heterogeneity in this strain (Avery, 2006). In concurrence with flow cytometric data, calculated CV's proved to be higher in both BG2-Epa1-HA mothers and buds than the corresponding CG2001-Epa1-HA cells. The differential expression observed in cells sharing

such close proximity during microscopy analysis also indicates variation is not the result of differing environmental inputs.

The possible mechanisms for such varied Epa1 expression, both within a clonal population and between various genetic backgrounds, will be further investigated in the following chapter.

Chapter 5 - Regulation of Epa1 Expression in *Candida glabrata*

5.1 Introduction

Similar to the *ALS* and *FLO* adhesin families in *C. albicans* and *S. cerevisiae* respectively, the *EPA* family consists of genes and proteins which share significant sequence identity. Such similarity may create functional redundancy, a possible explanation for the lack of a discernible *epa1Δ* phenotype *in vivo* where additional adhesins may compensate. Nevertheless, despite such sequence similarity the different adhesin proteins do appear to confer distinct cell surface properties allowing adhesion to a variety of substrates (Guo et al., 2000, Hoyer et al., 2008, Zupancic et al., 2008). One appealing hypothesis, borne out of the diverse range of niches occupied by pathogenic organisms, suggests that different adhesins are expressed under different conditions appropriate to their binding specificities. It has been proposed that differential gene expression driven by signals associated with different niches may regulate the varied expression of such adhesins (De Las Penas et al., 2003, Castano et al., 2005). Indeed subtelomeric silencing in *S. cerevisiae* may be regulated in response to cell stresses (Ai et al., 2002). Regulation of cell wall adhesins may therefore be highly regulated with such regulation being integral to niche adaptation and/or host infection.

Both the *EPA* and *FLO* family genes are predominately located in subtelomeric clusters, and close proximity to the telomere has been demonstrated to be important in regulating expression of both adhesin families (De Las Penas et al., 2003, Halme et al., 2004, Verstrepen et al., 2004, Castano et al., 2005). In a *C. glabrata* BG2 strain background the *EPA1* cluster (*HYR1*, *EPA1-3*) resides at the right telomere of chromosome E, *EPA4* and *EPA5* are present in the genome as an inverted repeat located at the right telomere of chromosome I, and *EPA6* and *EPA7* are located at either telomere on chromosome C (Fig. 38) (De Las Penas et al., 2003, Castano et al., 2005). With the exception of *EPA4/5*, which appears to be absent, these *EPA* genes have been identified at equivalent positions in *C. glabrata* ATCC2001 (de Groot et al., 2008, Thierry et al., 2008, Muller et al., 2009). The available genomic sequence for the type strain ATCC2001 runs from subtelomere to subtelomere but with gaps at the telomere regions (Sherman et al., 2006). Telomeric sequence for some chromosome ends in strain BG2 is available however, therefore it is known that the *EPA1* start codon is located approximately 24.6kb from its respective telomere in this strain. Consequently the *EPA1* ORF occupies a position markedly distanced from the telomere when compared to any of *EPA2-7*. Indeed *EPA*

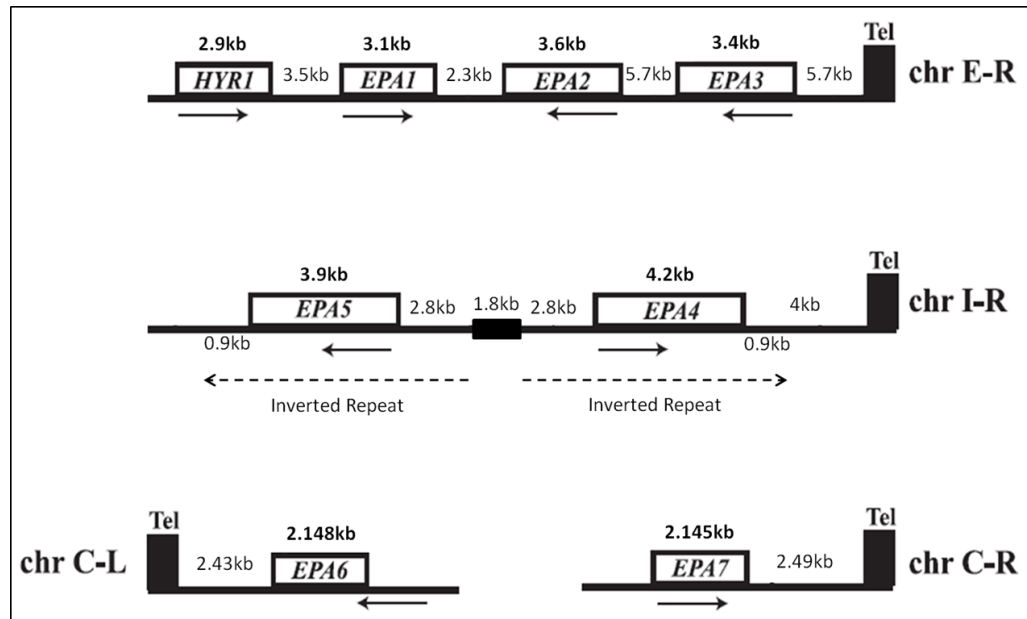


Figure 38 – Schematic representation of the positions of *EPA1*-to-*EPA7* in the genome of *C. glabrata* strain BG2 at four telomeres. The *EPA1* cluster is located at the right telomere of chromosome E (chr E-R), the *EPA4/EPA5* cluster resides at the right telomere of chromosome I (chr I-R), and *EPA6* and *EPA7* are located at either ends of chromosome C (chr C-L and chr C-R). Slightly modified from (Rosas-Hernandez et al., 2008).

2-5 are known to be subjected to *SIR3*-dependent, transcriptional silencing when exponential cells are grown *in vitro*. Conversely, and likely due to its increased distance from the telomere, *EPA1* is expressed under such conditions (De Las Penas et al., 2003). Nevertheless *EPA1* levels are increased in a *sir3* Δ BG2 background indicating that although not efficiently silenced the *EPA1* locus is subject to some repressive chromatin effects (De Las Penas et al., 2003). Silencing of *EPA1* appears to be particularly relevant in stationary phase BG2 cells where the transcript is weakly detectable and greatly increased in a *sir3* Δ background (Castano et al., 2005). *EPA6* and *EPA7* also appear to be subject to position dependent transcriptional silencing. Studies using *URA3*-based insertion assays have demonstrated a requirement for all three *C. glabrata* Sir proteins; Sir2, Sir3 and Sir4, in silencing at the *EPA1-7 loci* (Rosas-Hernandez et al., 2008). The Sir complex mediates silencing at both the silent mating type loci and telomeres in *S. cerevisiae* and is recruited to DNA via the action of a number of DNA binding proteins including Rap1. Identification of consensus Rap1 binding sites at *C. glabrata* telomeres suggests a similar function in this organism and indeed disruption of *RAP1* does de-repress transcription of silenced *EPA* genes (De Las Penas et al., 2003, North and Verdin, 2004, Castano et al., 2005).

The apparent degree of silencing exerted at telomeres appears to differ between chromosome ends (De Las Penas et al., 2003). *URA3* insertion assays demonstrated that unlike the *EPA4/5* cluster, where silencing occurred at all integration sites, there was graduated silencing across the *EPA1-3* cluster and the *EPA7* telomere (De Las Penas et al., 2003, Castano et al., 2005). Rather silencing decreased across the *EPA1-3* cluster and *EPA7* telomere as insertion sites became more and more centromeric. This is in agreement with previous data that *EPA1*, which has a relatively centromeric location compared to other *EPA* genes, is subject to only weak silencing. Different genetic requirements for silencing identified at these telomeres may contribute to such observed differences. The yKu70/yKu80 heterodimer, essential for *S. cerevisiae* silencing at all tested telomeres where it is known to regulate telomere length and aid in recruitment of Sir3 and Sir4, (Boulton and Jackson, 1996, Porter et al., 1996, Laroche et al., 1998), is not required for telomere position effect (TPE) silencing at the right end of chromosome E which includes the *EPA1-3* cluster (Rosas-Hernandez et al., 2008). In addition Rif1, likewise required for telomere length regulation in *C. glabrata* (Castano et al., 2005), has

been seen to exert various degrees of silencing at the different telomeres tested, with a discontinuous contribution to silencing observed across the *EPA1-3* telomere. Nevertheless *EPA1*, *EPA2* and *EPA3* are all induced in a *rif1* Δ background as measured by RT-PCR (Rosas-Hernandez et al., 2008). A proposed model for such differential telomere silencing suggests that certain *C. glabrata* telomeres encode *cis*-acting elements comparable to the silencer and proto-silencer elements described in *S. cerevisiae* (Fourel et al., 1999, Pryde and Louis, 1999, Rosas-Hernandez et al., 2008). Such elements may provide additional mechanisms to recruit silencing complexes and thus render telomeres more or less sensitive to changes in telomere length, such as was seen with *yku* Δ and *rif1* Δ mutants. Furthermore such a *cis*-acting element has been identified between *EPA3* and its telomere (Rosas-Hernandez et al., 2008). Silencing mediated by this element requires Sir3. However, analogous to *EPA1-3* expression, this does not appear to be dependent upon yKu70/80. In fact the silencing effect of this element increases with loss of yKu70 or yKu80, a likely consequence of shortened telomeres resulting in more available Sir complex. Indeed longer telomeres observed in *rif1* deletion strains do result in a partial release of this silencer mediated silencing (Rosas-Hernandez et al., 2008). Such results indicate that telomeres in *C. glabrata* are by no means equivalent (an observation mirrored in *S. cerevisiae*), and that the level of TPE and expression regulation is complex and differs between chromosome ends.

The above-mentioned observations highlight the potential complexity that may exist in the regulation of the subtelomeric *EPA* genes. This ranges from TPE to the contribution of silencer elements, and does not exclude possible promoter specific points of control and post-translational regulation of the product. The differing genetic interactions at different chromosome ends only add further to this complex arrangement. Such a level of complexity may be particularly important for a pathogenic organism such as *C. glabrata* by enabling individual modulation of *EPA* gene expression during the infection process. This chapter aims to elucidate mechanisms of regulation that impact on the heterogeneity of *EPA1* expression.

5.2 Impact of Virulence Related Environmental Conditions on Epa1 Expression and Heterogeneity

Adaptation to changing environments is a requirement for the survival of many microorganisms. Such adaptation is important for pathogens such as *C. glabrata* due to the wide range of host niches, with differing niche-specific conditions, that are encountered during the process of infection. While *C. glabrata* is a commensal of the gastrointestinal tract, it is capable of causing a wide range of diseases ranging from superficial mucosal infections to severe systemic candidiasis (Pfaller et al., 1998, Fidel et al., 1999, Kaur et al., 2005, Richter et al., 2005). *C. glabrata* can be isolated from the oral cavity, stomach, vaginal tract, bloodstream, kidney, liver and spleen (Fidel et al., 1999, De Las Penas et al., 2003, Castano et al., 2005, Schmidt et al., 2008). In addition, this pathogenic yeast occurs in environmental niches outside any mammalian host, having been isolated, for example, from rotten fruit (Nyanga et al., 2007, Schmidt et al., 2008). The ability of *C. glabrata* to survive and persist in such a diverse range of habitats indicates an efficient ability to adapt to changing environments.

Given the large repertoire of *EPA* adhesins that exist in this organism, and the attractive theory that different adhesins may be expressed in response to different environmental signals and at different times during infection, the effect of a number of infection-relevant conditions on expression of Epa1 was investigated.

5.2.1 Effect of Temperature

As mentioned above *C. glabrata* is an opportunistic human fungal pathogen that is commonly found in association with its host. Human body temperature is regulated to maintain an optimum of 37°C and, as expected, *C. glabrata* grows well at this temperature. I hypothesised that temperature could be a signal detected as a change of environment by *C. glabrata*, for example during entry to a host organism, leading to an alteration in expression profile accordingly. An elevated temperature of 37°C is a general requirement of hyphal induction in *C. albicans* (Sudbery, 2011) with several genes known to be expressed in a hyphal specific manner including the adhesins *HWP1* and *ALS3* (Hoyer et al., 1998, Hoyer et al., 2008). Since adhesion is believed to be an important stage in the infection process it was decided to determine if a switch in temperature from a standard laboratory growth temperature of 30°C to a host-resembling 37°C would modify Epa1 expression.

The effect of temperature change was analysed in both Epa1-HA tagged strains, CG2001-Epa1-HA and BG2-Epa1-HA. Cells were grown at the appropriate temperature for at least 15 hours before exponential phase cells were stained with anti-HA, Alexa Fluor[®] 488 antibody and analysed by flow cytometry. The results demonstrated that in the highly heterogeneous BG2-Epa1-HA strain a change in temperature from 30 to 37°C had only a small effect on Epa1-HA expression with a ~16.6% increase observed. This was accompanied by a small alteration in CV from 84 to 94 (Fig. 39). Conversely, the same temperature switch to 37°C in CG2001-Epa1-HA resulted in a more marked ~33.1% increase in Epa1-HA expression. In addition this increased expression was accompanied by a ~21% decrease in the CV value (Fig. 40). Despite temperature having a more marked effect on Epa1-HA expression in strain CG2001-Epa1-HA the observed increase was not associated with any marked difference in adhesion to Hep2 epithelial cells with only a ~6% increase being observed (Fig. 41).

5.2.2 Response to Nitrogen Limitation

Upon entry to the host environment access to certain nutrients may become limiting. Nitrogen limitation has previously been reported to induce morphological changes leading to invasive growth in pathogenic yeasts, including *C. glabrata* (Gimeno et al., 1992, Csank et al., 1998, Csank and Haynes, 2000). Invasive growth may be an important modification in response to environmental conditions that contributes to pathogenesis. Due to host conditions and possible implications for virulence, I decided to analyse the effect of nitrogen starvation on Epa1-HA expression in *C. glabrata*.

Previous studies involving nutrient limitation in *C. glabrata* utilised a 5% synthetic complete (SC) medium for which all SC components, including ammonium sulphate ((NH₄)₂SO₄), were at 5% of the standard concentration (Domergue et al., 2005). Therefore, in order to limit cells for nitrogen specifically both BG2-Epa1-HA and CG2001-Epa1-HA were grown in SC medium at 100% (37.8mM) and 5% (1.89mM) of the standard nitrogen concentration used for the medium in the form of (NH₄)₂SO₄, which constitutes the predominant nitrogen source, for at least 15 hours. Limiting nitrogen with the 5% condition had little effect on either mean Epa1-HA expression or heterogeneity (CV) in the BG2-Epa1-HA strain

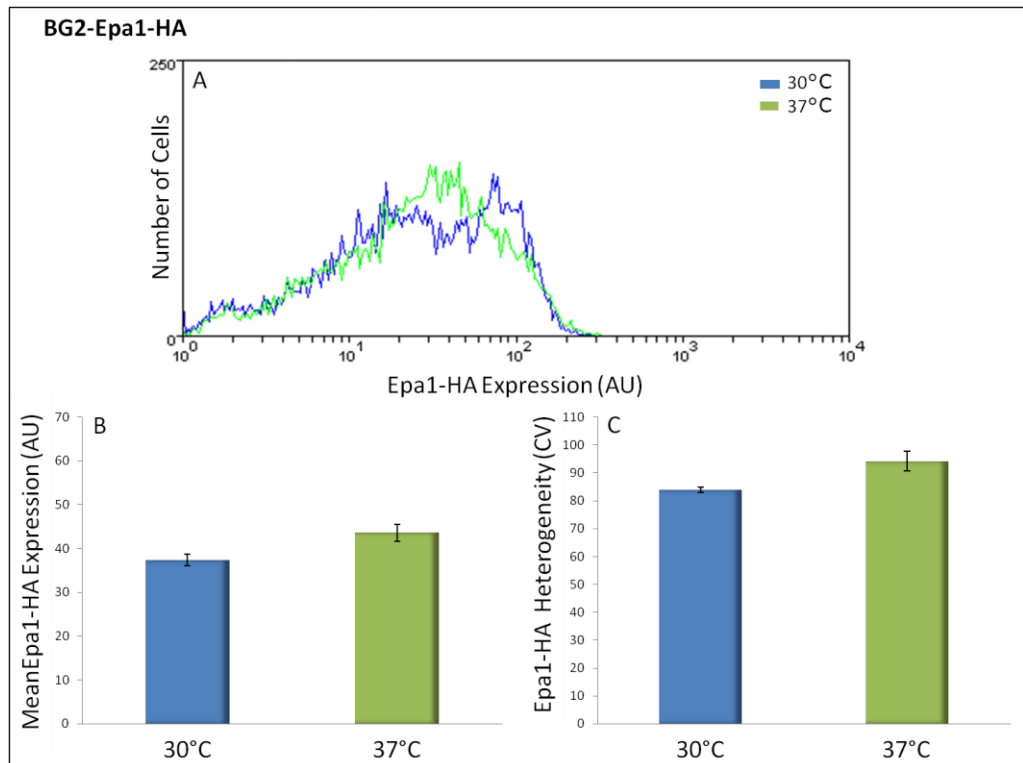


Figure 39 – The effect of Temperature on Epa1-HA expression in BG2-Epa1-HA. Cells were maintained at the appropriate temperature in YPD medium for at least 15 hours prior to analysis. In each instance, blue indicates expression at 30°C while green illustrates expression at 37°C. **(A)** Epa1-HA expression (AU) was analysed by flow cytometry following staining of exponential phase cells with anti-HA, Alexa Fluor® 488 conjugate antibody. **(B)** Mean Epa1-HA expression levels (AU) are shown and **(C)** heterogeneity is illustrated by Epa1-HA CV values. Data presented **(B, C)** are means of independent triplicate experiments \pm SEM.

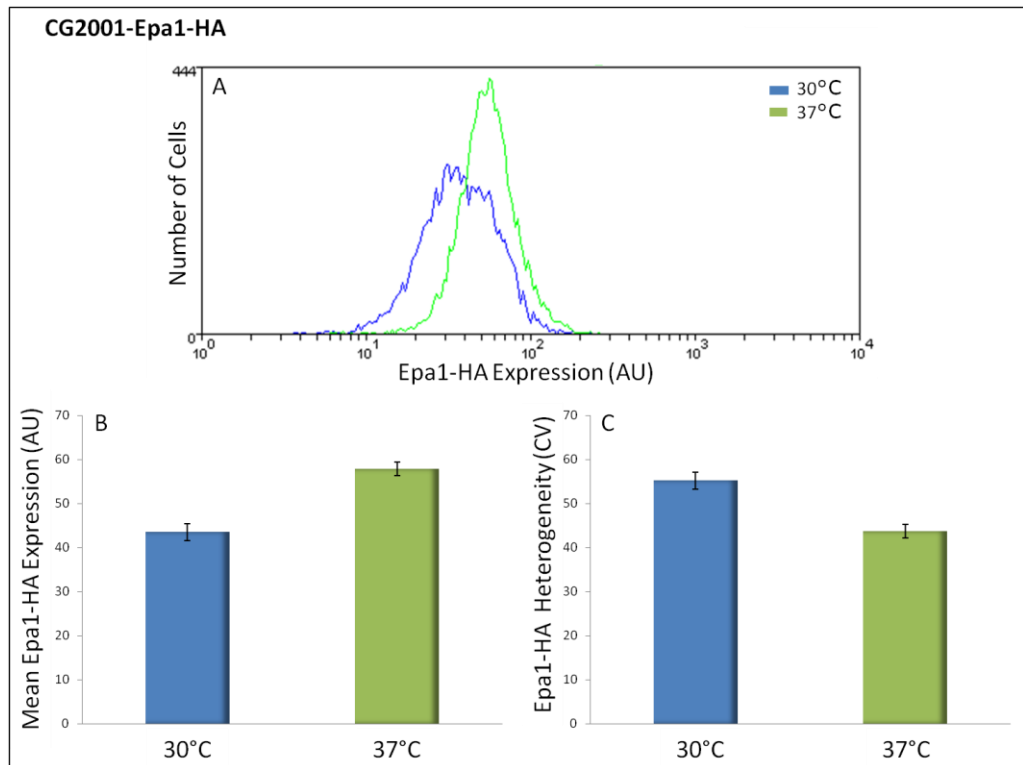


Figure 40 – The effect of Temperature on Epa1-HA expression in CG2001-Epa1-HA. Cells were maintained at the appropriate temperature in YPD medium for at least 15 hours prior to analysis. In each instance, blue indicates expression at 30°C while green illustrates expression at 37°C. **(A)** Epa1-HA expression (AU) was analysed by flow cytometry following staining of exponential phase cells with anti-HA, Alexa Fluor® 488 conjugate antibody. **(B)** Mean Epa1-HA expression levels (AU) are shown and **(C)** heterogeneity is illustrated by Epa1-HA CV values. Data presented **(B, C)** are means of independent triplicate experiments \pm SEM.

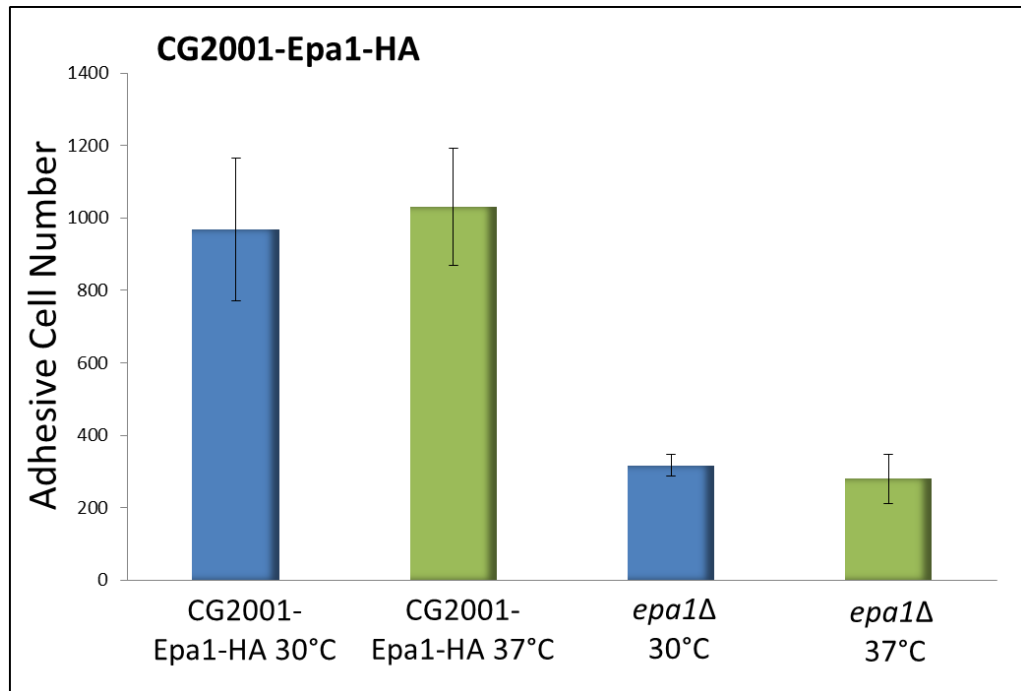


Figure 41 – The effect of temperature on adhesion of CG2001-Epa1-HA cells to Hep2 epithelial cell. Cells were grown overnight in YPD medium at either 30°C or 37°C, before dilution into fresh YPD medium and further growth at the appropriate temperature to exponential phase. Adhesion assays to Hep2 epithelial cells were performed, after which adhesive cells were removed and plated on YPD agar. The resulting number colony forming units (cfu) was used to determine adherent cell numbers. Data presented are means of adherent cell number calculated from independent triplicate experiments \pm SEM.

background (Fig. 42). An effect of nitrogen was slightly more apparent in the CG2001-Epa1-HA strain background, which demonstrates tighter heterogeneity regulation. In this instance limitation for nitrogen resulted in a 15.8% increase in mean Epa1-HA expression and 8.7% decrease in CV from 68.1 to 62.2 (Fig. 43).

5.2.3 Response to pH Level

The diverse niches occupied by *C. glabrata* within the host environment vary greatly in terms of their ambient pH. Within the human host such pH levels can range from the relatively acidic regions of the stomach and vaginal tract through to the more neutral and basic regions found in the bloodstream and many organs. In addition pH changes over time within a single niche have also been documented, for example in the oral cavity where pH can vary markedly due to changes in diet, the metabolism of other microflora and salivary flow. In addition pH of the vaginal tract can vary from its usual acidic level to slightly alkaline during the menstrual cycle (Davis, 2009, Davis, 2003). Pathogenic fungi must therefore be able to adapt to pH changes within the host and survival in such diverse pH environments suggests that *C. glabrata* possess an effective pH adaptation strategy (Schmidt et al., 2008).

The effect of pH on Epa1-HA expression and heterogeneity was analysed by flow cytometry, following anti-HA antibody staining, in both strain backgrounds; BG2-Epa1-HA and CG2001-Epa1-HA. Three different physiologically relevant pH values were tested; an acidic pH of 4 such that is found in the human vaginal cavity, pH7.4 which represents the pH of human blood and many tissues, and a pH of 8 similar to the more alkaline conditions of the gastrointestinal tract (Schmidt et al., 2008, Davis, 2009). These experiments were performed using Pan Fungal Medium (PFM) which was developed specifically for the standardisation of experiments involving the analysis of pH responses in yeasts and filamentous fungi (Schmidt et al., 2008). Cells were maintained at the appropriate pH for at least 15 hours prior to analysis. This investigation revealed pH to have little effect on either Epa1-HA mean expression or heterogeneity in the BG2-Epa1-HA strain background, although lowest mean Epa1-HA expression levels were evident at pH7.4. Heterogeneity levels also remained quite similar in BG2-Epa1-HA cells grown at the three pHs (Fig. 44). Alteration of growth medium pH had a greater effect on mean Epa1-HA expression and heterogeneity in a CG2001-Epa1-HA strain background (Fig. 45). In this

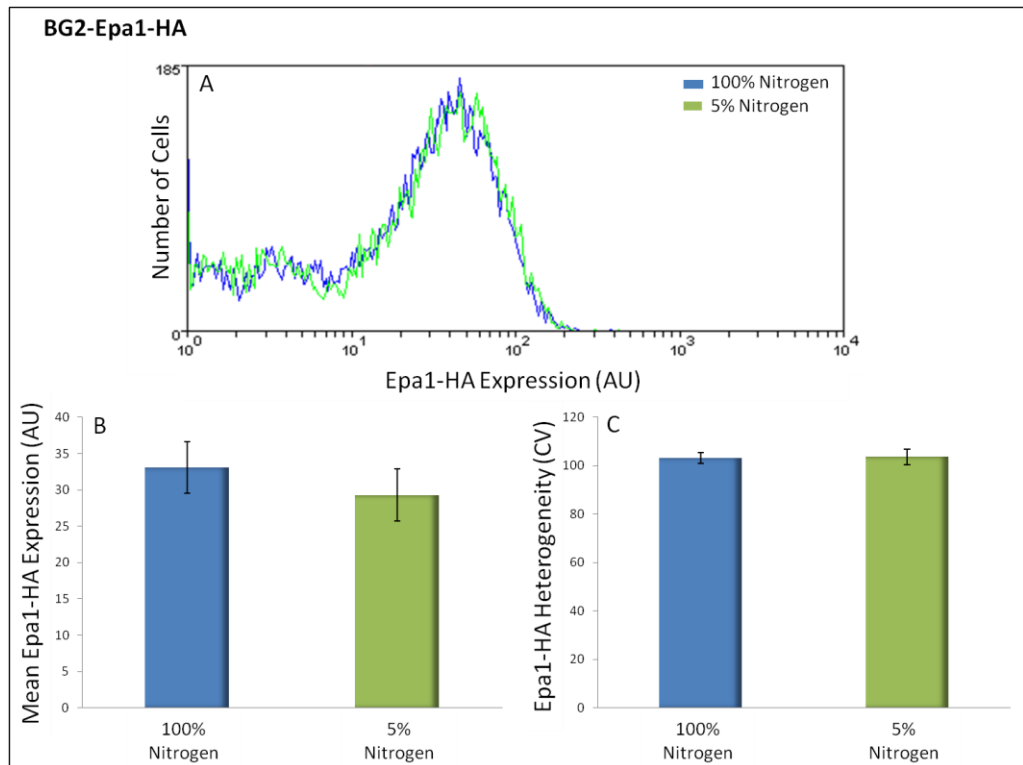


Figure 42 – The effect of Nitrogen limitation on Epa1-HA expression in BG2-Epa1-HA. Cells were grown in SC medium supplemented with the relevant concentration of ammonium sulphate ((NH₄)₂SO₄) for at least 15 hours prior to analysis. In each instance, blue indicates 100% Nitrogen ((NH₄)₂SO₄) while green illustrates 5% Nitrogen ((NH₄)₂SO₄) in otherwise unmodified SC medium. **(A)** Epa1-HA expression (AU) was analysed by flow cytometry following staining of exponential phase cells with anti-HA, Alexa Fluor® 488 conjugate antibody. **(B)** Mean Epa1-HA expression levels (AU) are shown and **(C)** heterogeneity is illustrated by Epa1-HA CV values. Data presented **(B, C)** are means of independent triplicate experiments ±SEM.

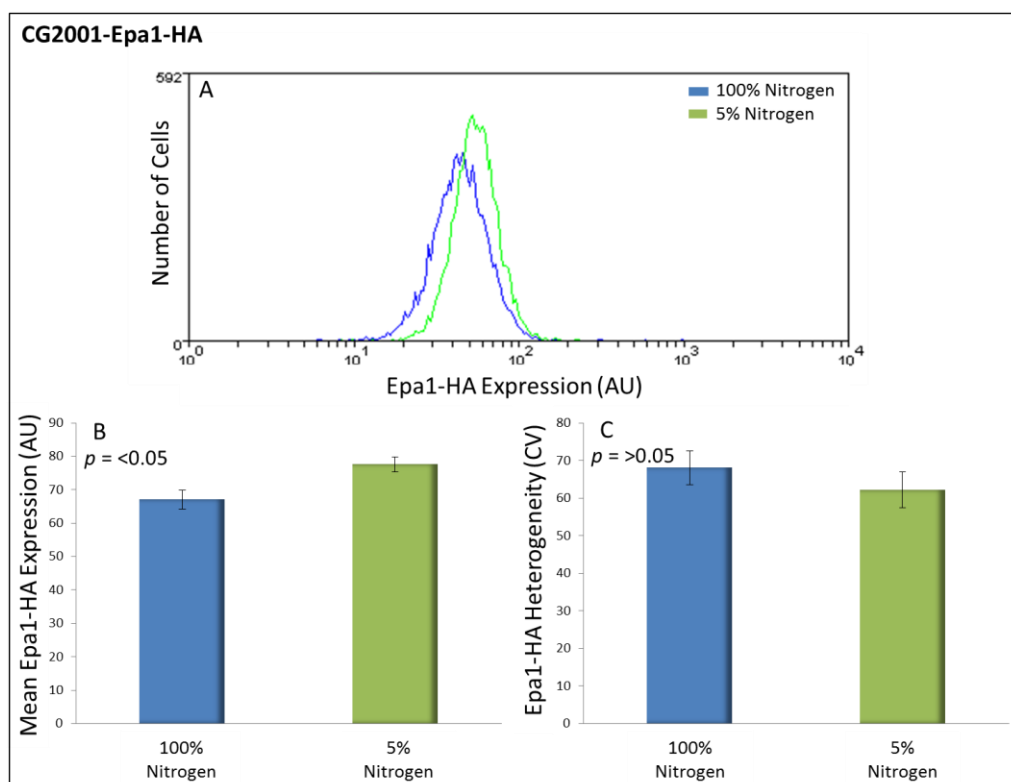


Figure 43 – The effect of Nitrogen limitation on Epa1-HA expression in CG2001-Epa1-HA. Cells were grown in SC medium supplemented with the relevant concentration of ammonium sulphate ($\text{gL}^{-1} (\text{NH}_4)_2\text{SO}_4$) for at least 15 hours prior to analysis. In each instance, blue indicates 100% Nitrogen ($\text{gL}^{-1} (\text{NH}_4)_2\text{SO}_4$) while green illustrates 5% Nitrogen ($\text{gL}^{-1} (\text{NH}_4)_2\text{SO}_4$) in otherwise unmodified SC medium. **(A)** Epa1-HA expression (AU) was analysed by flow cytometry following staining of exponential phase cells with anti-HA, Alexa Fluor® 488 conjugate antibody. **(B)** Mean Epa1-HA expression levels (AU) are shown and **(C)** heterogeneity is illustrated by Epa1-HA CV values. The differences in Epa1-HA expression and CV observed between the two growth conditions were deemed to be either, significant ($p < 0.05$), or not significant ($p > 0.05$) according to the Student's t-test (Materials and Methods). Data presented **(B, C)** are means of independent triplicate experiments \pm SEM.

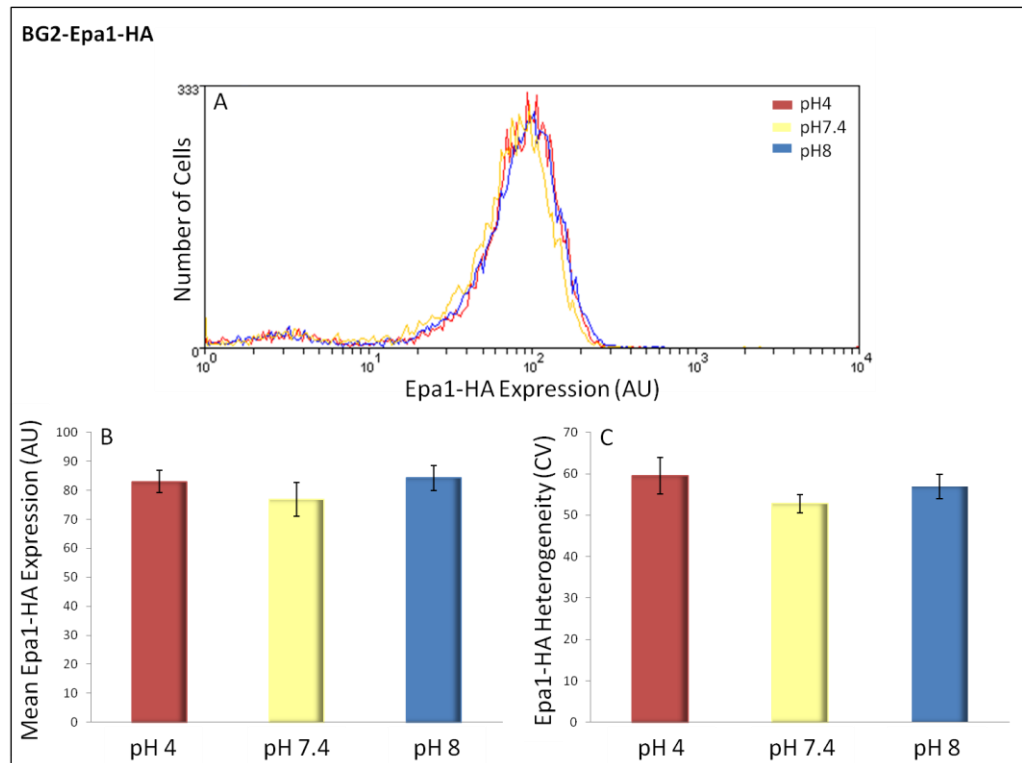


Figure 44 – The effect of ambient pH on Epa1-HA expression in BG2-Epa1-HA. In each instance, red indicates pH4, yellow indicate pH7.4, and blue indicates pH8. Cells were grown in PFM at the appropriate pH for at least 15 hours prior to analysis. **(A)** Epa1-HA expression (AU) was analysed by flow cytometry following staining of exponential phase cells with anti-HA, Alexa Fluor® 488 conjugate antibody. **(B)** Mean Epa1-HA expression levels (AU) are shown and **(C)** heterogeneity is illustrated by Epa1-HA CV values. Data presented **(B, C)** are means of independent triplicate experiments \pm SEM.

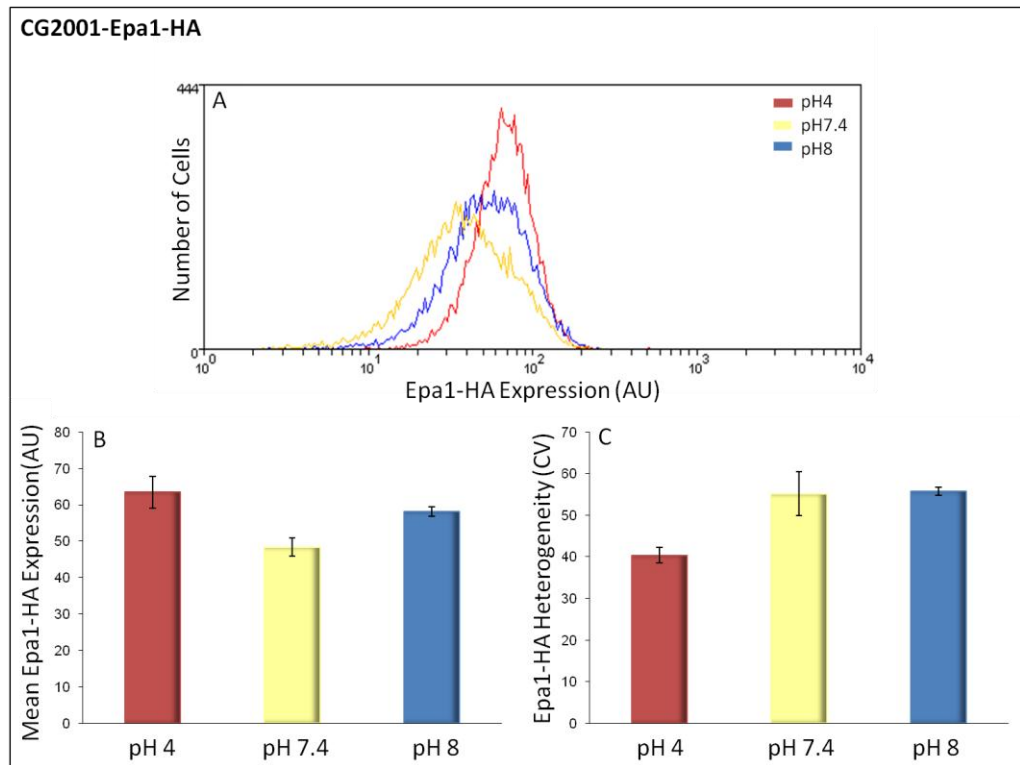


Figure 45 – The effect of ambient pH on Epa1-HA expression in CG2001-Epa1-HA. In each instance, red indicates pH4, yellow indicate pH7.4, and blue indicates pH8. Cells were grown in PFM at the appropriate pH for at least 15 hours prior to analysis. **(A)** Epa1-HA expression (AU) was analysed by flow cytometry following staining of exponential phase cells with anti-HA, Alexa Fluor[®] 488 conjugate antibody. **(B)** Mean Epa1-HA expression levels (AU) are shown and **(C)** heterogeneity is illustrated by Epa1-HA CV values. Differences of statistical significance were identified using a Student's t-test (see text and Materials and Methods). Data presented **(B, C)** are means of independent triplicate experiments \pm SEM.

instance the lowest level of Epa1-HA expression was seen at pH7.4, with mean Epa1-HA expression being significantly (24% and 16%) lower than that observed at pH4 and pH8 respectively according to the Student's t-test. The highest expression level, at pH4, corresponded to the lowest level of heterogeneity, (CV=40.4), in this strain background. By contrast CVs for Epa1-HA expression at pH7.4 and pH8 are very similar at 55.2 and 55.8 respectively. Thus heterogeneity at these latter pH values was approximately 37% higher than at pH4, a difference that was indeed deemed statistically significant (Fig.45).

5.3 Transcriptional Silencing affects *EPA1*/Epa1 Expression and Heterogeneity

As discussed in the main introduction to this chapter a number of studies have demonstrated that inhibition of transcriptional silencing, both directly, including *SIR3* deletion, and indirectly, can release telomeric silencing and de-repress *EPA* expression including *EPA1* (De Las Penas et al., 2003, Castano et al., 2005, Rosas-Hernandez et al., 2008). Consequently I wanted to determine whether transcriptional silencing contributed to the heterogeneity of Epa1 expression in our two strains.

5.3.1 *Sir3-Dependent EPA1 Transcription in a BG2 Strain Background*

Analogous to BG2-Epa1-HA, which enables visualisation of Epa1-HA protein expression at the cell surface in a BG2 strain background the *EPA1*-GFP transcriptional fusion (BG2-*EPA1*-GFP), demonstrated a high level of expression heterogeneity in a BG2 background as demonstrated in chapter 4 (Fig. 29, 30). Flow cytometric analysis of a *sir3*Δ mutant constructed in this *EPA1*-GFP BG2 background (Materials and Methods) indicated *EPA1* heterogeneity to be markedly dependent on Sir-mediated transcriptional silencing (Fig. 46). Loss of transcriptional silencing at the telomeres via deletion of *SIR3* resulted in a 57% decrease in the observed *EPA1*-GFP heterogeneity, from CV ~107 to ~46 (Fig. 46A, C). In addition, the results demonstrated that the decreased heterogeneity observed following loss of transcriptional silencing was accompanied by a ~53% increase in mean *EPA1*-GFP expression (Fig. 46A, B). These changes in Epa1-HA expression and CV demonstrated *p* values <0.05 according to the Student's t-test and were thus deemed statistically significant. The increase in *EPA1*-GFP expression seemed attributable to the loss of a subpopulation of low GFP

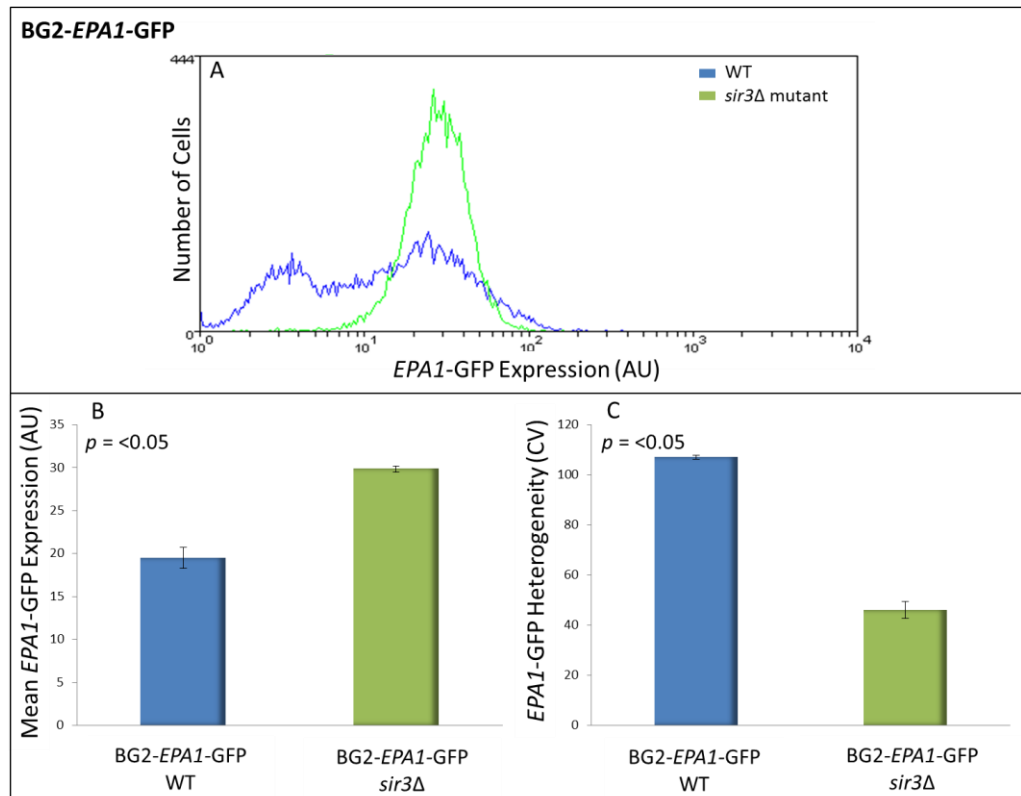


Figure 46 – The role of Sir3-dependent transcriptional silencing on cell surface Epa1 expression in the BG1-EPA1-GFP strain. Wild type (WT) and *sir3Δ* mutant cells were grown to exponential phase in YPD medium before analysis by flow cytometry. In each instance WT cells are represented in blue while *sir3Δ* mutant cells are indicated in green. **(A)** EPA1-GFP expression (AU) was analysed by flow cytometry. **(B)** Mean EPA1-GFP expression levels (AU) are shown and **(C)** heterogeneity is illustrated by EPA1-GFP CV values. The differences in Epa1-HA expression and CV observed between WT and *sir3Δ* mutant cells were deemed to be either, significant ($p < 0.05$), or not significant ($p > 0.05$) according to the Student's t-test (Materials and Methods). Data presented **(B,C)** are means of independent triplicate experiments \pm SEM.

expressing cells that was present in the wild type (Fig 46A). Loss of this highly silenced population of cells would also be expected to be a major contributing factor to the decreased heterogeneity exhibited by *EPA1*-GFP *sir3Δ* mutant cells. The results thus indicate that transcriptional silencing plays a major role in the regulation of *EPA1* expression and its heterogeneity.

5.3.2 *Sir3-Dependent Transcriptional Silencing in CG2001-Epa1-HA*

In order to identify the effect of Sir-dependent transcriptional silencing on cell surface Epa1 protein expression, which is more relevant for infection, a *sir3Δ* mutant was initially constructed in the Epa1-HA tagged strain CG2001-Epa1-HA (Materials and Methods). Subsequent flow cytometric analysis of this CG2001-Epa1-HA *sir3Δ* mutant strain, following anti-HA, Alexa Fluor® 488 conjugate antibody staining, revealed unexpected results. The CG2001-Epa1-HA *sir3Δ* mutant demonstrated a ~28% decrease in mean Epa1-HA expression compared to the wild type (Fig. 47). In addition, and in contrast to results obtained in a BG2 strain above, inhibition of transcriptional silencing had virtually no effect on Epa1-HA heterogeneity in CG2001-Epa1-HA, with wild type and *sir3Δ* mutant CV values of ~55 and ~53 respectively (Fig. 47). This result may be related to the much lower level of Epa1-HA heterogeneity that is already present in wild type cells of this strain background compared to the BG2 strain background (4.2.4). The population of low expressing cells evident in the BG2 strain background (BG2-Epa1-HA and BG2-*EPA1*-GFP) is absent from CG2001-Epa1-HA and it is this sub-population that was found to be eliminated upon *sir3* deletion in BG2-*EPA1*-GFP. It is noted that this comparison is between strains expressing an *EPA1*-GFP transcriptional fusion and Epa1-HA translational fusion, which in itself creates the potential for differing results. Nevertheless, one possible explanation for the results is that an already-tight regulation of Epa1-HA expression across a CG2001-Epa1-HA cell population (i.e. low heterogeneity) relates to weak silencing in this background (addressed further in 5.3.5).

A single copy plasmid containing the *SIR3* ORF under the control of its native promoter and terminator was constructed to complement the *sir3Δ* mutant. This involved amplification of the *SIR3* region as a SacI fragment which was then inserted into the single copy *C. glabrata* plasmid pCgACT-14 (Kitada et al., 1996) to yield pCgACT-14-*SIR3* (Materials and Methods). This plasmid includes tryptophan as a selection marker and

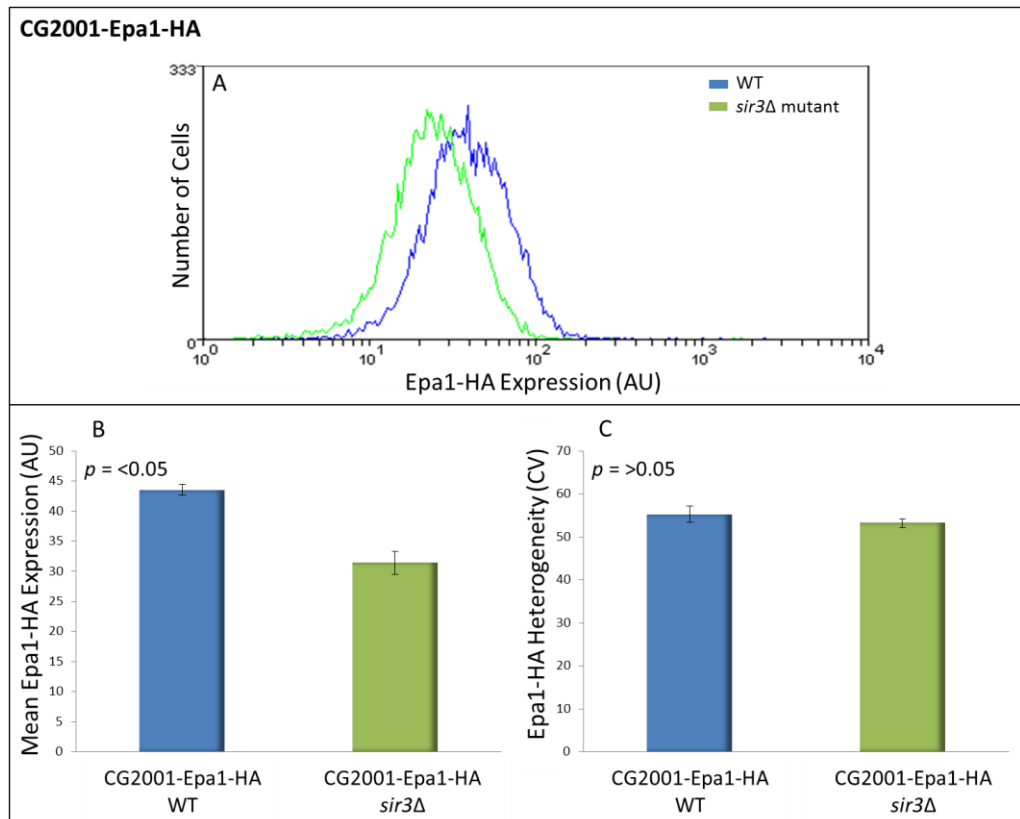


Figure 47 – The role of Sir3-dependent transcriptional silencing on cell surface Epa1 expression in the CG2001-Epa1-HA strain. Wild type (WT) and *sir3Δ* mutant cells were grown to exponential phase in YPD medium before analysis by flow cytometry. In each instance wild type cells are represented in blue while *sir3Δ* mutant cells are indicated in green. **(A)** Epa1-HA expression (AU) was analysed by flow cytometry following staining of exponential phase cells with anti-HA, Alexa Fluor® 488 conjugate antibody. **(B)** Mean Epa1-HA expression levels (AU) are shown and **(C)** heterogeneity is illustrated by Epa1-HA CV values. The differences in Epa1-HA expression and CV observed between WT and *sir3Δ* mutant cells were deemed to be either, significant ($p < 0.05$), or not significant ($p > 0.05$) according to the Student's t-test (Materials and Methods). Data presented **(B, C)** are means of independent triplicate experiments \pm SEM.

could therefore be transformed into CG2001-Epa1-HA *sir3* Δ mutant cells. Analysis of transformed cells by flow cytometry demonstrated that introduction of functional *SIR3* successfully complemented the *sir3* Δ mutant, with Epa1-HA expression reverting back to wild type levels (Fig. 48A). Heterogeneity levels, as expected, remained relatively unaffected (Fig. 48B). Unfortunately, the tryptophan selection marker made pCgACT-14-*SIR3* inappropriate for complementation of BG2-*EPA1*-GFP. The limited available selection markers ultimately resulted in multiple genetic manipulations proving difficult in a BG2 background.

5.3.3 Corroboration of Strain Dependent Sir-Mediated Transcriptional Silencing of *Epa1*-HA

The results presented above suggest a strain dependent regulation of *EPA1*/Epa1 expression by transcriptional silencing. This mechanism of regulation appeared to be more influential in the BG2 background (BG2-*EPA1*-GFP). By contrast, loss of Sir3 activity in the CG2001-Epa1-HA strain actually produced a decrease in mean Epa1-HA expression. Despite such indications that Sir-dependent *EPA1* silencing may differ according to strain background it must be considered that these experiments were performed using different reporters of expression. The effects of *SIR3* deletion were determined using an *EPA1*-GFP transcriptional fusion in the BG2 background while the *C. glabrata* CG2001 HTU Δ , a derivative of the type strain, was analysed through use of an Epa1-HA construct. A corresponding *EPA1*-GFP transcriptional fusion in the CG2001 HTU Δ background was not available. Construction of such a strain, using a GFP fragment flanked by 50bp regions of *EPA1* homology, was ineffective. It was, however, determined to focus on cell surface Epa1 expression which is more functionally relevant in terms of infection. Attempts were made to create a *sir3* Δ mutant of the BG2-Epa1-HA strain, but these proved unsuccessful mainly due to the difficulty of having limited available selection markers. Non-specific growth was evident when using selection markers that were available, such as hygromycin, and resulted in large numbers of colonies to be tested by diagnostic PCR, no successful transformants were detected. As discussed in chapter 4 (4.2.3) the *EPA1*-HA transforming fragment included *URA3* as a selection marker. Attempts were made to remove this *URA3* marker and select for successful transformants on 5FOA, which inhibits growth of Ura⁺ cells, thus allowing the *URA3* marker to be utilised in BG2-Epa1-HA for deletion of Sir3. Non-specific growth again proved

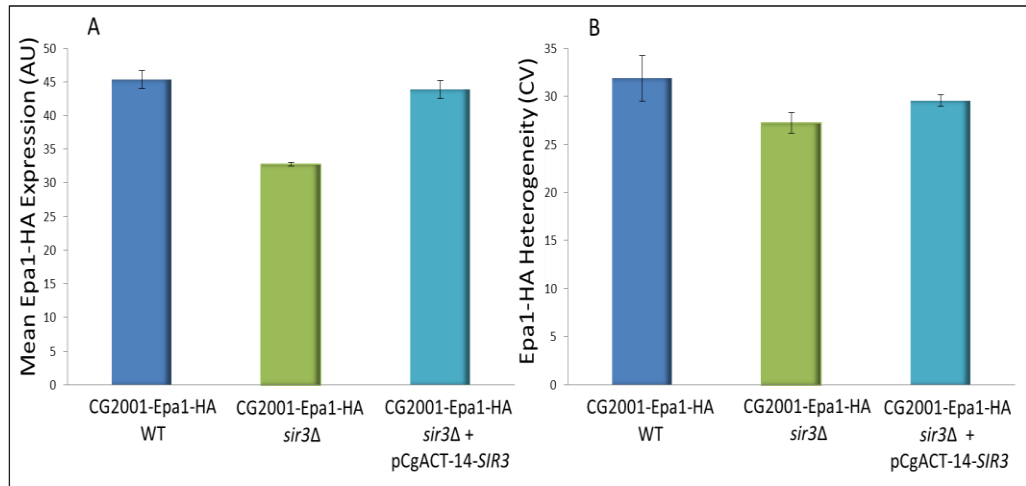


Figure 48 – Complementation of CG2001-Epa1-HA *sir3Δ* cells with pCgACT-14-*SIR3*. Cells were grown to exponential phase in YNB without tryptophan to ensure retention of pCgACT-14-*SIR3* prior to staining with anti-HA, Alexa Fluor® 488 conjugate antibody and analysis by flow cytometry. Wild type (WT) cells are shown in dark blue, *sir3Δ* cells are shown in green, and cells complemented with pCgACT-14-*SIR3* are shown in light blue. **(A)** Mean Epa1-HA expression levels (AU) are shown and **(B)** heterogeneity is illustrated by Epa1-HA CV values. Data presented **(A, B)** are means of independent triplicate experiments \pm SEM.

problematic, possibly due to the sub-set of cells that demonstrate silencing at the *EPA1* locus in this strain background which may mask the presence of *URA3*.

In order to substantiate that Sir-mediated regulation of Epa1 does differ according to strain background I needed to compare strains in which Epa1 expression was measured by the same method. Consequently it was decided to use Epa1-HA tagged strains, BG2-Epa1-HA and CG2001-Epa1-HA, in which transcriptional silencing would be inhibited by some other method, namely nicotinic acid (NA) limitation (Domergue et al., 2005). Further to this, *sir3Δ* mutants were constructed in untagged BG2 and CG2001 HTUΔ strains with cell surface Epa1 expression measured using an anti-Epa1 antibody (Kaur et al., 2007) kindly donated by B. Cormack (John Hopkins University).

5.3.3.1 Inhibition of Silencing in CG2001-Epa1-HA and BG2-Epa1-HA by Nicotinic Acid Limitation

C. glabrata is auxotrophic for NA and as a result requires an external supply in order to assimilate NAD⁺ and enable function of the NAD⁺-dependent histone deacetylase Sir2, an essential component of the transcriptional silencing machinery. Previous studies have successfully repressed transcriptional silencing of *EPA* genes in *C. glabrata* by limiting growth media for NA (Domergue et al., 2005). These authors also demonstrated that gene de-repression by NA limitation was specifically caused by inhibition of Sir2 activity and thus inhibition of Sir-mediated silencing. By limiting cells for NA it was possible to inhibit transcriptional silencing and analyse the effects on Epa1-HA expression in the two different strain backgrounds.

Cells were limited for NA as previously described, by growth in SC medium supplemented with either the standard amount of NA (3.25μM; 100%) or 5% NA (0.1625μM) (Domergue et al., 2005). Cells were grown overnight in the experimental medium before re-inoculation into appropriate SC medium and further growth to reach exponential phase. The results obtained with Sir-dependent transcriptional silencing by NA limitation broadly agreed with the data from *sir3Δ* mutants, indicating Sir-dependent regulation of Epa1 indeed to be dependent upon strain background. Thus, NA limitation had a greater effect on Epa1-HA expression in strain BG2-Epa1-HA, with CV values decreasing from ~88 to ~63 upon inhibition of silencing (Fig. 49). By contrast, inhibition of

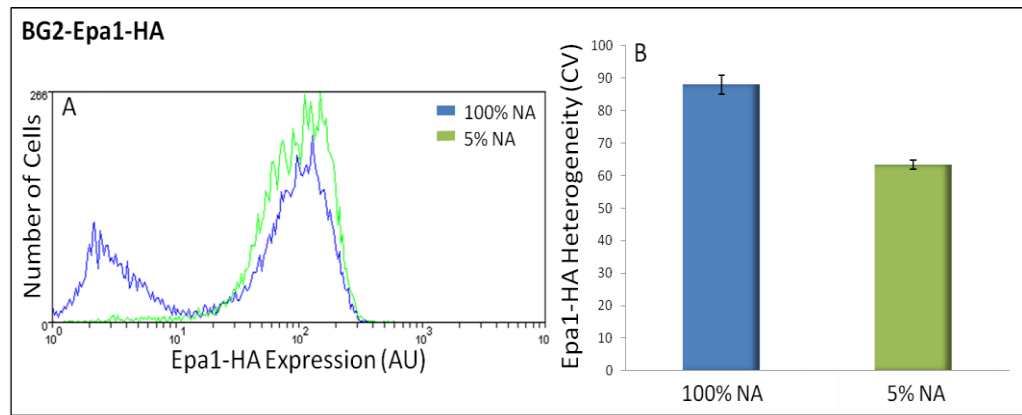


Figure 49 – Inhibiting transcriptional silencing by NA limitation and its effect on Epa1-HA heterogeneity (CV) in BG2-Epa1-HA cells. Results obtained from growth in 100% NA are shown in blue, while those from 5% NA are depicted in green. Cells were grown overnight in SC medium with either 100% or 5% NA before being re-inoculated into the appropriate fresh SC medium and grown to exponential phase. **(A)** Epa1-HA expression (AU) was analysed by flow cytometry following staining of cells with anti-HA, Alexa Fluor® 488 conjugate antibody. **(B)** Heterogeneity of Epa1-HA expression is demonstrated by Epa1-HA CV values. Data presented are means of independent triplicate experiments \pm SEM.

silencing by limiting NA availability had no effect on Epa1-HA expression heterogeneity in a CG2001-Epa1-HA background with CV values remaining at ~ 35 (Fig. 50). Mean Epa1-HA expression analysis was also in agreement with the results obtained with *sir3* Δ mutants. The decreased heterogeneity in strain BG2-Epa1-HA was accompanied by $\sim 37\%$ increase in mean Epa1-HA expression when cells were limited for NA (Fig. 51A). Similarly, as seen for the CG2001-Epa1-HA *sir3* Δ mutant, wild type cells of this background demonstrated $\sim 27\%$ decreased mean Epa1-HA expression when limited for NA (Fig. 51B). The latter observation, while unexpected, was therefore corroborated with a *sir3* Δ mutant and NA limitation. Control experiments utilising CG2001-Epa1-HA *sir3* Δ mutant cells grown in SC medium supplemented with either 100% or 5% NA revealed no marked additional phenotype in mean Epa1-HA expression or Epa1-HA heterogeneity (CV) following growth in NA limited SC medium (Fig. 52). This result is in concordance with the previous identification that NA limitation induced *EPA* de-repression is specifically due to an inhibition of transcriptional silencing (Domergue et al., 2005).

5.3.3.2 – Analysis of Cell Surface Epa1 Expression in *sir3* Δ Mutant Cells via an Anti-Epa1 Antibody

The construction of *sir3* Δ deletion mutants in untagged-Epa1 BG2 and CG2001 HTU Δ strains (Materials and Methods) enabled cell surface Epa1 expression to be measured in both backgrounds through use of an anti-Epa1 antibody (Kaur et al., 2007) kindly donated by B. Cormack (John Hopkins University). This antibody was not mono-specific for Epa1 but also capable of recognising Epa6 and Epa7 and possibly other Epa adhesins. Consequently, in order to obtain antibodies with a higher specificity for Epa1, pre-absorption was performed using an *epa1* Δ deletion strain grown under conditions of limited NA to induce expression of other *EPA* genes (Domergue et al., 2005), (Materials and Methods). Specificity of the pre-absorbed antibody for Epa1 was checked using the wild type BG2 and *epa1* Δ deletion strains, again grown in limited NA, along with a secondary Alexa Fluor[®] 488 conjugate antibody and analysis by flow cytometry. This revealed that the pre-absorbed antibody was indeed specific for Epa1 as virtually no staining was observed in *epa1* Δ cells compared to its non-pre-absorbed counterpart or compared to staining observed for wild type cells.

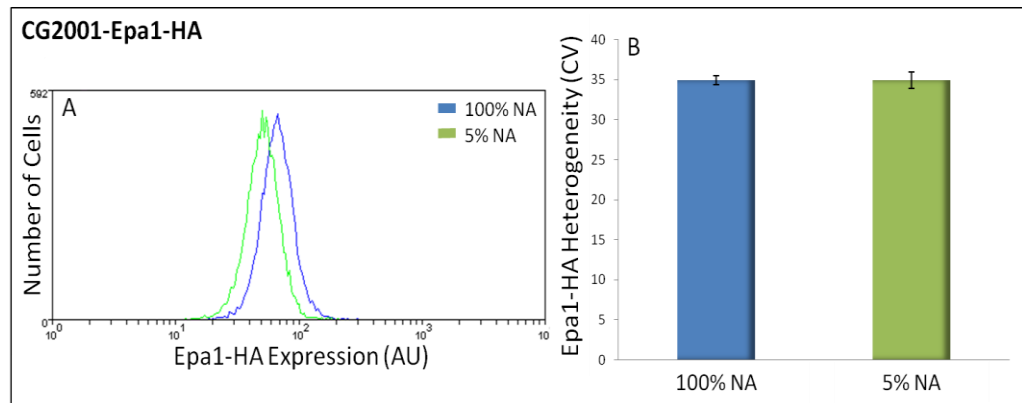


Figure 50 – Inhibiting transcriptional silencing by NA limitation and its effect on Epa1-HA heterogeneity (CV) in CG2001-Epa1-HA cells. Results obtained from growth in 100% NA are shown in blue, while those from 5% NA are depicted in green. Cells were grown overnight in SC medium with either 100% or 5% NA before being re-inoculated into the appropriate fresh SC medium and grown to exponential phase. **(A)** Epa1-HA expression (AU) was analysed by flow cytometry following staining of cells with anti-HA, Alexa Fluor® 488 conjugate antibody. **(B)** Heterogeneity of Epa1-HA expression is demonstrated by Epa1-HA CV values. Data presented are means of independent triplicate experiments \pm SEM.

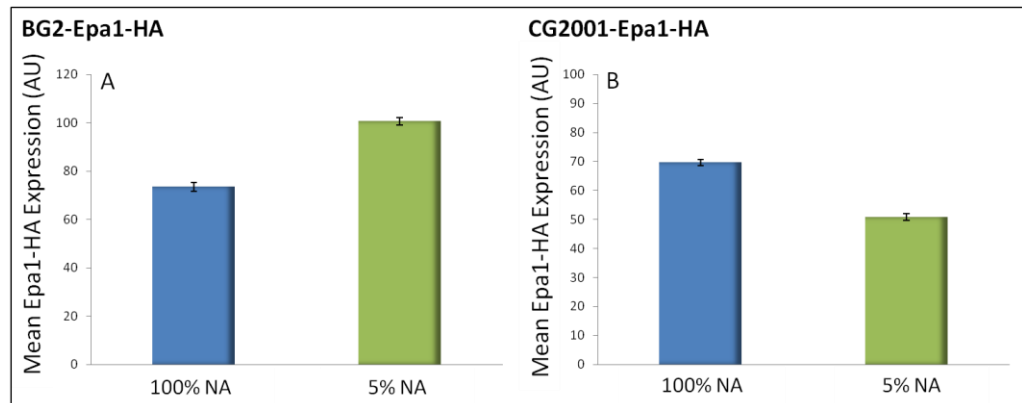


Figure 51 – Inhibiting transcriptional silencing by NA limitation and its effect on mean Epa1-HA expression (AU) in **(A)** BG2-Epa1-HA and **(B)** CG2001-Epa1-HA strain backgrounds. Results obtained from growth in 100% NA are shown in blue, while those from 5% NA are depicted in green. Cells were grown overnight in SC medium with either 100% or 5% NA before being re-inoculated into the appropriate fresh SC medium and grown to exponential phase. Cells were then stained with anti-HA, Alexa Fluor® 488 conjugate antibody and analysed by flow cytometry. Data presented are means of independent triplicate experiments \pm SEM.

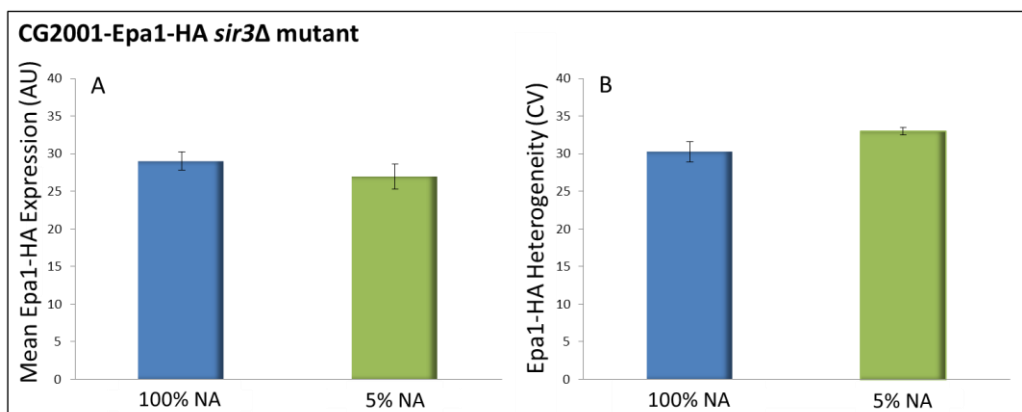


Figure 52 – Inhibiting transcriptional silencing by NA limitation and its effect on Epa1-HA expression in the CG2001-Epa1-HA *sir3Δ* mutant. Results obtained from growth in 100% NA are shown in blue, while those from 5% NA are depicted in green. Cells were grown overnight in SC medium with either 100% or 5% NA before being re-inoculated into the appropriate fresh SC medium and grown to exponential phase. Following anti-HA, Alexa Fluor® 488 conjugate antibody staining cells were analysed by flow cytometry. **(A)** Mean Epa1-HA expression (AU) levels and **(B)** Epa1-HA heterogeneity (CV) values are shown. Data presented are means of independent triplicate experiments \pm SEM.

Analysis of Epa1 cell surface expression in BG2-*sir3Δ* and CG2001-*sir3Δ* deletion strains by flow cytometry using this pre-absorbed anti-Epa1 antibody was in agreement with previous data obtained for *sir3Δ* deletion mutants (5.3.1 and 5.3.2) and following NA limitation (5.3.3.1) (Fig. 53, 54). Inhibition of silencing in the BG2 strain background by this method again caused a marked decrease in Epa1 expression heterogeneity of ~48% accompanied by a more than two-fold increase in mean Epa1 level (Fig. 53). By contrast, and as expected according to previous data, Epa1 expression heterogeneity in the CG2001-*sir3Δ* deletion mutant remained virtually unchanged compared to wild type cells with CV values of ~58 and ~56 being obtained respectively. In further corroboration of the earlier results obtained during this study, mean Epa1 expression levels were seen to decrease by ~11% upon *sir3Δ* deletion (Fig. 54).

5.3.4 The Effect of Transcriptional Silencing on EPA1 Transcript Levels also depends on Strain Background

As *EPA1*-GFP transcriptional fusions were not available in the two strains being tested, *EPA1* transcript levels were determined by qRT-PCR following inhibition of transcriptional silencing, via NA limitation. In addition by using wild type strains expressing native (not HA-tagged) Epa1, it was possible to rule out any artifactual effect that insertion of such a tag may have. Cells of the relevant untagged strains, BG2 and CG2001 HTUΔ, were grown in the presence of standard and limited NA concentrations as described above (5.3.3.1). As discussed this method produces cells with "standard" and limited levels of Sir2-mediated transcriptional silencing, respectively (Domergue et al., 2005). Thus, extraction of RNA from such cells enabled comparison of *EPA1* mRNA transcript levels in the two strains in response to inhibition of silencing. The results were similar to those for Epa1 protein expression at the cell surface in the two Epa1-HA tagged versions of these strains. Inhibition of silencing by NA limitation induced increased levels of *EPA1* transcript in the BG2 background whilst *EPA1* transcript levels were decreased in the CG2001 HTUΔ strain background (Fig. 55). The results are consistent with regulation at the transcript level determining the effects also seen at the protein level.

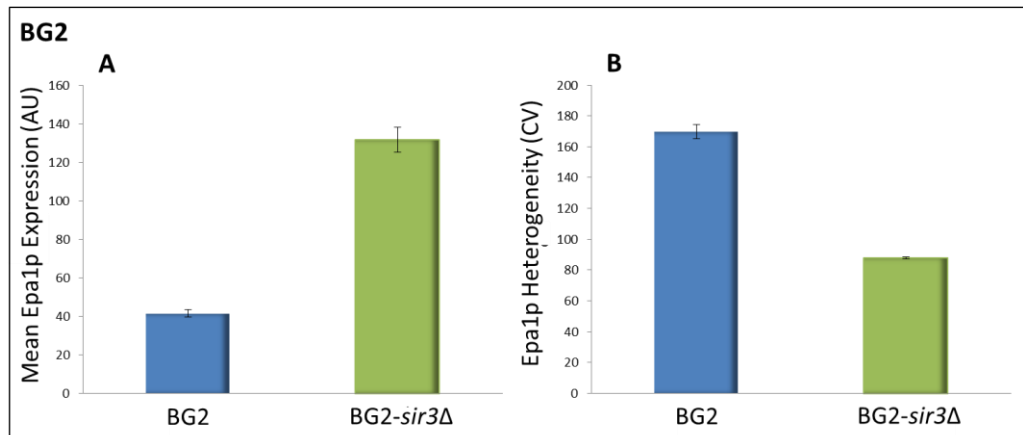


Figure 53 – The role of Sir3-dependent transcriptional silencing on cell surface Epa1 expression in a BG2 strain background. Wild type (blue) and *sir3Δ* deletion mutant (green) cells were grown to exponential phase in YPD medium before probing for Epa1 using an anti-Epa1 antibody and a secondary Alexa Fluor[®] 488 conjugate antibody before analysis by flow cytometry. **(A)** Mean Epa1p expression levels (AU) are shown and **(B)** heterogeneity is illustrated by Epa1p expression CV values. Data presented are means of independent triplicate experiments \pm SEM.

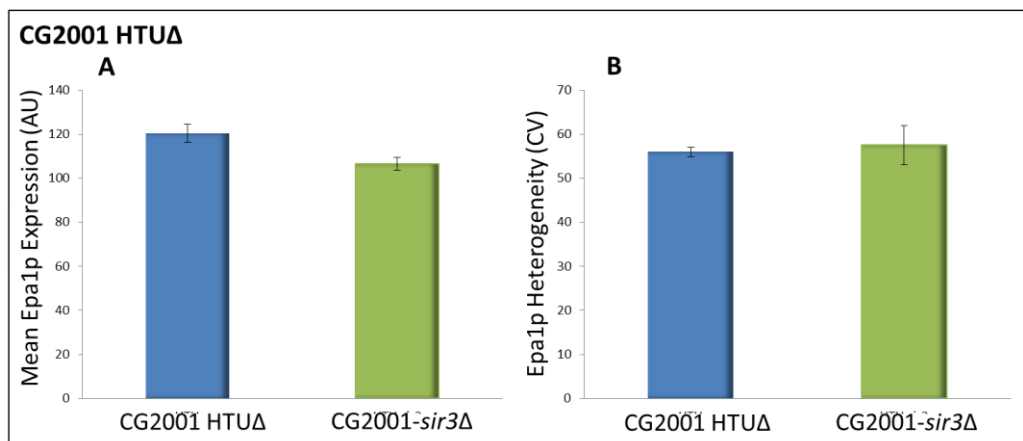


Figure 54 – The role of Sir3-dependent transcriptional silencing on cell surface Epa1 expression in a BG2 strain background. Wild type (blue) and *sir3Δ* deletion mutant (green) cells were grown to exponential phase in YPD medium before probing for Epa1 using an anti-Epa1 antibody and a secondary Alexa Fluor[®] 488 conjugate antibody before analysis by flow cytometry. **(A)** Mean Epa1p expression levels (AU) are shown and **(B)** heterogeneity is illustrated by Epa1p expression CV values. Data presented are means of independent triplicate experiments \pm SEM.

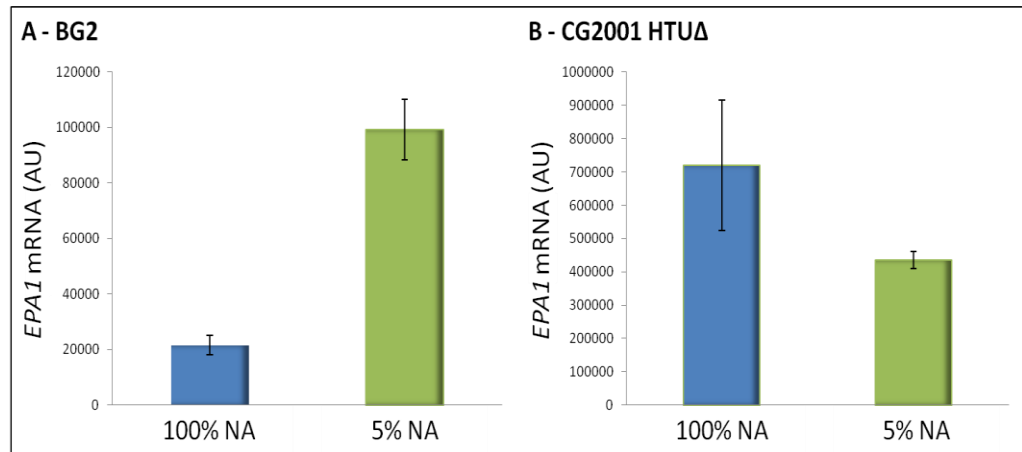


Figure 55 – *EPA1* mRNA levels in **(A)** BG2 and **(B)** CG2001 HTUΔ following NA limitation to inhibit transcriptional silencing. Cells were grown overnight in SC medium containing either 100% NA (blue) or 5% NA (green) before re-inoculation into the appropriate fresh SC medium and growth to exponential phase. RNA was extracted from $\sim 1 \times 10^7$ cells grown under the relevant condition, and *EPA1* mRNA quantified using standardised cDNA additions in all reactions. The data shown are means from three independent experiments (each analysed in triplicate) \pm SEM.

5.3.5 *Sir3 Mediated Silencing appears to be Less Efficient in a CG2001-EPA1-HA Background*

5.3.5.1 *Addition of a Second SIR3 Copy Increases Heterogeneity in CG2001-Epa1-HA*

The observations discussed thus far pertaining to differences in Epa1-HA expression heterogeneity between the two tested strains, along with differences in Sir-mediated regulation of such heterogeneity and of mean expression levels, could suggest that there is weaker transcriptional silencing of *EPA1* in CG2001 HTUΔ than in a BG2 genetic background. Such silencing differences could result from differences in the availability of components of the silencing machinery between strains, among other possibilities. Sir3 has been implicated in *EPA1* regulation both by previous studies (De Las Penas et al., 2003, Castano et al., 2005, Rosas-Hernandez et al., 2008) and my own data (above). The larger distance of *EPA1* from the telomere when compared to other *EPA* genes would be consistent with Sir3, in particular, being pivotal for the efficiency of silencing since it is this protein that propagates spreading of the Sir complex and silencing out and away from the telomere (Renauld et al., 1993, Talbert and Henikoff, 2006). These points, along with the fact that I had already constructed a single copy plasmid containing the *SIR3* ORF, pCgACT-14-*SIR3* (5.3.2), led me to study the effect that an additional copy of *SIR3* may have on silencing of Epa1-HA in the CG2001-Epa1-HA strain. The pCgACT-14-*SIR3* single copy plasmid was transformed into CG2001-Epa1-HA cells and the effect on Epa1-HA expression analysed by anti-HA, Alexa Fluor® 488 conjugate antibody staining and flow cytometry. This analysis showed that introduction of a second *SIR3* copy resulted in an Epa1-HA expression profile in CG2001-Epa1-HA cells that resembled more closely that of the more heterogeneous BG2-Epa1-HA strain (Fig. 56). Introduction of pCgACT-14-*SIR3* yielded a marked increase in Epa1-HA heterogeneity, from CV ~32 to CV ~62 accompanied by a ~37% decrease in mean Epa1-HA expression (Fig. 56).

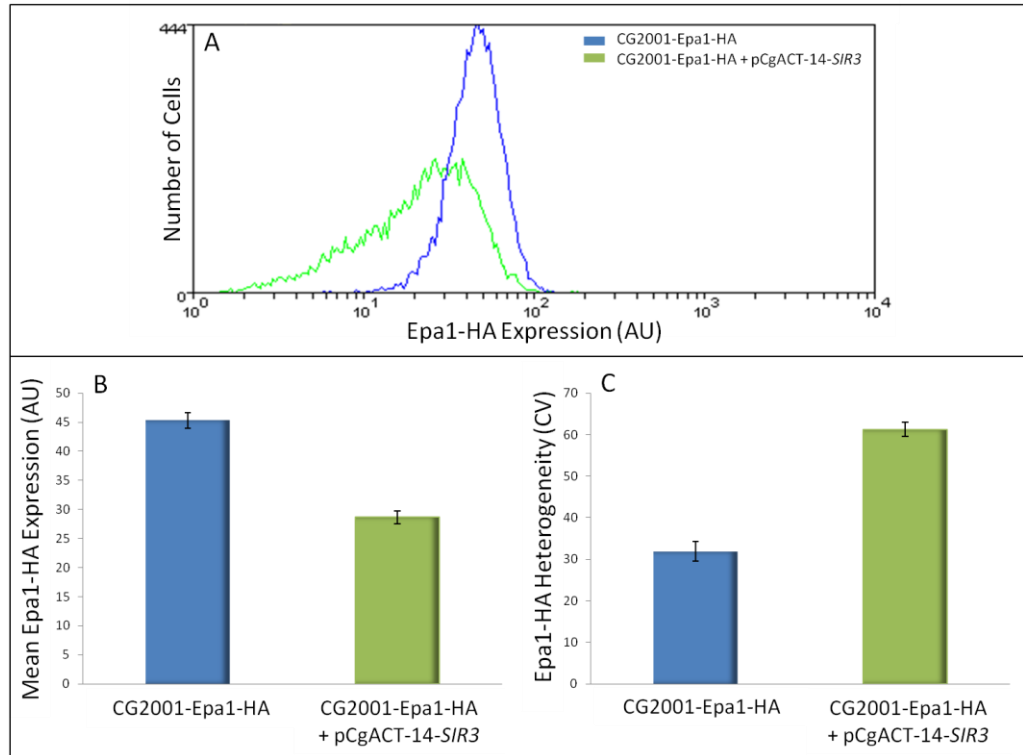


Figure 56 – Effect of ectopic *SIR3* expression on Epa1-HA expression among exponential phase cells of CG2001-Epa1-HA either transformed (green) or not (blue) with pCgACT-14-*SIR3*. **(A)** Flow cytometric histogram of Epa1-HA expression following cell staining with anti-HA, Alexa Fluor[®] 488 conjugate antibody. **(B)** Mean Epa1-HA expression levels (AU) are shown and **(C)** heterogeneity is illustrated by Epa1-HA CV values. Data presented **(B, C)** are means of independent triplicate experiments \pm SEM.

5.3.5.2 *SIR3* Transcript Level appears not to Contribute to the Weakened *EPA1* Silencing Observed in CG2001HTUΔ

As illustrated above, addition of a second copy of *SIR3* to CG2001-Epa1-HA led to an increase in Epa1-HA heterogeneity, more closely resembling Epa1-HA expression in BG2-Epa1-HA. This result added weight to the suggestion that *EPA1* exhibits weakened silencing in a CG2001-Epa1-HA background compared to BG2-Epa1-HA, partly corroborated by *SIR3* expression. It was considered possible that strain dependent Sir3-mediated *EPA1* silencing may have its roots in *SIR3* transcript level differences between the strains. In order to test this I measured the *SIR3* transcript level in both strain backgrounds by qRT-PCR, using the wild type strains BG2 and CG2001 HTUΔ. Levels of the *SIR3* transcript were actually ~1.6 fold higher in the weakly silenced CG2001 HTUΔ strain than in the BG2 strain where transcriptional silencing has been shown to be more influential upon *EPA1* and Epa1-HA expression (Fig. 57). The results indicated that the strain dependency of *EPA1* silencing was not determined by the transcript level of *SIR3*. It is possible that the higher levels of *SIR3* transcript in the CG2001 HTUΔ may reflect some compensatory response for the apparent low silencing efficiency of this strain.

5.3.6 Analysis of NA-Limitation and *EPA1* Expression in a Range of Clinical *C. glabrata* Isolates

As Sir-mediated transcriptional silencing of *EPA1* appeared dependent upon strain background it was decided to test this across a larger range of *C. glabrata* isolates. Clinical isolates acquired from a variety of sources, (Table 9) and kindly donated by Michael Petrou (Imperial College London), were used in this particular study. Each isolate was grown in SC medium supplemented with either 100% or 5% NA to produce populations in which Sir-mediated silencing was either active or inhibited respectively (5.3.3.1). RNA was then extracted from exponential phase cells and *EPA1* transcript levels analysed by qRT-PCR.

Inter-strain differences for Sir-mediated regulation of *EPA1* were evident across the tested clinical isolates (Fig. 58). Strains CI-21, CI-32, CI-146 CI-172, and NCYC388 (a laboratory strain) exhibited increased *EPA1* transcript levels when limited for NA; in this regard, these isolates

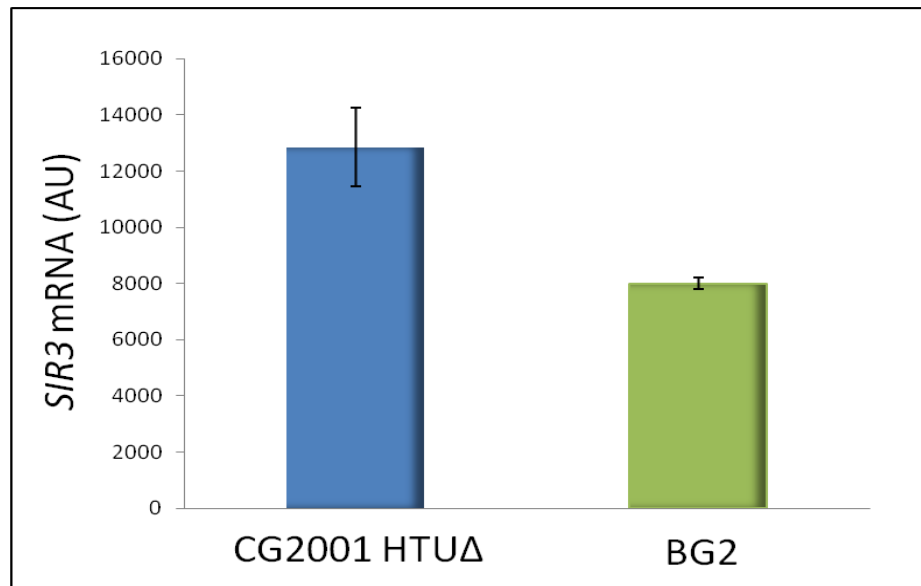


Figure 57 – *SIR3* mRNA levels in CG2001 HTUΔ (blue) and BG2 (green) strain backgrounds. Cells were grown in YPD under standard conditions to reach exponential phase. RNA was extracted from $\sim 1 \times 10^7$ cells, and *SIR3* mRNA quantified using standardised cDNA additions in all reactions. The data shown are means from three independent experiments (each analysed in triplicate) \pm SEM.

Table 9 – *C. glabrata* Clinical Isolates^a

Clinical Isolate	Source	Sir-Mediated Silencing ^b
CI-21	Blood	BG2-Like
CI-22	Urine	No Effect
CI-31	SPT	CG2001 HTUΔ-Like
CI-32	Urine	BG2-Like
CI-39	Pelvic Drain	CG2001 HTUΔ-Like
CI-82	Blood	CG2001 HTUΔ-Like
CI-105	Bile	No Effect
CI-134	Wound (Sternum)	No Effect
CI-146	Lung Biopsy	BG2-Like
CI-172	Tongue	BG2-Like
NCYC388	NCYC Collection	BG2-Like

^aIsolates were kindly supplied by Michael Petrou (Imperial College London)

^bOutcomes derived from Fig. 58

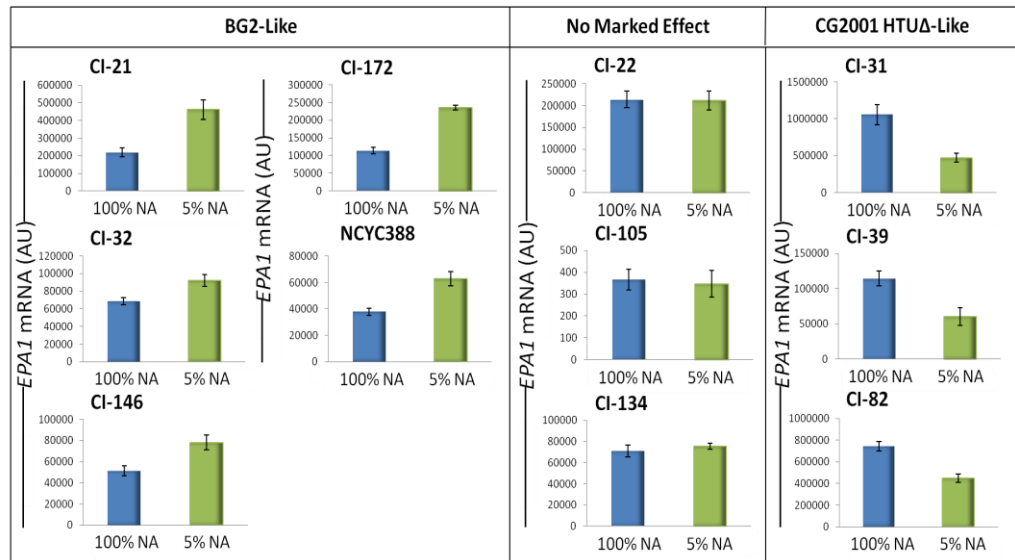


Figure 58 – Classification of *C. glabrata* clinical isolates into either; BG2-like, no effect, or CG2001 HTUΔ-like, according to the effect of silencing inhibition by NA limitation on *EPA1* transcript level. Cells were grown overnight in SC medium containing either 100% NA (blue) or 5% NA (green) before re-inoculation into the appropriate fresh SC medium and growth to exponential phase. RNA was extracted from $\sim 1 \times 10^7$ cells grown under the relevant condition, and *EPA1* mRNA quantified using standardised cDNA additions in all reactions. The data shown are means from three independent experiments (each analysed in triplicate) \pm SEM.

were deemed to be 'BG2-like'. On the other hand, strains CI-31, CI-39, and CI-82, were more 'CG2001 HTUΔ-like', with decreased *EPA1* transcript levels when silencing was inhibited. Of the eleven tested clinical isolates, three, CI-22, CI-105, and CI-134 showed no marked change in *EPA1* expression when limited for NA.

The extent to which *EPA1* expression is regulated by Sir-mediated silencing thus varies depending on strain background. The BG2-like clinical isolates apparently relied to a greater extent on such regulation to silence *EPA1*. It is tempting to speculate that these isolates may also resemble the BG2 strain background by demonstrating high levels of *EPA1*/Epa1-HA heterogeneity. The way in which each individual clinical isolate responded to inhibited silencing did not appear related to where the particular isolate was sourced from. For example, CI-21 and CI-82 were both isolated from blood but demonstrate 'BG2-Like' and 'CG2001 HTUΔ-Like' *EPA1* silencing respectively (Table 9).

5.3.6.1 The Extent of EPA1 Silencing Correlates with Cell Surface Epa1 Heterogeneity in Clinical C. glabrata Isolates

Preceding data for BG2 and CG2001 HTUΔ strain backgrounds indicate that transcriptional silencing of *EPA1* is linked to the level of Epa1 heterogeneity. Based on this it was predicted that the apparent marked variation in silencing-dependent *EPA1* expression across the range of tested clinical isolates (discussed above 5.3.6) should have implications for heterogeneity. This was tested by probing Epa1 cell surface expression with anti-Epa1 antibody (5.3.3.2) (Kaur et al., 2007), in exponential phase cells, grown under standard YPD conditions, and analysed by flow cytometry. Like the BG2 strain, all isolates in which *EPA1* silencing was released under conditions of inhibited transcriptional silencing, by low NA, exhibited a broad Epa1 expression heterogeneity under standard conditions (Fig. 59). Both low- and high-Epa1 subpopulations were expressed, accompanied by a generally lower mean Epa1 level when compared to 'CG2001 HTUΔ-like' isolates (Fig. 59). By contrast, isolates in which inhibition of silencing caused a decrease in *EPA1* expression exhibited lower Epa1 expression heterogeneity and higher mean Epa1 expression, thus resembling the CG2001 HTUΔ strain background (Fig. 59). Clinical isolates in which *EPA1* expression appeared to be unaffected by silencing inhibition also resembled the CG2001 HTUΔ strain in terms of Epa1 heterogeneity,

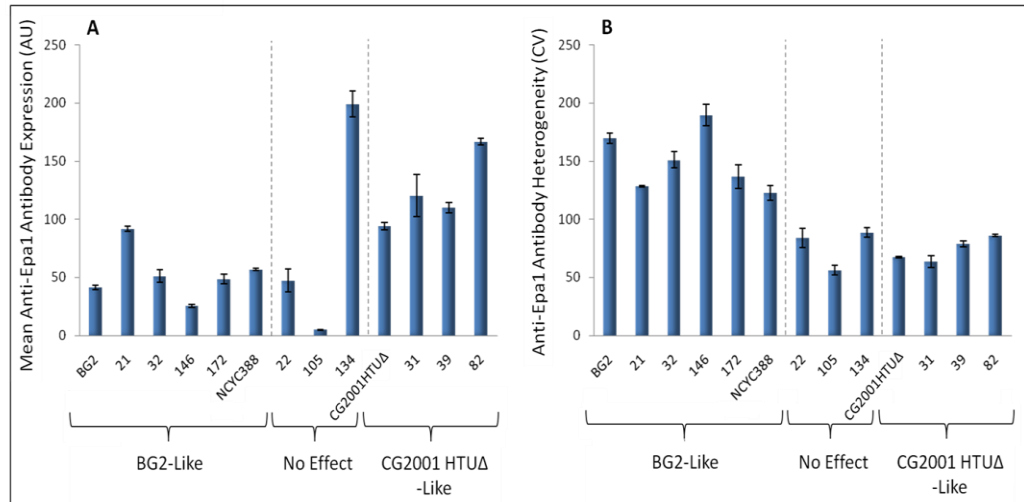


Figure 59 – Flow cytometric analysis of **(A)** mean Epa1 expression (AU) and **(B)** Epa1 heterogeneity (CV) in *C. glabrata* clinical isolates classified into either; 'BG2-like', 'no effect', or 'CG2001 HTUΔ-like', according to the effect of silencing inhibition by NA limitation on *EPA1* transcript level. 'BG2-like' strains were BG2, NCYC388 and isolates 21, 32, 146 and 172. 'CG2001 HTUΔ-like' strains were CG2001 HTUΔ and isolates 31, 39 and 82. The other strains were isolates 22, 105 and 134. Cells were grown to exponential phase in YPD medium before probing with an anti-Epa1 antibody and a secondary Alexa Fluor® 488 conjugated antibody. Samples were then analysed by flow cytometry. Data presented are means of independent triplicate experiments ±SEM.

their mean expression levels, however, were more varied (Fig. 59). Ultimately a positive relationship between silencing-dependent *EPA1* expression (low NA: high NA expression ratio) and heterogeneity (CV), was identified across the range of clinical isolates studies (Fig. 60), indicating that strain-specific gene silencing is likely a key determinant of strain-to-strain variation in the heterogeneity of Epa1 expression.

5.4 Variation in *EPA1* Distance from the Chromosome End is not a Likely Cause of Strain Dependent Sir-Regulation

The *C. glabrata* type strain ATCC2001, from which CG2001 HTUΔ and subsequently CG2001-Epa1-HA is derived has had its genome sequenced from sub-telomere to sub-telomere (Dujon et al., 2004, Sherman et al., 2006). Consequently this genome sequence contains gaps at each of the chromosome ends and it is not possible to determine the exact distance of the *EPA1* ORF from the end of the chromosome using these data. By contrast, although a complete genome sequence is not available, sequence data for the *EPA1* cluster at the right end of chromosome E, including the telomere, has been determined for strain BG2 (De Las Penas et al., 2003). Thus it is known that the *EPA1* ORF start site is at ~24.6kb from the chromosome end in a BG2 strain background.

Results thus far in this project suggest that *EPA1* in strain CG2001 HTUΔ experiences weakened silencing compared to BG2. In addition BG2 displays greater Epa1-HA expression heterogeneity, which is suppressed by loss of transcriptional silencing. As these differences appear not to be a result of defective *SIR3* expression in CG2001 HTUΔ it was hypothesised that the distance of *EPA1* from the chromosome end may differ between these two strains. Indeed silencing at the right side of the *EPA1* chromosome is known to decrease as sites become more distant to the telomere (De Las Penas et al., 2003, Castano et al., 2005), similar to many other chromosomes and other organisms. In addition chromosomal rearrangements have been reported to create differences between *C. glabrata* strains in terms of chromosome number and by the creation of chimeric chromosomes (Muller et al., 2009, Polakova et al., 2009). Recombination can occur at high frequency at the subtelomeres resulting in polymorphism among different chromosome ends and between individuals; such recombination could lead to alterations in the distance of *EPA1* from

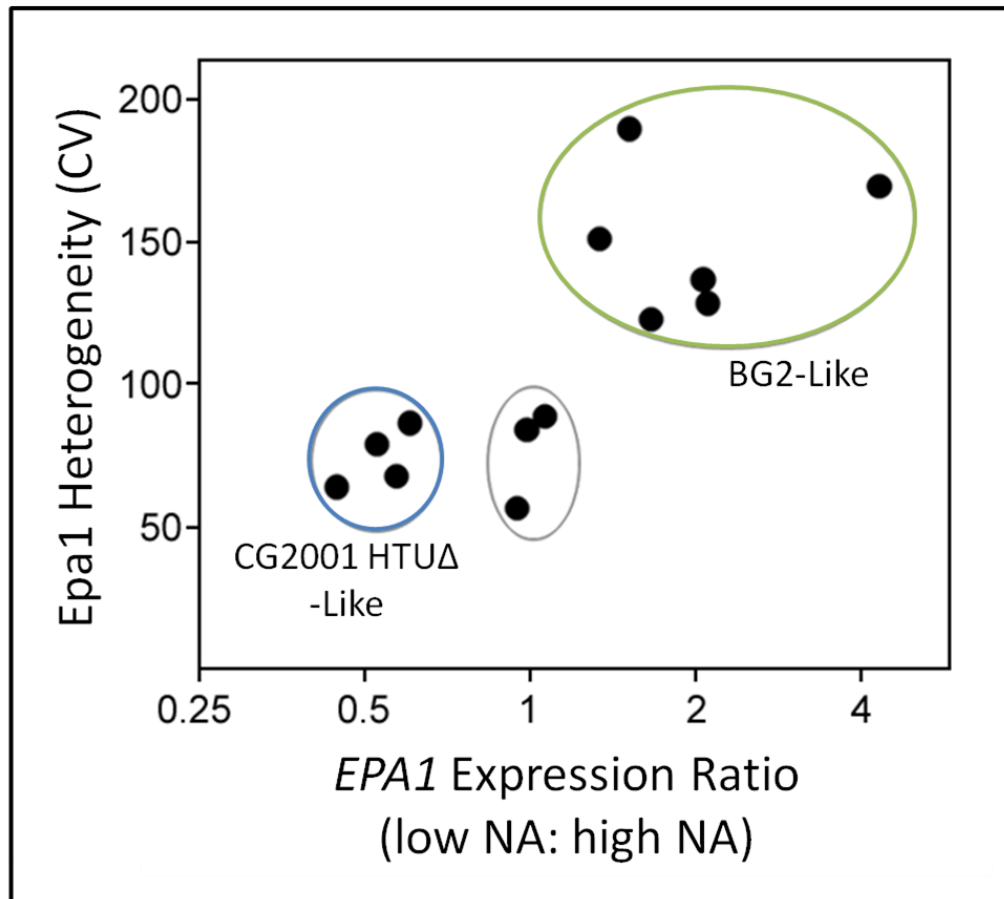


Figure 60 – Relationship between silencing and heterogeneity of Epa1 expression across all tested strains. 'BG2-like' strains (green) were BG2, NCYC388 and isolates 21, 32, 146 and 172. 'CG2001 HTUΔ-like' strains (blue) were CG2001 HTUΔ and isolates 31, 39 and 82. The other strains (grey) were isolates 22, 105 and 134. *EPA1* expression ratio data is based on results obtained by qRT-PCR following inhibition of silencing by growth in limited NA medium (illustrated in Fig. 58). Heterogeneity (CV) values were obtained following probing with an anti-Epa1 antibody and a secondary Alexa Fluor® 488 conjugated antibody followed by flow cytometry analysis, as presented in (Fig. 59B).

the end of its chromosome between strains (Louis and Vershinin, 2005, Verstrepen and Fink, 2009). Following this hypothesis, and owing to the weakened silencing observed, it was considered logical to test whether *EPA1* in the CG2001 HTUΔ strain is located further from the end of chromosome E than in BG2.

5.4.1 Strategy to look for Differences in the Distance of EPA1 from the Chromosome End in Two Strain Backgrounds

Since telomere regions are absent from the complete genome sequence of the *C. glabrata* type strain I required an experimental method to allow comparison of *EPA1* position in CG2001 HTUΔ and BG2. This was achieved by digestion of genomic DNA (isolated from each strain in agarose plugs to prevent fragmentation of DNA) with a restriction enzyme cutting at a known distance centromere-proximal from the *EPA1* start codon in both strains. Digested DNA was separated using field inversion gel electrophoresis (FIGE) and the resulting Southern blot probed for *EPA1* (Fig. 61). In order to ensure specific identification of the *EPA1* containing fragment a 416bp probe recognising the 120bp repeat regions within the gene was utilised. These repeats are located within the ser/thr rich region of *EPA1* and both the protein and nucleotide sequences are specific to *EPA1* (Frieman et al., 2002, De Las Penas et al., 2003). Corroboration of probe specificity was achieved using NCBI blast searches with *EPA1* being the only hit. The size of the resulting *EPA1* containing fragments could then be compared between strains BG2 and CG2001 HTUΔ.

5.4.2 Distance of EPA1 from the Chromosome End does not appear to Differ between Strains

Using the method described above, genomic DNA agarose plugs were digested with either *PmeI* or *StuI*. In each instance digestions were performed in triplicate with 3 separate agarose plugs being digested with each enzyme for each strain. Due to the lack of complete sequence data in BG2 only a limited selection of restriction sites with known positions in both strains were available. There is a 19bp difference in the location of the *StuI* restriction site upstream of *EPA1*, with the site in CG2001 HTUΔ being 19bp further upstream than in BG2. This difference however is too small to be detected with this method of gel separation and thus should not affect the results. The *PmeI* restriction site is at 7458bp and 6853bp upstream of the

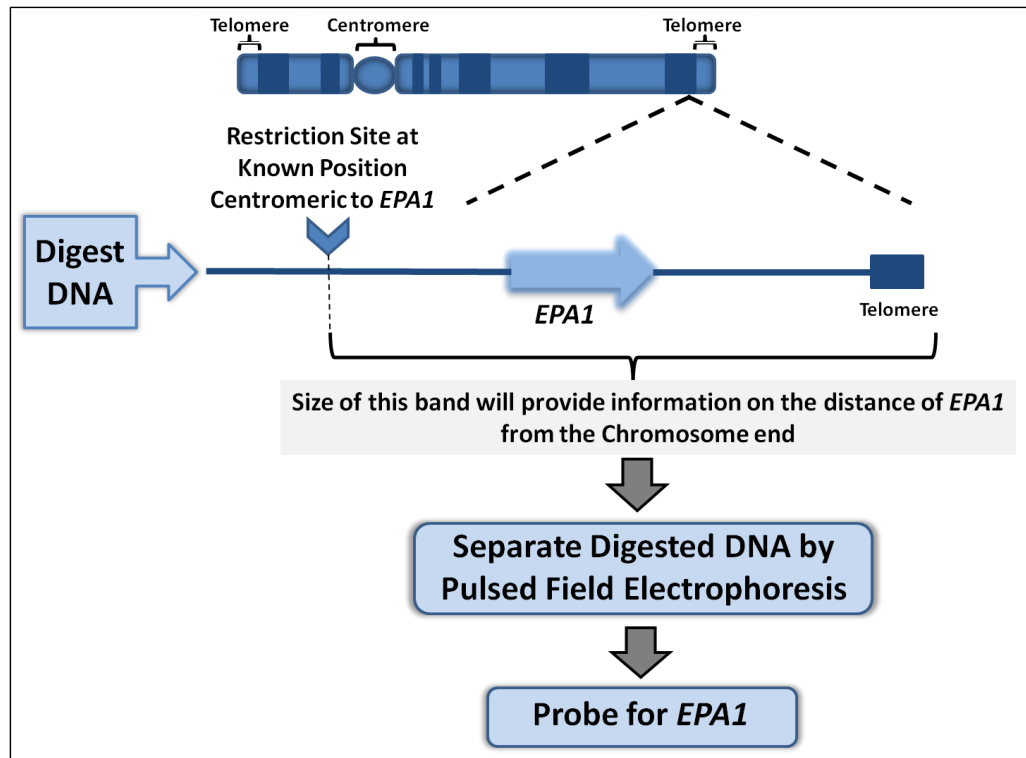


Figure 61 – Strategy employed to identify differences in position of the *EPA1* ORF from the chromosome end in two strain backgrounds.

EPA1 start codon in BG2 and CG2001 HTUΔ respectively. A difference of 605bp will thus exist irrespective of any variation in chromosome length telomeric to *EPA1*, with BG2 being 605bp longer. This difference was taken into account during the examination for size variation between strains.

Previous studies have determined the effect of distance from the telomere on transcriptional silencing through use of *URA3* insertions. Such analyses at the right end of chromosome E (Chr-E-R) revealed a strong silencing effect up to 14.8kb from the telomere with weak silencing being identified by a distance of 20.6kb just downstream of *EPA1* (De Las Penas et al., 2003, Rosas-Hernandez et al., 2008). Thus across a distance of 5.8kb silencing appears to increase from weak to strong and although not quantified this increase seems to be in the region of ~2.5 fold (De Las Penas et al., 2003). A gradient of silencing has previously been observed across the *EPA1-3* locus (Chr E-R) and is weakened as distance from the telomere increases (De Las Penas et al., 2003, Rosas-Hernandez et al., 2008). Assuming that, following the initial region of high repression observed at the *EPA1-3* telomere, silencing decreases continuously with distance from the telomere, this previous data indicates a distance of ~2.9kb may be required to see even a 25% difference in silencing efficiency between two sites in the region of *EPA1*.

Separation of digested genomic DNA followed by Southern blot and probing for *EPA1* suggested the gene to be a similar distance from the chromosome end in both strain backgrounds (Fig. 62A). Individual band sizes were determined using a standard curve method with mean sizes being generated from the triplicate digests performed for each strain. After accounting for the 605bp and 19bp differences in *PmeI* and *StuI* restriction site positions respectively band sizes exhibited by the different strain backgrounds were compared. The results of *PmeI* digestion indicated the BG2 *EPA1* to be located ~451bp further from the telomere than *EPA1* in CG2001 HTUΔ (Fig. 62B). By contrast digestion with *StuI* suggested *EPA1* to be more telomere distal in a CG2001 HTUΔ background with the observed fragment being ~762bp longer than the equivalent fragment in BG2 (Fig. 62C). These contradictory differences are rather small and may be indicative of the margin of error for this experimental procedure. Furthermore, based on data from previous studies (De Las Penas et al., 2003, Rosas-Hernandez et al., 2008) it seems unlikely that the small size of the differences detected would be sufficient to have a marked effect on *EPA1* repression.

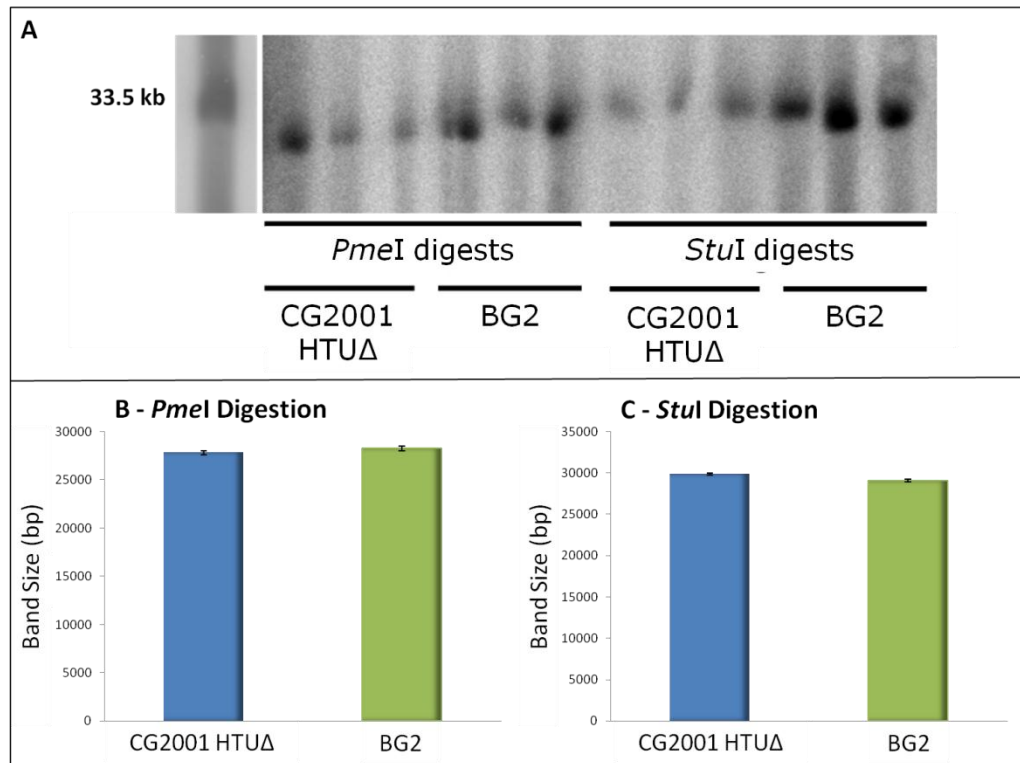


Figure 62 – (A) Field inversion gel electrophoresis (FIGE) depicting sizes of bands released following digestion of genomic DNA isolated in agarose plugs with either *PmeI* or *StuI* for both CG2001 HTUΔ and BG2 strain backgrounds. Fragment size was determined using a standard curve method for **(B)** *PmeI* and **(C)** *StuI* digests, in CG2001 HTUΔ (blue) and BG2 (green) backgrounds, from three independent experiments \pm SEM.

5.5 Contribution of Additional Post-Translational Factors to Epa1 Heterogeneity

Epa1 expression heterogeneity in a BG2 background seems to be regulated primarily by Sir-dependent transcriptional silencing. Such a strong reliance on transcriptional silencing to regulate Epa1 heterogeneity may mask other possible factors contributing to heterogeneity. CG2001-Epa1-HA provides a good model in which to elucidate such additional factors due to the Sir-independent regulation of Epa1 heterogeneity that is observed in this strain. The roles of a number of potential post-translational factors in control of Epa1 heterogeneity were thus investigated in CG2001-Epa1-HA.

5.5.1 Lipid Raft Heterogeneity does not contribute to Epa1 Heterogeneity

Lipid Rafts have been defined as nano-scale (10-200nm) dynamic membrane microdomains enriched for sterols and sphingolipids (Pike, 2006). Protein localisation to these assemblies is primarily mediated by a GPI anchor, acylation, or certain transmembrane domains (Lingwood et al., 2009). Indeed GPI-anchored proteins have been found to be enriched in lipid rafts (Martin and Konopka, 2004, Pike, 2004, Brown and Rose, 1992). In addition lipid rafts are known to be highly heterogeneous, exhibiting heterogeneity in both their composition and distribution (Pike, 2004, Mishra and Joshi, 2007). During microscopic analysis it was noted that in many cells Epa1-HA expression was not distributed uniformly around the cell surface but rather occurred in patches, suggestive of possible lipid raft localisation (Fig. 63). Consequently I wanted to determine whether Epa1 was localising to lipid rafts and if heterogeneity in the distribution and composition of these rafts could be contributing to Epa1 heterogeneity at the cell surface.

Sterols and sphingolipids constitute the major lipid raft building blocks and thus inhibition of these components can also inhibit the formation of lipid rafts. In order to determine the role of lipid raft heterogeneity in Epa1-HA expression heterogeneity I inhibited both sphingolipid and sterol biosynthesis through treatment of cells with myriocin and ketoconazole respectively, and analysed the effects by flow cytometry and fluorescence microscopy. In all instances cells were grown overnight in appropriately supplemented YPD medium before re-inoculation and further growth to exponential phase prior to analysis.

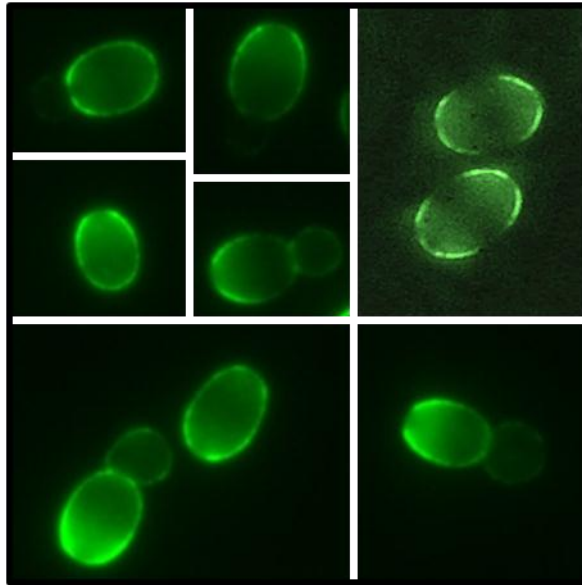


Figure 63 – Visualisation of Epa1-HA cell surface expression in exponential phase *C. glabrata* cells by fluorescence microscopy following staining with anti-HA, Alexa Fluor[®] 488 conjugate antibody

5.5.1.1 Inhibition of Sphingolipid Biosynthesis to Disrupt Lipid Raft Formation

Inhibition of sphingolipid biosynthesis was achieved through the use of myriocin which specifically inhibits the activity of serine palmitoyltransferase. This enzyme catalyses the first committed stage of sphingolipid biosynthesis and thus depletes the intracellular pool of sphingolipid intermediates (Miyake et al., 1995, Martin and Konopka, 2004). Myriocin treated yeast exhibit depleted levels of both detergent resistant membranes and lipid rafts (Martin and Konopka, 2004). Myriocin inhibits serine palmitoyltransferase at picomole concentrations (Miyake et al., 1995) and has been successfully used as a lipid raft inhibitor in *C. albicans* budding cultures at a final concentration of 1 μ M (Martin and Konopka, 2004). I found, however, that a final myriocin concentration of 2 μ M provided more distinct effects, without affecting growth, and was the concentration used in this study.

Myriocin (2 μ M) treated cells, analysed by anti-HA, Alexa Fluor[®] 488 conjugate antibody staining and flow cytometry, actually demonstrated a ~39% increase in cell surface Epa1-HA (Fig. 64A). This result was unexpected since, as mentioned above, GPI-anchored proteins are often localised to lipid rafts and lipid raft inhibition might be expected to decrease cell surface Epa1-HA. Heterogeneity of Epa1-HA expression was largely unaffected, with CV values of ~47 and ~45 for untreated and myriocin treated cells respectively (Fig. 64B). To corroborate that the effects of myriocin were due to inhibition of sphingolipid synthesis, cells were exposed to both myriocin and phytosphingosine (30 μ M). Phytosphingosine is an intermediate of sphingolipid synthesis downstream of serine palmitoyltransferase and has previously been shown to rescue cells from the effects of myriocin (Martin and Konopka, 2004). Phytosphingosine did largely rescue cells from the effect of myriocin here, with cell surface Epa1-HA levels returning closer to the level in untreated cells (Fig. 64A). Again heterogeneity remained similar to that in untreated cells (Fig. 64B). Consistent with phytosphingosine specifically compensating for sphingolipid loss in myriocin-treated cells, when cells were treated with phytosphingosine alone no decrease in cell surface Epa1-HA expression occurred (Fig. 64A).

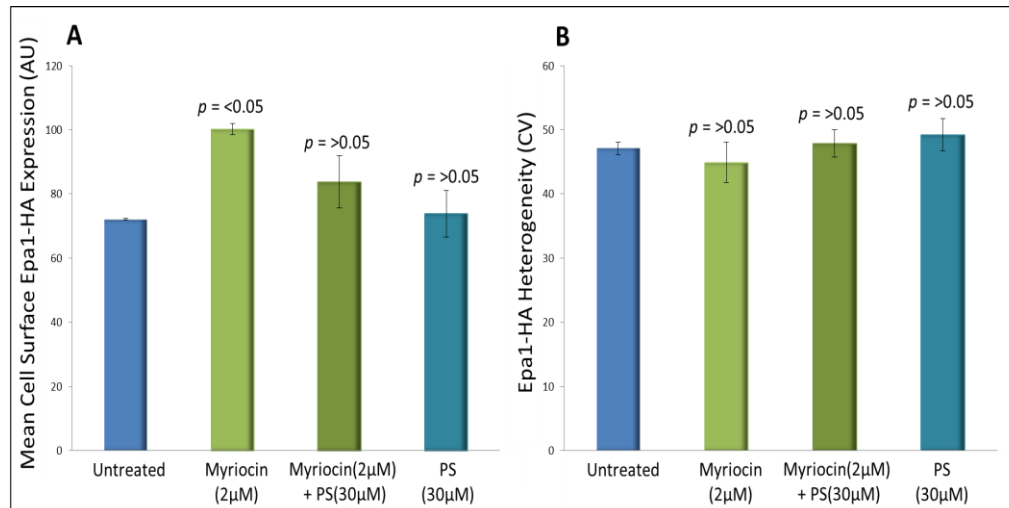


Figure 64 – Mean cell surface Epa1-HA expression (AU) **(A)** and heterogeneity (CV) **(B)** following treatment of CG2001-Epa1-HA cells with; myriocin (light green), myriocin + phytosphingosine (PS) (dark green), and phytosphingosine (PS) alone (dark blue) compared to untreated cells (bright blue). Cells were grown overnight in appropriately supplemented YPD medium before re-inoculation and further growth to reach exponential phase. Prior to analysis by flow cytometry cells were stained with anti-HA, Alexa Fluor® 488 conjugate antibody. The differences in Epa1-HA expression and CV observed in treated cells compared to the untreated control cells were deemed to be either, significant ($p < 0.05$), or not significant ($p > 0.05$) in each case according to the Student's t-test (Materials and Methods). Data presented are means of independent triplicate experiments \pm SEM.

5.5.1.2 Inhibition of Sterol Biosynthesis to disrupt Lipid Raft Formation

In order to inhibit sterol biosynthesis cells were grown in the presence of ketoconazole. Ketoconazole belongs to the azole family of antifungal agents and prevents the 14- α -demethylation of lanosterol in the ergosterol biosynthesis pathway (Ghannoum and Rice, 1999, Odds et al., 2003, Martin and Konopka, 2004). Ketoconazole concentrations of 100 μ M and particularly 300 μ M have previously been demonstrated to block sterol polarization in *C. albicans* hyphae. Polarization of these sterol-rich regions was also dependent upon sphingolipid biosynthesis. It is thus likely that such domains are representative of lipid rafts and indicates that the ketoconazole concentrations used are sufficient to inhibit lipid raft formation (Martin and Konopka, 2004). I discovered, however, that a final ketoconazole concentration of 300 μ M markedly affected the growth rate of cultures which could complicate interpretation of results, so this concentration was not used for this study.

Cells grown in the presence of ketoconazole were analysed by anti-HA, Alexa Fluor[®] 488 conjugate antibody staining followed by flow cytometry. The results indicated that, similar to the myriocin data, ketoconazole (100 μ M) treatment brought about a ~45% increase in Epa1-HA at the cell surface (Fig. 65A). Similarly in support of the myriocin data, heterogeneity was largely unaffected with CV values of ~47 and ~50 for untreated and treated cells respectively (Fig. 65B). Ketoconazole treatment is thought to be a specific inhibitor of sterol biosynthesis (Martin and Konopka, 2004), and the similar effects on Epa1-HA expression seen following myriocin treatment seem to corroborate that this antifungal agent is exerting its effect on Epa1-HA via inhibition of the sterol component of lipid rafts.

5.5.1.3 Inhibition of both Sphingolipid and Sterol Biosynthesis simultaneously caused increased Epa1-HA Expression

Lipid rafts are believed to be heterogeneous in terms not only of their protein composition but also their lipid composition (Mishra and Joshi, 2007). I considered whether inhibition of both sphingolipid and sterol biosynthesis combined was required to exert a major effect on lipid raft formation. I contemplated the possibility that reduced levels of sphingolipid may be compensated for by increased incorporation of sterols to raft domains, and vice versa. Indeed myriocin treatment in yeast has been

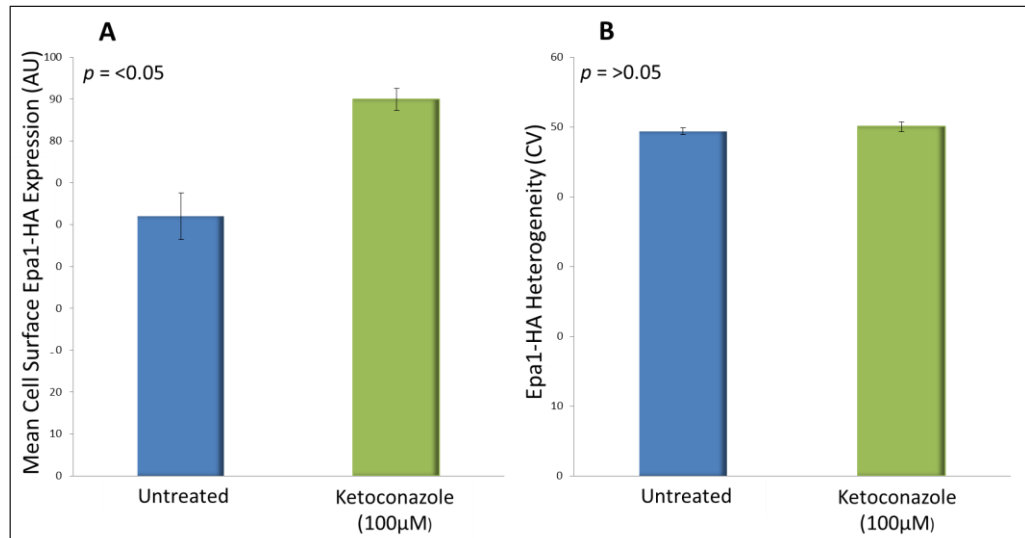


Figure 65 – Mean cell surface Epa1-HA expression (AU) (**A**) and heterogeneity (CV) (**B**) following treatment of CG2001-Epa1-HA cells with; ketoconazole (green) compared to untreated cells (blue). Cells were grown overnight in appropriately supplemented YPD medium before re-inoculation and further growth to reach exponential phase. Prior to analysis by flow cytometry cells were stained with anti-HA, Alexa Fluor[®] 488 conjugate antibody. The differences in Epa1-HA expression and CV observed between untreated and ketoconazole treated cells were deemed to be either, significant ($p < 0.05$), or not significant ($p > 0.05$) according to the Student's t-test (Materials and Methods). Data presented are means of independent triplicate experiments \pm SEM.

linked to increased ergosterol levels (Van Leeuwen et al., 2008). Combined treatment of cells with both myriocin and ketoconazole, inhibiting both major lipid raft components, did not elicit any decrease in cell surface Epa1-HA. Rather Epa1-HA was increased to a greater extent (~60%) than when either drug was used alone (Fig. 66A). Cell surface Epa1-HA CV values were again largely unaffected (Fig. 66B).

5.5.1.4 Inhibition of Lipid Rafts does not release the Patchy Expression Pattern Exhibited by Epa1-HA

Based on the above observations I considered whether or not inhibition of lipid raft components actually liberated Epa1 and allowed the GPI-anchored protein to spread across the whole cell surface rather than being confined to patches. Cell surface Epa1-HA expression was analysed by fluorescence microscopy following treatment with myriocin (2 μ M), ketoconazole (100 μ) or both. The observations revealed that localisation of Epa1-HA at the cell surface resembled that of untreated cells despite addition of the sphingolipid and sterol biosynthesis inhibitors. In all cases Epa1-HA expression often demonstrated irregular localisation with certain areas exhibiting stronger fluorescence than others. Inhibition of either sterol or sphingolipid biosynthesis, or both, did not make this localisation pattern more uniform (Fig. 67A-D).

5.5.1.5 Epa1-HA Fluorescence does not Co-localise with Filipin Staining in C. glabrata

An alternative approach, other than the use of sphingolipid/sterol inhibitors was employed to determine if Epa1-HA is localised to lipid rafts. Filipin staining was used to localise regions particularly enriched for sterols at the plasma membrane of *C. glabrata*. Filipin is a fluorescent polyene antibiotic that specifically binds sterols. This sterol dye absorbs ultraviolet light at 360nm while emitting visible blue light at 480nm and has been used to visualise membrane sterols in diverse cell types, from mammalian to yeast (Wachtler et al., 2003, Beh and Rine, 2004, Martin and Konopka, 2004, Jin et al., 2008, Van Leeuwen et al., 2008). Filipin stained cells were analysed by fluorescence microscopy. This indicated that the majority of cells exhibited uniform membrane staining (Fig. 68). Dual staining with both anti-HA, Alexa Fluor[®] 488 conjugate antibody and Filipin illustrated that patches of Epa1-HA fluorescence did not correspond with any sterol enriched areas for individual cells.

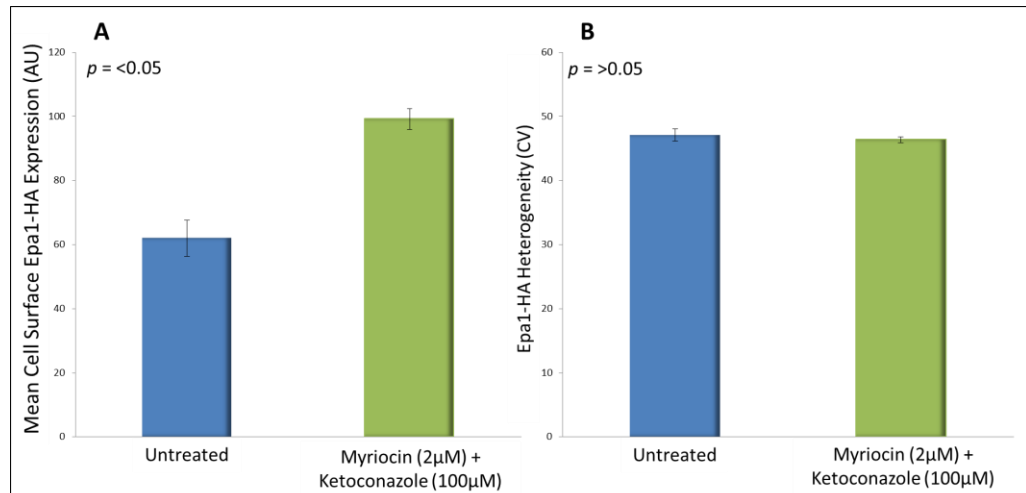


Figure 66 – Mean cell surface Epa1-HA expression (AU) (**A**) and heterogeneity (CV) (**B**) following treatment of CG2001-Epa1-HA cells with; myriocin and ketoconazole (green) compared to untreated cells (blue). Cells were grown overnight in appropriately supplemented YPD medium before re-inoculation and further growth to reach exponential phase. Prior to analysis by flow cytometry cells were stained with anti-HA, Alexa Fluor® 488 conjugate antibody. The differences in Epa1-HA expression and CV observed between untreated and myriocin + ketoconazole treated cells were deemed to be either, significant ($p=<0.05$), or not significant ($p=>0.05$) according to the Student's t-test (Materials and Methods). Data presented are means of independent triplicate experiments \pm SEM.

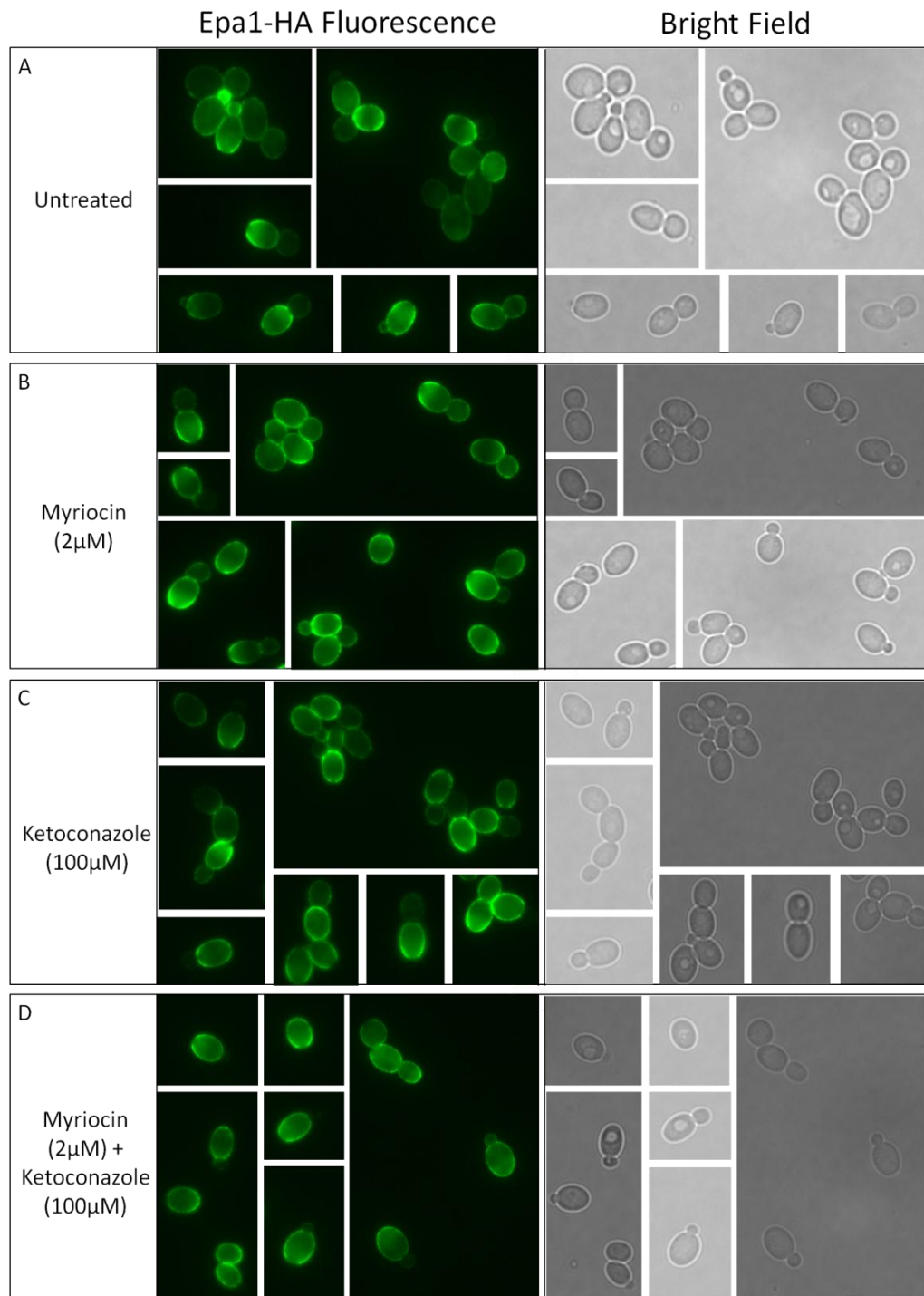


Figure 67 – Fluorescence microscopy of Epa1-HA expression in exponential phase cells of the CG2001-Epa1-HA strain in untreated **(A)**, Myriocin (2μM) treated **(B)**, Ketoconazole (100μM) treated **(C)**, and Myriocin + Ketoconazole treated **(D)** cells.

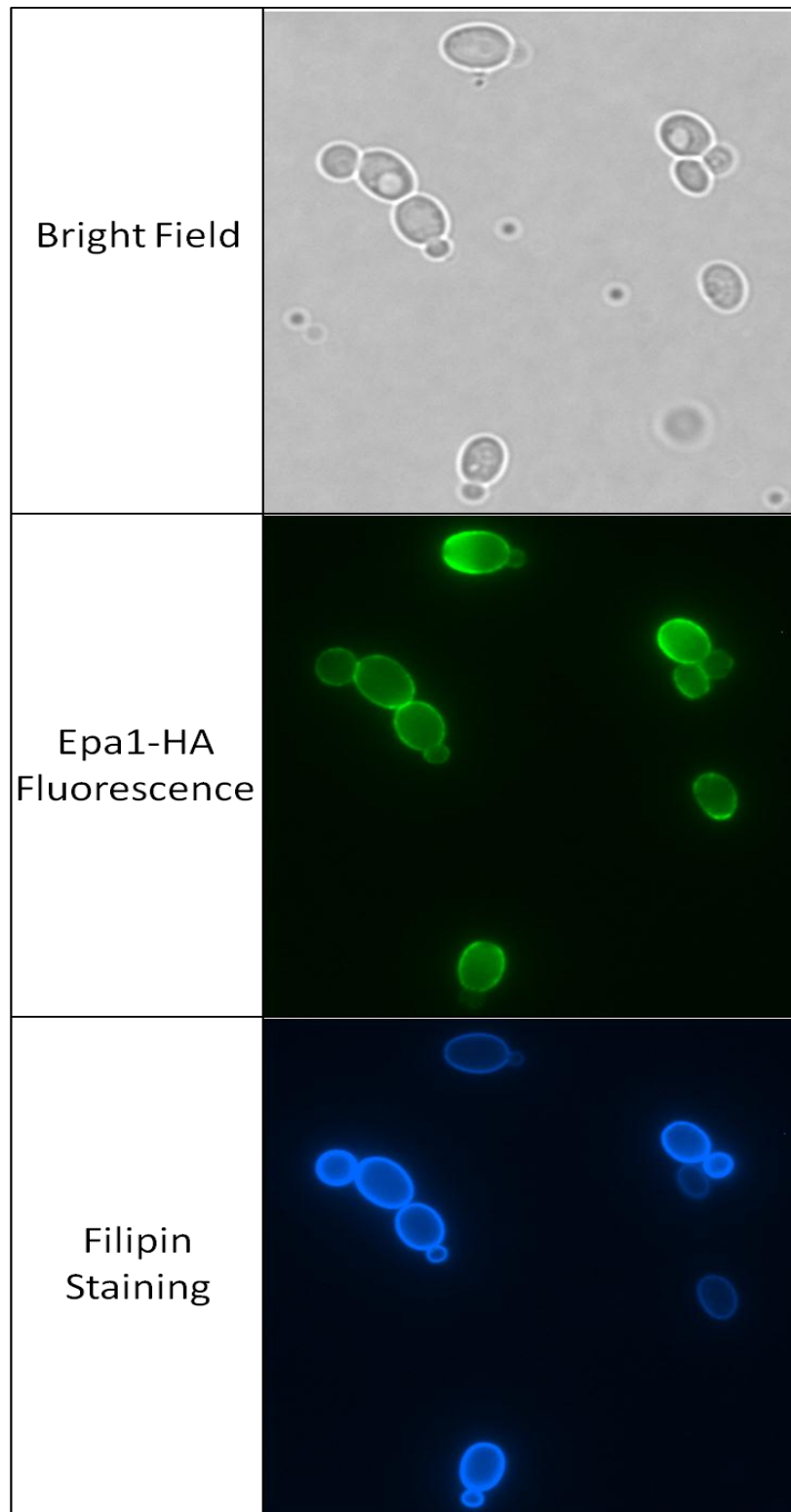


Figure 68 – Dual Staining of CG2001-Epa1-HA with anti-HA, Alexa Fluor[®] 488 conjugate antibody and Filipin to visualise Epa1-HA expression and sterol rich regions of the membrane simultaneously. Cells were grown to exponential phase in YPD medium prior to staining and then analysed by fluorescence microscopy. The different fluorochromes, Alexa Fluor[®] 488 and Filipin, were imaged using the FITC and DAPI filters respectively

C. glabrata cells predominantly exist as budding yeast blastoconidia, with pseudohyphal growth only being identified under conditions of limited nitrogen (Csank and Haynes, 2000). The uniform filipin staining observed for *C. glabrata* cells may be a consequence of their bud morphology and indicate a lack of obvious lipid compartmentalisation. Indeed studies in *C. albicans* revealed that both budding and pseudohyphal cells exhibited uniform filipin staining with distinct patches only being identified at the hyphal tip during this highly polarised form of growth (Martin and Konopka, 2004).

5.5.2 Epa1-HA Localisation does not appear Dependent on the Actin Cytoskeleton

The actin cytoskeleton can become tethered to the lipid membrane seemingly via its interaction with proteins that bind the inner-leaflet of the bi-layer. Such interactions are thought to play a pivotal role in membrane compartmentalisation and the control of membrane raft dynamics and composition (Mishra and Joshi, 2007, Viola and Gupta, 2007). A role for actin in the polarization of lipid rafts during hyphal growth in *C. albicans* has also been demonstrated (Martin and Konopka, 2004). In addition, clustered GPI-anchored proteins have been suggested to associate with transmembrane proteins that, in-turn, interact with a membrane associated complex attached to the actin cytoskeleton (Suzuki and Sheetz, 2001). Consequently I wanted to determine if actin patches show a localisation pattern similar to that observed for Epa1-HA. Following staining with Alexa Fluor 488 conjugated phalloidin (Invitrogen), which specifically binds actin, exponential phase cells were analysed by fluorescence microscopy. The microscopy photographs obtained are not completely clear, however, they do indicate actin patches to be rather diffuse and often concentrated in the bud cell. Therefore this pattern of fluorescence localisation did not resemble that seen for Epa1-HA (Fig. 69). This is in agreement with data obtained for *S. cerevisiae* and *C. albicans* whereby a typical actin staining pattern includes discrete patches localised to the surface of the growing bud or hyphae consistent with the actin cytoskeleton mediating polarized growth (Martin and Konopka, 2004, Holland and Avery, 2009).

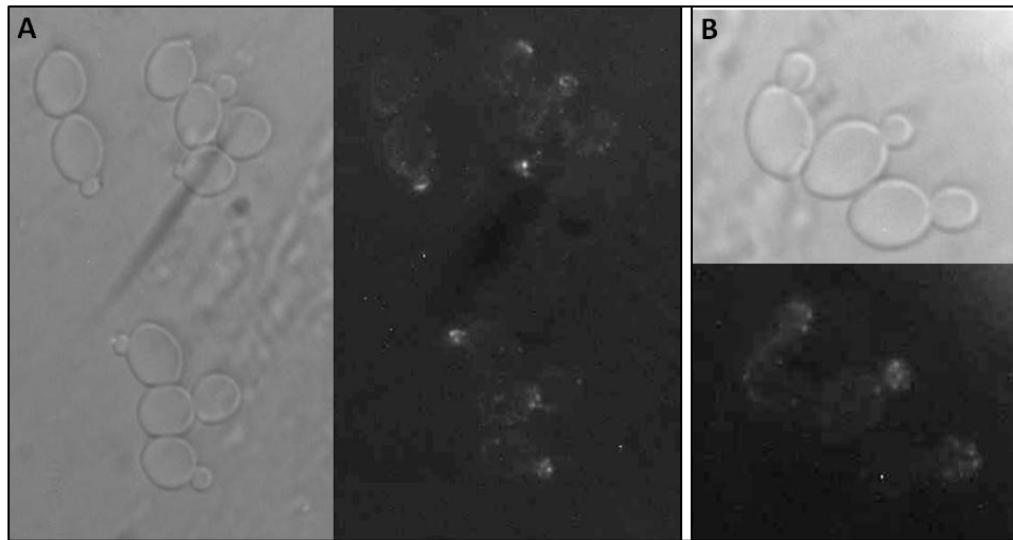


Figure 69 – Visualisation of actin patches in the CG2001-Epa1-HA strain background. Cells were grown to exponential phase in YPD medium and fixed with formaldehyde (4% v/v). Following staining with Alexa Flour 488 phalloidin cells were imaged by fluorescence microscopy. **(A)** Bright field image is shown on the left or **(B)** top with the corresponding fluorescence image on **(A)** the right or **(B)** bottom.

5.5.3 Removal of Epa1 from the Cell Surface via Yps Proteases does not appear to have a Role in Heterogeneity

The *YPS* genes, referred to as yapsins, encode GPI-linked aspartyl proteases that have been identified in a number of fungi and are known to have roles in cell wall integrity (Krysan et al., 2005, Albrecht et al., 2006, Kaur et al., 2007). *C. albicans* populations deleted for their respective *YPS* genes (*SAP9* and *SAP10*) demonstrate modified adhesion properties and reduced virulence in an *in vitro* model of oral infection (Albrecht et al., 2006). The *C. glabrata* genome encodes a family of eleven *YPS* genes (*YPS1-11*) which have been identified as an important virulence trait in this pathogen (Kaur et al., 2007). It has been proposed that GPI-anchored cell wall proteins may act as substrates for these proteases and the *C. glabrata* Yps-family, in particular Yps1 and Yps7, have been implicated in the proteolytic processing of Epa1 to remove it from the cell wall (Kaur et al., 2007). Due to such roles in cell wall integrity and virulence in addition to the proteolytic processing of Epa1, it was decided to test whether the action of these proteases may contribute to Epa1 heterogeneity at the cell surface.

5.5.3.1 The Yps Proteins do not appear to have a Role in Controlling Epa1 Heterogeneity

Previous analysis of Epa1 cell surface expression over time revealed expression to be highest in the hours immediately after inoculation into fresh medium. Expression of the protein then began to decline as cells progressed into stationary phase with lowest levels being observed at 10 hours post inoculation (Kaur et al., 2007). Time-course experiments performed during this study and described in chapter 4 were consistent with those observations (Fig. 34). By contrast to wild type cells, *yps(1-11)* Δ and *yps1* Δ *yps7* Δ mutant strains, created in a BG2 background, maintained their Epa1 cell surface expression at maximal levels throughout a 10hr time-course with *yps1* Δ and *yps7* Δ single mutants demonstrating only a 2-fold decrease (Kaur et al., 2007).

As Yps1 and Yps7 appear to be particularly relevant in regard to Epa1 regulation at the cell surface it was decided first to analyse their effects on Epa1-HA heterogeneity. A *yps7* Δ deletion strain, CG2001-Epa1-HA *yps7* Δ (Materials and Methods), was analysed by flow cytometry at both 3 hours, where Epa1 expression is high, and 10 hours, by which time Epa1 expression normally has declined (except in *yps* Δ mutants) (Kaur et al., 2007). Expression values 3 hours post-inoculation were very similar for

CG2001-Epa1-HA WT and CG2001-Epa1-HA *yps7* Δ mutant strains. At 10 hours CG2001-Epa1-HA wild type levels had declined by $\sim 70\%$ in both the wild type and *yps7* Δ mutant. The results revealed that Epa1-HA levels were not maintained in the CG2001-Epa1-HA *yps7* Δ mutant over and above those in the wild type (Fig. 70A). Similarly Epa1-HA heterogeneity also remained virtually unchanged in the *yps7* Δ mutant, with CV values of ~ 47 (3 hours) and ~ 63 (10 hours) compared to the corresponding wild type values of ~ 49 and ~ 63 respectively (Fig. 70B).

This analysis indicated that *YPS7* deletion in a CG2001-Epa1-HA background was not sufficient to exert a marked effect on Epa1-HA expression. Therefore, and owing to the more marked effect previously observed in an *yps1* Δ *yps7* Δ double mutant (Kaur et al., 2007) I constructed (Materials and Methods), and studied the effect of this double deletion on Epa1-HA expression and heterogeneity. Flow cytometry analysis at the 3 hour time-point did reveal a $\sim 22\%$ higher Epa1-HA level in the CG2001-Epa1-HA *yps1* Δ *yps7* Δ mutant strain (Fig. 71A). Heterogeneity, as with CG2001-Epa1-HA *yps7* Δ , again remained virtually unaffected in the double deletion strain compared to wild type, with CV values of ~ 59 and ~ 57 , respectively (Fig. 71B). Although Cg2001-Epa1-HA *yps1* Δ *yps7* Δ cells continued to exhibit cell surface Epa1-HA levels higher than in wild type cells at the 10 hour time-point, maximal (3 hour) Epa1-HA levels were not maintained following further growth of the mutant to 10 hours (Fig. 71A). Heterogeneity in the CG2001-HA *yps1* Δ *yps7* Δ strain again remained unaffected at this later time point with a CV value (~ 69), very similar to the wild type (Fig. 71B). Thus, the results indicated that neither Yps1 nor Yps7 have a role in controlling Epa1-HA heterogeneity in a CG2001-Epa1-HA background.

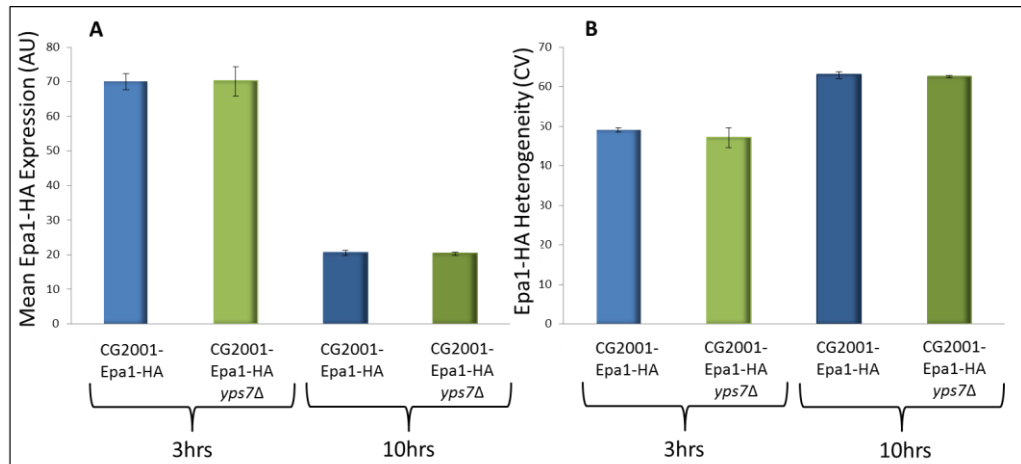


Figure 70 – Mean Epa1-HA level (AU) **(A)** and heterogeneity (CV) **(B)** of CG2001-Epa1-HA wild type (blue) and *yps7Δ* (green) strains at both 3 hours and 10 hours post inoculation. Cells were grown in YPD medium and analysed by flow cytometry following staining with anti-HA, Alexa Fluor® 488 conjugate antibody. Data presented are means of independent triplicate experiments \pm SEM.

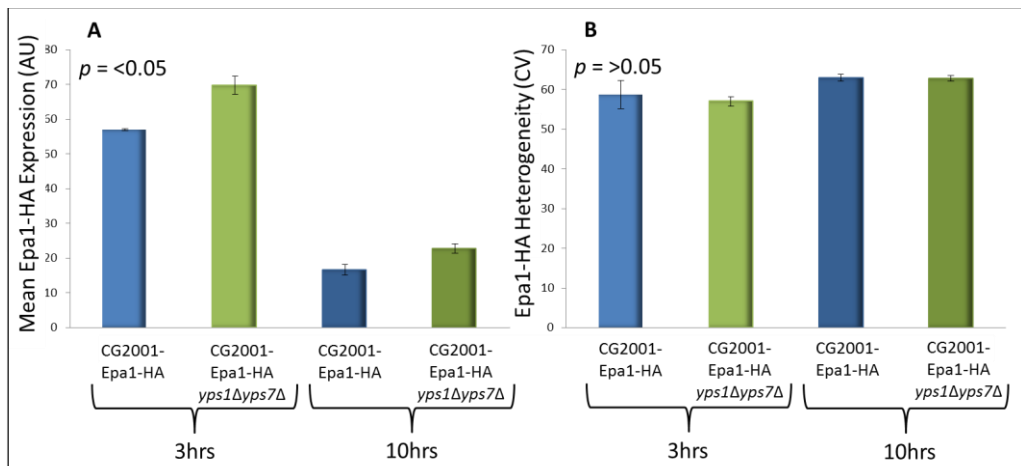


Figure 71 – Mean Epa1-HA level (AU) **(A)** and heterogeneity (CV) **(B)** of CG2001-Epa1-HA wild type (blue) and *yps1Δyps7Δ* (green) strains at both 3 hours and 10 hours post inoculation. Cells were grown in YPD medium and analysed by flow cytometry following staining with anti-HA, Alexa Fluor® 488 conjugate antibody. The differences in Epa1-HA expression and CV observed between the wild type and *yps1Δyps7Δ* strains at each time-point were deemed to be either, significant ($p < 0.05$), or not significant ($p > 0.05$) according to the Student's t-test (Materials and Methods). The p values indicated correspond to both timepoints on their respective bar chart **(A or B)**. Data presented are means of independent triplicate experiments \pm SEM.

5.5.4 Heterogeneity in Epa1 Expression Occurs Independently of Total Mannoprotein Level at the Cell Surface

The major constituents of the *C. glabrata* cell wall are 1,3- β -glucan, 1,6- β -glucan, chitin and mannoproteins. Despite having similar cell wall organisation to *S. cerevisiae*, the mannoprotein content of *C. glabrata* cell walls is \sim 50% higher than that observed in either *S. cerevisiae* or *C. albicans* (de Groot et al., 2008). GPI-anchored proteins, such as Epa1, which are often heavily mannosylated during the glycosylation stage of their maturation process, form the largest mannoprotein group (de Nobel et al., 1990, Brul et al., 1997, Levitz and Specht, 2006, de Groot et al., 2008, Lommel and Strahl, 2009). I considered whether heterogeneity exists generally for mannoprotein expression, and whether any such heterogeneity could contribute to Epa1 expression heterogeneity.

5.5.4.1 Visualisation of Total Mannoprotein Levels and Comparison with Epa1-HA Expression

Cell-to-cell variation in mannoprotein content was tested by probing cells with a fluorescent concanavalin-A conjugate, ConA-Alexa Fluor[®] 647 (Invitrogen), which binds mannose (Biondo et al., 2005) followed by flow cytometry. Mannoprotein levels were shown to be markedly uniform across a cell population with a CV of \sim 30. In contrast Epa1-HA was quite heterogeneous (CV \sim 53) even in this CG2001-Epa1-HA strain. Furthermore, dual staining for both Epa1-HA and Con-A, utilising both anti-HA, Alexa Fluor[®] 488 conjugate antibody and ConA-Alexa Fluor[®] 647 respectively, revealed that the highest and lowest 13% of Epa1-HA expressing cells had a similar level of mannoprotein staining (Fig. 72A, B). The evidence indicated that there was no relationship between the Epa1-HA and total-mannoprotein content of single cells.

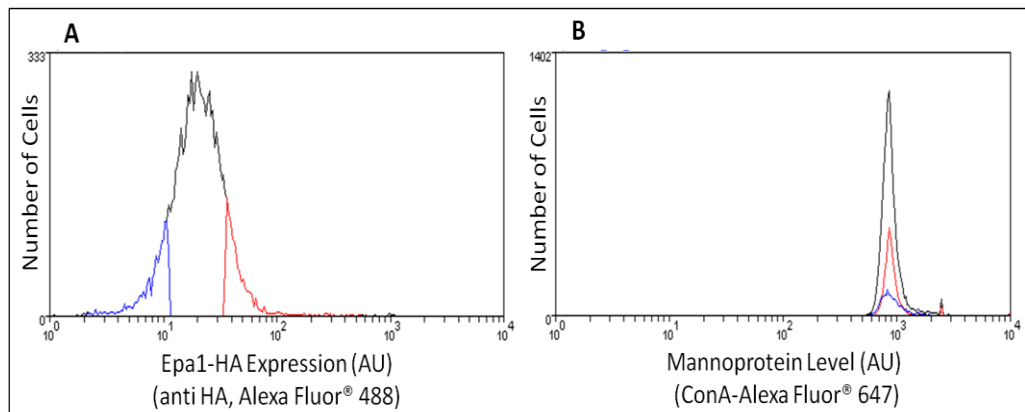


Figure 72 – Dual staining of CG2001-Epa1-HA for Epa1-HA expression (AU) with anti-HA, AlexaFluor[®] 488 conjugate antibody (**A**) and mannoprotein levels (AU) with ConA-Alexa Fluor[®] 647 conjugate (**B**) at the cell surface. Cells were grown to exponential phase prior to staining with one or both fluorescent conjugates. Analysis was performed by flow cytometry using FITC and APC-A filters to measure AlexaFluor[®] 488 and ConA-Alexa Fluor[®] 647 fluorescence respectively. Cells single stained with anti-HA, AlexaFluor[®] 488 only, and ConA-Alexa Fluor[®] 647 only, were used to create compensation controls on the flow cytometer which account for any overlap between the two fluorochromes. High expressing Epa1-HA cells are shown in red while low expressing Epa1-HA cells are shown in blue (**A**). Red and blue peaks (**B**) represent the corresponding mannoprotein level for high- and low-expressing Epa1-HA cells respectively. The above data are representative of three independent experiments.

5.6 Heterogeneity of Epa1 Expression is Primarily Determined at the mRNA Level

Heterogeneity in *EPA1* expression is evident at both the cell surface protein level (Epa1-HA) and at the mRNA level (*EPA1*-GFP) in the BG2 strain background. This evidence alongside such heterogeneity being Sir-dependent strongly suggested that the variation is determined primarily at the mRNA level. Although CG2001-Epa1-HA does not exhibit the same level of heterogeneity or Sir-dependence, heterogeneity regulation could still occur at the transcriptional level. Indeed with a number of post-translational factors being ruled out in section 5.5 regulation at the mRNA level seems plausible even in this strain. I wanted to corroborate that regulation occurs at the mRNA level in both strains, by testing whether the level of transcript directly correlates with the heterogeneous amount of Epa1-HA at the cell surfaces of individual cells.

5.6.1 Epa1 Cell Surface Expression Level Correlates with EPA1 Transcript Level

In order to test whether *EPA1* transcript level is directly correlated to expression of Epa1 protein at the cell surface, cells from each strain were sorted into high- and low-Epa1-HA expressing subpopulations. Initially exponential phase cells were stained using anti-HA, AlexaFluor® 488 conjugate antibody, sorting of the highest and lowest 13% Epa1-HA expressing subpopulations was then performed by flow cytometry fluorescence-activated cell sorting (FACS). Extraction of RNA from these sub-populations followed by qRT-PCR allowed the level of transcript to be related to the level of Epa1-HA protein at the cell surface in individual cells. The results illustrated that cells with high levels of Epa1-HA at their cell surface also exhibited a higher level of *EPA1* transcript than low Epa1-HA expressing cells. This was true for both BG2-Epa1-HA and CG2001-Epa1-HA strains (Fig. 73). The greater heterogeneity of Epa1-HA in BG2-Epa1-HA was illustrated by a ~7-fold increase in *EPA1* mRNA from low to high Epa1-HA cells, compared to an increase of almost half this in CG2001-Epa1-HA. These results demonstrated that transcript level is directly related to cell surface protein level and support the suggestion that Epa1-HA expression heterogeneity is controlled at the mRNA level in both strain backgrounds.

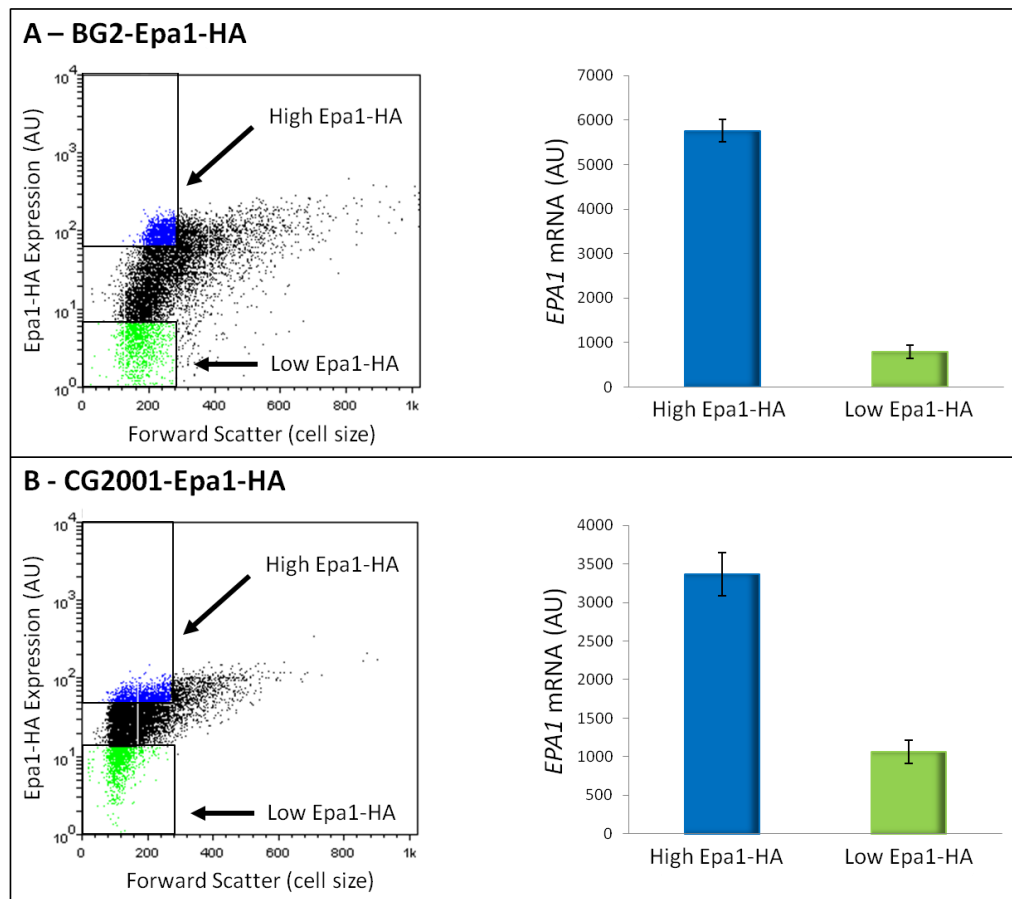


Figure 73 – Correlation between Epa1-HA protein and *EPA1* mRNA levels of individual *C. glabrata* **(A)** BG2-Epa1-HA and **(B)** CG2001-Epa1-HA cells. Exponential phase cells grown in YPD medium were gated and sorted by FACS, according to Epa1-HA expression level (as indicated with anti-HA, Alexa Fluor® 488 conjugate antibody). The gates shown were set to sort cells within the same forward scatter (cell size) range. RNA was isolated from $\sim 1 \times 10^6$ cells of the high- (blue) and the low-Epa1-HA (green) expressing subpopulations, and *EPA1* mRNA was quantified with qRT-PCR using standardized cDNA additions in all reactions. The data shown are means from three independent experiments (each analysed in triplicate) \pm SEM.

5.7 Analysis of the *EPA1* Promoter

The data presented thus far suggest that Epa1-HA heterogeneity in both tested strain backgrounds is controlled at the mRNA level. With BG2-Epa1-HA, the predominant form of transcriptional *EPA1* regulation is mediated by Sir-regulated silencing. This however is not the case for CG2001-Epa1-HA. Additional factors such as the binding of activators or other repressors to the *EPA1* promoter may also contribute to Epa1-HA heterogeneity. For instance *FLO11* expression in *S. cerevisiae* appears to be both position and promoter dependent (Halme et al., 2004). Regulation from the promoter may be particularly important in the CG2001-Epa1-HA background, where Sir-dependent silencing seems less influential. Promoter analysis was therefore performed in order to identify any possible binding sites that may impact on *EPA1* expression.

5.7.1 The *EPA1* Predicted Promoter Region Contains an Alpha2-Repressor Consensus Sequence

It was decided to characterise the likely *EPA1* promoter region, performing a bioinformatic analysis to ascertain the location of any putative transcription factor binding sites. A predicted promoter region was located at 73bp-122bp upstream of the *EPA1* start codon using the BGD Promoter Prediction (NNPP) version 2.2 tool for Eukaryotes (Reese, 2001) (http://www.fruitfly.org/seq_tools/promoter.html). The promoter sequence identified was identical in both strain backgrounds. Analysis of this predicted promoter region using the *S. cerevisiae* promoter data base (Zhu and Zhang, 1999), which has previously been applied to *C. glabrata* (Srikantha et al., 2003), revealed a MATalpha2 and a Gcn4 consensus sequence within the identified promoter region. Gcn4 has a role in the activation of amino acid biosynthetic genes in response to amino acid starvation (Hinnebusch and Natarajan, 2002). Epa1 has not been identified in such processes. Furthermore as discussed in section 5.2.2 nutrient starvation in the form of nitrogen limitation appeared to have no marked effect on Epa1-HA expression. Consequently, efforts were focused on identifying a possible role for *C. glabrata* Alpha-2 in *EPA1* regulation.

5.7.2 *Alpha2 Repressor Level appears not to Control EPA1 Expression*

In *S. cerevisiae* $\alpha 2$ functions as a repressor and is able to repress a-specific genes within alpha cells and thus aid in mating type regulation (Herskowitz, 1989, Zhong et al., 1999). Three mating type loci similar to the MAT, HML and HMR loci in *S. cerevisiae* have been identified in *C. glabrata* and termed MTL1, MTL2 and MTL3. *C. glabrata* has also been shown to maintain distinct a and α mating types despite no observable sexual cycle (Srikantha et al., 2003, Muller et al., 2008). In addition, *S. cerevisiae* genes known to be repressed by the a1/ $\alpha 2$ repressor are decreased in *SIR2*, *SIR3*, and *SIR4* mutants (Wyrick et al., 1999). This may also implicate the repressor in regulation of Epa1 in the CG2001-Epa1-HA strain background, where decreased Epa1-HA expression is observed when Sir activity is inhibited. The two predominant strain backgrounds used in this study CG2001 HTU Δ and BG2 have been identified as mating type α and a respectively (Muller et al., 2008, Ramirez-Zavaleta et al., 2010). Based on the evidence discussed above and provided by the promoter analysis it was postulated that any variation in $\alpha 2$ repressor levels may contribute to Epa1-HA heterogeneity, particularly in strain CG2001-Epa1-HA.

In order to characterise potential variation in the levels of $\alpha 2$ transcript in relation to Epa1 expression, cells were sorted by flow cytometry FACS according to Epa1-HA level and RNA extracted from these sorted cells was used for qRT-PCR (as described in 5.6.1). If $\alpha 2$ was indeed a direct repressor of *EPA1*, with the extent of repression being linked to $\alpha 2$ mRNA expression, we would expect higher levels of $\alpha 2$ mRNA to be present in low Epa1-HA expressing cells, and vice versa. However, the analysis revealed that CG2001-Epa1-HA cells expressing low Epa1-HA also demonstrated lower levels of $\alpha 2$ mRNA compared to those of for high Epa1-HA expressing cells (Fig. 74). Thus, $\alpha 2$ expression does not correlate with Epa1 repression suggesting that the repressor may not be responsible for controlling Epa1 expression and heterogeneity. Since $\alpha 2$ transcript levels were actually found to positively correlate with Epa1-HA expression it is possible that the repressor may act on an alternative *EPA1* repressor to affect expression of the adhesin indirectly. However, the promoter analysis did not reveal any obvious candidates. Furthermore if such a

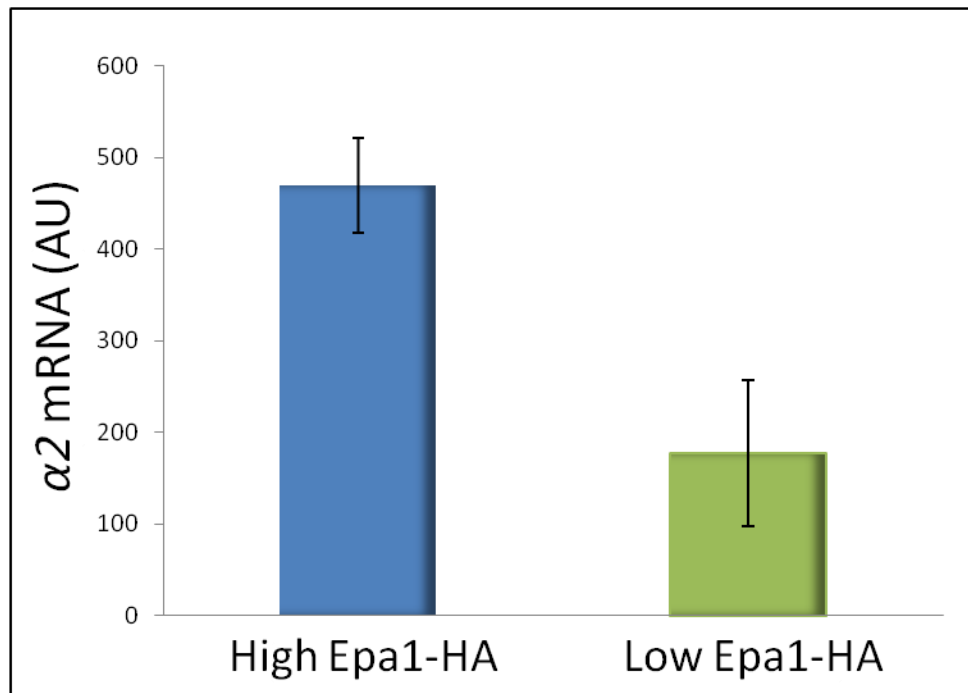


Figure 74 – Correlation between Epa1-HA protein and $\alpha 2$ mRNA levels of individual *C. glabrata* CG2001-Epa1-HA cells. Exponential phase cells grown in YPD medium were gated and sorted by FACS, according to Epa1-HA expression level (as indicated with anti-HA, Alexa Fluor® 488 conjugate antibody). Cells were sorted within the same forward scatter (cell size) range. RNA was isolated from $\sim 1 \times 10^6$ cells of the high- (blue) and the low-Epa1-HA (green) expressing subpopulations, and $\alpha 2$ mRNA was quantified with qRT-PCR using standardized cDNA additions in all reactions. The data shown are means from three independent experiments (each analysed in triplicate) \pm SEM.

mechanism did exist, loss of silencing, known to de-repress silent $\alpha 2$ in *C. glabrata* (Ramirez-Zavaleta et al., 2010), may be expected to increase Epa1-HA expression in CG2001-Epa1-HA cells, however, the opposite is seen. Not surprisingly, $\alpha 2$ transcript could not be detected in sorted BG2-Epa1-HA cells owing to the a-mating type of this strain, although leakiness in $\alpha 2$ expression has been inferred (Ramirez-Zavaleta et al., 2010).

5.8 Alignments of *EPA1* Sequence from Two Strain Backgrounds

In order to substantiate that differences in Epa1 regulation between the two *C. glabrata* strains are not due to sequence differences in and around the *EPA1* ORF, sequence alignments were performed using the NCBI Blast Alignment tool. *EPA1* is the same length in both strains and alignment revealed only 14bp to be different between the two genes. These differences corresponded to nine amino acid substitutions throughout the length of the translated protein with four of these substitutions being to amino acids which are chemically similar in each strain (Fig. 75). None of the changes are in the region of the GPI-anchor, which begins at residue 1010, nor are they present in the N-terminal domain (amino acids 1-332) which mediates ligand binding (Frieman et al., 2002). Consequently, such changes would not be expected to affect either ligand binding or, more importantly in terms of cell surface expression, attachment to the cell wall. Rather, amino acid substitutions were located in the C-terminal Ser/Thr rich domain. This region has been identified as important in the projection of Epa1 out from the cell wall, with changes in the length of this region leading to altered detection at the cell surface (Frieman et al., 2002). However since the proteins from each strain remain the same length such an effect is unlikely to create differences between our two strains and does not explain any differences in transcriptional regulation observed. Furthermore, differences in heterogeneity were seen with Epa1-HA in each strain: the Epa1-HA construct was derived from plasmid pMS15 for both strains, and therefore the sequence was the same. Upstream and downstream nucleotide sequences were also found to be highly similar between native *EPA1* the two strains. Alignments demonstrated that 501bp of upstream sequence had 99% sequence identity between the two strains with 288bp upstream of the *EPA1* start codon, encompassing the predicted promoter region, being 100% identical. The sequence up to 501bp down-

ATCC2001	1	MILNPALFLNKCVCYITTLILLLLLTNGGYATSSNDISLASKDPTTFPLGCSPIITPPKKG	60
BG2	1	MILNPALFLNKCVCYITTLILLLLLTNGGYATSSNDISLASKDPTTFPLGCSPIITPPKKG	60
ATCC2001	61	LSMELYSYDFRKKGSYPCWDAAYLDPNYPRTGYKSHRLLAKVDGVTGNINFYHATKGC	120
BG2	61	LSMELYSYDFRKKGSYPCWDAAYLDPNYPRTGYKSHRLLAKVDGVTGNINFYHATKGC	120
ATCC2001	121	PQLGHLPASYNYPKPLTMTNFTMLLYGYFRPKVTGFHTFTISADLLFVNFAGNAFDCC	180
BG2	121	PQLGHLPASYNYPKPLTMTNFTMLLYGYFRPKVTGFHTFTISADLLFVNFAGNAFDCC	180
ATCC2001	181	RRDSSADHFGNYQAYAIWGSKTAKDELTVHLDAGVYYPIRLFYNNREYDALSFTFKTES	240
BG2	181	RRDSSADHFGNYQAYAIWGSKTAKDELTVHLDAGVYYPIRLFYNNREYDALSFTFKTES	240
ATCC2001	241	NENTVDFSEYFFSLDDTEEGCPGLISYDSSCASVKTSKIIGIDYHETPNENLVPIITKT	300
BG2	241	NENTVDFSEYFFSLDDTEEGCPGLISYDSSCASVKTSKIIGIDYHETPNENLVPIITKT	300
ATCC2001	301	IYHLGIPCTGTTTTPLCGSGFYDPLANKCVTINTSSTSSVTKTTSHHTSKEVSFHSSISS	360
BG2	301	IYHLGIPCTGTTTTPLCGSGFYDPLANKCVTINTSSTSSVTKTTSHHTSKEVSFHSSISS	360
ATCC2001	361	QKTLIPKSIKSPYGIKSIQSIPTMETSSSEISSEYAFSDVISTPSSHSPYTKKHSSLNSS	420
BG2	361	QKTLIPKSIKSPYGIKSIQSIPTMETSSSEISSEYAFSDVISTPSSHSPYTKKHSSLNSS	420
ATCC2001	421	SYTSTVIHSLTSYSISQGFSTSLSEQNITSKSSDKFSTATSMNSITQSSIIISQSSST	480
BG2	421	SYTSTVIHSLTSYSISQGFSTSLSEQNITSKSSDKFSTATSMNSITQSSIIISQST	480
ATCC2001	481	NNENYTTTSMHTSSDKISTETLNNSISTTTSILFNSNSTILKNNTTIISSDKDTHYHPVN	540
BG2	481	NNENYTTTSMHTSSDKISTETLNNSISTTTSILFNSNSTILKNNTTIISSDKDTHYHPVN	540
ATCC2001	541	PTIIVCSTNKTEIICASITQPSISNSNNHWSSSVLRFNSTTVRSTLPSSAGSNETSINVFF	600
BG2	541	PTIIVCSTNKTEIICASITQPSISNSNNHWSSSVLRFNSTTVRSTLPSSAGSNETSINVFF	600
ATCC2001	601	SSSTESNA ⁺ STSTSTSNK ⁺ TVRSTLPSSAGSNETSINVFFSSSTESNTSTSTSTSNK ⁺	660
BG2	601	SSSTESN ⁺ STSTSTSNK ⁺ MVRSTLPSSAGSNETSISVFFSSSTESNTSTSTSTSNK ⁺	660
ATCC2001	661	VRSTLPSSAGSNETSINVFFSSSTESNA ⁺ STSTSTSNKTVRSTLPSSAGIIMTSLSQRN	720
BG2	661	VRSTLPSSAGSNETSINVFFSSSTESN ⁺ STSTSTSNKTVRSTLPSSAGIIMTSLSQRN	720
ATCC2001	721	NKSASSYASSNSKCYNTADSCRKRVHSTPSYLLTSSYTSEGVDYDCSLVSTKLIKINDTNC ^L	780
BG2	721	NKSASSYASSNSKCYNTADSCRKRVHSTPSYLLTSSYTSEGVDYDCSLVSTKLIKINDTNC ⁺	780
ATCC2001	781	NNKH ⁺ TTKCLKTSVTTTIP ⁺ LEIKTARKSSNTIGLHSYPTSSPNKSISSAPIIGYISSF	840
BG2	781	NNKH ⁺ TTKCLKTSVTTTIP ⁺ LEIKTARKSSNTIGLHSYPTSSPNKSISSAPIIGYISSF	840
ATCC2001	841	KTIKTASPSYQTSDLTITTTITSLNPNPGSTAVENTHESNDKSRKTSSNDISSKHSVIKET	900
BG2	841	KTIKTASPSYQTSDLTITTTITSLNPNPGSTAVENTHESNDKSRKTSSNDISSKHSVIKET	900
ATCC2001	901	KDAVESSNKSHQNTLKCSSIIIASSSHNSYESLGGTTLTLTLKSVYSPQNNDLPLFLEI	960
BG2	901	KDAVESSNKSHQNTLKCSSIIIASSSHNSYESLGGTTLTLTLKSVYSPQNNDLPLFLEI	960
ATCC2001	961	SEVNPSRTVLPESKMMQYLTSTEERNKTARNTIATNIVSISTFHFELEGNAIRMGYTQL	1020
BG2	961	SEVNPSRTVLPESKMMQYLTSTEERNKTARNTIATNIVSISTFHFELEGNAIRMGYTQL	1020
ATCC2001	1021	LLMLIGIIVMNIGT 1034	
BG2	1021	LLMLIGIIVMNIGT 1034	

Figure 75 – Protein alignment of Epa1 from ATCC2001 (top) and BG2 (bottom). Amino acid differences are highlighted in red with a '+' indicating a change to a chemically similar amino acid.

-stream of the *EPA1* ORF was also 99% identical between the two strains.

5.9 Regulation of Other *EPA* Genes Relative to Epa1-HA

The hypothesis that different *EPA* genes may be expressed at different times during infection (De Las Penas et al., 2003, Castano et al., 2005) led me to question whether this could reflect heterogeneity exhibited by cells, pre-infection, in order for subpopulations to be pre-equipped for survival at any location. In this case, "pre-adopted" subpopulations would be "selected" on arrival at the specific host niche, rather than regulation occurring as a response. It may be that cells demonstrating low levels of Epa1 show high expression of other Epa adhesins and vice versa. Epa proteins have been shown to confer distinct cell surface properties (Zupancic et al., 2008) and heterogeneity generation could be a way of creating subpopulations of cells within the larger population that are primed for infection at specific sites.

5.9.1 EPA6 and EPA7 mRNA Levels are Correlated with Cell Surface Epa1-HA Expression

In order to test the hypothesis, cells that had been sorted by flow cytometry FACS according to their Epa1-HA expression were analysed for expression of *EPA6* and *EPA7* by qRT-PCR (as described in 5.6.1). Such analysis therefore allows a direct comparison between the level of Epa1 at the cell surface and the corresponding expression of additional *EPA* genes in the same cells. This analysis revealed that *EPA6* and *EPA7* mRNA expression correlated with cell surface Epa1-HA for both BG2-Epa1-HA and CG2001-Epa1-HA (Fig. 76). Although this method of analysis does not give a direct measure of heterogeneity the differences between high and low values may give an idea of what heterogeneity could exist. *EPA6* and *EPA7* transcription varies ~17 fold and ~6 fold, respectively, between low-Epa1-HA and high-Epa1-HA cells of the BG2-Epa1-HA strain. In comparison the differences were smaller (~3 fold for both genes) in CG2001-Epa1-HA. This is similar to the difference measured for *EPA1* mRNA in such sorted cells (section 5.6.1). This may indicate higher levels of heterogeneity also for *EPA6* and *EPA7* in the BG2-Epa1-HA background. As a comparison, qRT-PCR for *ACT1* was also performed on sorted populations. Expression levels also appeared to be correlated to the Epa1-HA expression level, possibly

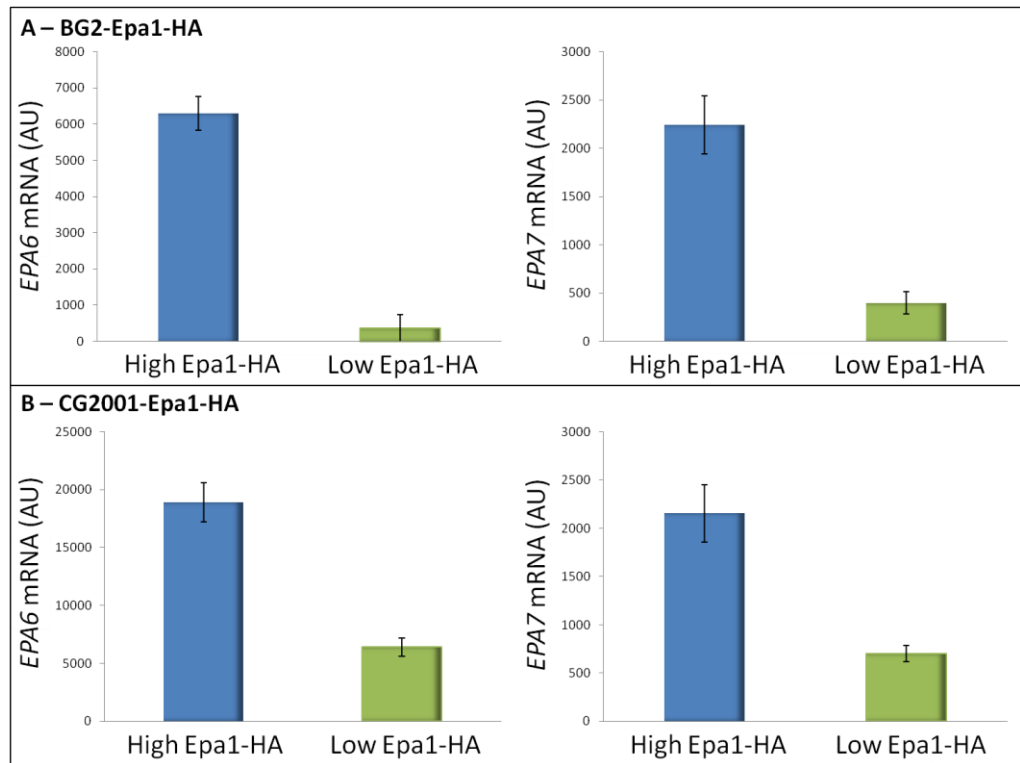


Figure 76 – Correlation between Epa1-HA protein and *EPA6* and *EPA7* mRNA levels of individual *C. glabrata* **(A)** BG2-Epa1-HA and **(B)** CG2001-Epa1-HA cells. Exponential phase cells grown in YPD medium were gated and sorted by FACS, according to Epa1-HA expression level (as indicated with anti-HA, Alexa Fluor® 488 conjugate antibody). Cells were sorted within the same forward scatter (cell size) range. RNA was isolated from $\sim 1 \times 10^6$ cells of the high- (blue) and the low-Epa1-HA (green) expressing subpopulations, and *EPA6* (left) and *EPA7* (right) mRNA was quantified with qRT-PCR using standardized cDNA additions in all reactions. The data shown are means from three independent experiments (each analysed in triplicate) \pm SEM.

suggesting a more global effect on transcription that is not simply limited to the *EPA* genes. The variation in *ACT1* expression across low- to high-Epa1 expressing cells was ~ 2 fold and ~ 3 fold for CG2001-Epa1-HA and BG2-Epa1-HA, respectively. This was less than the differences seen for *EPA6* and *EPA7* mRNA between low- and high-Epa1 expressing cells for the respective strains. It is possible that the differences seen for *ACT1* may be indicative of the margin of error for the experiment, for instance loading differences and are thus artifactual.

5.9.2 *Sir-Regulated Transcriptional Silencing of Additional EPA Genes*

Results described earlier demonstrated an apparent difference in the dependence of *EPA1* expression and heterogeneity on Sir-regulated transcriptional silencing according to strain background. In order to determine if this difference also applied to additional *EPA* genes the expression of *EPA6* and *EPA7* was measured by qRT-PCR under conditions of 'standard' and limited silencing for both strain backgrounds by limiting growth medium for NA (as described in section 5.3.3.1). This analysis was also performed in the CG2001-Epa1-HA *sir3* Δ strain in order to corroborate results obtained via NA limitation.

In the BG2 strain, data for both *EPA6* and *EPA7* agreed with the effect on *EPA1*, in that expression of both genes increased upon limitation of silencing (Fig. 77). In the CG2001 HTU Δ strain, by contrast, although *EPA6* mRNA decreased upon loss of silencing by both limited NA and *SIR3* deletion, as is also seen for *EPA1* in this strain, *EPA7* expression was increased in both instances (Fig. 78). Thus for the latter strain at least these results indicate that different *EPA* genes within the same strain may depend to different extents on regulation by Sir-dependent transcriptional silencing. Indeed analysis of more *EPA* genes may reveal this also to be the case in the BG2 background.

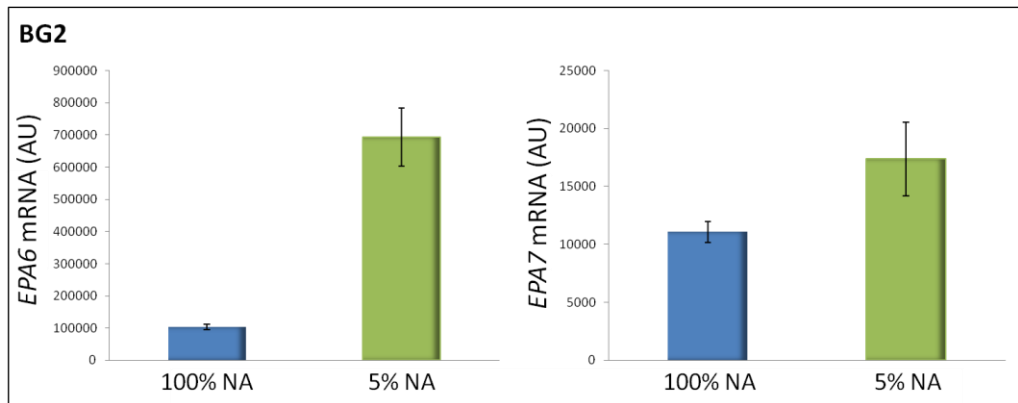


Figure 77 – *EPA6* (left) and *EPA7* (right) mRNA levels in BG2 following NA limitation to inhibit transcriptional silencing. Cells were grown overnight in SC medium containing either 100% NA (blue) or 5% NA (green) before re-inoculation into the appropriate fresh SC medium and growth to exponential phase. RNA was extracted from $\sim 1 \times 10^7$ cells grown under the relevant condition, and *EPA6* and *EPA7* mRNA quantified using standardised cDNA additions in all reactions. The data shown are means from three independent experiments (each analysed in triplicate) \pm SEM.

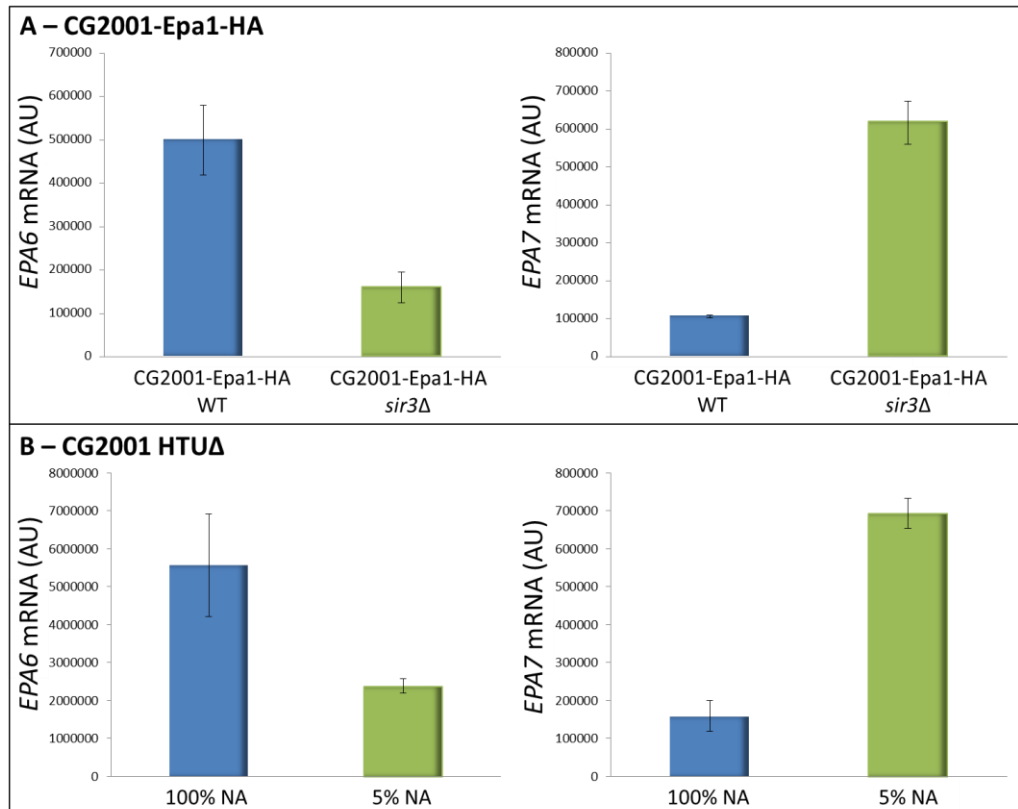


Figure 78 – *EPA6* (left) and *EPA7* (right) mRNA levels in **(A)** CG2001-Epa1-HA (blue) and CG2001-Epa1-HA *sir3Δ* (green) cells grown to exponential phase in YPD and **(B)** CG2001 HTUΔ cells following NA limitation to inhibit transcriptional silencing. Cells were grown overnight in SC medium containing either 100% NA (blue) or 5% NA (green) before re-inoculation into the appropriate fresh SC medium and growth to exponential phase. **(A, B)** RNA was extracted from $\sim 1 \times 10^7$ cells grown under the relevant condition, and *EPA6* and *EPA7* mRNA quantified using standardised cDNA additions in all reactions. The data shown are means from three independent experiments (each analysed in triplicate) \pm SEM.

5.10 Discussion

During the course of the study described in this chapter, the contribution of various factors to Epa1 expression were studied in order to elucidate possible sources of cell-to-cell heterogeneity in expression of this adhesin. During the process of host infection, pathogens may encounter a wide range of host niches and therefore environmental conditions can be highly variable. The effect of several virulence related conditions on Epa1 expression and heterogeneity were thus analysed; these included temperature, nitrogen limitation and ambient pH. Analyses demonstrated all three environmental conditions to have a greater effect on Epa1 expression in the CG2001-Epa1-HA strain, which has lower heterogeneity than the BG2-Epa1-HA strain. However the effects were relatively small. Heterogeneity was minimally affected by the environmental variables for both strains, particularly BG2-Epa1-HA. In CG2001-Epa1-HA, temperature change and pH evoked the most marked effect on Epa1-HA expression and heterogeneity.

In the case of ambient pH, CG2001-Epa1-HA exhibited the highest Epa1 expression and lowest heterogeneity at pH4. This acidic pH relates to the highly specific niche of the vaginal cavity and *C. glabrata* is known to be well adapted for colonisation in this environment (Schmidt et al., 2008, Davis, 2009). An attractive hypothesis is that different Epa1 proteins are expressed at different points during infection, possibly driven by signals associated with different host niches (De Las Penas et al., 2003, Castano et al., 2005). It may also be possible that heterogeneity occurs to different extents within the host as a survival mechanism. For example cells expressing low levels of Epa1 may be better adapted to disseminated blood stream infection, where adhesion may not be of primary importance, and avoidance of the immune system, possibly due to lower levels of immunogenic proteins at the pathogen surface. High expression on the other hand may be required when mucosal surfaces are encountered. Heterogeneity may allow *C. glabrata* populations to establish infection at any niche in addition to becoming systemic. As such the acidic pH of the vaginal cavity may serve as a useful signal identifying this particular niche as a specific site where adhesion is required causing reduced heterogeneity. By contrast growth pHs of 7.4 and 8, which represent a much broader range of host niches, did exhibit higher levels of heterogeneity.

Increasing growth temperature to that of mammalian hosts (37°C) has been linked to increased cell surface hydrophobicity in a number of *C. glabrata* isolates. This is thought to influence the adhesion properties of cells and be an indicator of increased adhesin incorporation at the cell wall (Hazen et al., 1986, Ishigami et al., 2006, de Groot et al., 2008). Increased Epa1-HA expression in CG2001-Epa1-HA, identified in this study, at 37°C is in agreement with increased incorporation of adhesins at the higher temperature, however this did not coincide with increased adhesion. It may be worth noting that Epa1-HA levels in CG2001-Epa1-HA are already high when compared to the BG2 background even when cells are grown at 30°C, indeed this strain has previously been shown to possess high cell surface hydrophobicity (de Groot et al., 2008). Consequently maximal adhesion to Hep2 epithelial cells may already be achieved at the lower temperature for this strain.

The relative lack of environmental effects on Epa1-HA expression in BG2-Epa1-HA, compared to CG2001-Epa1-HA, may not be completely unexpected in that different isolates of *C. glabrata* have been shown to react differently to the same growth conditions (Hazen et al., 1986, Luo and Samaranayake, 2002). In addition the present study has shown Epa1-HA expression and heterogeneity in BG2-Epa1-HA to be heavily dependent upon Sir-mediated transcriptional silencing. It may be logical to suggest that regulation exerted by the transcriptional silencing machinery could be sufficient to mask major environmental effects on Epa1 expression heterogeneity. In *S. cerevisiae* increased temperature has in fact been shown to increase transcriptional silencing at telomeres (Bi et al., 2004). Since transcriptional silencing is already active in BG2-Epa1-HA no additional silencing effect may be created by increased temperature. It is also possible that the active silencing in BG2-Epa1-HA, in addition to any increased silencing at 37°C, could simply counteract any increased expression induced directly by a switch in temperature. However, based on results observed for CG2001-Epa1-HA (which lacks *EPA1* silencing), where only a small increase in Epa1-HA expression is observed, any hidden effects would likely be minimal.

Increased Epa1-HA expression following the temperature shift in CG2001-Epa1-HA could be connected to an increase in silencing since inhibition of silencing in this strain results in a slight decrease in Epa1-HA expression. Introduction of an extra copy of *SIR3*, however, actually caused increased silencing. Nevertheless increased silencing seen in *S.*

cerevisiae at 37°C is not brought about by alterations in *SIR3* expression. Rather, it was hypothesised that altered thermodynamics drive increased Sir-nucleosome and Sir-Sir interactions (Bi et al., 2004). Such effects may not be sufficient to facilitate silencing of *EPA1* in CG2001-Epa1-HA cells grown at 37°C. By contrast, increasing the total level of *SIR3*, by introduction of an extra copy, may be sufficient to induce silencing of *EPA1* in this strain background. Sir3 overexpression is known to facilitate the spread of silent chromatin (Renauld et al., 1993, Talbert and Henikoff, 2006). Consequently ectopic expression of *SIR3* likely affects Sir-complex formation and spreading. This may be particularly pertinent to *EPA1* which resides at >20kb from the chromosome end. Thus, addition of this second copy of *SIR3* did bring observable Epa1 expression more in line with that seen for BG2-Epa1-HA, in which silencing appeared to be more efficient.

Although above results would be consistent with *EPA1* residing at a position closer to the telomere in strain BG2-Epa1-HA than in CG2001-Epa1-HA, any marked difference in the distance of *EPA1* from the chromosome end between the two tested strain backgrounds could not be identified. Indeed, based on previous literature (De Las Penas et al., 2003, Rosas-Hernandez et al., 2008) it was estimated that an approximate size difference of ~2.9kb would be needed to see even a 25% alteration in transcriptional silencing at the *EPA1* locus. Nonetheless, small differences were detected, with *EPA1* in BG2 estimated to be ~451bp further from the telomere and ~752bp closer to the telomere than its CG2001 HTUΔ counterpart following *PmeI* and *StuI* digestion, respectively. Given the relatively small size differences compared to the total fragment sizes being measured and distances required to see an effect, in addition to their contradictory estimations, it is possible that they may be indicative of the margin of error for this experimental procedure. Lack of large size difference is consistent with insertion, deletion or recombination events within regions between *EPA1* and the telomere not being responsible for the altered Sir-dependency observed in the two strains. In addition alignment of *EPA1* between the two strains revealed them to be highly similar, and identical in length. *EPA1* in these two particular strains was already known to contain the same number of 120bp minisatellite repeats (Thierry et al., 2008). Furthermore, studies have revealed no marked size difference in chromosome E, on which *EPA1* resides, between a large number of *C. glabrata* strains (Muller et al., 2009). Thus, other factors are likely necessary to reduce the efficiency of *EPA1* transcriptional silencing in

CG2001-Epa1-HA. Such other factors did not include decreased levels of *SIR3* transcript, which were actually higher in CG2001 HTUΔ than in the BG2 strain background where silencing was more efficient. It has also been shown elsewhere that the level of observable silencing is not necessarily related to the level of Sir transcript or protein (Bi et al., 2004). Taking these results into account, silencing of *EPA1* in CG2001-Epa1-HA may be due to inefficient propagation of silencing out towards the *EPA1* locus. A genome wide screen in *S. cerevisiae* identified a number of negative regulators which were able to antagonize the spread of Sir activity (Raisner and Madhani, 2008). Such regulators could be one important factor for reduced silencing of *EPA1* in CG2001-Epa1-HA, suppressible by *SIR3* over-expression. Along similar lines, heterogeneity in expression of such negative regulators could also have a role in controlling the heterogeneous Epa1 silencing observed for BG2-Epa1-HA. It is possible that the higher *SIR3* mRNA levels recorded in a CG2001-Epa1-HA background represent a response of this strain to compensate, albeit inefficiently, for any reduction in the spread of silenced chromatin.

The role of transcriptional silencing in *EPA1* regulation was not only found to differ between the two predominant strains of this study; CG2001-Epa1-HA and BG2-Epa1-HA, but also between a number of clinical *C. glabrata* isolates thus demonstrating inter-strain variation of Sir-dependency of *EPA1* heterogeneity. Epa1 expression in CG2001-Epa1-HA was affected by a loss of transcriptional silencing only in that there was a decrease in overall expression; heterogeneity was unaffected. The decrease observed, particularly since discounting a direct effect of the $\alpha 2$ repressor, could represent a decrease in the level of available transcriptional machinery due to de-repression of previously silenced genes. By contrast Epa1 expression in BG2 was markedly increased by a reduction in transcriptional silencing. This resulted in decreased heterogeneity due to loss of the low expressing population of cells. Although the method of analysis used to determine the role of silencing in a number of clinical isolates by nicotinic acid limitation did not enable comparison of heterogeneity levels, it did enable identification of three distinct groups. 1) *EPA1* is subject to transcriptional silencing which is released upon inhibition of silencing (BG2-like), 2) Inhibition of silencing has no marked effect on *EPA1* expression, and 3) *EPA1* expression decreases when silencing is inhibited (CG2001 HTUΔ-like). Such results underscore the propensity of different *C. glabrata* isolates to react

differently to the same stimulus (Hazen et al., 1986, Luo and Samaranayake, 2002). Furthermore, this study identified the Sir-dependency of *EPA1* expression to be correlated with Epa1 cell surface heterogeneity in these isolates being greatest in cells subject to silencing (BG2-like). The analyses did not suggest that the role of Sir-dependent silencing in *EPA1* regulation was related to the source of each isolate. Isolates sourced from the same human niche exhibited different dependencies on transcriptional silencing in *EPA1* regulation. Previous studies in *C. albicans* have indicated, with the exception of increased *ALS4* in vaginal specimens, that *ALS* transcriptional activity is relatively consistent despite the location from which specimens were collected (Hoyer et al., 2008). Rather than the most appropriate adhesin being expressed at a particular host site in response to environmental cues this indicated the presence of multiple adhesins at each niche (Hoyer et al., 2008). This could be consistent with a greater relative role for cell-to-cell heterogeneity in host infection.

It was found that, however, although *EPA1* expression in CG2001 HTUΔ is not heavily reliant on Sir-mediated transcriptional silencing, *EPA7* within this strain is. Upon inhibition of silencing, expression of *EPA7* was markedly increased, much in the same way as *EPA1* expression increases under the same conditions in a BG2 background. Two different methods of regulation therefore seem to exist for *EPA* expression, at least in CG2001 HTUΔ, and this may enable differential *EPA* expression within the host at different sites. Similar differences in *EPA* gene regulation were not seen in a BG2 background however, but could possibly be revealed with the analysis of more *EPA* genes. Alternatively, BG2 which exhibits high *EPA1* heterogeneity, and possibly higher *EPA6* and *EPA7* variation (discussed further below) may be more reliant on silencing driven cell-to-cell adhesin heterogeneity as a mechanism to allow colonisation of whichever host site is encountered. CG2001 HTUΔ on the other hand, where heterogeneity is markedly lower, may be more reliant on expression of the most appropriate *EPA* gene at a given site.

The lack of Sir-mediated transcriptional silencing exerted on Epa1 in CG2001-Epa1-HA enabled the use of the strain to elucidate the effect of potential post translation factors on Epa1 expression and heterogeneity. The effects of lipid rafts, cleavage from the cell surface by the action of Yps aspartyl proteases and overall levels of mannoprotein at the cell surface were analysed. According to the results, although inhibition of lipid raft

components did lead to increased mean Epa1-HA expression, such domains do not appear to be involved in confinement of Epa1 to specific regions at the cell surface and heterogeneity of such lipid-enriched regions is not related to Epa1-HA heterogeneity. Similarly, removal of Epa1 from the cell surface by the action of Yps aspartyl proteases (Kaur et al., 2007) was found to have little role in the regulation of Epa1 heterogeneity. In addition the extent of heterogeneity exhibited by Epa1 was not mirrored by heterogeneity in total mannoprotein, indicating that Epa1 expression at the cell surface varies independently of this.

In contrast to the lack of the above post-translational modes of control over Epa1 expression heterogeneity, it was apparent that cell surface Epa1 protein level was correlated with *EPA1* transcript level in both strain backgrounds. Thus even in CG2001-Epa1-HA, in which Epa1 is not subject to Sir-mediated silencing and heterogeneity is lower than observed in BG2-Epa1-HA, heterogeneity in Epa1 expression appeared to be controlled at the transcriptional level. This is consistent with transcriptional regulation generally being a major contributor to gene expression noise (Avery, 2006). In line with this, cell-to-cell variation of adhesin-encoding *FLO* genes in *S. cerevisiae* is controlled at the transcriptional level by a combination of both global and promoter specific factors that contribute to gene silencing (Halme et al., 2004, Octavio et al., 2009). The transcription factors Flo8, Mss11, and Msn1 regulate *FLO* gene expression in *S. cerevisiae* (Halme et al., 2004, Verstrepen et al., 2004, Octavio et al., 2009), with the corresponding Flo8 and Mss11 regulators in *C. glabrata* being implicated in *EPA6* gene expression (Mundy and Cormack, 2009). Bioinformatic analysis, however, revealed a putative $\alpha 2$ repressor binding site within the promoter of *EPA1*. This repressor is known to have a role in decreased gene expression exhibited upon release of silencing in *S. cerevisiae* (Wyrick et al., 1999). Subsequent investigation in the present study revealed that increased expression of $\alpha 2$ transcript did not correlate with lower levels of Epa1-HA at the single cell level. Therefore, it is unlikely that $\alpha 2$ is responsible for Epa1 expression heterogeneity, or the decreased expression seen in CG2001-Epa1-HA upon inhibition of silencing. Evidence from previous studies supports the lack of a role for the $\alpha 2$ repressor in Epa1 expression regulation. Such studies have reported that silencing of the *MTL3* locus, within which the *C. glabrata* $\alpha 1$ and $\alpha 2$ genes are located, is dependent on yKu70 and yKu80 (Ramirez-Zavaleta et al., 2010):

however, *yKu* deletion in *C. glabrata* has been shown to have no effect on *EPA1* expression (Rosas-Hernandez et al., 2008). The $\alpha 2$ consensus sequence was identified in the promoters of both *C. glabrata* strain backgrounds. However, $\alpha 2$ is also unlikely to have a role regulating *Epa1* expression in the BG2 background since the a-mating type means that $\alpha 2$ is transcriptionally silent in this strain. Although the transcript is eventually detectable due to leaky expression (Ramirez-Zavaleta et al., 2010), such low levels are unlikely to influence *EPA1* expression in this background. In addition Sir-dependent silencing appears to be the primary mode of *EPA1* regulation in BG2 cells and the increased expression of *Epa1* seen upon loss of silencing is also evidence against a role for the repressor in this strain.

Like *EPA1*, expression of *EPA6* and *EPA7* was also found to be correlated with *Epa1*-HA cell surface levels in both strains. This suggested that control over expression of several *EPA* genes is exerted at the transcriptional level, possibly in a combined *EPA* regulation mechanism. An additional factor, however, that must be taken into account is the correlation also with *ACT1* expression seen among the sorted populations. Despite this correlation the difference in *ACT1* expression observed between high- and low-*Epa1*-HA expressing cells was lower than that observed for the *EPA* genes in either tested strain background. It is possible that the differences seen for *ACT1* are artifactual and may be indicative of the margin of error for the experiment. Alternatively a more global regulation of heterogeneity may be occurring, which extends beyond just the *EPA* genes, i.e. the extremes of *EPA1* expression also correlate with the extremes of expression for other genes, such as *ACT1*. Indeed, all genes demonstrate some heterogeneity even if the effect is small. An additional possible explanation for the correlated *ACT1* expression may be that high *Epa1* cells are primed not only for adhesion but also for the accompanying tissue invasion; the cytoskeleton is known to be important for polarized growth, thought to be involved in tissue invasion in *C. albicans* (Martin and Konopka, 2004), so higher expression of *ACT1* may be beneficial in this regard. Further insights could be gained by a broader study including the analysis of many genes in high- and low-*Epa1* expressing subpopulations by transcriptomics analyses. This study into the expression *EPA6* and *EPA7* suggested that *EPA6* and *EPA7* in the BG2 strain may exhibit high heterogeneity, which might indicate that high *EPA* heterogeneity is a common trait of this strain.

Regulation of Epa1 heterogeneity thus seems to be complex and although the results discussed in this chapter indicate that control is exerted at the mRNA level, this could be part of a broader response influenced by several factors yet to be elucidated. Further complication stems from the fact that different strains, and indeed different *EPA* genes within these strains, seem to be differentially affected by the same stimuli. In particular, in the case of this study, a differential dependence of Epa1 expression and heterogeneity on Sir-mediated transcriptional silencing was identified.

Chapter 6 - Concluding Remarks

6.1 Concluding Remarks

Research efforts in recent years have greatly improved our understanding of the molecular mechanisms that govern (fungal) pathogenesis, including the gene products that contribute to virulence. This understanding has been mirrored by the emergence of cell-to-cell heterogeneity as a major research area, with recognition of its likely role as a virulence determinant in pathogens (Avery, 2006, Verstrepen and Fink, 2009). Indeed, in principle, it may take just a few virulent cells within a larger mostly-avirulent population to initiate infection. Importantly conventional microbiological analyses produce culture-averaged data which can mask variation within the population. This study aimed to identify and further characterise heterogeneity within yeast populations. Despite initially promising, but ultimately misleading, indications of bi-stable Rad6 expression within *S. cerevisiae*, the major focus of this work became analysis of the well studied *C. glabrata* adhesin Epa1. The pathogenic yeast *C. glabrata* is responsible for a variety of mucosal and disseminated infections (Kaur et al., 2005), the latter of which can be associated with high levels of mortality (Wisplinghoff et al., 2004). Adhesion, being one of the first host-pathogen interactions to occur, is thought to be an important step in the initiation of infection and many pathogens produce adhesins to help mediate this process (de Groot et al., 2008, Hoyer et al., 2008, Silva et al., 2011).

During the course of this study Epa1 gene and protein expression was observed to exhibit marked variation between individual cells. This phenotype appears to be primarily mediated by Sir-dependent transcriptional silencing. In agreement with this observation, Epa1 protein expression was controlled primarily at the mRNA level, consistent with transcriptional regulation being a major contributor to noise in gene expression generally (Avery, 2006). Indeed epigenetic gene silencing has been shown to regulate differential expression of the *S. cerevisiae* *FLO* genes which constitute functional homologues of the *EPA* gene family (Halme et al., 2004). Variation in the adhesion capacity of different *C. glabrata* strains has been reported previously (de Groot et al., 2008). In addition marked genome plasticity has been observed across isolates (Muller et al., 2009, Polakova et al., 2009). It may not be surprising then, that the existence of Sir-dependent Epa1 heterogeneity was related to strain background with the two predominant strains utilised during this study exhibiting different heterogeneity levels. Furthermore both high- and

low- heterogeneity phenotypes were evident across clinical isolates recovered from various host niches and appeared to correlate with the level of *EPA1* silencing exhibited in those strains.

It is tempting to speculate that different strains could have different virulences possibly due to their heterogeneity levels (heterogeneity may provide a virulence advantage). The incidence of both high- and low-heterogeneity isolates from patients, however, highlights the importance of additional factors in pathogenesis. This is not to say that *Epa1* heterogeneity would not confer any influence over virulence within the host. Indeed *Epa1* expression of individual cells was shown to be correlated with adherence capacity, thus establishing a functional consequence of heterogeneity and a link to virulence potential. Moreover phenotypic heterogeneity is proposed to aid survival during times of stress and environmental fluctuation (Avery, 2006, Bishop et al., 2007, Smith et al., 2007, Acar et al., 2008), such as may be encountered within the mammalian host as cells invade the bloodstream and/or colonise different epithelia and organs. To that end it might be predicted that isolates with the greatest heterogeneity (i.e., those exhibiting Sir-mediated *EPA* silencing), may have some survival advantage and possibly a greater virulence potential. For instance, low-*Epa1* expressing cells could be better adapted for bloodstream infection where adhesion to a surface may be less important or better protected from immune recognition. For instance, *C. glabrata* BG2 cells deleted for the *Yps* proteases, which cleave *Epa1* from the cell surface in this strain background, demonstrate increased activation of macrophages, alongside decreased survival within these phagocytic cells, and attenuated virulence (Kaur et al., 2007). These observations may suggest a survival advantage for cells expressing low levels of *Epa1* whereby lower levels of immunogenic proteins at the cell surface could suppress macrophage activation. Alternatively such cells may express higher levels of other proteins, such as other adhesins equipped for attachment to various surfaces; be it different host cell types, other yeast, or indwelling medical devices. Furthermore, the dynamic phenotypic changes identified, due to the fact that high- or low-expressing *Epa1* cells revert to mixed populations within a few generations with mothers producing buds of different expression phenotypes, are predicted to be increasingly favoured as the frequency at which an organism's environment changes increases (Acar et al., 2008).

An appealing hypothesis proposes that Epa proteins, which are known to vary in their ligand-binding specificities (Zupancic et al., 2008), are differentially regulated to facilitate adherence to different host surfaces during the course of infection. Such regulation may be driven by the various potential environmental cues encountered (De Las Penas et al., 2003, Castano et al., 2005, de Groot et al., 2008, Zupancic et al., 2008). Certainly, environmental conditions such as NA limitation and exposure to weak acids commonly found in antifungals have been shown to affect expression of *EPA* genes such as *EPA6* (Domergue et al., 2005, Mundy and Cormack, 2009). The impact of silencing on heterogeneity here results in a tendency towards increased numbers of cells expressing low rather than high-*EPA1*. Strains demonstrating high levels of Epa1 heterogeneity could be ones in which the dominant adhesin differs most between different cells. For instance, as alluded to above, cells demonstrating low levels of Epa1 may produce high levels of an alternative adhesin in place of Epa1 at the cell surface, so adding another layer of diversity. This may allow the population as a whole to be pre-equipped for adhesion to more diverse surface types. Furthermore, such switching of the dominant Epa between subpopulations could aid in immune system evasion akin to the systems utilised by a number of parasites (Verstrepen and Fink, 2009). Indeed the ability to switch Epa1 expression state was demonstrated here. Transcriptional analysis performed during this study, however, suggests that alternative Epa proteins may not be expressed in place of Epa1, at least in the case of Epa6 and Epa7 where low levels of *EPA1* mRNA appeared to correlate with low transcript levels for these other two adhesins. Nevertheless the BG2 and ATCC2001 strains encode 17 and 23 *EPA* genes respectively (Kaur et al., 2005, de Groot et al., 2008), in addition to over 60 other adhesin-like GPI-proteins identified in *C. glabrata* (de Groot et al., 2008). Any one of these may have the potential to mediate adherence and thus replace Epa1 at the cell surface. Such non-Epa adhesins may include Pwp7p and Ade1p both of which have roles in adherence to endothelial cells and form members of a recently identified and characterized family of *C. glabrata* GPI-anchored CWPs, absent in *S. cerevisiae* and *C. albicans* (Desai et al., 2011). It is also plausible that low expressing cells exhibit relatively low levels of a high number of adhesins in order to broaden "specificity" rather than high expression of one or two dominant adhesins. Alternately such cells may contain increased levels of non-adhesin cell wall proteins.

Interestingly, following exposure to weak acids that are used as preservatives in antifungal treatments (sorbic acid and paraben), *EPA6* expression increases (Mundy and Cormack, 2009). This increase, however, occurs only in a subset of cells, similar to the phenomenon observed for *FLO11* of *S. cerevisiae* under conditions of N-limitation (Halme et al., 2004). This establishes the possibility of heterogeneity existing in expression of Epa's other than Epa1. Furthermore the influence of the weak acid preservative treatments on expression differed between *EPA6*, *EPA7*, and *EPA1* (Mundy and Cormack, 2009) thus providing an example of differential regulation not only of *EPA6* but also between different *EPA* genes. *EPA6* is also known to be induced during stationary phase, apparently due to the hypoxic environment (Mundy and Cormack, 2009). This environment is consistent with that found within biofilms and both *EPA6* and *EPA7* are expressed under biofilm conditions (Iraqi et al., 2005). In contrast, Epa1 expression is maximal during exponential growth, the protein being cleaved from the cell wall as cultures enter stationary phase (Kaur et al., 2007), an observation confirmed in this study. Given the similar ligand-binding specificities of Epa1 and Epa7 (Zupancic et al., 2008), differential regulation may ensure persistence of the adhesion properties of high-Epa1 cells upon the switch to stationary phase, such as during biofilm formation on host mucosa or on indwelling medical devices, a stage which often precedes candidiasis. It has been suggested that within the human host, adherent *C. glabrata* cells exist in a semi-stationary phase throughout most of their lifetime (de Groot et al., 2008). Results collected during this project indicate that a strain exhibiting high-Epa1 heterogeneity can extend such heterogeneous expression into stationary phase, irrespective of the accompanying decrease in mean expression. Thus Epa1 heterogeneity could influence virulence even in stationary conditions.

An important future challenge will include investigation in to how such heterogeneity in adhesin gene expression may impact survival within the host and ultimately virulence. Such studies may require the use of infection models, initially utilising both high-and low-Epa1 heterogeneity strains to identify possible differences in dissemination and the ability to colonise host sites following initial infection. Identification of a possible virulence advantage in highly heterogeneous strains would subsequently need to be linked specifically to Epa1 heterogeneity. This would likely require specific manipulation of Epa1 expression heterogeneity. *SIR3* deletion would be a non-specific approach as inhibition of transcriptional

silencing would have pleiotropic effects. Alternatively Epa1 heterogeneity could be manipulatable by introducing alternative promoters, as has been done with other genes (Blake et al., 2006, Smith et al., 2007). In addition, although both high- and low-Epa1 heterogeneity strains evidently occur in patients, analysis of larger numbers of such clinical isolates may provide some statistical data indicating whether one phenotype is dominant over the other within the host environment. A large analysis of this type could also provide more robust information on the relationship between source site and Epa1 heterogeneity. In addition, the hypothesis that individual cells express different dominant adhesins, enabling attachment to different surfaces could be tested through adhesion assays using sorted Epa1 subpopulations and various host cell types as well as synthetic surfaces. Ultimately, several key questions concerning Epa1 heterogeneity in this pathogenic yeast still need to be answered, in particular, further characterisation of the mechanisms underlying such variation and the advantages that they may confer upon a population.

References

- ACAR, M., METTETAL, J. T. & VAN OUDENAARDEN, A. 2008. Stochastic switching as a survival strategy in fluctuating environments. *Nat Genet*, 40, 471-5.
- AI, W., BERTRAM, P. G., TSANG, C. K., CHAN, T. F. & ZHENG, X. F. 2002. Regulation of subtelomeric silencing during stress response. *Mol Cell*, 10, 1295-305.
- ALBRECHT, A., FELK, A., PICOVA, I., NAGLIK, J. R., SCHALLER, M., DE GROOT, P., MACCALLUM, D., ODDS, F. C., SCHAFER, W., KLIS, F., MONOD, M. & HUBE, B. 2006. Glycosylphosphatidylinositol-anchored proteases of *Candida albicans* target proteins necessary for both cellular processes and host-pathogen interactions. *J Biol Chem*, 281, 688-94.
- ALSFORD, S., HORN, D. & GLOVER, L. 2009. DNA breaks as triggers for antigenic variation in African trypanosomes. *Genome Biol*, 10, 223.
- ANDERSEN, P. L., XU, F. & XIAO, W. 2008. Eukaryotic DNA damage tolerance and translesion synthesis through covalent modifications of PCNA. *Cell Res*, 18, 162-73.
- AVERY, S. V. 2006. Microbial cell individuality and the underlying sources of heterogeneity. *Nat Rev Microbiol*, 4, 577-87.
- AVERY, S. V., MALKAPURAM, S., MATEUS, C. & BABB, K. S. 2000. Copper/zinc-Superoxide dismutase is required for oxytetracycline resistance of *Saccharomyces cerevisiae*. *J Bacteriol*, 182, 76-80.
- BANNISTER, A. J., ZEGERMAN, P., PARTRIDGE, J. F., MISKA, E. A., THOMAS, J. O., ALLSHIRE, R. C. & KOUZARIDES, T. 2001. Selective recognition of methylated lysine 9 on histone H3 by the HP1 chromo domain. *Nature*, 410, 120-4.
- BARRETT, M. P., BURCHMORE, R. J., STICH, A., LAZZARI, J. O., FRASCH, A. C., CAZZULO, J. J. & KRISHNA, S. 2003. The trypanosomiasis. *Lancet*, 362, 1469-80.
- BAYLISS, C. D. 2009. Determinants of phase variation rate and the fitness implications of differing rates for bacterial pathogens and commensals. *FEMS Microbiol Rev*, 33, 504-20.
- BEH, C. T. & RINE, J. 2004. A role for yeast oxysterol-binding protein homologs in endocytosis and in the maintenance of intracellular sterol-lipid distribution. *J Cell Sci*, 117, 2983-96.
- BERTANI, G. 1951. Studies on lysogenesis. I. The mode of phage liberation by lysogenic *Escherichia coli*. *J Bacteriol*, 62, 293-300.
- BI, X., YU, Q., SANDMEIER, J. J. & ELIZONDO, S. 2004. Regulation of transcriptional silencing in yeast by growth temperature. *J Mol Biol*, 344, 893-905.
- BIONDO, C., MESSINA, L., BOMBACI, M., MANCUSO, G., MIDIRI, A., BENINATI, C., CUSUMANO, V., GERACE, E., PAPASERGI, S. & TETI, G. 2005. Characterization of two novel cryptococcal mannoproteins recognized by immune sera. *Infect Immun*, 73, 7348-55.
- BISHOP, A. L., RAB, F. A., SUMNER, E. R. & AVERY, S. V. 2007. Phenotypic heterogeneity can enhance rare-cell survival in 'stress-sensitive' yeast populations. *Mol Microbiol*, 63, 507-20.
- BLAKE, W. J., BALAZSI, G., KOHANSKI, M. A., ISAACS, F. J., MURPHY, K. F., KUANG, Y., CANTOR, C. R., WALT, D. R. & COLLINS, J. J. 2006. Phenotypic consequences of promoter-mediated transcriptional noise. *Mol Cell*, 24, 853-65.
- BLASCO, M. A. 2007. The epigenetic regulation of mammalian telomeres. *Nat Rev Genet*, 8, 299-309.

- BOOTHROYD, C. E., DREESEN, O., LEONOVA, T., LY, K. I., FIGUEIREDO, L. M., CROSS, G. A. & PAPAVALIIOU, F. N. 2009. A yeast-endonuclease-generated DNA break induces antigenic switching in *Trypanosoma brucei*. *Nature*, 459, 278-81.
- BOULTON, S. J. & JACKSON, S. P. 1996. Identification of a *Saccharomyces cerevisiae* Ku80 homologue: roles in DNA double strand break rejoining and in telomeric maintenance. *Nucleic Acids Res*, 24, 4639-48.
- BRANZEI, D. & FOIANI, M. 2007. Interplay of replication checkpoints and repair proteins at stalled replication forks. *DNA Repair (Amst)*, 6, 994-1003.
- BRANZEI, D., VANOLI, F. & FOIANI, M. 2008. SUMOylation regulates Rad18-mediated template switch. *Nature*, 456, 915-20.
- BREEDEN, L. L. 2003. Periodic transcription: a cycle within a cycle. *Curr Biol*, 13, R31-8.
- BROWN, D. A. & ROSE, J. K. 1992. Sorting of GPI-anchored proteins to glycolipid-enriched membrane subdomains during transport to the apical cell surface. *Cell*, 68, 533-44.
- BRUL, S., KING, A., VAN DER VAART, J. M., CHAPMAN, J., KLIS, F. & VERRIPS, C. T. 1997. The incorporation of mannoproteins in the cell wall of *S. cerevisiae* and filamentous Ascomycetes. *Antonie Van Leeuwenhoek*, 72, 229-37.
- BRUN, J., CHIU, R., LOCKHART, K., XIAO, W., WOUTERS, B. G. & GRAY, D. A. 2008. *hMMS2* serves a redundant role in human PCNA polyubiquitination. *BMC Mol Biol*, 9, 24.
- BUHLER, M. & GASSER, S. M. 2009. Silent chromatin at the middle and ends: lessons from yeasts. *EMBO J*, 28, 2149-61.
- BUSCAGLIA, C. A., CAMPO, V. A., DI NOIA, J. M., TORRECILHAS, A. C., DE MARCHI, C. R., FERGUSON, M. A., FRASCH, A. C. & ALMEIDA, I. C. 2004. The surface coat of the mammal-dwelling infective trypomastigote stage of *Trypanosoma cruzi* is formed by highly diverse immunogenic mucins. *J Biol Chem*, 279, 15860-9.
- BUSCAGLIA, C. A., CAMPO, V. A., FRASCH, A. C. & DI NOIA, J. M. 2006. *Trypanosoma cruzi* surface mucins: host-dependent coat diversity. *Nat Rev Microbiol*, 4, 229-36.
- CALCAGNO, A. M., BIGNELL, E., WARN, P., JONES, M. D., DENNING, D. W., MUHLSCHLEGEL, F. A., ROGERS, T. R. & HAYNES, K. 2003. *Candida glabrata* *STE12* is required for wild-type levels of virulence and nitrogen starvation induced filamentation. *Mol Microbiol*, 50, 1309-18.
- CALDERWOOD, M. S., GANNOUN-ZAKI, L., WELLEMS, T. E. & DEITSCH, K. W. 2003. *Plasmodium falciparum* var genes are regulated by two regions with separate promoters, one upstream of the coding region and a second within the intron. *J Biol Chem*, 278, 34125-32.
- CASTANO, I., KAUR, R., PAN, S., CREGG, R., PENAS ADE, L., GUO, N., BIERY, M. C., CRAIG, N. L. & CORMACK, B. P. 2003. Tn7-based genome-wide random insertional mutagenesis of *Candida glabrata*. *Genome Res*, 13, 905-15.
- CASTANO, I., PAN, S. J., ZUPANCIC, M., HENNEQUIN, C., DUJON, B. & CORMACK, B. P. 2005. Telomere length control and transcriptional regulation of subtelomeric adhesins in *Candida glabrata*. *Mol Microbiol*, 55, 1246-58.
- CASTILLON, G. A., WATANABE, R., TAYLOR, M., SCHWABE, T. M. & RIEZMAN, H. 2009. Concentration of GPI-anchored proteins upon ER exit in yeast. *Traffic*, 10, 186-200.

- CHEN, S. C., SLAVIN, M. A. & SORRELL, T. C. 2011. Echinocandin antifungal drugs in fungal infections: a comparison. *Drugs*, 71, 11-41.
- CHIU, R. K., BRUN, J., RAMAEKERS, C., THEYS, J., WENG, L., LAMBIN, P., GRAY, D. A. & WOUTERS, B. G. 2006. Lysine 63-polyubiquitination guards against translesion synthesis-induced mutations. *PLoS Genet*, 2, e116.
- CHOI, H. K., JEONG, S. J., LEE, H. S., CHIN, B. S., CHOI, S. H., HAN, S. H., KIM, M. S., KIM, C. O., CHOI, J. Y., SONG, Y. G. & KIM, J. M. 2009. Blood stream infections by *Candida glabrata* and *Candida krusei*: a single-center experience. *Korean J Intern Med*, 24, 263-9.
- CONLAN, R. S. & TZAMARIAS, D. 2001. Sfl1 functions via the co-repressor Ssn6-Tup1 and the cAMP-dependent protein kinase Tpk2. *J Mol Biol*, 309, 1007-15.
- CONRAD, M. N., WRIGHT, J. H., WOLF, A. J. & ZAKIAN, V. A. 1990. RAP1 protein interacts with yeast telomeres in vivo: overproduction alters telomere structure and decreases chromosome stability. *Cell*, 63, 739-50.
- CORMACK, B. P., GHORI, N. & FALKOW, S. 1999. An adhesin of the yeast pathogen *Candida glabrata* mediating adherence to human epithelial cells. *Science*, 285, 578-82.
- CSANK, C. & HAYNES, K. 2000. *Candida glabrata* displays pseudohyphal growth. *FEMS Microbiol Lett*, 189, 115-20.
- CSANK, C., SCHROPPEL, K., LEBERER, E., HARCUS, D., MOHAMED, O., MELOCHE, S., THOMAS, D. Y. & WHITEWAY, M. 1998. Roles of the *Candida albicans* mitogen-activated protein kinase homolog, Cek1p, in hyphal development and systemic candidiasis. *Infect Immun*, 66, 2713-21.
- DAVIS, D. 2003. Adaptation to environmental pH in *Candida albicans* and its relation to pathogenesis. *Curr Genet*, 44, 1-7.
- DAVIS, D. A. 2009. How human pathogenic fungi sense and adapt to pH: the link to virulence. *Curr Opin Microbiol*, 12, 365-70.
- DE GROOT, P. W., DE BOER, A. D., CUNNINGHAM, J., DEKKER, H. L., DE JONG, L., HELLINGWERF, K. J., DE KOSTER, C. & KLIS, F. M. 2004. Proteomic analysis of *Candida albicans* cell walls reveals covalently bound carbohydrate-active enzymes and adhesins. *Eukaryot Cell*, 3, 955-65.
- DE GROOT, P. W., HELLINGWERF, K. J. & KLIS, F. M. 2003. Genome-wide identification of fungal GPI proteins. *Yeast*, 20, 781-96.
- DE GROOT, P. W. & KLIS, F. M. 2008. The conserved PA14 domain of cell wall-associated fungal adhesins governs their glycan-binding specificity. *Mol Microbiol*, 68, 535-7.
- DE GROOT, P. W., KRANEVELD, E. A., YIN, Q. Y., DEKKER, H. L., GROSS, U., CRIELAARD, W., DE KOSTER, C. G., BADER, O., KLIS, F. M. & WEIG, M. 2008. The cell wall of the human pathogen *Candida glabrata*: differential incorporation of novel adhesin-like wall proteins. *Eukaryot Cell*, 7, 1951-64.
- DE GROOT, P. W., RAM, A. F. & KLIS, F. M. 2005. Features and functions of covalently linked proteins in fungal cell walls. *Fungal Genet Biol*, 42, 657-75.
- DE GROOTE, F. H., JANSEN, J. G., MASUDA, Y., SHAH, D. M., KAMIYA, K., DE WIND, N. & SIEGAL, G. 2011. The Rev1 translesion synthesis polymerase has multiple distinct DNA binding modes. *DNA Repair (Amst)*, 10, 915-25.
- DE JONG, I. G., HACCOU, P. & KUIPERS, O. P. 2011. Bet hedging or not? A guide to proper classification of microbial survival strategies. *Bioessays*, 33, 215-23.

- DE LAS PENAS, A., PAN, S. J., CASTANO, I., ALDER, J., CREGG, R. & CORMACK, B. P. 2003. Virulence-related surface glycoproteins in the yeast pathogen *Candida glabrata* are encoded in subtelomeric clusters and subject to *RAP1*- and *SIR*-dependent transcriptional silencing. *Genes Dev*, 17, 2245-58.
- DE NOBEL, J. G., KLIS, F. M., PRIEM, J., MUNNIK, T. & VAN DEN ENDE, H. 1990. The glucanase-soluble mannoproteins limit cell wall porosity in *Saccharomyces cerevisiae*. *Yeast*, 6, 491-9.
- DE RUIJTER, A. J., VAN GENNIP, A. H., CARON, H. N., KEMP, S. & VAN KUILENBURG, A. B. 2003. Histone deacetylases (HDACs): characterization of the classical HDAC family. *Biochem J*, 370, 737-49.
- DEITSCH, K. W., DEL PINAL, A. & WELLEMS, T. E. 1999. Intra-cluster recombination and var transcription switches in the antigenic variation of *Plasmodium falciparum*. *Mol Biochem Parasitol*, 101, 107-16.
- DELNERI, D., COLSON, I., GRAMMENOUDI, S., ROBERTS, I. N., LOUIS, E. J. & OLIVER, S. G. 2003. Engineering evolution to study speciation in yeasts. *Nature*, 422, 68-72.
- DESAI, C., MAVRIANOS, J. & CHAUHAN, N. 2011. *Candida glabrata* Pwp7p and Aed1p are required for adherence to human endothelial cells. *FEMS Yeast Res*, 11, 595-601.
- DIAS, J. C. 2009. Elimination of Chagas disease transmission: perspectives. *Mem Inst Oswaldo Cruz*, 104 Suppl 1, 41-5.
- DOERING, T. L. & SCHEKMAN, R. 1996. GPI anchor attachment is required for Gas1p transport from the endoplasmic reticulum in COP II vesicles. *EMBO J*, 15, 182-91.
- DOETSCH, P. W., MOREY, N. J., SWANSON, R. L. & JINKS-ROBERTSON, S. 2001. Yeast base excision repair: interconnections and networks. *Prog Nucleic Acid Res Mol Biol*, 68, 29-39.
- DOMERGUE, R., CASTANO, I., DE LAS PENAS, A., ZUPANCIC, M., LOCKATELL, V., HEBEL, J. R., JOHNSON, D. & CORMACK, B. P. 2005. Nicotinic acid limitation regulates silencing of *Candida* adhesins during UTI. *Science*, 308, 866-70.
- DOUGLAS, L. J. 2003. *Candida* biofilms and their role in infection. *Trends Microbiol*, 11, 30-6.
- DRANGINIS, A. M., RAUCEO, J. M., CORONADO, J. E. & LIPKE, P. N. 2007. A biochemical guide to yeast adhesins: glycoproteins for social and antisocial occasions. *Microbiol Mol Biol Rev*, 71, 282-94.
- DUJON, B., SHERMAN, D., FISCHER, G., DURRENS, P., CASAREGOLA, S., LAFONTAINE, I., DE MONTIGNY, J., MARCK, C., NEUVEGLISE, C., TALLA, E., GOFFARD, N., FRANGEUL, L., AIGLE, M., ANTHOUARD, V., BABOUR, A., BARBE, V., BARNAY, S., BLANCHIN, S., BECKERICH, J. M., BEYNE, E., BLEYKASTEN, C., BOISRAMÉ, A., BOYER, J., CATTOLICO, L., CONFANIOLERI, F., DE DARUVAR, A., DESPONS, L., FABRE, E., FAIRHEAD, C., FERRY-DUMAZET, H., GROUPI, A., HANTRAYE, F., HENNEQUIN, C., JAUNIAUX, N., JOYET, P., KACHOURI, R., KERREST, A., KOSZUL, R., LEMAIRE, M., LESUR, I., MA, L., MULLER, H., NICAUD, J. M., NIKOLSKI, M., OZTAS, S., OZIER-KALOGEROPOULOS, O., PELLEZ, S., POTIER, S., RICHARD, G. F., STRAUB, M. L., SULEAU, A., SWENNEN, D., TEKAIA, F., WESOLOWSKI-LOUVEL, M., WESTHOF, E., WIRTH, B., ZENIOMEYER, M., ZIVANOVIC, I., BOLOTIN-FUKUHARA, M., THIERRY, A., BOUCHIER, C., CAUDRON, B., SCARPELLI, C., GAILLARDIN, C., WEISSENBACH, J., WINCKER, P. & SOUCIET, J. L. 2004. Genome evolution in yeasts. *Nature*, 430, 35-44.

- DURASINGH, M. T., VOSS, T. S., MARTY, A. J., DUFFY, M. F., GOOD, R. T., THOMPSON, J. K., FREITAS-JUNIOR, L. H., SCHERF, A., CRABB, B. S. & COWMAN, A. F. 2005. Heterochromatin silencing and locus repositioning linked to regulation of virulence genes in *Plasmodium falciparum*. *Cell*, 121, 13-24.
- DZIKOWSKI, R. & DEITSCH, K. W. 2009. Genetics of antigenic variation in *Plasmodium falciparum*. *Curr Genet*, 55, 103-10.
- EISENHABER, B., BORK, P. & EISENHABER, F. 2001. Post-translational GPI lipid anchor modification of proteins in kingdoms of life: analysis of protein sequence data from complete genomes. *Protein Eng*, 14, 17-25.
- EL-SAYED, N. M., MYLER, P. J., BARTHOLOMEU, D. C., NILSSON, D., AGGARWAL, G., TRAN, A. N., GHEDIN, E., WORTHEY, E. A., DELCHER, A. L., BLANDIN, G., WESTENBERGER, S. J., CALER, E., CERQUEIRA, G. C., BRANCHE, C., HAAS, B., ANUPAMA, A., ARNER, E., ASLUND, L., ATTIPOE, P., BONTEMPI, E., BRINGAUD, F., BURTON, P., CADAG, E., CAMPBELL, D. A., CARRINGTON, M., CRABTREE, J., DARBAN, H., DA SILVEIRA, J. F., DE JONG, P., EDWARDS, K., ENGLUND, P. T., FAZELINA, G., FELDBLYUM, T., FERELLA, M., FRASCH, A. C., GULL, K., HORN, D., HOU, L., HUANG, Y., KINDLUND, E., KLINGBEIL, M., KLUGE, S., KOO, H., LACERDA, D., LEVIN, M. J., LORENZI, H., LOUIE, T., MACHADO, C. R., MCCULLOCH, R., MCKENNA, A., MIZUNO, Y., MOTTRAM, J. C., NELSON, S., OCHAYA, S., OSOEGAWA, K., PAI, G., PARSONS, M., PENTONY, M., PETTERSSON, U., POP, M., RAMIREZ, J. L., RINTA, J., ROBERTSON, L., SALZBERG, S. L., SANCHEZ, D. O., SEYLER, A., SHARMA, R., SHETTY, J., SIMPSON, A. J., SISK, E., TAMMI, M. T., TARLETON, R., TEIXEIRA, S., VAN AKEN, S., VOGT, C., WARD, P. N., WICKSTEAD, B., WORTMAN, J., WHITE, O., FRASER, C. M., STUART, K. D. & ANDERSSON, B. 2005. The genome sequence of *Trypanosoma cruzi*, etiologic agent of Chagas disease. *Science*, 309, 409-15.
- FERRARI, S., ISCHER, F., CALABRESE, D., POSTERARO, B., SANGUINETTI, M., FADDA, G., ROHDE, B., BAUSER, C., BADER, O. & SANGLARD, D. 2009. Gain of function mutations in *CgPDR1* of *Candida glabrata* not only mediate antifungal resistance but also enhance virulence. *PLoS Pathog*, 5, e1000268.
- FIDEL, P. L., JR., VAZQUEZ, J. A. & SOBEL, J. D. 1999. *Candida glabrata*: review of epidemiology, pathogenesis, and clinical disease with comparison to *C. albicans*. *Clin Microbiol Rev*, 12, 80-96.
- FITZPATRICK, D. A., LOGUE, M. E., STAJICH, J. E. & BUTLER, G. 2006. A fungal phylogeny based on 42 complete genomes derived from supertree and combined gene analysis. *BMC Evol Biol*, 6, 99.
- FOUREL, G., REVARDEL, E., KOERING, C. E. & GILSON, E. 1999. Cohabitation of insulators and silencing elements in yeast subtelomeric regions. *EMBO J*, 18, 2522-37.
- FRANK, M., DZIKOWSKI, R., AMULIC, B. & DEITSCH, K. 2007. Variable switching rates of malaria virulence genes are associated with chromosomal position. *Mol Microbiol*, 64, 1486-98.
- FREITAS-JUNIOR, L. H., HERNANDEZ-RIVAS, R., RALPH, S. A., MONTIEL-CONDADO, D., RUVALCABA-SALAZAR, O. K., ROJAS-MEZA, A. P., MANCIO-SILVA, L., LEAL-SILVESTRE, R. J., GONTIJO, A. M., SHORTE, S. & SCHERF, A. 2005. Telomeric heterochromatin propagation and histone acetylation control mutually exclusive expression of antigenic variation genes in malaria parasites. *Cell*, 121, 25-36.

- FRIEMAN, M. B. & CORMACK, B. P. 2004. Multiple sequence signals determine the distribution of glycosylphosphatidylinositol proteins between the plasma membrane and cell wall in *Saccharomyces cerevisiae*. *Microbiology*, 150, 3105-14.
- FRIEMAN, M. B., MCCAFFERY, J. M. & CORMACK, B. P. 2002. Modular domain structure in the *Candida glabrata* adhesin Epa1p, a beta1,6 glucan-cross-linked cell wall protein. *Mol Microbiol*, 46, 479-92.
- FUJITA, M. & KINOSHITA, T. 2010. Structural remodeling of GPI anchors during biosynthesis and after attachment to proteins. *FEBS Lett*, 584, 1670-7.
- GAME, J. C. & CHERNIKOVA, S. B. 2009. The role of *RAD6* in recombinational repair, checkpoints and meiosis via histone modification. *DNA Repair (Amst)*, 8, 470-82.
- GANNOUN-ZAKI, L., JOST, A., MU, J., DEITSCH, K. W. & WELLEMS, T. E. 2005. A silenced *Plasmodium falciparum* var promoter can be activated in vivo through spontaneous deletion of a silencing element in the intron. *Eukaryot Cell*, 4, 490-2.
- GHANNOUM, M. A. & RICE, L. B. 1999. Antifungal agents: mode of action, mechanisms of resistance, and correlation of these mechanisms with bacterial resistance. *Clin Microbiol Rev*, 12, 501-17.
- GIMENO, C. J., LJUNGDAHL, P. O., STYLES, C. A. & FINK, G. R. 1992. Unipolar cell divisions in the yeast *S. cerevisiae* lead to filamentous growth: regulation by starvation and RAS. *Cell*, 68, 1077-90.
- GRANT, S. M. & CLISSOLD, S. P. 1990. Fluconazole. A review of its pharmacodynamic and pharmacokinetic properties, and therapeutic potential in superficial and systemic mycoses. *Drugs*, 39, 877-916.
- GUARRO, J., GENEJ & STCHIGEL, A. M. 1999. Developments in fungal taxonomy. *Clin Microbiol Rev*, 12, 454-500.
- GUO, B., STYLES, C. A., FENG, Q. & FINK, G. R. 2000. A *Saccharomyces* gene family involved in invasive growth, cell-cell adhesion, and mating. *Proc Natl Acad Sci U S A*, 97, 12158-63.
- HALME, A., BUMGARNER, S., STYLES, C. & FINK, G. R. 2004. Genetic and epigenetic regulation of the *FLO* gene family generates cell-surface variation in yeast. *Cell*, 116, 405-15.
- HAYNES, K. 2001. Virulence in *Candida* species. *Trends Microbiol*, 9, 591-6.
- HAZEN, K. C., PLOTKIN, B. J. & KLIMAS, D. M. 1986. Influence of growth conditions on cell surface hydrophobicity of *Candida albicans* and *Candida glabrata*. *Infect Immun*, 54, 269-71.
- HECHT, A., STRAHL-BOLSINGER, S. & GRUNSTEIN, M. 1996. Spreading of transcriptional repressor *SIR3* from telomeric heterochromatin. *Nature*, 383, 92-6.
- HEDGES, S. B. 2002. The origin and evolution of model organisms. *Nat Rev Genet*, 3, 838-49.
- HEDGES, S. B., BLAIR, J. E., VENTURI, M. L. & SHOE, J. L. 2004. A molecular timescale of eukaryote evolution and the rise of complex multicellular life. *BMC Evol Biol*, 4, 2.
- HENRY, K. W., NICKELS, J. T. & EDLIND, T. D. 2000. Upregulation of *ERG* genes in *Candida* species by azoles and other sterol biosynthesis inhibitors. *Antimicrob Agents Chemother*, 44, 2693-700.
- HERSKOWITZ, I. 1989. A regulatory hierarchy for cell specialization in yeast. *Nature*, 342, 749-57.
- HIBBETT, D. S., BINDER, M., BISCHOFF, J. F., BLACKWELL, M., CANNON, P. F., ERIKSSON, O. E., HUHNENDORF, S., JAMES, T., KIRK, P. M., LUCKING, R., THORSTEN LUMBSCH, H., LUTZONI, F., MATHENY, P. B., MCLAUGHLIN, D. J., POWELL, M. J., REDHEAD, S., SCHOCH, C. L., SPATAFORA, J. W., STALPERS, J. A., VILGALYS, R., AIME, M. C., APTROOT, A., BAUER, R., BEGEROW, D., BENNY, G. L.,

- CASTLEBURY, L. A., CROUS, P. W., DAI, Y. C., GAMS, W., GEISER, D. M., GRIFFITH, G. W., GUEIDAN, C., HAWKSWORTH, D. L., HESTMARK, G., HOSAKA, K., HUMBER, R. A., HYDE, K. D., IRONSIDE, J. E., KOLJALG, U., KURTZMAN, C. P., LARSSON, K. H., LICHTWARDT, R., LONGCORE, J., MIADLIKOWSKA, J., MILLER, A., MONCALVO, J. M., MOZLEY-STANDRIDGE, S., OBERWINKLER, F., PARMASIO, E., REEB, V., ROGERS, J. D., ROUX, C., RYVARDEN, L., SAMPAIO, J. P., SCHUSSLER, A., SUGIYAMA, J., THORN, R. G., TIBELL, L., UNTEREINER, W. A., WALKER, C., WANG, Z., WEIR, A., WEISS, M., WHITE, M. M., WINKA, K., YAO, Y. J. & ZHANG, N. 2007. A higher-level phylogenetic classification of the Fungi. *Mycol Res*, 111, 509-47.
- HINNEBUSCH, A. G. & NATARAJAN, K. 2002. Gcn4p, a master regulator of gene expression, is controlled at multiple levels by diverse signals of starvation and stress. *Eukaryot Cell*, 1, 22-32.
- HOEGE, C., PFANDER, B., MOLDOVAN, G. L., PYROWOLAKIS, G. & JENTSCH, S. 2002. RAD6-dependent DNA repair is linked to modification of PCNA by ubiquitin and SUMO. *Nature*, 419, 135-41.
- HOEIJMAKERS, J. H. 2001. Genome maintenance mechanisms for preventing cancer. *Nature*, 411, 366-74.
- HOLLAND, S. L. & AVERY, S. V. 2009. Actin-mediated endocytosis limits intracellular Cr accumulation and Cr toxicity during chromate stress. *Toxicol Sci*, 111, 437-46.
- HORN, D. & BARRY, J. D. 2005. The central roles of telomeres and subtelomeres in antigenic variation in African trypanosomes. *Chromosome Res*, 13, 525-33.
- HORN, D. & MCCULLOCH, R. 2010. Molecular mechanisms underlying the control of antigenic variation in African trypanosomes. *Curr Opin Microbiol*, 13, 700-5.
- HORN, D. L., NEOFYTOS, D., ANAISSIE, E. J., FISHMAN, J. A., STEINBACH, W. J., OLYAEI, A. J., MARR, K. A., PFALLER, M. A., CHANG, C. H. & WEBSTER, K. M. 2009. Epidemiology and outcomes of candidemia in 2019 patients: data from the prospective antifungal therapy alliance registry. *Clin Infect Dis*, 48, 1695-703.
- HOYER, L. L., GREEN, C. B., OH, S. H. & ZHAO, X. 2008. Discovering the secrets of the *Candida albicans* agglutinin-like sequence (ALS) gene family--a sticky pursuit. *Med Mycol*, 46, 1-15.
- HOYER, L. L. & HECHT, J. E. 2001. The ALS5 gene of *Candida albicans* and analysis of the Als5p N-terminal domain. *Yeast*, 18, 49-60.
- HOYER, L. L., PAYNE, T. L., BELL, M., MYERS, A. M. & SCHERER, S. 1998. *Candida albicans* ALS3 and insights into the nature of the ALS gene family. *Curr Genet*, 33, 451-9.
- HUANG, H., KAHANA, A., GOTTSCHLING, D. E., PRAKASH, L. & LIEBMAN, S. W. 1997. The ubiquitin-conjugating enzyme Rad6 (Ubc2) is required for silencing in *Saccharomyces cerevisiae*. *Mol Cell Biol*, 17, 6693-9.
- HUANG, Y. 2002. Transcriptional silencing in *Saccharomyces cerevisiae* and *Schizosaccharomyces pombe*. *Nucleic Acids Res*, 30, 1465-82.
- HUBSCHER, U., MAGA, G. & SPADARI, S. 2002. Eukaryotic DNA polymerases. *Annu Rev Biochem*, 71, 133-63.
- HUH, D. & PAULSSON, J. 2011. Non-genetic heterogeneity from stochastic partitioning at cell division. *Nat Genet*, 43, 95-100.
- IKEZAWA, H. 2002. Glycosylphosphatidylinositol (GPI)-anchored proteins. *Biol Pharm Bull*, 25, 409-17.
- IRAQUI, I., GARCIA-SANCHEZ, S., AUBERT, S., DROMER, F., GHIGO, J. M., D'ENFERT, C. & JANBON, G. 2005. The Yak1p kinase controls

- expression of adhesins and biofilm formation in *Candida glabrata* in a Sir4p-dependent pathway. *Mol Microbiol*, 55, 1259-71.
- ISHIGAMI, M., NAKAGAWA, Y., HAYAKAWA, M. & IIMURA, Y. 2006. *FLO11* is the primary factor in flor formation caused by cell surface hydrophobicity in wild-type flor yeast. *Biosci Biotechnol Biochem*, 70, 660-6.
- JIN, H., MCCAFFERY, J. M. & GROTE, E. 2008. Ergosterol promotes pheromone signaling and plasma membrane fusion in mating yeast. *J Cell Biol*, 180, 813-26.
- KACHOURI-LAFOND, R., DUJON, B., GILSON, E., WESTHOF, E., FAIRHEAD, C. & TEIXEIRA, M. T. 2009. Large telomerase RNA, telomere length heterogeneity and escape from senescence in *Candida glabrata*. *FEBS Lett*, 583, 3605-10.
- KAERN, M., ELSTON, T. C., BLAKE, W. J. & COLLINS, J. J. 2005. Stochasticity in gene expression: from theories to phenotypes. *Nat Rev Genet*, 6, 451-64.
- KAPTEYN, J. C., HOYER, L. L., HECHT, J. E., MULLER, W. H., ANDEL, A., VERKLEIJ, A. J., MAKAROW, M., VAN DEN ENDE, H. & KLIS, F. M. 2000. The cell wall architecture of *Candida albicans* wild-type cells and cell wall-defective mutants. *Mol Microbiol*, 35, 601-11.
- KARRAS, G. I. & JENTSCH, S. 2010. The *RAD6* DNA damage tolerance pathway operates uncoupled from the replication fork and is functional beyond S phase. *Cell*, 141, 255-67.
- KAUFMANN, B. B. & VAN OUDENAARDEN, A. 2007. Stochastic gene expression: from single molecules to the proteome. *Curr Opin Genet Dev*, 17, 107-12.
- KAUR, R., CASTANO, I. & CORMACK, B. P. 2004. Functional genomic analysis of fluconazole susceptibility in the pathogenic yeast *Candida glabrata*: roles of calcium signaling and mitochondria. *Antimicrob Agents Chemother*, 48, 1600-13.
- KAUR, R., DOMERGUE, R., ZUPANCIC, M. L. & CORMACK, B. P. 2005. A yeast by any other name: *Candida glabrata* and its interaction with the host. *Curr Opin Microbiol*, 8, 378-84.
- KAUR, R., MA, B. & CORMACK, B. P. 2007. A family of glycosylphosphatidylinositol-linked aspartyl proteases is required for virulence of *Candida glabrata*. *Proc Natl Acad Sci U S A*, 104, 7628-33.
- KIM, K. Y., TRUMAN, A. W., CAESAR, S., SCHLENSTEDT, G. & LEVIN, D. E. 2010. Yeast Mpk1 cell wall integrity mitogen-activated protein kinase regulates nucleocytoplasmic shuttling of the Swi6 transcriptional regulator. *Mol Biol Cell*, 21, 1609-19.
- KITADA, K., YAMAGUCHI, E. & ARISAWA, M. 1995. Cloning of the *Candida glabrata* *TRP1* and *HIS3* genes, and construction of their disruptant strains by sequential integrative transformation. *Gene*, 165, 203-6.
- KITADA, K., YAMAGUCHI, E. & ARISAWA, M. 1996. Isolation of a *Candida glabrata* centromere and its use in construction of plasmid vectors. *Gene*, 175, 105-8.
- KLIS, F. M., BOORSMA, A. & DE GROOT, P. W. 2006. Cell wall construction in *Saccharomyces cerevisiae*. *Yeast*, 23, 185-202.
- KLIS, F. M., BRUL, S. & DE GROOT, P. W. 2010. Covalently linked wall proteins in ascomycetous fungi. *Yeast*, 27, 489-93.
- KLIS, F. M., SOSINSKA, G. J., DE GROOT, P. W. & BRUL, S. 2009. Covalently linked cell wall proteins of *Candida albicans* and their role in fitness and virulence. *FEMS Yeast Res*, 9, 1013-28.
- KROGH-MADSEN, M., ARENDRUP, M. C., HESLET, L. & KNUDSEN, J. D. 2006. Amphotericin B and caspofungin resistance in *Candida*

- glabrata* isolates recovered from a critically ill patient. *Clin Infect Dis*, 42, 938-44.
- KRYSAN, D. J., TING, E. L., ABEIJON, C., KROOS, L. & FULLER, R. S. 2005. Yapsins are a family of aspartyl proteases required for cell wall integrity in *Saccharomyces cerevisiae*. *Eukaryot Cell*, 4, 1364-74.
- LANGIE, S. A., KNAAPEN, A. M., RAMAEKERS, C. H., THEYS, J., BRUN, J., GODSCHALK, R. W., VAN SCHOOTEN, F. J., LAMBIN, P., GRAY, D. A., WOUTERS, B. G. & CHIU, R. K. 2007. Formation of lysine 63-linked poly-ubiquitin chains protects human lung cells against benzo[a]pyrene-diol-epoxide-induced mutagenicity. *DNA Repair (Amst)*, 6, 852-62.
- LAROCHE, T., MARTIN, S. G., GOTTA, M., GORHAM, H. C., PRYDE, F. E., LOUIS, E. J. & GASSER, S. M. 1998. Mutation of yeast *Ku* genes disrupts the subnuclear organization of telomeres. *Curr Biol*, 8, 653-6.
- LESAGE, G. & BUSSEY, H. 2006. Cell wall assembly in *Saccharomyces cerevisiae*. *Microbiol Mol Biol Rev*, 70, 317-43.
- LEVITZ, S. M. 2010. Innate recognition of fungal cell walls. *PLoS Pathog*, 6, e1000758.
- LEVITZ, S. M. & SPECHT, C. A. 2006. The molecular basis for the immunogenicity of *Cryptococcus neoformans* mannoproteins. *FEMS Yeast Res*, 6, 513-24.
- LEWIS, K. 2007. Persister cells, dormancy and infectious disease. *Nat Rev Microbiol*, 5, 48-56.
- LINGWOOD, D., KAISER, H. J., LEVENTAL, I. & SIMONS, K. 2009. Lipid rafts as functional heterogeneity in cell membranes. *Biochem Soc Trans*, 37, 955-60.
- LIU, G. G., TANNY, J. C., KRUGER, R. G., WALZ, T. & MOAZED, D. 2005. Assembly of the SIR complex and its regulation by O-acetyl-ADP-ribose, a product of NAD-dependent histone deacetylation. *Cell*, 121, 515-27.
- LO, H. J., KOHLER, J. R., DIDOMENICO, B., LOEBENBERG, D., CACCIAPUOTI, A. & FINK, G. R. 1997. Nonfilamentous *C. albicans* mutants are avirulent. *Cell*, 90, 939-49.
- LOMMELE, M. & STRAHL, S. 2009. Protein O-mannosylation: conserved from bacteria to humans. *Glycobiology*, 19, 816-28.
- LOPES, M., FOIANI, M. & SOGO, J. M. 2006. Multiple mechanisms control chromosome integrity after replication fork uncoupling and restart at irreparable UV lesions. *Mol Cell*, 21, 15-27.
- LOPEZ, C. R., RIBES-ZAMORA, A., INDIVIGLIO, S. M., WILLIAMS, C. L., HARICHARAN, S. & BERTUCH, A. A. 2011. Ku Must Load Directly onto the Chromosome End in Order to Mediate Its Telomeric Functions. *PLoS Genet*, 7, e1002233.
- LOUIS, E. J. & VERSHININ, A. V. 2005. Chromosome ends: different sequences may provide conserved functions. *Bioessays*, 27, 685-97.
- LOWNDES, N. F., JOHNSON, A. L., BREEDEN, L. & JOHNSTON, L. H. 1992. SWI6 protein is required for transcription of the periodically expressed DNA synthesis genes in budding yeast. *Nature*, 357, 505-8.
- LUO, G. & SAMARANAYAKE, L. P. 2002. *Candida glabrata*, an emerging fungal pathogen, exhibits superior relative cell surface hydrophobicity and adhesion to denture acrylic surfaces compared with *Candida albicans*. *APMIS*, 110, 601-10.
- LUO, K., VEGA-PALAS, M. A. & GRUNSTEIN, M. 2002. Rap1-Sir4 binding independent of other Sir, yKu, or histone interactions initiates the assembly of telomeric heterochromatin in yeast. *Genes Dev*, 16, 1528-39.

- MAO, Y., ZHANG, Z., GAST, C. & WONG, B. 2008. C-terminal signals regulate targeting of glycosylphosphatidylinositol-anchored proteins to the cell wall or plasma membrane in *Candida albicans*. *Eukaryot Cell*, 7, 1906-15.
- MARTIN, S. W. & KONOPKA, J. B. 2004. Lipid raft polarization contributes to hyphal growth in *Candida albicans*. *Eukaryot Cell*, 3, 675-84.
- MAYOR, S. & RIEZMAN, H. 2004. Sorting GPI-anchored proteins. *Nat Rev Mol Cell Biol*, 5, 110-20.
- MCBRYANT, S. J., KRAUSE, C., WOODCOCK, C. L. & HANSEN, J. C. 2008. The silent information regulator 3 protein, SIR3p, binds to chromatin fibers and assembles a hypercondensed chromatin architecture in the presence of salt. *Mol Cell Biol*, 28, 3563-72.
- MCGUINNESS, D., MCGUINNESS, D. H., MCCAUL, J. A. & SHIELS, P. G. 2011. Sirtuins, bioageing, and cancer. *J Aging Res*, 2011, 235754.
- MILLER, L. G., HAJJEH, R. A. & EDWARDS, J. E., JR. 2001. Estimating the cost of nosocomial candidemia in the united states. *Clin Infect Dis*, 32, 1110.
- MISHRA, K. & SHORE, D. 1999. Yeast Ku protein plays a direct role in telomeric silencing and counteracts inhibition by rif proteins. *Curr Biol*, 9, 1123-6.
- MISHRA, S. & JOSHI, P. G. 2007. Lipid raft heterogeneity: an enigma. *J Neurochem*, 103 Suppl 1, 135-42.
- MIYAKE, Y., KOZUTSUMI, Y., NAKAMURA, S., FUJITA, T. & KAWASAKI, T. 1995. Serine palmitoyltransferase is the primary target of a sphingosine-like immunosuppressant, ISP-1/myriocin. *Biochem Biophys Res Commun*, 211, 396-403.
- MORACE, G., BORGHI, E., IATTA, R. & MONTAGNA, M. T. 2009. Anidulafungin, a new echinocandin: in vitro activity. *Drugs*, 69 Suppl 1, 91-4.
- MULLER, H., HENNEQUIN, C., GALLAUD, J., DUJON, B. & FAIRHEAD, C. 2008. The asexual yeast *Candida glabrata* maintains distinct a and alpha haploid mating types. *Eukaryot Cell*, 7, 848-58.
- MULLER, H., THIERRY, A., COPPEE, J. Y., GOUYETTE, C., HENNEQUIN, C., SISMEIRO, O., TALLA, E., DUJON, B. & FAIRHEAD, C. 2009. Genomic polymorphism in the population of *Candida glabrata*: gene copy-number variation and chromosomal translocations. *Fungal Genet Biol*, 46, 264-76.
- MUNDY, R. D. & CORMACK, B. 2009. Expression of *Candida glabrata* adhesins after exposure to chemical preservatives. *J Infect Dis*, 199, 1891-8.
- MUNIZ, M., MORSOMME, P. & RIEZMAN, H. 2001. Protein sorting upon exit from the endoplasmic reticulum. *Cell*, 104, 313-20.
- NEWMAN, J. R., GHAEMMAGHAMI, S., IHMELS, J., BRESLOW, D. K., NOBLE, M., DERISI, J. L. & WEISSMAN, J. S. 2006. Single-cell proteomic analysis of *S. cerevisiae* reveals the architecture of biological noise. *Nature*, 441, 840-6.
- NOBEL, S. M., FRENCH, S., KOHN, L. A., CHEN, V. & JOHNSON, A. D. 2010. Systematic screens of a *Candida albicans* homozygous deletion library decouple morphogenetic switching and pathogenicity. *Nat Genet*, 42, 590-8.
- NORRIS, A. & BOEKE, J. D. 2010. Silent information regulator 3: the Goldilocks of the silencing complex. *Genes Dev*, 24, 115-22.
- NORTH, B. J. & VERDIN, E. 2004. Sirtuins: Sir2-related NAD-dependent protein deacetylases. *Genome Biol*, 5, 224.
- NYANGA, L. K., NOUT, M. J., GADAGA, T. H., THEELEN, B., BOEKHOUT, T. & ZWIETERING, M. H. 2007. Yeasts and lactic acid bacteria microbiota from masau (*Ziziphus mauritiana*) fruits and their

- fermented fruit pulp in Zimbabwe. *Int J Food Microbiol*, 120, 159-66.
- OCTAVIO, L. M., GEDEON, K. & MAHESHRI, N. 2009. Epigenetic and conventional regulation is distributed among activators of *FLO11* allowing tuning of population-level heterogeneity in its expression. *PLoS Genet*, 5, e1000673.
- ODDS, F. C., BROWN, A. J. & GOW, N. A. 2003. Antifungal agents: mechanisms of action. *Trends Microbiol*, 11, 272-9.
- ORLEAN, P. & MENON, A. K. 2007. Thematic review series: lipid posttranslational modifications. GPI anchoring of protein in yeast and mammalian cells, or: how we learned to stop worrying and love glycosphospholipids. *J Lipid Res*, 48, 993-1011.
- PAGES, V. & FUCHS, R. P. 2002. How DNA lesions are turned into mutations within cells? *Oncogene*, 21, 8957-66.
- PAGES, V., SANTA MARIA, S. R., PRAKASH, L. & PRAKASH, S. 2009. Role of DNA damage-induced replication checkpoint in promoting lesion bypass by translesion synthesis in yeast. *Genes Dev*, 23, 1438-49.
- PAN, X. & HEITMAN, J. 2002. Protein kinase A operates a molecular switch that governs yeast pseudohyphal differentiation. *Mol Cell Biol*, 22, 3981-93.
- PAPPAS, P. G., REX, J. H., LEE, J., HAMILL, R. J., LARSEN, R. A., POWDERLY, W., KAUFFMAN, C. A., HYSLOP, N., MANGINO, J. E., CHAPMAN, S., HOROWITZ, H. W., EDWARDS, J. E. & DISMUKES, W. E. 2003. A prospective observational study of candidemia: epidemiology, therapy, and influences on mortality in hospitalized adult and pediatric patients. *Clin Infect Dis*, 37, 634-43.
- PAYNE, T. 2007. Protein secretion in *Saccharomyces cerevisiae*: PhD Thesis, University of Nottingham.
- PAYS, E. 2005. Regulation of antigen gene expression in *Trypanosoma brucei*. *Trends Parasitol*, 21, 517-20.
- PFALLER, M. A. & DIEKEMA, D. J. 2004. Twelve years of fluconazole in clinical practice: global trends in species distribution and fluconazole susceptibility of bloodstream isolates of *Candida*. *Clin Microbiol Infect*, 10 Suppl 1, 11-23.
- PFALLER, M. A., JONES, R. N., MESSER, S. A., EDMOND, M. B. & WENZEL, R. P. 1998. National surveillance of nosocomial blood stream infection due to species of *Candida* other than *Candida albicans*: frequency of occurrence and antifungal susceptibility in the SCOPE Program. SCOPE Participant Group. Surveillance and Control of Pathogens of Epidemiologic. *Diagn Microbiol Infect Dis*, 30, 121-9.
- PIKE, L. J. 2004. Lipid rafts: heterogeneity on the high seas. *Biochem J*, 378, 281-92.
- PIKE, L. J. 2006. Rafts defined: a report on the Keystone Symposium on Lipid Rafts and Cell Function. *J Lipid Res*, 47, 1597-8.
- PITTET, M. & CONZELMANN, A. 2007. Biosynthesis and function of GPI proteins in the yeast *Saccharomyces cerevisiae*. *Biochim Biophys Acta*, 1771, 405-20.
- POLAKOVA, S., BLUME, C., ZARATE, J. A., MENDEL, M., JORCK-RAMBERG, D., STENDERUP, J. & PISKUR, J. 2009. Formation of new chromosomes as a virulence mechanism in yeast *Candida glabrata*. *Proc Natl Acad Sci U S A*, 106, 2688-93.
- PORTER, S. E., GREENWELL, P. W., RITCHIE, K. B. & PETES, T. D. 1996. The DNA-binding protein Hdf1p (a putative Ku homologue) is required for maintaining normal telomere length in *Saccharomyces cerevisiae*. *Nucleic Acids Res*, 24, 582-5.
- PRYDE, F. E. & LOUIS, E. J. 1997. *Saccharomyces cerevisiae* telomeres. A review. *Biochemistry (Mosc)*, 62, 1232-41.

- PRYDE, F. E. & LOUIS, E. J. 1999. Limitations of silencing at native yeast telomeres. *EMBO J*, 18, 2538-50.
- RAISNER, R. M. & MADHANI, H. D. 2008. Genomewide screen for negative regulators of sirtuin activity in *Saccharomyces cerevisiae* reveals 40 loci and links to metabolism. *Genetics*, 179, 1933-44.
- RALPH, S. A., SCHEIDIG-BENATAR, C. & SCHERF, A. 2005. Antigenic variation in *Plasmodium falciparum* is associated with movement of var loci between subnuclear locations. *Proc Natl Acad Sci U S A*, 102, 5414-9.
- RALPH, S. A. & SCHERF, A. 2005. The epigenetic control of antigenic variation in *Plasmodium falciparum*. *Curr Opin Microbiol*, 8, 434-40.
- RAMIREZ-ZAVALETA, C. Y., SALAS-DELGADO, G. E., DE LAS PENAS, A. & CASTANO, I. 2010. Subtelomeric silencing of the MTL3 locus of *Candida glabrata* requires yKu70, yKu80, and Rif1 proteins. *Eukaryot Cell*, 9, 1602-11.
- RECKER, M., BUCKEE, C. O., SERAZIN, A., KYES, S., PINCHES, R., CHRISTODOULOU, Z., SPRINGER, A. L., GUPTA, S. & NEWBOLD, C. I. 2011. Antigenic variation in *Plasmodium falciparum* malaria involves a highly structured switching pattern. *PLoS Pathog*, 7, e1001306.
- REESE, M. G. 2001. Application of a time-delay neural network to promoter annotation in the *Drosophila melanogaster* genome. *Comput Chem*, 26, 51-6.
- RENAULD, H., APARICIO, O. M., ZIERATH, P. D., BILLINGTON, B. L., CHHABLANI, S. K. & GOTTSCHLING, D. E. 1993. Silent domains are assembled continuously from the telomere and are defined by promoter distance and strength, and by *SIR3* dosage. *Genes Dev*, 7, 1133-45.
- RICHARD, M. L. & PLAINE, A. 2007. Comprehensive analysis of glycosylphosphatidylinositol-anchored proteins in *Candida albicans*. *Eukaryot Cell*, 6, 119-33.
- RICHTER, S. S., GALASK, R. P., MESSER, S. A., HOLLIS, R. J., DIEKEMA, D. J. & PFALLER, M. A. 2005. Antifungal susceptibilities of *Candida* species causing vulvovaginitis and epidemiology of recurrent cases. *J Clin Microbiol*, 43, 2155-62.
- RIGDEN, D. J., MELLO, L. V. & GALPERIN, M. Y. 2004. The PA14 domain, a conserved all-beta domain in bacterial toxins, enzymes, adhesins and signaling molecules. *Trends Biochem Sci*, 29, 335-9.
- RIVIER, A. S., CASTILLON, G. A., MICHON, L., FUKASAWA, M., ROMANOVA-MICHAELIDES, M., JAENSCH, N., HANADA, K. & WATANABE, R. 2010. Exit of GPI-anchored proteins from the ER differs in yeast and mammalian cells. *Traffic*, 11, 1017-33.
- ROBINSON, N. P., BURMAN, N., MELVILLE, S. E. & BARRY, J. D. 1999. Predominance of duplicative VSG gene conversion in antigenic variation in African trypanosomes. *Mol Cell Biol*, 19, 5839-46.
- ROETZER, A., GABALDON, T. & SCHULLER, C. 2011. From *Saccharomyces cerevisiae* to *Candida glabrata* in a few easy steps: important adaptations for an opportunistic pathogen. *FEMS Microbiol Lett*, 314, 1-9.
- ROSAS-HERNANDEZ, L. L., JUAREZ-REYES, A., ARROYO-HELGUERA, O. E., DE LAS PENAS, A., PAN, S. J., CORMACK, B. P. & CASTANO, I. 2008. yKu70/yKu80 and Rif1 regulate silencing differentially at telomeres in *Candida glabrata*. *Eukaryot Cell*, 7, 2168-78.
- RUIZ-HERRERA, J., ELORZA, M. V., VALENTIN, E. & SENTANDREU, R. 2006. Molecular organization of the cell wall of *Candida albicans* and its relation to pathogenicity. *FEMS Yeast Res*, 6, 14-29.

- RUSCHE, L. N., KIRCHMAIER, A. L. & RINE, J. 2003. The establishment, inheritance, and function of silenced chromatin in *Saccharomyces cerevisiae*. *Annu Rev Biochem*, 72, 481-516.
- SAFDAR, A., CHATURVEDI, V., KOLL, B. S., LARONE, D. H., PERLIN, D. S. & ARMSTRONG, D. 2002. Prospective, multicenter surveillance study of *Candida glabrata*: fluconazole and itraconazole susceptibility profiles in bloodstream, invasive, and colonizing strains and differences between isolates from three urban teaching hospitals in New York City (Candida Susceptibility Trends Study, 1998 to 1999). *Antimicrob Agents Chemother*, 46, 3268-72.
- SALMON, T. B., EVERT, B. A., SONG, B. & DOETSCH, P. W. 2004. Biological consequences of oxidative stress-induced DNA damage in *Saccharomyces cerevisiae*. *Nucleic Acids Res*, 32, 3712-23.
- SANGLARD, D., ISCHER, F. & BILLE, J. 2001. Role of ATP-binding-cassette transporter genes in high-frequency acquisition of resistance to azole antifungals in *Candida glabrata*. *Antimicrob Agents Chemother*, 45, 1174-83.
- SCANNELL, D. R., BUTLER, G. & WOLFE, K. H. 2007. Yeast genome evolution--the origin of the species. *Yeast*, 24, 929-42.
- SCHERF, A., LOPEZ-RUBIO, J. J. & RIVIERE, L. 2008. Antigenic variation in *Plasmodium falciparum*. *Annu Rev Microbiol*, 62, 445-70.
- SCHMIDT, P., WALKER, J., SELWAY, L., STEAD, D., YIN, Z., ENJALBERT, B., WEIG, M. & BROWN, A. J. 2008. Proteomic analysis of the pH response in the fungal pathogen *Candida glabrata*. *Proteomics*, 8, 534-44.
- SEDGWICK, S. G., TAYLOR, I. A., ADAM, A. C., SPANOS, A., HOWELL, S., MORGAN, B. A., TREIBER, M. K., KANUGA, N., BANKS, G. R., FOORD, R. & SMERDON, S. J. 1998. Structural and functional architecture of the yeast cell-cycle transcription factor Swi6. *J Mol Biol*, 281, 763-75.
- SHAHBAZIAN, M. D. & GRUNSTEIN, M. 2007. Functions of site-specific histone acetylation and deacetylation. *Annu Rev Biochem*, 76, 75-100.
- SHEN, J., GUO, W. & KOHLER, J. R. 2005. CaNAT1, a heterologous dominant selectable marker for transformation of *Candida albicans* and other pathogenic *Candida* species. *Infect Immun*, 73, 1239-42.
- SHEPPARD, D. C., YEAMAN, M. R., WELCH, W. H., PHAN, Q. T., FU, Y., IBRAHIM, A. S., FILLER, S. G., ZHANG, M., WARING, A. J. & EDWARDS, J. E., JR. 2004. Functional and structural diversity in the Als protein family of *Candida albicans*. *J Biol Chem*, 279, 30480-9.
- SHERMAN, D., DURRENS, P., IRAGNE, F., BEYNE, E., NIKOLSKI, M. & SOUCIET, J. L. 2006. Genolevures complete genomes provide data and tools for comparative genomics of hemiascomycetous yeasts. *Nucleic Acids Res*, 34, D432-5.
- SHILATIFARD, A. 2006. Chromatin modifications by methylation and ubiquitination: implications in the regulation of gene expression. *Annu Rev Biochem*, 75, 243-69.
- SHIMA, D. T., HALDAR, K., PEPPERKOK, R., WATSON, R. & WARREN, G. 1997. Partitioning of the Golgi apparatus during mitosis in living HeLa cells. *J Cell Biol*, 137, 1211-28.
- SILVA, S., NEGRI, M., HENRIQUES, M., OLIVEIRA, R., WILLIAMS, D. W. & AZEREDO, J. 2011. Adherence and biofilm formation of non-*Candida albicans* *Candida* species. *Trends Microbiol*, 19, 241-7.
- SMITH, B. C., HALLOWS, W. C. & DENU, J. M. 2008. Mechanisms and molecular probes of sirtuins. *Chem Biol*, 15, 1002-13.

- SMITH, M. C., SUMNER, E. R. & AVERY, S. V. 2007. Glutathione and Gts1p drive beneficial variability in the cadmium resistances of individual yeast cells. *Mol Microbiol*, 66, 699-712.
- SMITS, G. J., SCHENKMAN, L. R., BRUL, S., PRINGLE, J. R. & KLIS, F. M. 2006. Role of cell cycle-regulated expression in the localized incorporation of cell wall proteins in yeast. *Mol Biol Cell*, 17, 3267-80.
- SOARES, E. V. 2011. Flocculation in *Saccharomyces cerevisiae*: a review. *J Appl Microbiol*, 110, 1-18.
- SOUTHERN, E. 2006. Southern blotting. *Nat Protoc*, 1, 518-25.
- SRIKANTHA, T., LACHKE, S. A. & SOLL, D. R. 2003. Three mating type-like loci in *Candida glabrata*. *Eukaryot Cell*, 2, 328-40.
- STRAHL-BOLSINGER, S., HECHT, A., LUO, K. & GRUNSTEIN, M. 1997. SIR2 and SIR4 interactions differ in core and extended telomeric heterochromatin in yeast. *Genes Dev*, 11, 83-93.
- SUDBERY, P., GOW, N. & BERMAN, J. 2004. The distinct morphogenic states of *Candida albicans*. *Trends Microbiol*, 12, 317-24.
- SUDBERY, P. E. 2011. Growth of *Candida albicans* hyphae. *Nat Rev Microbiol*.
- SUMNER, E. R., AVERY, A. M., HOUGHTON, J. E., ROBINS, R. A. & AVERY, S. V. 2003. Cell cycle- and age-dependent activation of Sod1p drives the formation of stress resistant cell subpopulations within clonal yeast cultures. *Mol Microbiol*, 50, 857-70.
- SUZUKI, K. & SHEETZ, M. P. 2001. Binding of cross-linked glycosylphosphatidylinositol-anchored proteins to discrete actin-associated sites and cholesterol-dependent domains. *Biophys J*, 81, 2181-9.
- TAKAHASHI, Y. H., SCHULZE, J. M., JACKSON, J., HENTRICH, T., SEIDEL, C., JASPERSEN, S. L., KOBOR, M. S. & SHILATIFARD, A. 2011. Dot1 and histone H3K79 methylation in natural telomeric and *HM* silencing. *Mol Cell*, 42, 118-26.
- TALBERT, P. B. & HENIKOFF, S. 2006. Spreading of silent chromatin: inaction at a distance. *Nat Rev Genet*, 7, 793-803.
- THIERRY, A., BOUCHIER, C., DUJON, B. & RICHARD, G. F. 2008. Megasatellites: a peculiar class of giant minisatellites in genes involved in cell adhesion and pathogenicity in *Candida glabrata*. *Nucleic Acids Res*, 36, 5970-82.
- THOMPSON, G. R., 3RD, WIEDERHOLD, N. P., VALLOR, A. C., VILLAREAL, N. C., LEWIS, J. S., 2ND & PATTERSON, T. F. 2008. Development of caspofungin resistance following prolonged therapy for invasive candidiasis secondary to *Candida glabrata* infection. *Antimicrob Agents Chemother*, 52, 3783-5.
- TONG, L. & DENU, J. M. 2010. Function and metabolism of sirtuin metabolite O-acetyl-ADP-ribose. *Biochim Biophys Acta*, 1804, 1617-25.
- TORRES, E. M., SOKOLSKY, T., TUCKER, C. M., CHAN, L. Y., BOSELLI, M., DUNHAM, M. J. & AMON, A. 2007. Effects of aneuploidy on cellular physiology and cell division in haploid yeast. *Science*, 317, 916-24.
- TRICK, W. E., FRIDKIN, S. K., EDWARDS, J. R., HAJJEH, R. A. & GAYNES, R. P. 2002. Secular trend of hospital-acquired candidemia among intensive care unit patients in the United States during 1989-1999. *Clin Infect Dis*, 35, 627-30.
- ULRICH, H. D. 2002. Degradation or maintenance: actions of the ubiquitin system on eukaryotic chromatin. *Eukaryot Cell*, 1, 1-10.
- ULRICH, H. D. 2005. The *RAD6* pathway: control of DNA damage bypass and mutagenesis by ubiquitin and SUMO. *Chembiochem*, 6, 1735-43.

- ULRICH, H. D. 2009. Regulating post-translational modifications of the eukaryotic replication clamp PCNA. *DNA Repair (Amst)*, 8, 461-9.
- UNK, I., HAJDU, I., BLASTYAK, A. & HARACSKA, L. 2010. Role of yeast Rad5 and its human orthologs, *HLTF* and *SHPRH* in DNA damage tolerance. *DNA Repair (Amst)*, 9, 257-67.
- VAN LEEUWEN, M. R., SMANT, W., DE BOER, W. & DIJKSTERHUIS, J. 2008. Filipin is a reliable in situ marker of ergosterol in the plasma membrane of germinating conidia (spores) of *Penicillium discolor* and stains intensively at the site of germ tube formation. *J Microbiol Methods*, 74, 64-73.
- VERDIN, E., DEQUIEDT, F. & KASLER, H. G. 2003. Class II histone deacetylases: versatile regulators. *Trends Genet*, 19, 286-93.
- VERSTREPEN, K. J. & FINK, G. R. 2009. Genetic and epigenetic mechanisms underlying cell-surface variability in protozoa and fungi. *Annu Rev Genet*, 43, 1-24.
- VERSTREPEN, K. J., REYNOLDS, T. B. & FINK, G. R. 2004. Origins of variation in the fungal cell surface. *Nat Rev Microbiol*, 2, 533-40.
- VERZIJLBERGEN, K. F., FABER, A. W., STULEMEIJER, I. J. & VAN LEEUWEN, F. 2009. Multiple histone modifications in euchromatin promote heterochromatin formation by redundant mechanisms in *Saccharomyces cerevisiae*. *BMC Mol Biol*, 10, 76.
- VIOLA, A. & GUPTA, N. 2007. Tether and trap: regulation of membrane-raft dynamics by actin-binding proteins. *Nat Rev Immunol*, 7, 889-96.
- VOSS, T. S., HEALER, J., MARTY, A. J., DUFFY, M. F., THOMPSON, J. K., BEESON, J. G., REEDER, J. C., CRABB, B. S. & COWMAN, A. F. 2006. A var gene promoter controls allelic exclusion of virulence genes in *Plasmodium falciparum* malaria. *Nature*, 439, 1004-8.
- WACHTLER, V., RAJAGOPALAN, S. & BALASUBRAMANIAN, M. K. 2003. Sterol-rich plasma membrane domains in the fission yeast *Schizosaccharomyces pombe*. *J Cell Sci*, 116, 867-74.
- WATERS, L. S., MINESINGER, B. K., WILTROUT, M. E., D'SOUZA, S., WOODRUFF, R. V. & WALKER, G. C. 2009. Eukaryotic translesion polymerases and their roles and regulation in DNA damage tolerance. *Microbiol Mol Biol Rev*, 73, 134-54.
- WATERS, L. S. & WALKER, G. C. 2006. The critical mutagenic translesion DNA polymerase Rev1 is highly expressed during G(2)/M phase rather than S phase. *Proc Natl Acad Sci U S A*, 103, 8971-6.
- WEIG, M., JANSCH, L., GROSS, U., DE KOSTER, C. G., KLIS, F. M. & DE GROOT, P. W. 2004. Systematic identification in silico of covalently bound cell wall proteins and analysis of protein-polysaccharide linkages of the human pathogen *Candida glabrata*. *Microbiology*, 150, 3129-44.
- WHEELER, R. T. & FINK, G. R. 2006. A drug-sensitive genetic network masks fungi from the immune system. *PLoS Pathog*, 2, e35.
- WHITTAKER, R. H. 1959. On the broad classification of organisms. *Q Rev Biol*, 34, 210-26.
- WHITTAKER, R. H. 1969. New concepts of kingdoms or organisms. Evolutionary relations are better represented by new classifications than by the traditional two kingdoms. *Science*, 163, 150-60.
- WINGARD, J. R. 1994. Infections due to resistant *Candida* species in patients with cancer who are receiving chemotherapy. *Clin Infect Dis*, 19 Suppl 1, S49-53.
- WISPLINGHOFF, H., BISCHOFF, T., TALLENT, S. M., SEIFERT, H., WENZEL, R. P. & EDMOND, M. B. 2004. Nosocomial bloodstream infections in US hospitals: analysis of 24,179 cases from a prospective nationwide surveillance study. *Clin Infect Dis*, 39, 309-17.

- WOLF, D. M. & ARKIN, A. P. 2002. Fifteen minutes of fim: control of type 1 pili expression in *E. coli*. *OMICS*, 6, 91-114.
- WU, J., SUKA, N., CARLSON, M. & GRUNSTEIN, M. 2001. *TUP1* utilizes histone H3/H2B-specific *HDA1* deacetylase to repress gene activity in yeast. *Mol Cell*, 7, 117-26.
- WYRICK, J. J., HOLSTEGE, F. C., JENNINGS, E. G., CAUSTON, H. C., SHORE, D., GRUNSTEIN, M., LANDER, E. S. & YOUNG, R. A. 1999. Chromosomal landscape of nucleosome-dependent gene expression and silencing in yeast. *Nature*, 402, 418-21.
- YANG, B., BRITTON, J. & KIRCHMAIER, A. L. 2008. Insights into the impact of histone acetylation and methylation on Sir protein recruitment, spreading, and silencing in *Saccharomyces cerevisiae*. *J Mol Biol*, 381, 826-44.
- YIN, Q. Y., DE GROOT, P. W., DE KOSTER, C. G. & KLIS, F. M. 2008. Mass spectrometry-based proteomics of fungal wall glycoproteins. *Trends Microbiol*, 16, 20-6.
- ZHANG, H. & LAWRENCE, C. W. 2005. The error-free component of the RAD6/RAD18 DNA damage tolerance pathway of budding yeast employs sister-strand recombination. *Proc Natl Acad Sci U S A*, 102, 15954-9.
- ZHAO, X., OH, S. H., CHENG, G., GREEN, C. B., NUESSEN, J. A., YEATER, K., LENG, R. P., BROWN, A. J. & HOYER, L. L. 2004. ALS3 and ALS8 represent a single locus that encodes a *Candida albicans* adhesin; functional comparisons between Als3p and Als1p. *Microbiology*, 150, 2415-28.
- ZHONG, H., MCCORD, R. & VERSHON, A. K. 1999. Identification of target sites of the alpha2-Mcm1 repressor complex in the yeast genome. *Genome Res*, 9, 1040-7.
- ZHU, J. & ZHANG, M. Q. 1999. SCPD: a promoter database of the yeast *Saccharomyces cerevisiae*. *Bioinformatics*, 15, 607-11.
- ZHU, X. & GUSTAFSSON, C. M. 2009. Distinct differences in chromatin structure at subtelomeric X and Y' elements in budding yeast. *PLoS One*, 4, e6363.
- ZUPANCIC, M. L., FRIEMAN, M., SMITH, D., ALVAREZ, R. A., CUMMINGS, R. D. & CORMACK, B. P. 2008. Glycan microarray analysis of *Candida glabrata* adhesin ligand specificity. *Mol Microbiol*, 68, 547-59.

List of Figures

Figure 1 – Saccharomycotina phylogenetic tree.....	10
Figure 2 – <i>C. glabrata</i> pseudohyphal growth.....	11
Figure 3 – <i>C. albicans</i> cellular morphology.....	11
Figure 4 – <i>C. glabrata</i> biofilms.....	15
Figure 5 – Fungal cell wall molecular architecture.....	20
Figure 6 – Structure of the GPI-anchored precursor protein and the GPI core.....	23
Figure 7 – Epa PA14 domain.....	27
Figure 8 – Sir2-dependent histone deacetylation reaction.....	30
Figure 9 – Sir complex assembly at telomeres.....	33
Figure 10 – The looping model of discontinuous silencing.....	36
Figure 11 – Mechanisms of DNA damage tolerance.....	39
Figure 12 – Bypass of DNA lesions by TLS.....	41
Figure 13 – Mechanisms of <i>VSG</i> switching in <i>T. brucei</i>	49
Figure 14 – Model for <i>VAR</i> gene activation according to nuclear localisation in <i>P. falciparum</i>	53
Figure 15 – Mechanisms mediating heterogeneous <i>FLO</i> gene expression in <i>S. cerevisiae</i>	55
Figure 16 – Maps of plasmids utilised and constructed during this study..	61
Figure 17 – DNA ladders for agarose gel electrophoresis.....	75
Figure 18 – DNA ladder for FIGE.....	86
Figure 19 – <i>S. cerevisiae</i> Rad6-GFP translational fusion (Invitrogen) expression.....	92
Figure 20 – Single copy <i>S. cerevisiae</i> plasmids utilised and constructed during this study.....	95
Figure 21 – Complementation of Rad6-GFP <i>SIR2</i> and <i>SWI6</i> deletion strains.....	96
Figure 22 – Flow cytometry of high- and low-expressing Rad6-GFP cells...98	98
Figure 23 – Rad6-GFP expression level switching.....	98
Figure 24 – PCR Gel confirming presence of the Rad6-GFP cassette in both high- and low-Rad6-GFP cells.....	100
Figure 25 – Diagnostic PCR for generation of an <i>S. cerevisiae</i> <i>RAD6</i> -GFP transcriptional fusion strain.....	100
Figure 26 – Flow cytometry of the <i>RAD6</i> -GFP transcriptional fusion.....	102
Figure 27 – Flow cytometry of a remade <i>S. cerevisiae</i> Rad6-GFP translational fusion.....	102

Figure 28 - Flow cytometry of an <i>EPA1</i> -GFP transcriptional fusion strain.....	107
Figure 29 - Adhesion and reversion of sorted high- and low-Epa1-HA expressing cells.....	109
Figure 30 - The CV of <i>EPA1</i> -GFP expression calculated according to Newman et al (2006).....	111
Figure 31 - Construction of strains expressing triple-HA tagged Epa1.....	113
Figure 32 - Flow cytometry and fluorescence microscopy of the CG2001-Epa1-HA strain.....	115
Figure 33 - Comparison of Epa1-HA expression and heterogeneity in two strain backgrounds.....	116
Figure 34 - Flow cytometric analysis of Epa1-HA expression and heterogeneity during growth in batch culture for two strain backgrounds.....	118
Figure 35 - Partitioning of Epa1-HA during cell division.....	120
Figure 36 - Comparison of bud cell area and bud cell Epa1-HA expression in two strain backgrounds.....	122
Figure 37 - (Non) heritability of Epa1-HA expression.....	124
Figure 38 - Schematic representation of <i>EPA1-EPA7</i> positions in the <i>C. glabrata</i> genome.....	131
Figure 39 - Effect of temperature on Epa1-HA expression and heterogeneity in the BG2-Epa1-HA strain.....	136
Figure 40 - Effect of temperature on Epa1-HA expression and heterogeneity in the CG2001-Epa1-HA strain.....	137
Figure 41 - Effect of temperature on adhesion of CG2001-Epa1-HA cells to Hep2 epithelial cells.....	138
Figure 42 - Nitrogen limitation in the BG2-Epa1-HA strain and its role in Epa1-HA expression and heterogeneity.....	140
Figure 43 - Nitrogen limitation in the CG2001-Epa1-HA strain and its role in Epa1-HA expression and heterogeneity.....	141
Figure 44 - Growth of BG2-Epa1-HA cells at various pH's and the effect on Epa1-HA expression and heterogeneity.....	142
Figure 45 - Growth of CG2001-Epa1-HA cells at various pH's and the effect on Epa1-HA expression and heterogeneity.....	143
Figure 46 - Sir-dependent transcriptional silencing of Epa1 in the BG2-Epa1-HA strain.....	145
Figure 47 - The role of Sir-dependent transcriptional silencing on Epa1-HA expression and heterogeneity in CG2001-Epa1-HA.....	147

Figure 48 – Complementation of CG2001-Epa1-HA <i>sir3</i> Δ.....	149
Figure 49 – Epa1-HA expression heterogeneity following inhibition of transcriptional silencing by NA limitation in BG2-Epa1-HA cells.....	151
Figure 50 – Epa1-HA expression heterogeneity following inhibition of transcriptional silencing by NA Limitation in CG2001-Epa1-HA cells.....	153
Figure 51 – Mean Epa1-HA expression following inhibition of transcriptional silencing by NA limitation in BG2-Epa1-HA and CG2001-Epa1-HA cells...	154
Figure 52 – Inhibition of transcriptional silencing by NA limitation in the CG2001-Epa1-HA <i>sir3</i> Δ deletion strain background.....	154
Figure 53 – Analysis of Sir-dependent transcriptional silencing in an untagged Epa1 BG2 strain using an anti-Epa1 antibody.....	156
Figure 54 – Analysis of Sir-dependent transcriptional silencing in an untagged Epa1 CG2001 HTUΔ strain using an anti-Epa1 antibody.....	156
Figure 55 – <i>EPA1</i> transcript levels following NA limitation in two strain backgrounds.....	157
Figure 56 – Ectopic expression of <i>SIR3</i> in the CG2001-Epa1-HA background.....	159
Figure 57 – <i>SIR3</i> mRNA levels in two <i>C. glabrata</i> strain backgrounds.....	161
Figure 58 – Inhibition of transcriptional silencing across a range of clinical <i>C. glabrata</i> isolates.....	162
Figure 59 – Epa1 expression and heterogeneity across a range of clinical <i>C. glabrata</i> isolates.....	164
Figure 60 – Relationship between silencing and heterogeneity of Epa1 expression across all tested <i>C. glabrata</i> strains.....	166
Figure 61 – Strategy to determine differences in the distance of <i>EPA1</i> from the chromosome end between two strain backgrounds.....	168
Figure 62 – FIGE gel analysis to determine the distance of <i>EPA1</i> from the chromosome end in two strain backgrounds.....	170
Figure 63 – Fluorescence microscopy of Epa1-HA cell surface expression.....	172
Figure 64 – Epa1-HA expression and heterogeneity following treatment of cells with myriocin.....	174
Figure 65 – Epa1-HA expression and heterogeneity following treatment of cells with ketoconazole.....	176
Figure 66 – Epa1-HA expression and heterogeneity following treatment of cells with myriocin and ketoconazole.....	178
Figure 67 – Fluorescence microscopy to image Epa1-HA expression following treatment of cells with: myriocin, ketoconazole, or both.....	179

Figure 68 – Dual staining of cells for Epa1-HA and membrane sterols.....	180
Figure 69 – Actin staining of cells.....	182
Figure 70 – Effect of <i>YPS7</i> deletion on Epa1-HA expression and heterogeneity.....	185
Figure 71 – Effect of <i>YPS1</i> and <i>YPS7</i> double deletion on Epa1-HA expression and heterogeneity.....	185
Figure 72 – Dual staining of cells for Epa1-Ha and cell surface mannoprotein.....	187
Figure 73 – Correlation between Epa1-HA protein and <i>EPA1</i> mRNA levels.....	189
Figure 74 – Correlation between Epa1-HA protein and $\alpha 2$ mRNA levels...192	
Figure 75 – Protein alignment of Epa1 from the ATCC2001 type strain and BG2.....	194
Figure 76 – Correlation between Epa1-HA protein and <i>EPA6</i> and <i>EPA7</i> mRNA levels.....	196
Figure 77 – <i>EPA6</i> and <i>EPA7</i> mRNA levels following NA limitation the BG2 strain background.....	198
Figure 78 – <i>EPA6</i> and <i>EPA7</i> mRNA levels following NA limitation or <i>sir3</i> Δ deletion in the CG2001 HTU Δ strain background.....	199

List of Tables

Table 1 – Cell wall composition of <i>C. glabrata</i> , <i>S. cerevisiae</i> , and <i>C. albicans</i>	20
Table 2 – Amino acid and antibiotic concentrations.....	67
Table 3 – Phusion® High Fidelity polymerase PCR reaction mixture.....	70
Table 4 – Taq DNA polymerase PCR reaction mixture.....	71
Table 5 – PCR primers.....	72
Table 6 – Sequencing primers.....	73
Table 7 – qRT-PCR primers.....	84
Table 8 – Solutions for dCT ³² P-labelled probe hybridisation.....	88
Table 9 – <i>C. glabrata</i> clinical isolates, their source, and grouped according to the dependence of <i>EPA1</i> expression on Sir-mediated transcriptional silencing.....	161